Design Synthesis Exercise

Final Report

H.J.P. Gaens (4352858)
T. Harms (4348850)
R. Hendrickx (4380908)
S. Hofman (4353862)
T. Pruijsers (4147030)
R.V. van Sunten (4381807)
L.N. Van de Sype (4379233)
S.I.M.C. Verhellen (4355423)
R.C. Wink (4351657)

Low-Noise Medium-Range Airliner

Group 25

Delft University of Technology

TU Delft Delft University of Technology

Challenge the future

Design of a Low-Noise Medium-Range Airliner

Technical Design Report

by

Group 25

H.J.P. Gaens (4352858)
T. Harms (4348850)
R. Hendrickx (4380908)
S. Hofman (4353862)
T. Pruijsers (4147030)
R.V. van Sunten (4381807)
L.N. Van de Sype (4379233)
S.I.M.C. Verhellen (4355423)
R.C. Wink (4351657)

As part of the Spring 2017 Design Synthesis Exercise

At Delft University of Technology, Faculty of Aerospace Engineering

	Course:	AE3200
	Identification:	DID-2
Tutor:	Dr. ir. S. Hartjes	Air Transport Operations
Coaches:	T. Gaida MSc.	Aircraft Noise and Climate Effects
	N. Zhong MSc.	Novel Aerospace Materials

Preface

This report presents the concluding chapter of the Spring 2017 Design Synthesis Exercise (DSE) at the Faculty of Aerospace Engineering of Delft University of Technology. The project serves as closure of the Bachelor of Aerospace Engineering by means of an integrated design project, incorporating previously studied material as well as innovation. During a period of ten weeks, a team of nine Bachelor of Science students have been involved in the preliminary design of a low-noise medium-range airliner. This resulted in the *Silent Regional Jet 110*. More elaborate information about the progress and development of the design leading up to this point can be found in the preceding reports; the Project Plan, the Baseline and the Mid-term reports.

First of all, the group would like to express its sincere gratitude to dr. ir. Sander Hartjes for his coaching, guidance, advice, involvement and valuable and informative feedback as tutor during the project. Appreciation also goes out to Timo Gaida MSc. and Nan Zhong MSc. for their role as coaches. Furthermore all teachers and staff members the group was able to consult for advice are thanked for their feedback and support: dr. ir. O. Bergsma (SI&C), dr. ir. A. Elham (FPP), ir. M. Hoogreef (FPP), dr. ir. G. La Rocca (FPP), ir. J. Melkert (FPP), dr. ir. A. Sahai (ANCE), ir. J. Sinke (SI&C), ir. N. Timmer (Aero), dr. ir. W. Verhagen (ATO) and dr. ir. R. Vos (FPP).

Last but not least, the organisational committee of the DSE and Delft University of Technology are thanked for providing the group the opportunity and facilities to complete this project.

This project has been an intense but valuable learning experience, both on technical and personal level. The group is proud on the final output of the design and team effort throughout the project. The tasks were not just completed as a group of students but rather as a devoted team, driven, ambitious and cohesive. It is therefore with great pleasure that DSE group 25 presents their design of a low-noise medium-range airliner, the SRJ110.

Hendrik Gaens
Tim Harms
Rik Hendrickx
Sam Hofman
Tom Pruijsers
Ralph van Sunten
Luka Van de Sype
Saranne Verhellen
Ruben Wink

28 June 2017
Delft, The Netherlands

Summary

This report describes the work that has been performed in the final phase of the low-noise medium-range airliner project and subsequently, presents the corresponding results. This final phase of the design synthesis exercise mostly consisted of more detailed technical analysis in order to, in the end, reach a final design concept. The final concept carries the name SRJ110, signifying 'Silent Regional Jet' and the amount of passengers the aircraft is designed to carry. This summary will present the reader with an overview of the work that is performed as well as the results that are achieved.

The report first gives an overview of the requirements posed on the project and thus the final design. While the requirements have not been changed in the final phase, they remained crucial throughout the whole design process. The most basic requirements are summarised here. Firstly, the aircraft is required to transport 110 passengers with standard economy service levels. In terms of performance, the SRJ110 is required to have a cruise speed of at least Mach 0.7 at an altitude of 25,000 ft or an equivalent ground speed of 216 m/s. The range should equal or exceed 1,500 NM at maximum payload. Furthermore, the aircraft should be able to operate from London City Airport (LCY) with an 80% load factor for a 1,000 NM mission, imposing stringent requirements on the SRJ's performance because of the urban environment LCY is located in. Moreover, reference noise levels should be 5 dB lower than FAR noise certification points. In addition, the area exposed to more than 65 dBA should be reduced by 30%. For fuel efficiency and ecology, the SRJ has to at least match the performance of the Embraer E190-E2. In terms of safety and operating costs, the aircraft should at least rival the Avro RJ100. Further requirements were worked out in the chapter 2.

Afterwards, a market analysis was performed. It is essential to know the market and the possibilities it offers before developing a product. The main competitors are identified to be the Embraer E190-E2, the Sukhoi Superjet 100, the Mitsubishi MRJ90 and the Bombardier CS100. Every continent was considered and discussed in terms of their market and potential. Apart from Europe, which is and will remain the largest market, Latin America and Asia continue to prove to be growing markets. A 90- and 130-seater variant will create the possibility to compete over a wider range of the market, as well as lowering production and development costs for the whole programme. In total, it is projected that 450 to 500 SRJ110s can be sold over a period of 15 years. A competitive listing price for the SRJ110 would be between 50-55 million USD. For a more detailed view on the market analysis, the future market outlook, the study of regional markets and the production and unit price estimate, please consult chapter 3.

Subsequently, a risk assessment is performed. A number of technical risks are identified and analysed. Their likelihood and the severity of the consequences are assigned a grade. Multiplication of those two grades results in a value for threat for every identified risk. The most threatening ones are summarised here. The risk with the highest grade is for the aircraft to be not sufficiently sustainable. Not meeting the noise requirement is also a threatening risk. Subsequently, an increase in cost as compared to the requirement is considered a serious risk. There also is the risk of having excessive cabin noise due to the wing-mounted engine. Finally, there is the risk of leaving unused excess engineering budget. For every one of these five critical risks, a mitigation method was thought of. For the mitigation methods and more information on the process of risk assessment in general, please consult chapter 4.

The last part before the start of the technical part of the report is the concept selection. In the baseline phase, a large amount of possible concepts were produced. From the baseline report four concepts were selected: one conventional jet concept, one similar concept with engines on top of the wing, one conventional turboprop concept and finally a concept characterised by a push prop and canard. In the midterm report, the first concept was merged with the second. Finally, that particular concept scored best in the trade-off.

A very important aspect of the design process is the weight estimation and the design space determination. An overview of the process of the Class I weight estimation, the Class II weight estimation and the design space is given. The iterative process that has been maintained throughout the design process is described. Finally, a maximum take of mass of 45,734 kg, an operative empty mass of 26,193 kg, a fuel mass of 8,871 kg and a maximum zero-fuel mass of 36,863 kg were found. According to design space, a thrust of 135.18 kN and a wing area of 87.82 m^2 were obtained. For a more detailed look into the process, and detailed breakdown of the mass of all subsystems, please consult chapter 6.

The stability and control characteristics of the aircraft are determined subsequently. The starting point for this analysis is the preliminary tail sizing, mainly based on reference aircraft. Then, three different loading diagrams are generated, for three different wing positions. The loading diagrams give the most forward and backward centre of gravity positions. From these three data sets, two lines can be extrapolated showing forward and backward centre of gravity for each possible position of the wing. Afterwards, the critical

stability and controllability relations are calculated. From these follows the scissor plot, that defines the relation between the position of centre of gravity and the horizontal tail surface. Superposing these two graphs gives the ideal design point, defining tail surface and position of the leading edge of the mean aerodynamic chord. These two parameters are determined to be 14.75 m^2 and 13.74 m. Furthermore, the horizontal tail arm is equal to 17.89 m. For the vertical tail, an area of 14.59 m^2 was found and a tail arm of 15.39 m. The landing gear is determined to be 1.7 m high, shorter than that of comparable aircraft. For wheelbase and exact landing gear position, as well as for the detailed stability and control process, please consult chapter 7.

The next extensive field of research is the aerodynamic analysis. At first, through analysis and trade-off airfoils are selected. The NASA SC(2)-0614 airfoil is selected for the root part of the wing. Around halfway the wing, where a kink is located the NASA SC(2)-0612, is applied. At the tip of the wing, the airfoil is even thinner, the SC(2)-0610 is chosen there. The planform is designed after. An aspect ratio of 8.925, a surface area of 87.82 m^2, a wingspan of 28 m, a quarter chord sweep of 25 ° and a taper ratio of 0.25 are the most important parameters that have been found. Additionally, a wing tip device has been designed in order to increase efficiency. The device on the SRJ110 is a combination of a raked wingtip and a blended winglet. The wingtip device lowers the drag by 3.25%. Subsequently, a full wing analysis is performed by *XFLR5*. The following values were found during the analysis: a maximum lift coefficient of 1.73, a stall angle of 18.75°, a cruise angle of attack of 2.5° and a moment coefficient at cruise of -0.6068. The drag estimation was performed after using book methods. Adding up all drag types, a total drag coefficient of 0.032 is found. Moreover, the design of high lift devices is treated. The aircraft will have two sets of flaps: an inboard double slotted flap and an outboard single slotted Fowler flap. The effects of the high lift devices on the aerodynamic performance are described in more detail in chapter 8. Finally, ailerons, elevators and rudder are elaborated on.

Another critical aspect in the design of an aircraft is the structural analysis. First, the material choice is elaborated upon. Carbon fibre reinforced plastic T800H is selected as the main material in the aircraft, both for the wings and the fuselage. For the wing, the structural design of the wing box is performed. Shear load and moment diagrams were generated, illustrating the forces and moments acting on the wing at every point along the span. From there, accounting for the stresses created within the wing box, the internal wing lay-out is determined. Spar and skin thickness are defined at different locations along the span. For a more detailed look on the process and for the final results, please consult chapter 9.2. The fuselage is the other major part of the aircraft in need of a structural analysis. Again, forces and moments within the fuselage are analysed. This is done for the situation of a hard landing (load case of 3.75 g). The fuselage and its structural elements were analysed using the boom method. Stresses within were calculated and subsequently skin thickness, stringer thickness and size were determined. Hoop stress and fatigue were elaborated upon as well.

Subsequently, the flight performance is analysed. The cruise altitude, cruise speed and fuel consumption are investigated. A cruise speed of 229 m/s and a cruise altitude of $FL350$ are deemed best regarding fuel consumption and feasibility. This would equate to a cruise Mach number of 0.77 or equivalent ground speed of 229 m/s. The corresponding fuel efficiency is equal to 0.0376 $kg/PAX/NM$ at these conditions, 12% better than the set requirement. In terms of harmful particle emissions, the SRJ also scores better than the requirements. For a more elaborate description of the process and analysis, please consult section 10.1. The climb performance is another important aspect of the flight performance. The climb rate and climb gradient were analysed for a range of speeds and altitudes, as well as for one engine inoperative situations and rejected landings. Due to the multitude of results, please consult 10.2 for the description and all the results. Airfield performance was analysed as well: an important parameter, given the requirement to operate from short runways such as the one at London City. The take-off distance, consisting of both ground roll and airborne phase, is 1,054 m long. Airfield performance for 'hot and high' conditions were also analysed. At a temperature of 50°C and an air pressure of 100,609 Pa, the take off distance has grown to 1,293 m. With this value, the aircraft can theoretically still take off from London City, if some of the clearways are used for the climb phase. For the landing distance calculations, the steep approach procedure has to be taken into account. The total certified landing distance is found to be 925 m, well under the FAR certified distance of 1,112 m at LCY.

On top of the large design and analysis subjects above, smaller though important subsystems have been designed during this final phase of the design synthesis exercise. The fuel system has been designed, with fuel tanks, lay-out of piping, valves, pumps, vents and redundancy and safety features. The tank volume is determined to be 14 m^3: more than was accounted for in the performance and weight analysis. Weather protection systems have been designed as well in the form of a heat duct in the leading edge for de-icing purposes. The electrical system and flight control system have been thought out and are represented using flow diagrams. The detailed explanation on the subsystem design can be read in chapter 11.

A paramount part of this design synthesis exercise is the noise mitigation. Firstly, research is done concerning the concept of noise, most notable noise sources, noise regulations, noise contours and noise of

comparable aircraft. For certification, noise is measured at three different locations, for different conditions. Flyover noise is the noise after take-off perceived by an observer standing directly under the climb path of the aircraft. Lateral noise is determined as the maximum noise during the ground run of the take-off phase, measured 450 m from the side. Approach noise is similar to flyover noise in observer location, but in the approach configuration. From how similar contemporary aircraft perform, it is determined that lateral noise require special attention in order to satisfy the given requirements. After a theoretical analysis about noise, possible noise mitigation measures are investigated. In the end, mitigation measures are selected to be applied to the SRJ110. For aerodynamic noise mitigation, metal brushes are attached to the trailing edge, reducing wing noise by around 3 dB. Furthermore, flap tip fences are applied on the outboard flaps, reducing noise by up to 7 dB on flap level. For slat noise, wing fences are placed at the ends of the slats, minimising drag and noise generated by turbulent flow around the slat edges. Sealing the slat-track cut-out boasts another improvement in noise. Finally, landing gear fairings are applied. Fairings reduce noise with up to 3.5 $EPNdB$ on aircraft level. On top of that, the main landing gear doors are sized in a way that if the landing gear is down and the doors close, the cavity left in the wing is minimal, and so will the noise. In terms of engine noise mitigation, jet and fan noise are distinguished. Jet noise levels are low to begin with, given the choice for a high-bypass turbofan. Chevrons yield an extra noise reduction of up to 5 $EPNdB$. Given the high bypass ratio of the engine, fan noise is more pronounced. The gearbox in the geared turbofan that was selected can lower fan speeds, lowering aerodynamic noise. An important part of the noise mitigation of the SRJ110 concept is the position of the engines. Research by the FAA, Boeing and NASA predict reductions for lateral noise of 4.3 up to 5 $EPNdB$, on aircraft level. Possible increase in cabin noise is mitigated by extra shielding, insulation and active noise control, similar to the Active Noise and Vibration Suppression system in the Bombardier Q400. The distance between fuselage and engine edge is 1.81 m. Additionally, an integrated noise model analysis has been performed. In this model, noise values and contours of the RJ85 and the SRJ110 are compared. The SRJ110 boasts a 23.1% reduction in noise area during departure. The difference is even larger during approach, where the SRJ110 outperforms the Avro by 56.2%. Final noise levels found for the SRJ110 in $EPNdB$ are 89.0 for the approach point, 82.1 for sideline noise and 75.9 during flyover. For more detail on noise mitigation and the performance of the SRJ110 in terms of noise, please consult chapter 13.

The final design configuration of the aircraft has been summarised in the next chapter. The fuselage is designed in a 2-2 configuration. A seat width of 47 cm is decided upon. The aisle width is equal to 50 cm at the narrowest point, which complies with all CS25 requirements. In total, the cabin diameter at its widest point is 283 cm. The total fuselage diameter is 3.03 m and the cabin of the aircraft is 26.3 m long. Emergency exits and required clearance, as well as lavatories and gallies have been sized for. 110 passengers can be seated at a standard seat pitch of 31 in. At a 30 in pitch, 114 passengers can be seated, and with an inch of legroom less, the SRJ110 can carry 118 passengers. A two-class configuration with six first class seats would allow for 97 economy passengers. Overhead compartments have a volume of 8.1 m^3. The main cargo holds can store up to 15 m^3 of goods. A seat plan, a representation of the cross-section, as well as the design philosophy and CS25 compliance can be found in section 14.1. In section 8.2, a table can be found with all final dimensions and characteristics of the wing. Tail and landing gear dimensions are summarised again, but were already elaborated upon in previous sections, and will therefore not be repeated at this point of the summary.

The last important technical part is the cost analysis. For a detailed look at the processes that were followed and assumptions that were made, please consult chapter 15. The main outcomes of the cost analysis are presented here. Research, development and testing costs are projected to be 754.27 million USD. Manufacturing costs for 500 produced aircraft is estimated to be 21.39 billion USD. This would yield a unit price of 54.80 million USD. A detailed breakdown of the direct operating cost was done. The total direct operating cost of the SRJ110 is 3,026 USD/h. Return of investment and profit for the manufacturer was also considered.

The technical phases of the report are followed by a verification and validation for all technical divisions. Furthermore, operations, logistics and sustainability are discussed.

After the technical design is set, a compliance check was performed in order to verify if all requirements for the project are met. Three incompliances are noted. Firstly, the target unit price of 40 million USD has not been met. This was identified beforehand and agreed upon with the customer. Furthermore, an incompliance with respect to the CS25 regulations has been identified. Every aspect treated during this project is, as far as reasonably identifiable, in compliance with CS25. However, CS25 is very extensive, and many the requirements are beyond the scope of this project. A compliance with CS25 can not be given however if not every single requirement is met. Moreover a slight discrepancy is left on the noise exposed area. Even though the area was reduced by 29.2%, a margin of 0.8% still needs to be attained in a future stage. Due to software limitations, one of the most important noise mitigation measures is not yet taken into account; wing shielding. Hence the design team is confident that the requirement will be met in a later stage.

Contents

Nomenclature

Greek Symbols

α_{0L}	Wing zero-lift angle of attack	[°]
α_{cruise}	Cruise angle of attack	[°]
α_{stall}	Stall angle of attack	[°]
β	Prandlt-Glauert correction factor	[-]
η	Airfoil efficiency factor	[-]
Γ	Dihedral angle	[°]
γ	Climb gradient	[°]
λ	Taper ratio	[-]
$\Lambda_{1/2c}$	Half chord sweep angle	[°]
$\Lambda_{1/4c}$	Quarter chord sweep angle	[°]
Λ_{LE}	Leading edge sweep angle	[°]
ρ	Air density	$[kg/m^3]$
$\sigma_{c_{max}}$	Maximum compressive stress	$[MPa]$
$\sigma_{t_{max}}$	Maximum tensile stress	$[MPa]$
$\sigma_{vM_{max}}$	Maximum von Mises stress	$[MPa]$
τ_{max}	Maximum shear stress	$[MPa]$

Latin Symbols

$\bar{Y}$	Spanwise location of the MAC	$[m]$
A	Aspect ratio	[-]
B	Wheelbase	$[m]$
b	Wingspan	$[m]$
b_{fus}	Fuselage width	$[m]$
c	Wing chord	$[m]$
C_l	Two dimensional lift coefficient	[-]
C_{D_0}	Zero-lift drag coefficient	[-]
C_{D_i}	Induced drag coefficient	[-]
$C_{D_{min}}$	Minimum drag coefficient	[-]
C_{D_w}	Wave drag coefficient	[-]
C_D	Drag coefficient	[-]
C_d	Airfoil drag coefficient	[-]
C_{L_0}	Wing zero lift coefficient	[-]
C_{L_α}	Wing lift gradient	$[1/rad]$
C_{l_α}	Airfoil lift gradient	$[1/rad]$
$C_{L_{des}}$	Wing lift design coefficient	[-]
$C_{l_{des}}$	Airfoil lift design coefficient	[-]
$C_{L_{max}}$	Maximum wing lift coefficient	[-]
$C_{l_{max}}$	Maximum airfoil lift coefficient	[-]
$C_{l_{mindrag}}$	Minimum drag airfoil lift coefficient	[-]
C_L	Lift coefficient	[-]
C_l	Two dimensional lift coefficient	[-]
$C_{m_{1/4}}$	Quarter chord moment coefficient	[-]
$C_{m_{ac}}$	Aerodynamic moment coefficient	[-]
c_r	Root chord	$[m]$
c_t	Tip chord	$[m]$
D	Drag force	$[N]$
d_{fus}	Fuselage diameter	$[m]$
e	Oswald efficiency factor	[-]
g	Gravitational acceleration	$[m/s^2]$
h_{cr}	Cruise altitude	$[m]$
h_{fus}	Fuselage height	$[m]$
I	Moment of inertia	$[m^4]$
i_w	Wing incidence angle	[°]
L	Lift force	$[N]$
l	Tail arm	$[m]$
L/D	Lift to drag ratio	[-]
l_{fus}	Fuselage length	$[m]$
l_{nc}	Nose cone length	$[m]$
l_{tc}	Tail cone length	$[m]$
M	Mach number	[-]
m	Mass	$[kg]$
M_{DD}	Drag divergence Mach number	[-]
n_{max}	Maximum loading factor	[-]
S	Wing surface area	$[m^2]$
S_h	Horizontal tail surface area	$[m^2]$
S_v	Vertical tail surface area	$[m^2]$
S_{wet}	Wetted wing surface area	$[m^2]$
T	Thrust force	$[N]$
t	Thickness	$[mm]$
t/c	Thickness-over-chord ratio	[-]
T/W	Thrust loading	$[N/N]$
V	Airspeed	$[m/s]$
V_L	Landing speed	$[m/s]$
V_D	Dive speed	$[m/s]$
V_e	Exhaust velocity	$[m/s]$
V_{stall}	Stall speed	$[m/s]$
W/S	Wing loading	$[N/m^2]$
x/c	Arbitrary chord location	[-]
X_{LEMAC}	Position of the LE point of wing MAC	$[m]$

Abbreviations

EAS	Equivalent airspeed	$[m/s]$
$EPNL$	Effective perceived noise level	$[EPNdB]$
FM	Fuel mass	$[kg]$
FW	Fuel weight	$[N]$
LCC	Low cost carrier	[-]
LCY	London City Airport	[-]
MAC	Mean aerodynamic chord	$[m]$
MLM	Maximum landing mass	$[kg]$
$MTOM$	Maximum take-off mass	$[kg]$
$MTOW$	Maximum take-off weight	$[N]$
$MZFM$	Maximum zero-fuel mass	$[kg]$
$NASA$	National Aeronautics and Space Administration	[-]
OEM	Operating empty mass	$[kg]$
OEW	Operating empty weight	$[N]$
P	Payload	$[kg]$
$RAMS$	Reliability, Availability, Maintainability and Safety	[-]
RC	Rate of climb	[m/s]

$RDTE$	Research, development and testing phase	[-]
RPM	Rounds per minute	$[rev/min]$
SEL	Sound exposure level	[dBA]
SFC	Specific fuel consumption	$[kg/Ns]$
SPL	Sound pressure level	$[dB]$
SPL_A	A-weighted sound pressure level	$[dBA]$
SRJ	Silent Regional Jet	[-]
TAS	True airspeed	$[m/s]$
CAEP	Committee on Aviation Environmental Protection	[-]
CS25	Certification Specifications for Large Aeroplanes issued by EASA	[-]
DOC	Direct Operating Cost	[-]
EASA	European Aviation Safety Agency	[-]
FAA	Federal Aviation Administration	[-]
FAR	Federal Aviation Regulations	[-]
ICAO	International Civil Aviation Organisation	[-]
NACA	National Advisory Committee for Aeronautics	[-]
PAX	Passengers	[#]

Subscripts

$A-h$	Aircraft-less-tail	[-]
av	Average	[-]
bc	Begin of cruise	[-]
$clean$	Clean condition	[-]
cr	Critical	[-]
$cruise$	Cruise condition	[-]
ec	End of cruise	[-]
fus	Fuselage	[-]
ge	Ground effect	[-]
h	Horizontal tail	[-]
$land$	Landing condition	[-]
rot	Rotation	[-]
st	Stringer	[-]
TO	Take-off condition	[-]
v	Vertical tail	[-]

1 Introduction

Ever since the first prototype of the *Wright Flyer*, challenges and innovations have been the heartbeat of the aviation industry. While the strict science of flight has been resolved since then, focus is nowadays on the development of aircraft systems able to comply with the modern society and the living quality standards. Efforts in terms of noise reduction and pollutant emissions minimisation have already been undertaken in the past sixty years. However, the noise level experienced at certain airports due to air traffic operations remains problematic. Therefore, the need of satisfying the current demand for quieter and more environmentally friendly design solutions is a key priority in the aviation industry.

Being aware of this contemporary problem, the Faculty of Aerospace Engineering at the Delft University of Technology has hired a team of nine Aerospace Engineering students to work full time on the preliminary design of a low-noise medium-range airliner. The mission need statement for this project is defined as follows: *provide a market-competitive, medium-range airliner with reduced noise pollution and fuel consumption compared to the best available alternatives; the Avro RJ100 and Embraer E2 respectively*. The project objective statement states that *the objective of this project is to provide the preliminary design of a revolutionary medium-range airliner, specifically aimed at operating from noise-sensitive airports, without significantly compromising efficiency, capacity, cost, environmental impact and safety with nine students in ten weeks*. In order to develop such a system, several technical analyses have been undertaken. Accuracy, reliability, safety and sustainability have driven the design to a successful end. The ultimate goal of this report is therefore to present the final aircraft configuration of the low-noise medium-range airliner designed by the DSE group 25, namely the *Silent Regional Jet 110*. The team is confident that the developed aircraft will meet competitive standards with the potential capability of widening the current market opportunities.

This report is structured as follows. First of all, a summary of the requirements introduced in the Mid-term Report is provided in chapter 2. Elaboration on the market opportunities, the risks and the design selection process presented in the Baseline Report is undertaken in chapters 3, 4 and 5, respectively. In order to initiate intricate technical analyses of the design, an accurate weight estimation and determination of the design space were needed. These results are presented in chapter 6. The different technical analyses, together with the final results, are subsequently included in chapters 7 to 10. The order the analyses are discussed in is as follows. The Stability & Control analysis is presented first, followed by the Aerodynamic, Structural and finally the Flight Performance analysis. Chapter 11 discusses the different subsystems to be implemented into the design of the SRJ110. A close look at the noise concept and the related regulations, as well as the noise mitigation measures for the SRJ110 is taken in chapters 12 and 13. Once all the technical analyses are complete, the final aircraft design configuration is introduced in chapter 14. A detailed cost analysis of the final design is performed in chapter 15. In order to verify and validate the methods used for the various technical analyses, a verification and validation campaign is performed in chapter 16. Operations and logistics, as well as the sustainability strategy are then discussed in chapters 17 and 18, respectively. Before determining the post-DSE activities in chapter 20, a compliance matrix has been generated in chapter 19.

2 Requirements Analysis and Overview

Requirements on the aircraft characteristics are the starting point of the design. These follow from stakeholder wishes as well as from technical, legal and operational constraints. The initial requirements as stated by the customer, c.q. top level requirements, are discussed in section 2.1. Section 2.2 translates these requirements to the so called system requirements such that the design team is capable of meeting the requirements in a technical or engineering sense. Additionally, a more detailed set of requirements is derived and described in section 2.3, namely the subsystem requirements.

2.1 Top Level Requirements

The top level requirements are listed below. As mentioned before, this is the starting point of the development since the design shall comply with the needs of the customer. Moreover, the design team is responsible for analysis of the top level requirements to determine their feasibility and attainability. In the final stage, the design team will evaluate if the design meets the requirements by means of a compliance matrix.

- Capacity and Operations
  - A minimum seating capacity of 110 seats is required with service levels similar to Embraer E190 (with respect to seat pitch, galleys, lavatories, etc.).
- Performance
  - Cruise speed should exceed Mach 0.7 at 25,000 ft.
  - Maximum range should exceed 1,500 NM.
  - Should be able to operate from London City Airport with an 80% load factor for a 1,000 NM mission.
- Safety and reliability
  - Similar or better than comparable aircraft (Avro RJ100).
- Sustainability
  - The pollutant emissions should be better or at least similar to the Embraer E2 currently under development.
  - Fuel efficiency at least 10% better per PAX/NM than the Embraer E2 family currently under development.
  - Noise levels (as compared to the Avro RJ100).
    - Reference noise levels should be 5 dB lower than FAR noise certification points.
    - The area of exposed to Sound Exposure Levels of greater than 65 dBA should be reduced by 30%.
- Cost
  - Unit cost of 40 million USD to account for manufacturing and return on investment.
  - Direct operating cost lower than Avro RJ100.

2.2 System Requirements

The analysis of the requirements starts off with redefining the top level requirements such that these comply with the VALID criteria for stating requirements [1]. The VALID method ensures the requirements are clearly defined in a technical sense by subjecting them to five criteria. This requirement analysis is conducted and the outcome presented in this section, resulting in a significant amount of system requirements.

2.2.1 Capacity and Operational Requirements

With respect to the capacity and operational requirements, a single system requirement is derived. The seating capacity is considered to be of major importance to both the customer and the design team. For the latter because it drives the design of the fuselage. Consequently, it is identified as a driving requirement.

- SRJ110-OPS-CAP-A1 The aircraft shall have a seating capacity of at least 110 seats in full economy configuration. *Considered a driving requirement.*

2.2.2 Performance Requirements

The performance of the aircraft shall at least meet the following three requirements.

- SRJ110-PERF-CRU-A1 The aircraft's true air speed, c.q. ground speed, shall exceed 216 m/s. *Considered a driving requirement.*
- SRJ110-PERF-RAN-A1 The aircraft's maximum range shall exceed 1,500 NM at maximum payload. *Considered a driving requirement.*
- SRJ110-PERF-LCY-A1 The aircraft shall be able to operate from London City Airport (LCY) with an 80% load factor for a 1,000 NM mission. *Considered a key requirement.*

For the first requirement, the initial speed and altitude requirements have been translated in consultation with the customer as ground speed is said to be the most desired performance parameter. The second requirement adds an operational constraint, required payload, to the existing range of 1,500 NM. From experience it is known that this is key to operators satisfaction since their goal is to move passengers from A to B. Both of these requirements are identified to be driving requirements, since existing designs have already proven its feasibility. Finally, the third requirement is a key requirement because it is very specific and has been stressed by the customer.

2.2.3 Safety and Reliability Requirements

The system requirements related to safety and reliability are shown below.

- SRJ110-S&R-REL-A1 The aircraft shall have a dispatch reliability of at least 98%. *Considered a key requirement.*
- SRJ110-S&R-SAF-A1 The aircraft shall be in compliance with the CS25 regulations. *Considered a driving requirement.*

The reliability requirement is considered a key requirement. When this target is met, the product is commercially viable with respect to existing aircraft. Moreover, this parameter is an important indicator for potential operators of the aircraft and thus the customer. The Avro RJ100 has a dispatch reliability of 98%, therefore it is important to excel this number [2]. In case of safety, no parameter is unambiguous to represent the design's safety performance. Therefore the airworthiness regulations are set as a bare minimum to comply with. A non-airworthy aircraft will never be allowed to fly commercially, hence complying with the CS25 regulations is both important to the customer and the design team. As safety is a factor that should be implemented throughout the design, it is considered as a driving requirement.

2.2.4 Sustainability Requirements

Characteristics such as fuel burn and pollutant emissions are very important for aircraft operators, for both economical and corporate social responsibility reasons. The following requirements have been set:

- SRJ110-SUS-POL-A1 The aircraft shall have a margin to the CAEP 6 standard for NO_x emission of at least 50%. *Considered a driving requirement.*
- SRJ110-SUS-POL-B1 The aircraft's CO_2 emission shall be less than 134.3 $g/PAX/NM$. *Considered a driving requirement.*
- SRJ110-SUS-POL-C1 The aircraft's CO and HC emission shall be lower than 0.004263 and 0.004263 $g/PAX/NM$ respectively. *Considered a driving requirement.*
- SRJ110-SUS-POL-D1 The aircraft shall have of fuel burn equal to or less than 0.04263 $kg/PAX/NM$ based on a 100% loading factor. *Considered a key requirement.*

As mentioned in the top level requirements, the Embraer E2 family is currently under development and definitive numbers are not published yet. Consequently, it is extremely hard to quantify numbers at this stage due to the availability of data. Fortunately, it is known that the Embraer will meet the CAEP 6 standards resulting in the first requirement [3]. The second requirement is based on a complete combustion of Jet A fuel. Using the derived fuel consumption of the Embraer E190-E2, the requirement for CO_2 emission is converted to 134.3 $g/PAX/NM$ [4]. Besides the emission of CO_2, other pollutants such as CO and HC are emitted due the combustion of fuel as well. Emission data about family members of the E190-E2 engine is found in an ICAO database [5]. Hence, the requirement is set to perform at least better than current engines available. This equals 0.1 g/kg of fuel burnt for both pollutants. The reduction in pollutant emission is the

direct consequence of improved fuel efficiency thus decreased fuel burn. Hence the pollutant emission requirement is translated with respect to the fuel burn. Preliminary figures from Embraer show that the new generation E190-E2 will have 16% less fuel burn compared to the current generation [4]. The fuel burn value for the current E190 is 0.0564 $kg/PAX/NM$ based on a 90 PAX configuration [6]. Hence the value for the E190-E2 lies around 0.04738 $kg/PAX/NM$. The top level requirement is to be at least 10% below this number. Even though the sustainability system requirements are linked with each other - less fuel burn results in less emission - only the fourth and final one is identified as being key. Operators are familiar with this parameter which is often used to compare performance between aircraft.

With respect to another key aspect of the to be designed aircraft, which is noise, a two requirements have been defined. The first is derived from an EASA database, the latter from data obtained by an existing noise model, INM (Integrated Noise Model) [7].

- SRJ110-SUS-POL-E1 The aircraft noise shall not exceed 256.8 $EPNdB$ cumulatively, 83.1 $EPNdB$ laterally, 81.1 $EPNdB$ at flyover and 92.6 $EPNdB$ during approach. *Considered a driving requirement.*

- SRJ110-SUS-POL-F1 The area exposed to Sound Exposure Levels of greater than 65 dBA shall be less than 35.2 km^2.

The FAA regulations (FAR) prescribe noise pollution limits at three different certification points. These regulations are equal to the regulations set by EASA [8]. Moreover, EASA provides a database with numerous aircraft noise measurements, including the AVRO RJ100 [7]. Consequently, the requirement is defined according to these measurements with 5 $EPNdB$ subtracted at every measurement point. The ICAO sets specific noise limits as well, however these are met automatically if the aircraft complies with the cumulative reduction of 15 $EPNdB$ with respect to the Avro. This will be elaborated on in section 12.3.

2.2.5 Cost Requirements

The cost requirements are both considered key, since cost is decisive for potential customers. According to ICAO, the DOC of a BAe 146-300, the predecessor of the Avro RJ100, is 2,585.00 USD per block hour [9]. This number is published in 2000, so an inflation correction is applied. Hence the requirement is defined by taking this updated value as upper limit.

- SRJ110-CST-CST-A1 The unit cost of the aircraft shall not exceed 40 million USD. *Considered a key requirement.*
- SRJ110-CST-DOC-A1 The DOC shall be less than 3,670.70 USD per block hour. *Considered a key requirement.*

2.3 Subsystem Requirements

The subsystem requirements are more detailed than the previously discussed system requirements. A significant number is directly related to the system requirements, as can be seen by the prefix. However, additional requirements are defined due to external constraints.

2.3.1 Capacity and Operational Requirements

KLM comfort standards are set as the standard for the to be designed aircraft, defining the seat pitch, width and number of facilities [10]. KLM is one of the main operators of the E190 and their standards are thus very common in the market. The aisle width is however a safety measure found in CS25 [11].

- SRJ110-OPS-CAP-A1-01 The seat pitch shall be at least 30 inch.
- SRJ110-OPS-CAP-A1-02 The seat width shall be at least 18 inch.
- SRJ110-OPS-CAP-A1-03 The aisle width shall be at least 20 inch at a height of 25 inches measured from the cabin floor.
- SRJ110-OPS-CAP-A1-04 The aircraft shall have at least two lavatories.
- SRJ110-OPS-CAP-A1-05 The aircraft shall have at least three galleys.

2.3.2 Performance Requirements

Operations from London City Airport (LCY) pose additional constraints on the performance of the aircraft due to the close proximity to the densely populated city center and noise abatement procedures. Runway length is limited and there are minimums for the climb gradient and glide slope for the so called steep approach procedure. On top of that, special certification is required. Based on the United Kingdom's Aeronautical Information Provider (AIP), the following technical requirements follow for operation to and from LCY [12].

- SRJ110-PERF-LCY-A1-01 The aircraft shall be able to fly an ILS approach at a 5.5° slope while maintaining approach speed within regulatory limits.
- SRJ110-PERF-LCY-A1-02 The aircraft shall be able to descend at a 7.9% gradient while maintaining approach speed V_{app} within regulatory limits.
- SRJ110-PERF-LCY-A1-03 The aircraft shall have a climb out gradient in case of missed approach of at least 3.5% in ISA sea level conditions.
- SRJ110-PERF-LCY-A1-04 The aircraft shall comply with appendix Q, article 25.1 of the EASA CS25 regulations for a steep approach landing.
- SRJ110-PERF-LCY-A1-05 The aircraft at MLW shall be able to land and come to a complete stop within a distance of 1,319 m from the threshold and 1,207 m while performing an ILS landing.
- SRJ110-PERF-LCY-A1-06 The aircraft shall be able to take off within a distance of 1,199 m at $MTOW$ accounting for the stopping distance in case of rejected take-off.

2.3.3 Miscellaneous Subsystem Requirements

The following subsystem requirements are not directly related to the system requirements but originate from other considerations that arose during the requirement discovery process.

Wingspan

To be able to serve as many as possible airports in the world, it is important to design an ICAO category C compliant aircraft. Hence a requirement on wingspan follows.

- SRX110-WIN-DIM-A1-01 The aircraft wingspan shall not exceed 36 m.

Cargo

With the requirements on number of PAX in mind, it is possible to establish an initial estimate for the required cargo volume for both the luggage compartments and cargo holds.

- SRX110-INT-LUG-A1-01 The aircraft shall have luggage compartments with a total volume of at least 5,000 litres.
- SRX110-CAR-LUG-A1-01 The aircraft shall have cargo holds with a total volume of at least 12,000 litres.

Resources

Finally, the available resources are a constraint. This design synthesis exercise is conducted in a limited time frame with a limited amount of students. As time equals money, the a limit on the development cost is set. The total development cost is based on the program cost of the Embraer E2-family [13].

- SRX110-RES-TEAM-A1-01 The preliminary design shall be performed by 9 students within 10 weeks.
- SRX110-RES-CST-A1-01 The development cost shall not exceed 1.7 billion USD.

3 Market Analysis

Knowing the market the aircraft will be sold on, its characteristics, opportunities and weaknesses is of crucial importance for making design decisions. This chapter firstly sketches an image of how the market came to be and its current situation, both discussed in section 3.1. What the future might hold is presented in section 3.2. Subsequently, specific trends and options relevant to the SRJ110 and its future are discussed in sections 3.3, 3.4 and 3.5. The chapter is concluded in section 3.6.

3.1 Current Market

Over the past years, the regional jet aircraft market has experienced a large growth in demand. The hub-to-hub model, which predicted large aircraft would fly between major airports, seems less interesting than the point-to-point model. Smaller, regional aircraft that fly on these smaller point-to-point routes are therefore seen as an increasingly interesting product [14].

Overall, air transportation remains a growing market. In 2016, passenger demand grew by 6.2%, and growth is expected to continue over the next years [15].

Up until now, the two most important players in the regional jet market are Bombardier and Embraer. Bombardier first entered the market with the CRJ700/900/1000 series, featuring passenger capacities ranging from 79 to 104. With the introduction of the E-Jets, Embraer surpassed Bombardier, delivering aircraft that offer more capabilities and have the ability to transport slightly more passengers at higher comfort levels. The E-Jets family, in setup most similar to the SRJ110, consist of the E170, E175, E190 and E195, offering a seating capacity range from 66 to 126 passengers. In total, 1317 Embraer E-Jets have been delivered, compared to 796 Bombardier CRJ700/705/900/1000 aircraft [16, 17]. However, the demand will stagnate as more and more manufacturers and models join the market and the competition becomes more fierce [18].

In 2011 the Superjet 100-95 (SSJ100) was launched, produced by the Russian aircraft manufacturer Sukhoi in cooperation with a number of international companies. 105 SSJ100's are delivered so far and the Superjet proves itself a worthy competitor of the E-Jets and CRJ series, since it has a 99.9% dispatch reliability so far [18]. The SSJ100 offers seating for up to 108 passengers. Although it is not equipped with the most high tech engines, it still offers a 6-9% improvement in fuel burn and operating costs versus the CRJ1000 and E190/E195 [18]. Additionally, it outclasses all previously available competitors in terms of passenger comfort. By choosing for a larger fuselage diameter, seating passengers in a 3-2 configuration instead of the 2-2 of the E-jets, a significantly more spacious cabin is achieved. The cabin boasts a higher ceiling, wider seats, a wider aisle and an increased seat pitch. The sales of the Sukhoi however are heavily impacted by politics and the negative perception regarding Russia. Sales in Western Europe do not seem to lift off anytime soon.

Mitsubishi, a large Japanese manufacturer, is working on its very own regional jet: the MRJ90. In most respects it is very similar to the Embraer E-jets, and to the SRJ110. In size it is comparable to the E190, with a passenger capacity of 92. The MRJ90 was planned to arrive in 2013. At the time it would have been technically superior to the competition. However, it is now still in its testing phase, already four years late, causing it to probably enter the market when the at least equally advanced Bombardier C Series and Embraer E2 will have been released as well. 233 MRJ's have been ordered so far [19].

As previously mentioned, Embraer works on a second E-jets series, mounting new engines and an entirely new wing and landing gear. In other aspects the E175-E2, E190-E2 and E195-E2 are generally similar to their first generation cousins. Deliveries are expected to start in 2018.

Lastly, Bombardier recently launched a larger alternative, bridging the gap between regional and transcontinental jetliners. The CS100 and CS300 have started operations in 2016, two years late and two billion dollars over budget. The CS300 is, with up to 160 passengers, not really comparable to the previously discussed aircraft. It competes in a larger class, with the Airbus A319neo and 737 MAX 7, among others. The CS100, while still quite large at 108-130 PAX, is a more comparable aircraft. 123 CS100 aircraft have been ordered to this day [20].

3.2 Future Prospects

Forecast International predicts that 3,817 regional aircraft will be produced from 2016 through 2025. The value of these aircraft equals 135.2 billion *USD* [21]. Fuel prices are currently low, resulting in a significantly lower contribution to operating costs. Still, fuel is a finite resource, and while fuel prices are not expected

to shoot up quickly, the political situation in the Middle East might play a significant role in this respect. Consequently, fuel usage is and will remain an aspect demanding improvement.

A *SuperJet International* market analysis predicts a demand for 6,200 regional jets between 2016 and 2035, of which 63% is in the 90-120 segment [15]. As stated previously, the market is stabilising. For the upcoming years, 340 units p.a. are expected to be produced. Towards 2025, this would be 420 aircraft per year [21]. As for market share, Embraer is predicted to produce 959 aircraft between 2016 and 2035. Bombardier will add 591 regional aircraft to the market and Mitsubishi 437 [21]. Table 3.1 provides an overview of the options available on the market and their characteristics.

Table 3.1: Market competitors characteristics [22–26].

Parameter:	**E190**:	**E190-E2**:	**SSJ100-95**:	**MRJ90**:	**CS100**:	**CRJ1000**:
Passengers [#]	96/100/114	97/106	87/98/108	88/92	108/125/135	97/104
Seat width $[in]$	18.25	18.25	18.5	18.5	19	17.3
Seat pitch $[in]$	29/30	31	30/32	29/31	30	31
Cabin height $[m]$	2	2	2.12	2.03	2.11	1.88
Aisle width $[in]$	19.75	19.75	20	18	19	16.1
$MTOW$ $[kg]$	47,790	56,400	45,880	39,600	60,781	41,640
$MPLW$ $[kg]$	13,063	13,080	12,245	-	18,711	11,966
Range $[NM]$	1,850	2,850	1,645	1,150	3,100	1,622
Take-off field length $MTOW$ $[m]$	1,598	1,670	1,931	1,490	1,463	2,120
Take-off field length 500 NM mission $[m]$	1,267	-	-	-	1,219	-
Landing field length $[m]$	1,226	1,315	1,630	1,480	1,387	1,750
Max operating speed $[Mach]$	0.82	0.82	0,81	0.78	0.82	0.82
Service ceiling $[ft]$	41,000	41,000	41,000	39,000	41,000	41,000
Max TO thrust per engine $[lbf]$	20,000	17,000-23,000	15,400-16,100	17,600	18,900	14,510
Emissions (% lower than CAEP6)						
HC	29.8	-	84	85	-	-
CO	8.6	-	-	70	-	-
NO_x	23.9	-	20	50	50	-
Smoke	77.1	-	44	85	-	-
CO_2	-	-	33	-	-	-
Unit cost [million USD]	46.2	53.6	35.4	47.3	76.5	49
Program cost [million USD]	-	-	1,500	1,500	5,400	-
First flight	2004	2016	2008	2015	2013	2009
Introduction	2005	2018	2011	2020	2016	2010
Deliveries	534	-	105	-	7	51
Orders	590	68	210	233	123	68

In conclusion, the demand for medium-range, regional passenger aircraft is high. However the demand has recently stabilised and will not grow at the same rate. Nevertheless, a large market has been created, with a constant and large demand. Many different players compete in the same category. Providing one can offer an aircraft with distinct improvements or characteristics - something this project clearly aims to do - and/or for a competitive price, this market is attractive with promising opportunities.

3.3 Operators and Target Market

Generally, airlines can be divided into two classes: full-service/legacy carriers and low-cost carriers (LCCs). During the last two decades, low-cost airlines have claimed an increasingly prominent place in the market. Since 2008, LCCs have grown from making up just over 20% of the market, to almost 50% in 2015 [15]. Traditional flag carriers have seen their share decline with an equal and opposite fraction. The SRJ110 will be designed to suit both types of airlines well. It should live up to all modern standards in terms of technology, safety and passenger comfort valued by legacy carriers. At the same time it has to offer offer best-in-class fuel efficiency. The noise reduction potential is an aspect of importance for all airlines: stringent noise requirements affect all air traffic. The significant decrease in noise pollution will therefore appeal to both legacy and low-cost carriers.

Another important aspect in identifying possible customers and a target market is geographically based. Over the last decades new markets have emerged, which continue to show growth today. One of the regions that is expected to show the most growth in the next twenty years is Africa. Countries such as South Africa, Ethiopia and Nigeria prove to be among the top growing economies in the world [15]. With an estimated 350 regional jets between 2016 and 2035, of which 180 in the 91-120 seat segment, the African continent is still the smallest market. However, it has to be noted that the addition of 180 aircraft in the segment comes on top of only 45 operative now: Africa is a relatively untapped market, boasting serious potential.

Two other markets in full growth are Latin America and south-east Asia. Mexico, Brazil and Indonesia are examples of large countries with significant populations and an increasingly strong economy. Latin America is expected to boast demand for 790 regional jets, of which 660 with between 91 and 120 passengers [15]. For Pacific Asia, these numbers are 455 and 330 respectively. The airliner market of both continents discussed is characterised by a very large LCC market share. In Mexico City (Mexico), 55% of the market is accounted for by LCCs. In São Paulo (Brazil), the share of LCCs is 34% and in Manila (Philippines) 37% [15]. As can be seen in figure 3.1b and 3.1d, the SRJ110, with its range of 1,500 NM at maximum payload, is a perfect fit for Latin American airlines. From Santiago (Chile), most of the major South American cities can be reached. From Rio de Janeiro for example, Montevideo, Buenos Aires, Lima, all other major Brazilian cities are within reach. From Mexico City, the SRJ110 is easily able to serve all of Mexico as well as the entirety of Central America and up to Los Angeles and Chicago. As for the rest of Asia, China and India are and will remain large economies with numerous large population centres; hence a potentially interesting market for the SRJ110.

North America is a mature market which boasts a constant and high demand. Low-cost carriers make up an important part of the US market. Canada, Mexico and the United States are vast countries. Distances are large, road connections are not great and passenger railroad systems are underdeveloped compared to Europe. Regional air transport is therefore a significant share of the North American airline market. Looking at figure 3.1d, the range of the Silent Regional Jet is well suited for the American market, covering a major part of the United States, as well as most of Mexico and the major population centres of Canada. The market analysis of *SuperJet International* projects an additional 815 91-120 passenger regional jets to be sold in North America between 2016 and 2035. In total 2,075 regional jets will join that market in the same time period [15].

The Middle East is another booming market. The market here is dominated by the three large Gulf carriers: Qatar Airways, Etihad Airways and Emirates Airlines. They are characterised by offering high comfort and quality service. LCCs are not a significant factor in the Gulf market. Again, in terms of range, the SRJ110 is a versatile option for Middle Eastern airlines, able to reach the whole Middle East until Istanbul, India, Central Asia and Eastern Africa.

Finally, Europe is and stays the single largest airline market. 1,095 91-120 seat jet aircraft are expected to be added to the European market in the coming twenty years [15]. Europe is characterised by a high dependency on seasons: demand rises significantly in summer. Therefore smaller aircraft are more versatile all year round. Investing in large aircraft to fulfil summer demand might render them obsolete in winter. Smaller aircraft serving lower density, niche routes seem to be a better strategy, proven by the success of major European LCCs such as Ryanair, Easyjet, Wizzair and more.

(a) Africa.

(b) Latin America.

(c) Europe and the Middle East.

(d) North America.

Figure 3.1: Visualisation of SRJ110 range from various airports on different continents [27].

3.4 Aircraft Family

A very interesting option to consider in order to increase the target market, sell more aircraft and reduce development cost, is the development of an aircraft family. In order to determine the optimal passenger numbers for derivative aircraft. For this, firstly the average percentual difference between aircraft in single-aisle families was studied. Averaging for the Airbus A320 family, the Boeing 737 MAX family, the Bombardier C Series and the Embraer-E2 family, it was found that on average family members differ 17% from the original model. For the SRJ with 110 passengers, this would mean a 90-seater and a 130-seater. Looking at market analysis, existing models and their sales numbers, it was validated that 90 and 130 would be the ideal passenger numbers to cover the regional aircraft spectrum. Offering the SRJ90, SRJ110 and SRJ130 would create a powerful setup for the manufacturer, able to form an alternative to the E2-series and C Series, and competing with these alternatives in every segment of the market. It gives airlines a chance to select aircraft of different capacities, to fulfil all their tasks in the best way possible, without having to resort to different aircraft manufacturers and with keeping commonality across the board. Both versions are well within size margins that will allow them to share almost all of the structure. While fuselage length will obviously differ and engines might be changed or optimised, fuselage lay-out, cockpit and wings can probably be almost identical. In other words, the added sales of the derivatives outweigh the additional development costs, overall making the program more profitable.

3.5 Business Market

Additionally, the idea arose to not only enter the passenger airliner market, but to also launch a business variant of the silent regional aircraft developed during this DSE. While the business jet market is large (20 billion USD of revenue per year and increasing steadily), the large airliner-class business jet segment only accounts for around 3% of the sales and will, over the next 10 years, be 15.85 billion USD of revenues (compared to 248 USD billion for the whole market) [28]. It has to be noted that this 'business airliner' segment consists of everything from Embraer 190 based jets to large Airbus A330 and Boeing 747 business variants. The SRJ will therefore compete in a share of the market that accounts for a lot less than this projected average of 15.85 billion USD per year.

At the moment, this business airliner market is dominated by the Boeing BBJ line, which accounts for 60% of aircraft sold. Airbus ACJ takes another 25% and Embraer (Lineage 1000) accounts for the remaining 15% [28]. Sukhoi's SSJ100 based SBJ, launched in 2017, is predicted to sell 2-3 items per year until 2025. The Lineage 1000 also accounts for 2-3 deliveries per year. The C Series based business jet from Bombardier, that will appear in 2021, is predicted to sell around 1 to 2 pieces per year.

It is clear that this market is really small. Entering the market with the concept that results from this DSE will, in the best case, result in two aircraft sold per year. Clearly, this segment of the business market is not a gold mine. If the conversion to business configuration is not associated with too much extra costs, it is an option to consider. Nevertheless, generally the focus should remain on passenger transport aircraft.

3.6 Conclusive Statement

In conclusion, the SRJ110 in its form undoubtedly has its place in the market. While competition is fierce, the demand for regional jet aircraft is high and still growing. Leading fuel consumption figures, a state-of-the-art design and a significant advantage in noise will create interest for the SRJ programme. The European market should be a priority for the SRJ110. Apart from the mature markets of the Western world, Latin America and Asia are markets with a wealth of opportunities. The amount of aircraft that is projected to be sold is based on sales number of comparable aircraft combined with future market predictions. Values for comparable aircraft were all considered taking factors such as market situation, country of origin, time scale and geopolitics into account. The sales will most likely be lower than the E-jets, given that Embraer was early to the market. However, they will be higher than the Superjet 100, as the Western world, due to the political climate, is still hesitant to buy a Russian built aircraft. A factor positively influencing the sales figure is the fact that the domestic market, Europe, is large; a factor that the MRJ suffers from for example, given the small Japanese market. Overall, it is projected that 450-500 SRJ110 aircraft can be sold in 15 years after introduction. SRJ90 and SRJ130 derivatives would give the possibility to have a higher impact on the market and to lower production and development costs for every single aircraft that is being built. For an SRJ90, a projected sales number is 350, while the SRJ130 could account for 200 aircraft sold, both based on similar families of aircraft. A competitive price for a modern, high-tech, innovative aircraft with top-notch fuel efficiency and the added bonus of significantly reduced noise, is around 50-55 million USD. The Embraer E190-E2 has a unit price of 53.6 million USD, and serves as the main benchmark. While the SRJ110 will be newer, more technologically advanced and boasts a higher passenger capacity which might justify a higher price, Embraer has earned its place in the market, so a lower price will make for a more competitive position within the market.

4 Risk Assessment

As the risks related to management and team organisation have been discussed in the Project Plan Report, risks related to aircraft operations in the Baseline Report and risks related to the trade-off phase in the Mid-term Report, the focus is now on the technical risks associated with the preliminary technical design and post-DSE phase of the low-noise medium-range airliner project [29–31]. The identification of possible risks is key in approaching the design process in a well-prepared manner. Section 4.1 first presents and analyses the technical risks identified by the team. The risks that are identified as very threatening are subsequently mitigated in section 4.2.

4.1 Risk Analysis

For the technical risk assessment in this stage of the design, a closer look was taken at the risks that could interfere with the successful future development of the design and risks threatening requirements compliance. In this section of the risk analysis, these risks are identified.

Grades for likelihood and consequence are attributed to the risks, in order to determine the threat. The threat is the multiplication of the likelihood and the consequence and determines the position of the risk on the risk map. All risks and their respective likelihood, consequence and threat grade can be seen in table 4.1. The grades are assigned as follows. For likelihood, the grades range between a '1' and a '5'. The connotation of the likelihood grades is *very likely*, *likely*, *probable*, *unlikely* and *very unlikely*. For the consequence, the connotations are *catastrophic*, *major*, *moderate*, *minor* and *marginal*. The consequences can be interpreted in several ways, e.g. catastrophic on design level implies major design driving changes and possibly not meeting deadlines. On operational level it might imply injuries and even casualties.

Table 4.1: Technical risk identification and assessment, with the most threatening risks in red.

#	Event:	Likelihood:	Consequence:	Threat:
1	Cost increase	4	3	12
2	Unused excess engineering budget	4	3	12
3	Imprecise post-DSE time allocation	4	2	8
4	Cabin noise due to wing-mounted engine	3	4	12
5	Not attaining adequate performance	2	4	8
6	Tip-over at OEW	2	5	10
7	Overdesigning structure and frame	3	3	9
8	Improper material selection	2	3	6
9	Errors in *Python* code	5	1	5
10	Improper assumptions	4	2	8
11	Aircraft not sufficiently sustainable	4	4	16
12	Noise requirement not met	3	5	15
13	Too many simplifications	4	2	8
14	Failure of composite components	2	4	8
15	Failure of metal components	1	4	4

In the following paragraphs the likelihood and consequence grades attributed to each of the technical risks are discussed. Please note that the risk events presented in table 4.1 are considered unanticipated.

1. **Cost increase:** An increase in cost can be caused by all analyses and processes of design. Since most of the design analyses is done at the same time, cost can easily increase as it is sensitive to all processes. Also, the current design stage is still early and there are a lot of details unknown. This is why this likelihood is seen as *likely* and the consequence is *moderate*. The team can negotiate with the customer for more budget and try to find a efficient way to reduce the costs.

2. **Unused excess engineering budget:** Given the requirements, the group tries to optimise in every way possible to excel in e.g. performance. However, it is *likely* that, by excelling, there will be excess engineering budget left unused. If so, the group misses an opportunity to make the aircraft better in other aspects, which has a *moderate* effect.

3. **Imprecise post-DSE time allocation:** Since the group is not familiar with the industrial phase of the design of an aircraft, i.e. testing, manufacturing, etc., it is *likely* that the time allocated to certain phases will be imprecise. This has a *minor* consequence, since this only involves a preliminary time allocation and the exact times can be determined more precisely in a later stage.

4. **Cabin noise due to wing-mounted engine:** The focus of the group was more on reducing external noise in several directions, thus it is *probable* that the comfort of the passengers considering noise is placed on a lower level of importance. However, passenger comfort is a main factor for an airline so this plays quite a *major* role for the customer.

5. **Not attaining optimal performance:** The group spent a lot of time on optimising the performance during the project with several status meetings with the customer and discussions with experts, so it is *unlikely* that they will not be able to attain an optimal performance, which would have *major* consequences for the group because it would make the design less attractive for the customer.

6. **Tip-over at OEW:** Since there is a stability and control team in charge of determining the centre of gravity, they are more than aware of this risk. *Unlikely* is an adequate expression for this event since the task of the team is essentially preventing this risk from happening. Since this flaw would be discovered only in production or even in operation, it will only have a *catastrophic* consequence, since making driving design changes at that stage is very expensive.

7. **Overdesigning structure and frame:** The emphasis of this project does not fully lie in the structural design of the aircraft, but on noise and operations. This is why the group has allocated less time to the structural analysis of the aircraft, resulting in an overdesign being *probable*. This overdesign has an *moderate* impact, since more weight estimations will be done after the preliminary technical design and the problem will arise soon enough to mitigate it without major consequences.

8. **Improper material selection:** In the aerospace industry, the materials have already been optimised up until a detailed extent. Having this information available makes a wrong choice of material *unlikely*. The effect of a wrong material choice will probably be a heavier aircraft, which is a *moderate* consequence. It is common for aircraft in design phase to gain weight [32].

9. **Errors in *Python* code:** Coding is used for a large part of the technical analysis and many lines full of code were written, which, in combination with human error, makes it *very likely* that errors are present. However, the errors can be found and debugged during verification activities, so the effect is considered *marginal*.

10. **Improper assumptions:** For the technical design, such as structural, performance and aerodynamic analysis, many assumptions are made in order to come up with results in this early stage of design. By making a large amount of assumptions, it is *likely* that some might be improper. Since detailed design will be performed post-DSE, the existing designs will be revised, hence the *minor* consequence.

11. **Aircraft not sufficiently sustainable:** Sustainability is a subject that can easily be adversely affected if insufficient time is allocated to it. This implies that the aircraft is *likely* not to be sustainable enough, given the amount of time the group has to divide over all design topics. Given that sustainable development is key for most companies the consequences would be at least *major*.

12. **Noise requirement not met:** Since quantitative noise analyses are scarce, it is hard to obtain realistic numbers on the noise until real life measurements are carried out. Hence, it is *probable* that in the end the aircraft will not make the noise requirements. Since this is one of the key requirements for the project and the noise only can be measured during flight tests, not meeting the requirement can have *catastrophic* consequences for the design.

13. **Too many simplifications:** Comparable with the assumptions, a large amount of simplifications are made in order to come up with results in this early stage of design. This is why it is considered to be *likely* that too many have been made, so that no realistic result is obtained. When detailed design is performed in a later stage, the design will be revised and simplifications will be removed, yielding a *minor* consequence.

14. **Failure of composite components:** If, in the end, the aircraft is well designed, it should be *unlikely* for composite parts to fail. The reason that it is just a little more likely than metal parts, is for the fact that the visual fatigue behaviour of composites is entirely different compared to metals. Also, since metals have already been used for a long time in the history of aerospace structure, composites are fairly new and will most probably still be optimised in the future, as more research is being carried out. However, the consequence if any structural component fails is at least *major*. Depending on the part and flight phase it can even be *catastrophic*.

15. **Failure of metal components:** The failure of metal components is *very unlikely*, since regular inspection can prevent cracks from growing too large. However, just like for the composite components, a failure has at least a *major* consequence.

All the risks from table 4.1 are plotted in a risk map as can be seen in figure 4.1. From the risk map, three categories can be distinguished. Risks in the top right corner are events with high risk or threat. These are indicated in red. Risks in the middle section are events with medium risk or threat. These events are represented in yellow. The bottom left corner shows the events with the lowest risk or threat, coloured in green. This map, in combination with the risk table, helps to define the top five of highest risks, which are mitigated in section 4.2.

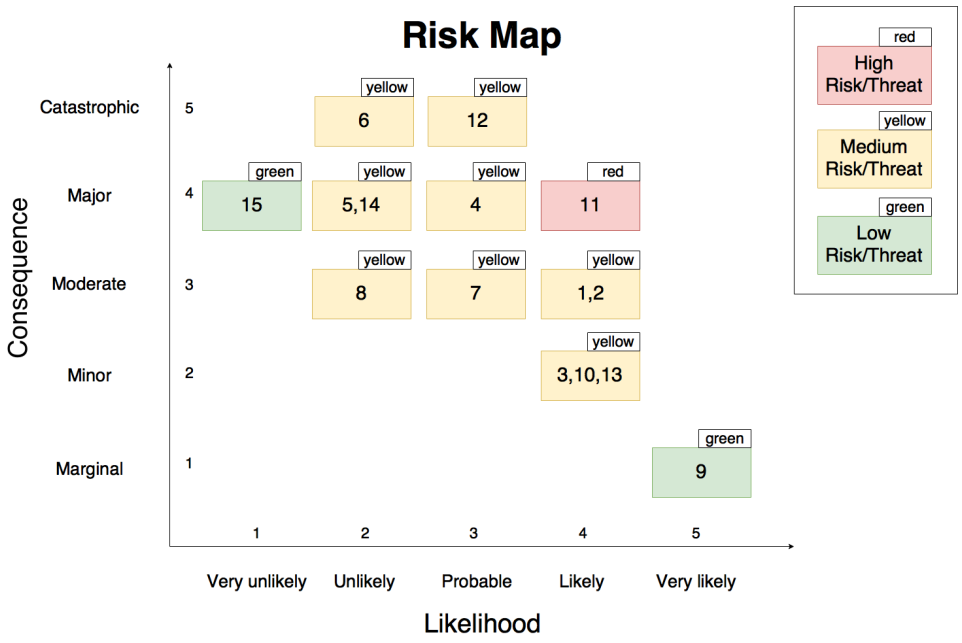

Figure 4.1: Risk map with the risks as numbered in table 4.1.

4.2 Risk Mitigation

As previously mentioned, in order to identify the most threatening risks, the likelihood grade is multiplied by the consequence grade. By doing this, risks 1, 2, 4, 11 and 12 are defined as the most threatening risks. The risk mitigation includes both the preventive actions, i.e. the actions taken to reduce the probability of occurrence, as well as severity mitigation actions, the actions that deal with limiting the consequences in case a particular event happens. In this way, the overall risks can be mitigated. The risks are mitigated as follows.

- **Risk 1: Cost increase:** Keeping in mind that cost is a driving factor throughout the design could help preventing this risk. Moreover, keeping an open and constructive dialogue with the customer in case of a budget shortage would definitely reduce the impact if it might occur as the customer has been informed already. Also, using excess engineering budget, if any, can help to cut the costs.

- **Risk 2: Unused excess engineering budget:** The group should constantly monitor that, if requirements are met and there is more room for optimisation, this extra budget is used smartly and not left unused.

- **Risk 4: Cabin noise due to wing-mounted engine:** The design team can come up with innovative solutions to mitigate the engine noise in the cabin if it turns out to be too high.
- **Risk 11: Aircraft not sufficiently sustainable:** This risk can be prevented by allocating a specific person as sustainability chief to watch over the design process and to ensure all work is performed on a sustainable basis. Mitigation measures will also be taken to deal with polluting waste products coming from production.
- **Risk 12: Noise Requirement not met:** Since the noise mitigation is based on a pure qualitative approach and information and sources are scarce, experts in the field of Aircraft Noise are visited on a regular basis. Their expertise in the field of aircraft noise can give the group a valuable extra dimension in the noise analysis and whether or not the aircraft will finally meet the noise requirements.

Now that the most threatening risks have been mitigated, a new risk map can be constructed. This risk map includes the mitigated top risks and visualises the effect of the mitigation. The risks that have undergone the mitigation all get '-1' on their grade for both likelihood and consequence. The new risk map can be seen in figure 4.2.

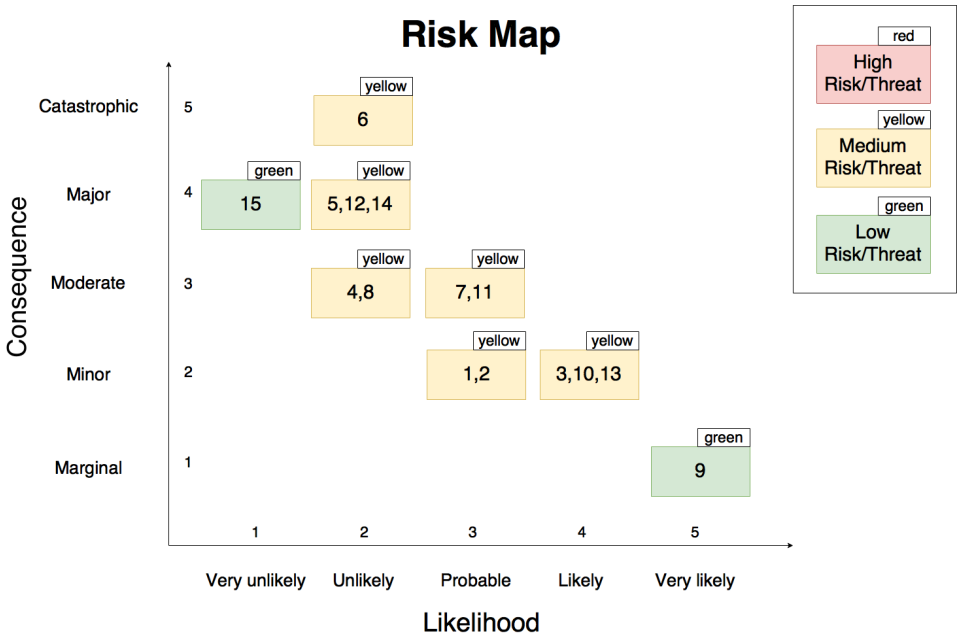

Figure 4.2: Risk map after risk mitigation, with the risks as numbered in table 4.1.

5 Concept Selection

The aircraft configuration presented and further developed in this report has resulted from an extensive design and trade-off process. First of all, the outcome of the generation process undertaken to initially identify a viable amount of concepts, as performed in the Baseline Report, is summarised in section 5.1 [29]. Consequently, the trade-off process, introduced in the Mid-term Report, and followed up by the selection of the most suited design configuration is treated in section 5.2 [31].

5.1 Initial Concept Generation

After establishing the system and subsystem requirements, aircraft configurations that would be able to meet these standards were to be found. In this phase of the design, it was key to consider every possible option. Therefore, the team brainstormed on both proven and tested, innovative and eccentric ideas. This resulted in design option trees for various aircraft components; propulsion type, engine type, engine placement, wing configuration, fuselage configuration, tail configuration and take-off and landing methods [29]. Consequently, unrealistic or clearly unfeasible options were eliminated. With all the remaining component options, sixteen combinations have been generated based on engineering sense keeping the stakeholder requirements in mind. Four aircraft have been selected to enter the more detailed design stage. This selection has been based on an elementary trade-off matrix where weight, noise, drag, maintainability, engine performance and complexity were assessed. Sketches of the four concepts are presented in figure 5.1.

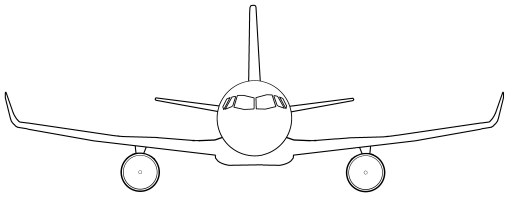

(a) Concept 1

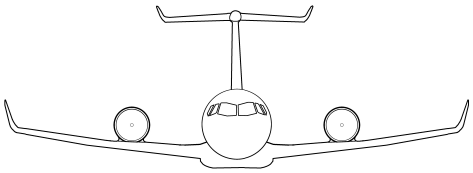

(b) Concept 2

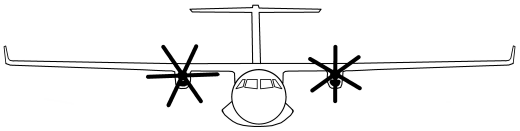

(c) Concept 3

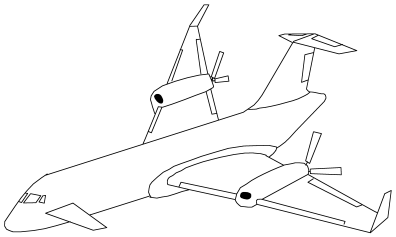

(d) Concept 4

Figure 5.1: Images of the four concepts generated in the Baseline Report [29].

Concept 1 is based on a conventional design, i.e. the SSJ100, Embraer E190 and Bombardier CS100. It has a low wing, turbofan engines under the wing and a conventional tail. The main reason why this aircraft is chosen is because the concept is proven, as it is the present day standard for regional to medium range airliners. Undoubtedly, good reasons for its popularity exist.

Concept 2 is somewhat similar to Concept 1, with a conventional fuselage and low wing. However, the engines are mounted on top of the wing as it is assumed to have a beneficial effect on noise. Moreover, improved take-off performance due to the Coandă effect is considered beneficial. Because of the possible exhaust interference, a T-tail was opted for.

Concept 3 would entail an improved version from aircraft similar to the Dash Q400 or ATR 72; a high wing propeller aircraft with a T-tail. At lower altitudes, the propellers could be more efficient than turbofan engines. Initially, the concept of hybrid propulsion was also proposed. This would be more easily implemented in a propeller configuration. However, a preliminary investigation revealed that the weight and storage penalty does not weigh up to the fuel savings. Therefore, this addition was discarded.

Concept 4 is the most innovative concept identified by the team. It incorporates a three-lifting surface, with a canard and a T-tail, with push-propellers attached on a mid-wing. This concept was based on the Piaggio Avanti. This is known as a quiet aircraft, therefore it has been decided to investigate if a scaled up version would offer the same benefits.

5.2 Final Concept Trade-off

In the Mid-term Report, the four remaining concepts have been analysed more in depth to arrive at a single concept for the final design stage [31]. As some configuration choices were not explored comprehensively, and there was still freedom in the component composition, the concepts were first 'frozen'. This has led to the merger of Concept 1 and 2. As a matter of fact, these concepts were only different in the placement of the engine, either under or on top of the wing, and a conventional or T-tail. The latter is also linked with the engine location. Therefore, the choice was made to continue with one concept that focuses on the use of a turbofan engine. Preliminary investigation showed that for noise and performance, the engine on top configuration would have significant benefits that outweighed the disadvantages. This also meant the inclusion of a T-tail. The revised Concept 1 is shown in figure 5.2.

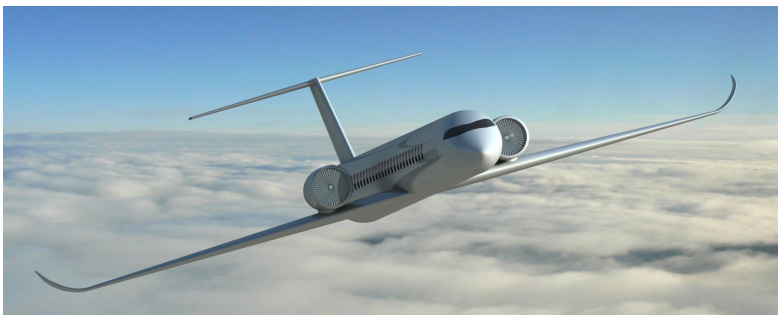

Figure 5.2: Render showing Concept 1 from the Mid-term Report.

For Concept 2, previously Concept 3, no significant design alterations were made. For noise mitigation, ducted fans were added as technological innovation. The amount of fans and propellers depends on further analysis. A rendered image is provided in figure 5.3.

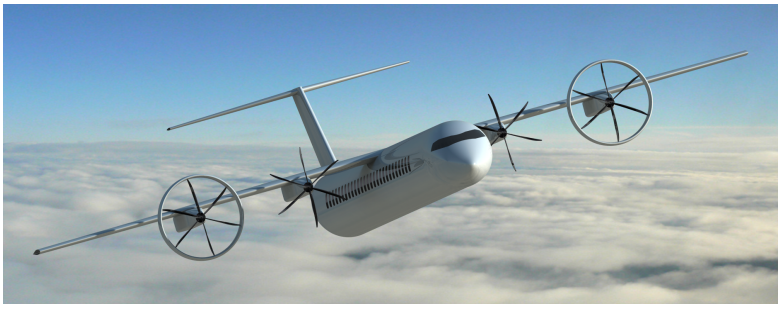

Figure 5.3: Render showing Concept 2 from the Mid-term Report.

Concept 4 is renamed to Concept 3. As with Concept 2, no large design alternations have been made. Again, ducted fans to the propellers are added with the amount depending on performance analysis. The concept incorporates three lifting surfaces, mid wing and push-propellers. The concept is presented in figure 5.4.

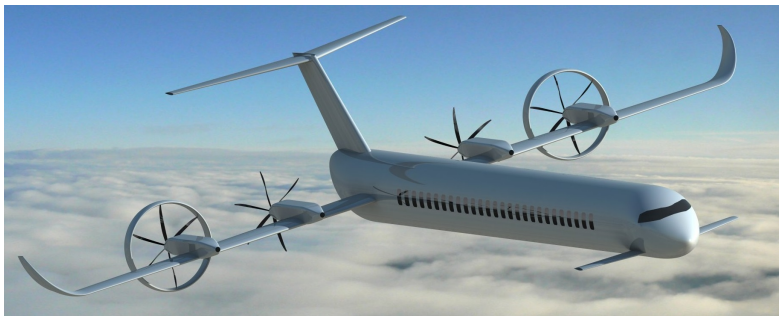

Figure 5.4: Render showing Concept 3 from the Mid-term Report.

5.2.1 Concept Evaluation

After the final concept generation, general configurations were fixed, with exception of the amount of engines, each of the three concepts was investigated extensively. Before this could be done, the design space was generated based on both jet and propeller aircraft. This determines many parameters the aircraft should comply with. A preliminary design and sizing was then performed for each concept. This included the fuselage, wing, tail, high lift devices, landing gear, engine, structures and material. Some of these characteristics were the same for all three concepts, however special attention was paid to the differences. After the preliminary sizing, a more extensive technical analysis was performed to assess and compare the three concepts. Performance, aerodynamic, structural, safety and cost characteristics were computed. This provided sufficient inputs to execute the final trade-off analysis. The three concepts were evaluated in terms of fuel efficiency, noise reduction potential, performance, technology readiness level, maintainability, versatility and unit cost. Weights were assigned to these criteria based on their relative importance. Subsequently, scores were assigned to each concept based on predefined scales as can be seen in table 5.1.

Table 5.1: Trade-off criteria, including weights.

Criteria:	**Weight:**	**0 points:**	**1 point:**	**2 points:**	**3 points:**	**4 points:**	**5 points:**
Fuel Efficiency	5	Does not meet req.	-	-	Meets req.	Exceeds req. by 7.5%	Exceeds req. by 15%
Noise Reduction Potential	4	-	Worst	-	Intermediate	-	Best
Performance	4	-	Worst	-	Intermediate	-	Best
Technology Readiness Level	3	Unfeasible	Theory	Laboratory Conditions	Prototype	Extrapolating Conditions	Existing
Maintainability	3	Impossible	Very Difficult	Difficult	Doable	Easy	Very Easy
Versatility	3	Impossible	Very Difficult	Difficult	Doable	Easy	Very Easy
Unit Cost	2	-	Worst	-	Intermediate	-	Best

5.2.2 Concept Comparison

In general, the jet aircraft configuration has superior performance characteristics. This follows from the requirements on speed and range. For a propeller aircraft, the speed of Mach 0.7 at 25,000 ft translates in a ground speed of 216 m/s, which is at the very edge of the normal operating regime. At the same time, the aircraft requires more capacity compared with reference propeller aircraft. The design was complicated by a limited choice in engines that could provide enough power. Five PW150 engines, applied at the Dash 8 Q400, would be required to meet the requirements, which is unfeasible. Therefore, a compromise was made in agreement with the customer. The amount of engines would be fixed at four and the range would be 1,500 NM as per the requirement. The ground speed was then optimised. This led to a possible maximum ground speed of 199 m/s; about 8% lower compared with the jet concept which can meet - and exceed - the speed and altitude requirement. Because the propeller aircraft could not fully satisfy the customer requirements, this has a significant impact in the trade-off score.

Also in terms of noise reduction potential, the jet aircraft design was found to be more promising compared to both propeller aircraft. This is mainly caused by recent and continuing innovation and improvements in turbofan engines with regards to noise mitigation. This development lacks behind for propeller engines. Additionally, the engine on top concept would allow for more shielding at certain measuring points. The evolution of turbofan engines also had an effect on the fuel performance and versatility score. For the former, turbofan engines are continuously getting cleaner and more fuel efficient while turboprops rely on relatively conventional technology. A coarse analysis showed that the projected fuel efficiency of the jet significantly exceeds the requirement while the margin for the propeller aircraft is noticeably smaller.

As it is expected the trend in turbofan improvements will continue, Concept 1 is more future proof in terms of applying new engine technology. Additionally, because the jet aircraft is not operating at the limit of engine capabilities, it will be easier to introduce a larger aircraft by incorporating more powerful engines. This can lead to a family of aircraft and increase in market share. This is not possible for the propeller aircraft, although smaller versions can be considered.

Maintainability is the only criterion where Concept 1 scores lower than the propeller aircraft. Because of the engine on top concept, it is more difficult to perform (line) maintenance as equipment is necessary to reach the engines. For Concept 2, the infrastructure and procedures already exist as a comparable aircraft is already in service, leading to a higher score. Concept 3 will require new maintenance procedures and mechanics training because of its unconventional nature, leading to a lower score than the other propeller aircraft.

Also, the feasibility and risk of the designs were evaluated. Concept 1 and 2 more or less exist on a smaller scale, however Concept 3 as a commercial airliner is completely revolutionary. Therefore, the three-lifting surface design entailed a significant risk in terms of technical feasibility, leading to a lower score compared with the other two configurations.

Finally, the unit cost of each concept was estimated. It was difficult to quantify cost based on a general configuration, therefore the concepts were mostly graded with respect to each other. Concept 1 scores highest because it is conventional and requires two engines. Concept 2 is conventional but requires four engines, which will most likely translate into a higher cost. Concept 3 is considered the most expensive as the innovative design and adaptions to the manufacturing process and training of workforce will entail significant investments.

5.2.3 Trade-off Result

The complete trade-off table can be consulted in table 5.2.

Table 5.2: Trade-off table.

Criteria:	**Concept 1:**		**Concept 2:**		**Concept 3:**	
	Points:	Weighted:	Points:	Weighted:	Points:	Weighted:
Fuel Efficiency	5	25	3	15	3	15
Noise Reduction Potential	5	20	3	12	3	12
Performance	5	20	3	12	3	12
Technology Readiness Level	4	12	4	12	3	9
Maintainability	3	9	4	12	3	9
Versatility	5	15	3	9	2	6
Unit Cost	5	10	3	6	1	2
Total		**111**		**78**		**65**

It can be seen that Concept 1, the jet aircraft with engines on top, is the clear winner with 111 points; 33 points more than Concept 2 and 46 points more than Concept 3. However, a sensitivity analysis was performed. The weights of the criteria was altered and criteria were excluded on at a time to make sure no single criterion would be decisive. In all cases, Concept 1 came out as the optimum design. This is expected as it scores the higher than or equal to the other concepts on 6 out of the 7 criteria. Therefore, the turbofan aircraft was unequivocally proposed for the final design stage.

6 Weight Estimation and Design Space Determination

This chapter describes one of the most integral analyses performed during the final stage of the design. The determination of the weight, on both component and gross level, is a dedicated process impacting the entire design process as will be shown in this chapter. The weight estimation itself, however, consists of only two processes; the Class I and Class II weight estimation method. The first method is described in section 6.1, the second in section 6.2. Moreover, section 6.3 describes the determination of the design space, as this has changed with respect to the previous Mid-term Report [31]. Finally, section 6.4 discusses the importance of the weight estimation and its central role within the design analysis by means of an N2-chart.

6.1 Class I Weight Estimation

The Class I method was performed earlier and has been presented in the Mid-term Report [31]. However, at that particular stage the analysis relied on rough estimates for e.g. aerodynamics and flight performance parameters. In contrast with that particular approach, the Class I estimation is now part of a more elaborate iterative process, taking into account more detailed and accurate numbers found during conducted research. The outcome of the method is nevertheless similar as it still estimates gross 'weights' of the aircraft, namely the maximum take-off mass $MTOM$, operative empty mass OEM and fuel mass FM. The estimation is based on a simple formula relating the previously mentioned gross weights, as shown in equation 6.1. Firstly, the payload P is fixed by the SRJ's nominal capacity, i.e. 110 passengers plus luggage. The average mass of a passenger including luggage is 97 kg, hence the maximum payload is 10,670 kg [33]. Secondly, to solve equation 6.1, OEM and FM should be rewritten as a function of the $MTOM$; the general idea behind the Class I weight estimation. For the operative empty weight, an empirical relation is found based on the OEM and $MTOM$ of reference aircraft. A significant amount of reference aircraft is selected to carefully set up this relation. The respective aircraft and their weights are displayed in table 6.1.

$$MTOM = OEM + P + FM \tag{6.1}$$

Table 6.1: Reference aircraft for the Class I weight estimation [34–38].

Jet:	OEM [kg]**:**	$MTOM$ [kg]**:**
Boeing 737-600	36,440	65,090
Bombardier CRJ1000	23,188	41,640
Bombardier CS100	35,221	60,781
Comac ARJ21-900	26,770	47,182
Airbus A318	39,500	68,000
Avro RJ100/BAe 146	24,993	44,225
Boeing 717-200	31,675	51,710
McDonnel Douglas MD90	39,415	70,760
Fokker 100	24,593	43,090
Sukhoi Superjet 100	24,250	45,880
Mitsubishi MRJ90	26,000	39,600
Embraer 190	24,250	45,880

A linear regression line is computed using equation 6.2. The R^2 value equals 0.9489, indicating the data points have an acceptable cohesion.

$$OEM = 0.5435 \cdot MTOM + 1640.4 \tag{6.2}$$

The final step is to determine a relation between the fuel mass FM and the maximum take-off mass $MTOM$. The fuel fractions method is therefore applied. This method assumes the mass an aircraft loses during flight is purely the result of fuel burn. By applying the fuel fraction for every flight phase, the fuel burned over the entire trip, as a ratio of the $MTOM$, is found. Hence, a mission profile is firstly constructed. The mission profile for the to be designed aircraft is displayed in figure 6.1. The profile considers both a diversion and loiter phase; safety measures that need to be implemented according to the regulations. A nominal flight, however,

would only last from phase 1 to 6 with phase 11 additionally to finalise the flight. The flight phases with their respective description and fuel fractions can be found in table 6.2. The fractions for loiter and cruise were part of the iterative process and required the cruise altitude, cruise speed, lift over drag and fuel consumption. To accurately compute these fractions, the Brequet range and endurance formulae were applied. These can be found in the Aerospace Design and Systems Engineering lecture slides [39].

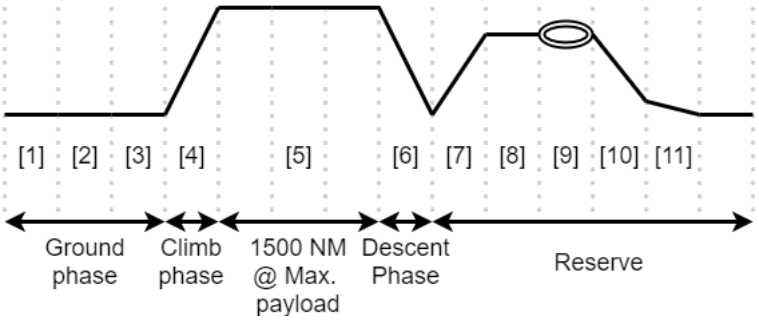

Figure 6.1: Mission profile for a commercial flight at maximum range.

Table 6.2: Fuel fractions. The numbers in the left column correspond to figure 6.1 [39]

Fuel fraction [-]:	Jet:	Flight phase description:
$W1/MTOM$	0.990	Engine start
$W2/W1$	0.995	Taxi
$W3/W2$	0.995	Take-off
$W4/W3$	0.980	Climb
$W5/W4$	0.873	Cruise
$W6/W5$	0.990	Descent
$W7/W6$	0.980	Climb
$W8/W7$	0.970	Cruise
$W9/W8$	0.983	Loiter
$W10/W9$	0.990	Descent
$W11/W10$	0.992	Landing

6.2 Class II Weight Estimation

The Class II weight estimation is the logical follow-up of the already discussed Class I weight estimation. Moreover, the outputs of the Class I weight estimation are part of the input of the more detailed Class II estimation. Furthermore, it is an intensive iterative process which will be stressed in the next section. As the previously conducted analysis computed the gross weights, OEM, $MTOM$ and FM, the method utilised in this section goes in more depth to component level. Consequently, the weights of a number of components, thirteen in total, are computed according to a method described by *Torenbeek* [40]. The respective components are the wing, fuselage, horizontal stabiliser, vertical stabiliser, high lift devices, main and nose landing gear, engines, electrical, pneumatic, and hydraulic equipment, autopilot, navigational equipment, furnishing and operational equipment, air conditioning and anti-icing and finally the auxiliary power unit (APU). The summation of all these components yields the operative empty weight of the aircraft, as shown by equation 6.3.

$$OEM = m_w + m_f + m_{hst} + m_{vst} + m_{HLD} + m_g + m_e + m_{eph} + m_{ap} + m_{nav} + m_{fur} + m_{ac} + m_{APU} \tag{6.3}$$

In alignment with the Class I estimation, this method is mostly based on statistics. However, a more significant amount of input data is required such as geometry of e.g. the wing planform and fuselage, next to the gross weights. This is because the statistical approach is not entirely similar to the Class I approach where assumptions were made on the magnitude of parameters. On the contrary, *Torenbeek* describes relations between key parameters of components and the estimated component weight. As an example, the method provides equations for estimating the wing weight as a function of the wingspan, wing thickness etc. Moreover, *Torenbeek* suggests correction factors for the use of different materials, mostly for different aluminium

alloys. Hence the outcome is deemed more reliable since it is based on empirical data. A detailed list of all input parameters can be found in the respective book [40].

6.3 Design Space

During the mid-term phase of the project, described in the Mid-term Report, the design space of the to be designed aircraft was determined [31]. However, using progressive insight from the final design stage the inputs are updated with respect to for instance aerodynamics and flight performance. This resulted in a significant increase in wing loading, whilst the thrust loading was similar to the previously found value.

6.3.1 Thrust and Wing Loading

The conditions treated remained the same, hence the design space is defined with the same analyses, as described in the Mid-term Report [31]. These cases were the following: stall, take-off, landing, cruise, climb, manoeuvring in cruise and one engine inoperative. The results are displayed in figure 6.2. The most optimal point is located as far to the bottom right as possible. However, several limiting cases have been chosen based on the feasibility of the other to be designed components. An example would be the $C_{L_{max,TO}}$, it should equal 1.8 such that the flaps design would be achievable. The final results are displayed in table 6.3.

Table 6.3: Outcome of the wing loading diagrams.

Parameter:	Value:
T/W $[N/N]$	0.30131
W/S $[N/m^2]$	5,107

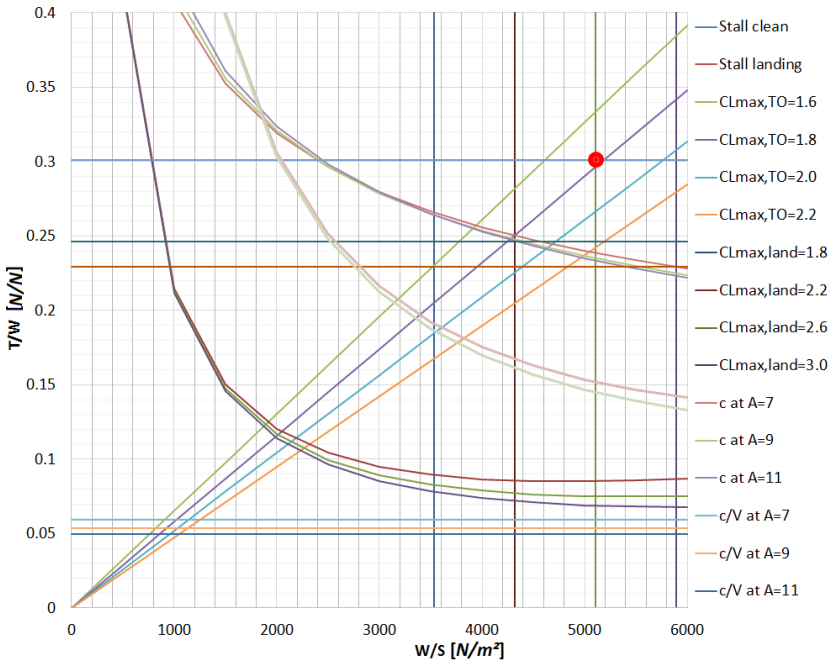

Figure 6.2: T/W vs. W/S diagram for the SRJ design. The optimal is indicated by a red dot.

6.3.2 Flight Envelope

The flight envelope or structural loading diagram illustrates the loads the aircraft shall be able to withstand at a range of equivalent air speeds, both for loads caused by manoeuvring and by wind gusts. The flight envelope is limited by either stall, manoeuvring or dive speed. The latter two are straightforwardly derived from the CS25 regulations [11]. Its main outputs, the limit load factor and dive speed, are of major importance for e.g. the structural analysis. The diagram was constructed before, but has been updated for the new design parameters during the final stage. Consequently, the approach is completely in line with the Mid-term Report [31]. The final diagram is shown in figure 6.3. It can be seen that the limit load factor is 2.5 and the dive speed V_D, which is the maximum speed indicated by the vertical line, equals 140 m/s EAS at 35,000 ft. After this line the aircraft will experience structural failure.

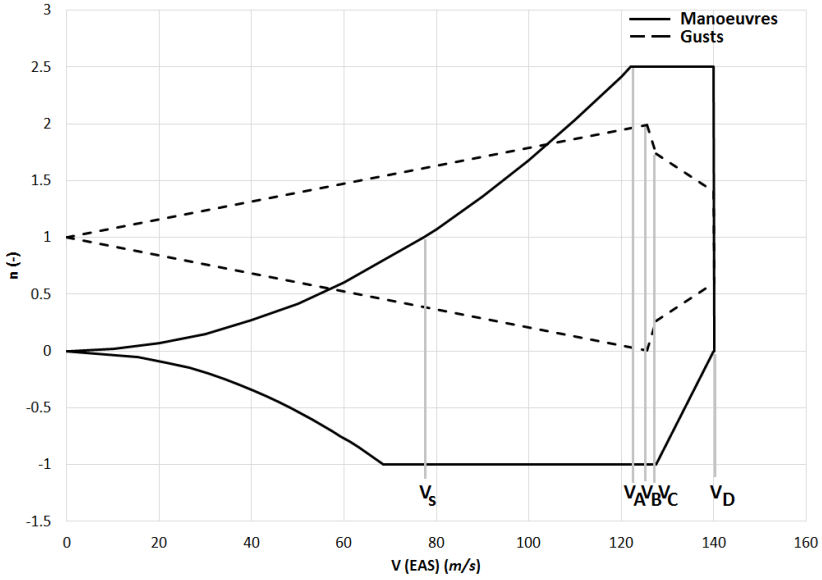

Figure 6.3: Flight envelope of the SRJ110.

6.4 Integrality, Iterations and Results

This section is dedicated to explaining the major importance of the weight estimation and the interrelations with other design processes, leading to an iterative process. Furthermore, it presents the final outcome of the Class I and Class II weight estimation methods, as the iterative process was terminated when an acceptable error of 1% was reached. Consequently, the iterations had a convergent character, so a solution existed.

The most convenient way to illustrate the importance of the weight estimation is by means of a N2-chart. A N2-chart is a two-dimensional diagram with the major processes centred on a diagonal. The existence of a diagonal indicates that different levels exist, both horizontally and vertically. Thereby the most important feature of a N2-chart is introduced. The horizontal levels represent the outputs of the central process located at the same level. On the contrary, the vertical levels indicate the inputs to the analysis located at that particular level. The N2-chart of this design stage is shown in figure 6.5 at the end of this chapter. The arrows indicate the input and output flow direction. The grey boxes, located on the diagonal, represent the design analyses.

It is obvious that the Class I weight estimation with its five input and five output blocks is paramount. The outputs however are strongly related to the inputs as by definition the Class I only determines the gross weights. As an example, the wing surface is not an output of the Class I weight estimation but with the W/S ratio found during the loading diagram analysis, it is possible to compute the wing surface S. Hence it is displayed as a Class I output. The gross weights in combination with the outcome of the initial numbers found during the loading diagrams, aerodynamic analysis, performance analysis, fuselage design and wing planform design induce the first iteration. Consequently, these five caused a chain reaction to the other processes. This loop lasted for the entire final design stage until the point that the error margin was acceptable. The more detailed description of the analyses can be found in the upcoming chapters. Next to the informative purpose the N2-chart serves, it clearly illustrates sensitivity of the design process. Obviously within every analysis sensitive parameters exist, an example for the previously discussed weight estimation would be SFC and L/D, originating from the performance and aerodynamic analysis respectively. However, the sensitivity of the general design process is also clearly depicted by this particular N2-chart. As already mentioned, the change in a single parameter causes of course an iteration with respect to the directly linked processes. In addition, these processes initiate a chain reaction of other processes that might be part of a feedback like loop. Consequently, all parameters indicated in the N2-chart are regarded as sensitive and therefore kept track off during the entire design process. The most critical cases were also identified, namely the tail arm l_H and fuselage lenght l_fus to the Class II Weight Estimation, the L/D and SFC to the Class I Weight estimation, $C_{L_{des}}$ to the aerodynamic analysis and the wing area S to the wing planform design. In conclusion, the N2-chart has been of great use during the development of the preliminary design of the SRJ.

The error margin of the weight estimation was within the discrepancy error of the utilised software, *Python*, after 53 iterations. The extensive amount of iterations guaranteed accurate results. The final gross weights are displayed in table 6.4. As defined by the Baseline Report, a contingency of 5% should be taken into account

with respect to the results that will be obtained in the final design stage [29].

Table 6.4: Gross weights.

Parameter:	Mass [kg]:
$MTOM$	45,734
OEM	26,193
FM	8,871
$MZFM$	36,863

With the gross weights and the final design in place, it is possible to run the Class II weight estimation once more to asses the weight breakdown. The mass per aircraft component is valuable to the design team to identify possible weight savings in a later stage. Moreover, it is a common way to validate the Class II weight estimation as will be done in chapter 16. The mass breakdown as a fraction of the operative empty mass is shown in figure 6.4. The mass of individual components is listed in table 6.5.

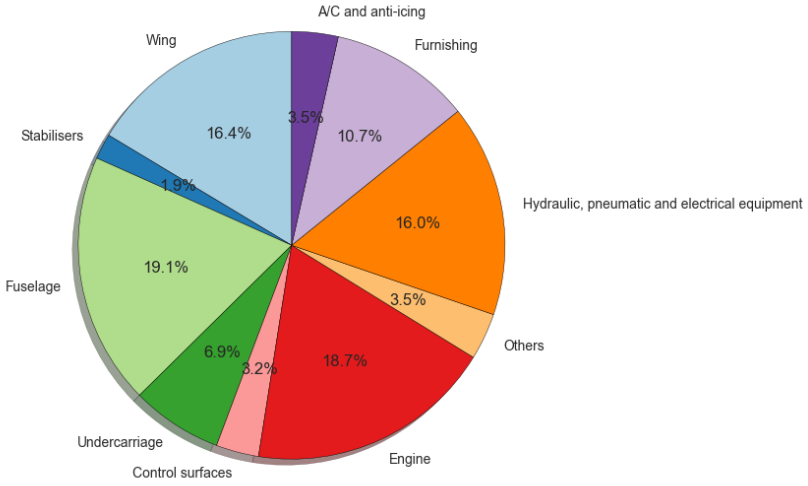

Figure 6.4: Pie chart of the mass of different components.

Table 6.5: Mass per aircraft component.

Component:	Component mass [kg]:
Wing	4,296
Stabilisers	503
Fuselage	4,991
Undercarriage	1,809
Control surfaces	849
Engines	4,900
Hydraulic, pneumatic and electrical equipment	4,201
Furnishing	2,804
A/C and anti-icing	920
Others	924

Finally, the results of the wing and thrust loading can be discussed; the thrust and wing area. The maximum thrust required is basically the most critical weight, $MTOW$, multiplied with the thrust loading originating from the thrust loading diagrams and displayed in table 6.3. This results in a thrust of 135.18 kN. The previously selected engine, the Pratt and Whitney PW1700G, still easily meets this requirement and because of its good prospected performance, 17,000 lbf or 76 kN, it remains the preferred engine to drive the SRJ110 [41]. The wing area is obtained similarly and the final result is 87.82 m^2.

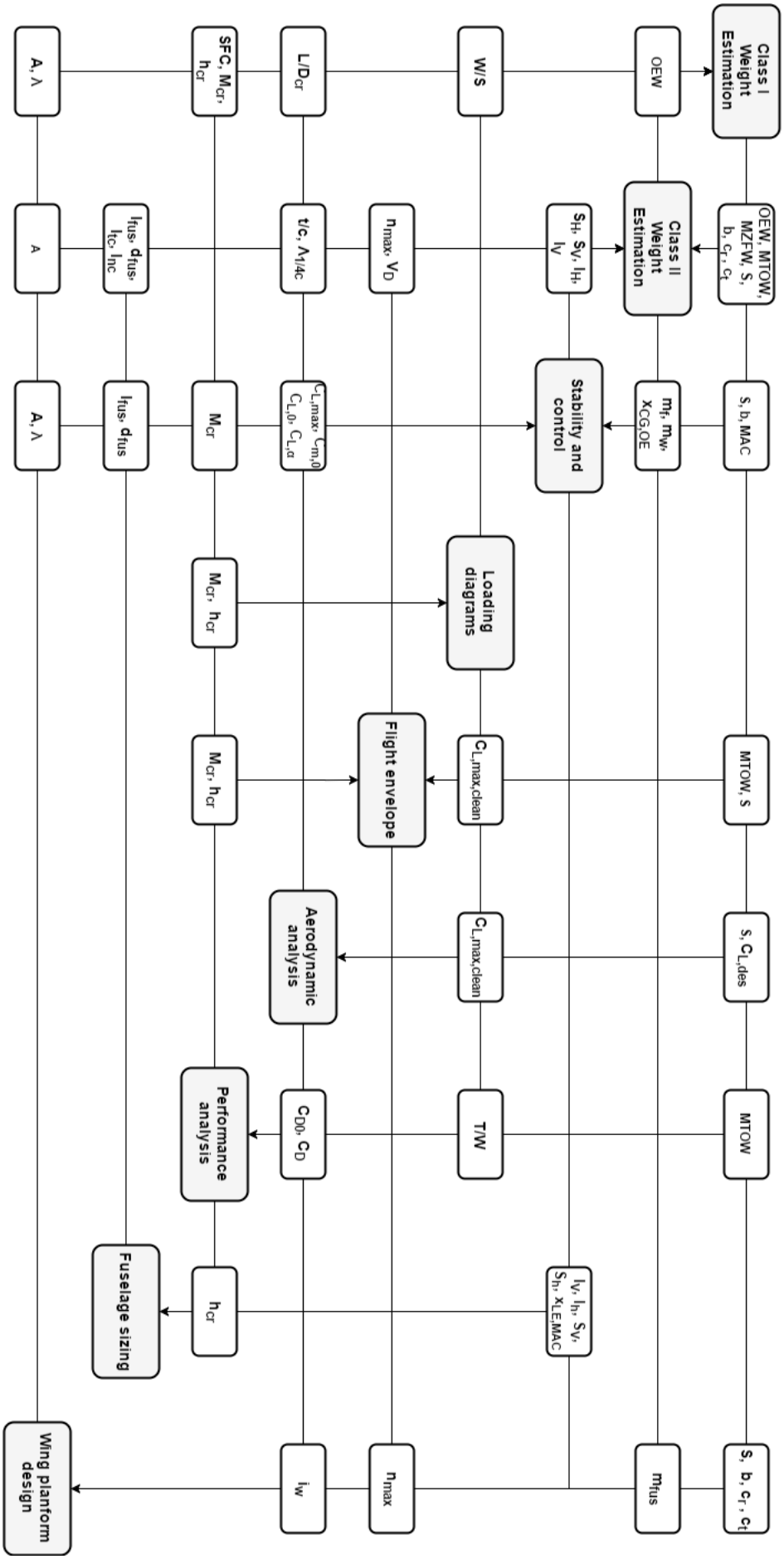

Figure 6.5: N2-chart of the performed analyses. The major processes are highlighted in grey, located on the diagonal.

7 Stability and Control Characteristics

Stability and controllability are key when designing aircraft, because it defines the aircraft behaviour whilst flying. Investigating such characteristics allows to determine important design parameters such as the wing longitudinal positioning and the horizontal tail surface area. In this chapter, the logical flow of actions undertaken to analyse the stability and control of the SRJ110 is presented. It follows the method presented in the Systems Engineering and Aerospace Design course, unless specified otherwise [32]. First, the maximum centre of gravity range during operation is identified by means of a loading diagram in section 7.2. Next, the impact of the longitudinal wing positioning on the centre of gravity location is evaluated in section 7.3. This is followed by the generation of the aircraft scissor plot in section 7.4, such that the maximum centre of gravity range can be compared to the allowable most front and aft centre of gravity location constrained by the stability and controllability of the aircraft. Subsequently, the tail surface area and the wing positioning selected from the above analysis are assessed in section 7.5. Following from the general aircraft stability, also the landing gear lateral and longitudinal position is determined in section 7.6. This is of importance for on-ground stability.

7.1 Preliminary Tail Sizing

In the Mid-term Report, a prediction of the tail sizing has been performed [31]. However, these tail dimensions mostly come from reference aircraft and do not account for the stability and controllability of the aircraft. It is therefore required to thoroughly investigate the tail sizing based on these criteria, in particular the horizontal tail surface area. Data from the preliminary analysis is summarised in table 7.1.

Table 7.1: Preliminary tail sizing of the SRJ110.

Parameter:	Value:
S_h [m^2]	23.03
S_v [m^2]	14.59
$\Lambda_{1/4c_h}$ [°]	26.5
λ_h [-]	0.36
A_h [-]	5.65
$\Lambda_{1/4c_v}$ [°]	40.25
λ_v [-]	0.72
A_v [-]	1.13

In the first instance, the tail configuration is set to be a T-tail. Investigation about the advantages and disadvantages of such a configuration with respect to a conventional tail configuration have been carried out. The conclusion is drawn that a T-tail is mostly implemented in order to avoid the engine wash in any flight conditions. In this way, in-flight vibrations are limited and deep stall is averted. However, main drawbacks of such a configuration are the increase of structural weight and the difficulties encountered during notably pre-flight inspections. Avoiding the engine wash principally drove the selection of the tail configuration for the to be designed aircraft. A T-tail is therefore selected for the SRJ110. The final tail configuration can be found in section 7.5.

7.2 Loading Diagram

The stability and control analysis of the SRJ110 is initiated by determining the maximum centre of gravity range during operation. A useful tool to highlight the centre of gravity variations caused by the loading of non-fixed items is the loading diagram. The loading diagram presented in this section is based on the weight initially derived from the Class II weight estimation performed in chapter 6. It does therefore not take into account the iterations later performed due to the design changes resulting from the Stability & Control analysis. The final tail sizing, however includes all the iterations.

In order to generate the loading diagram of the SRJ110, several parameters needed to be identified first. The weight of each component group as well as their centre of gravity is required. Following from the weight estimation performed in chapter 6, the weight components have been determined. Note that the loading

diagram has been built based on initial weight estimation. The evaluation of the centre of gravity of each component is performed either based on statistical values or basic approximations [32]. The centre of gravity of the fuselage group is assumed to be located at half the fuselage length, namely 18 m. At this stage of the analysis, the wing group is fixed at 50% of the mean aerodynamic chord. Furthermore, from reference aircraft with a similar engine configuration, the centre of gravity of the aircraft at operational empty weight is selected to be 24% of the MAC. This value is required in order to evaluate the position of the leading edge point of the wing mean aerodynamic chord, X_{LEMAC}. A X_{LEMAC} of 17.99 m is found using equation 7.1.

$$X_{LEMAC} = X_{FG} - X_{OE} + \frac{W_{WG}}{W_{FG}} \cdot (X_{WG} - X_{OE}) \tag{7.1}$$

In which X_{FG}, X_{WG} and X_{OE}, are respectively the centre of gravity of the fuselage group, the wing group and the aircraft at operational empty weight. W_{FG} and W_{WG} are the weight of the fuselage and wing group. The fuselage group includes the stabilisers, the fuselage structure and the various aircraft systems. The wing group consists of the wing structure, the undercarriage, the high lift devices and the engines mounted on top of the wings. In equation 7.1, X_{FG} and X_{LEMAC} are both expressed in the aircraft overall reference system measured from the aircraft nose, while X_{WG} and X_{OE} are expressed as a percentage of the MAC.

The mean aerodynamic chord is determined using equation 7.2.

$$MAC = \frac{2}{3} \cdot c_r \cdot \frac{1 + \lambda + \lambda^2}{1 + \lambda} \tag{7.2}$$

The next step is to determine the cargo hold volumes. From the requirements, a total cargo volume of 12 m^3 should be available for luggage storage as explained in section 14.1 [29]. Since 5 m^3 of luggage can directly be stored in the overhead bins cabin, only 1,009 kg needs to be stored in the front and rear cargo holds. From the Embraer E190 specifications, a percentage of the total cargo capacity for the front and rear cargo volume is found, respectively 54.76% and 45.24% [42]. These percentages are used as first estimates for the cargo volumes of the SRJ110, and the 1,009 kg of cargo are proportionally shared between the two holds. Other parameters assumed from the Embraer E190 are the location of the front and rear cargo hold door, respectively 9 and 23 m measured in the aircraft overall reference system [43].

Moreover, the position of the first passenger seat row measured in the aircraft overall reference system is found to be 5.7 m since the aircraft nose cone is evaluated to be 1.2 m, the cockpit section 2.5 m, the galley 0.91 m, the hallway 0.51 m and the seat pitch 0.7 m. Lastly, the fuel centre of gravity is assumed to be located at half the MAC, inside the wing.

The loading diagram particularly focuses on the centre of gravity variations due to the loading of cargo, passengers and fuel on board of the aircraft. In figure 7.1, the loading diagram of the aircraft is provided. This loading diagram has been generated when the OEM was evaluated at 25,128 kg. At the end of the Stability & Control analysis, iterations have been performed based on the updated tail parameters.

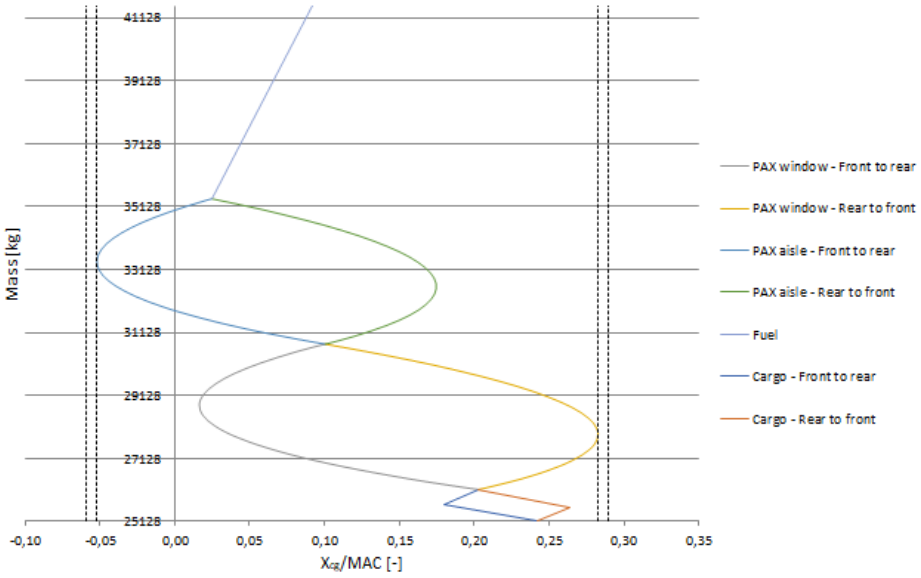

Figure 7.1: Initial loading diagram of the SRJ110.

In figure 7.1, the vertical dotted lines represent the 2% margin accounted for centre of gravity variations caused by passengers and attendants moving, landing gear retracting and food and drinks served [32].

7.3 Centre of Gravity Range

The impact of the longitudinal wing positioning with respect to the fuselage on the location of the aircraft centre of gravity is also investigated. This is achieved by varying the ratio $\frac{X_{LEMAC}}{l_{fus}}$ by 10%. In this way, an X_{LEMAC} of 14.39 m is found when the wing is shifted forward by 10% and of 21.59 m when the wing is moved 10% aft.

The next step consists of the determination of the aircraft centre of gravity at operational empty weight expressed in m in the aircraft overall reference system. This step firstly requires the moment each group component introduces with respect to the overall aircraft reference system. Summing up these moments and dividing the obtained result by the total operational empty weight leads to the value for the centre of gravity. This value is converted as a function of the MAC following equation 7.3.

$$X_{OE_{MAC}} = \frac{X_{OE_{CG}} - X_{LEMAC}}{MAC} \tag{7.3}$$

In this equation, $X_{OE_{CG}}$ is the aircraft centre of gravity at operational empty weight expressed in the aircraft overall reference system. X_{OE} is shifted backward to 0.85% of the MAC and is positioned at -0.238% of the MAC when the wing is respectively shifted 10% forward and backward. Findings are presented in table 7.2.

Table 7.2: Aircraft centre of gravity range as a function of the longitudinal wing positioning with respect to the fuselage.

Parameter:	X_{LEMAC}**:**	$X_{LEMAC+10\%}$**:**	$X_{LEMAC-10\%}$**:**
X_{LEMAC} length $[m]$	17.99	21.59	14.39
Most aft c.g. $[\%MAC]$	0.289	-0.218	0.954
Loading condition [-]	Rear to front Window PAX row 18	Rear to front Aft cargo	Rear to front Window PAX row 16
Most forward c.g. $[\%MAC]$	-0.059	-0.683	0.668
Loading condition [-]	Front to rear Aisle PAX row 16	Front to rear Aisle PAX row 16	Front to rear PAX Aisle PAX row 14
$MTOM$ c.g. $[\%MAC]$	0.113	-0.411	0.719

The values presented in table 7.2 include a 2% margin for the same reason as previously explained.

In figure 7.2, the centre of gravity range of the three different wing positioning in displayed.

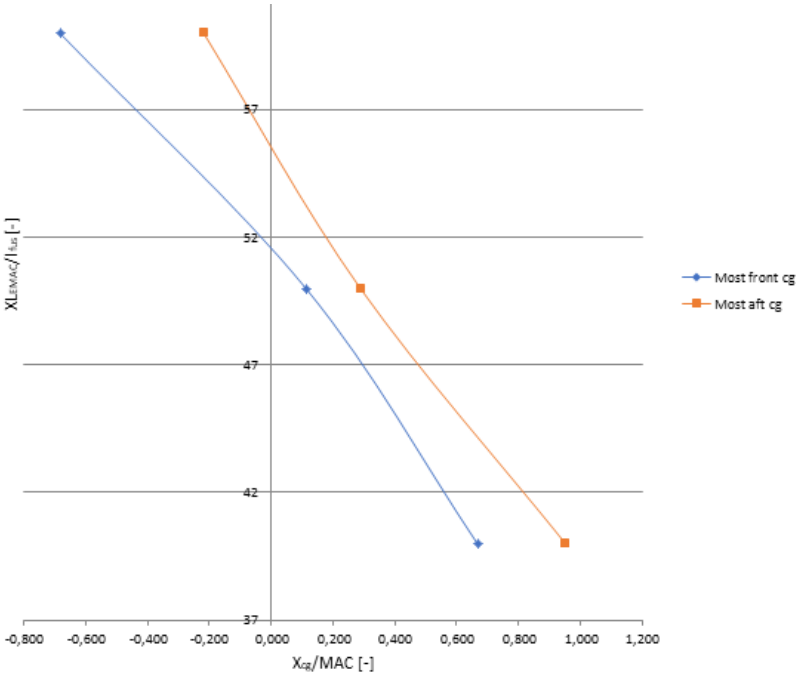

Figure 7.2: Centre of gravity range as a function of the X_{LEMAC}/l_{fus}.

This diagram has its real significance once combined with the scissor plot generated hereafter. As a matter of fact, combining these two plots allows to identify the most suitable tail surface area for the SRJ110. To do so, the curve of figure 7.2 needs to be approximated by a function. The best results were obtained when a polynomial of order to 2 was used to model the curves ($R^2 = 1$). Therefore, when the diagrams are combined, this should be taken into consideration and results should be carefully analysed.

7.4 Scissor Plot

The most aft and forward centre of gravity positions possible for a certain horizontal stabiliser surface area are constrained by the stability and controllability characteristics of the aircraft. For both stability and controllability, a critical relation can be constructed and a corresponding critical line can be plotted. Combined, the two lines result in a design space, defining the possible ranges of centre of gravity position and tail size. Determining these relationships is a complex task. A rough overview of the mathematical steps will be given in this section, as well as the resulting stability and controllability curves.

For stability, equation 7.4 holds.

$$\bar{x}_{np} = \bar{x}_{ac} + \frac{C_{L_{\alpha_h}}}{C_{L_{\alpha_{A-h}}}} \cdot \left(1 - \frac{d\epsilon}{d\alpha}\right) \cdot \frac{S_h \cdot l_h}{S \cdot \bar{c}} \cdot \left(\frac{V_h}{V}\right)^2 - SM \tag{7.4}$$

Rewriting equation 7.4, one can obtain $\frac{S_h}{S}$ as a function of $\bar{x}_{ac}$. This relation is given in equation 7.5. The stability analysis is performed in its critical situation, namely cruise. All inputs, such as lift coefficient and Mach correction will be done for the cruise condition. SM is the stability margin, and is assumed equal to 5%.

$$\frac{S_h}{S} = \frac{1}{\frac{C_{L_{\alpha_h}}}{C_{L_{\alpha_{A-h}}}} \cdot \left(1 - \frac{d\epsilon}{d\alpha}\right) \cdot \frac{l_h}{\bar{c}} \cdot \left(\frac{V_h}{V}\right)^2} \cdot \bar{x}_{cg} - \frac{\bar{x}_{ac} - 0.05}{\frac{C_{L_{\alpha_h}}}{C_{L_{\alpha_{A-h}}}} \cdot \left(1 - \frac{d\epsilon}{d\alpha}\right) \cdot \frac{l_h}{\bar{c}} \cdot \left(\frac{V_h}{V}\right)^2} \tag{7.5}$$

In equation 7.5, $\bar{x}_{np}$ and $\bar{x}_{ac}$ are the positions of the neutral point and the aerodynamic centre as a fraction of the mean aerodynamic chord. The position of aerodynamic centre, $\bar{x}_{ac}$ is a combination of wing aerodynamic centre, fuselage contribution and nacelle contribution. For a T-tail configuration, the tail/wing speed ratio V_h/V can be assumed equal to 1 [32]. $C_{L_{\alpha_h}}$, the lift slope of the horizontal tail, is determined using the *DATCOM* method given in equation 7.6.

$$C_{L_{\alpha_h}} = \frac{2 \cdot \pi \cdot A_h}{2 + \sqrt{4 + \left(\frac{A_h \cdot \beta}{\eta}\right)^2 \cdot \left(1 + \frac{\tan^2 \Lambda_{0.5 \cdot C_h}}{\beta^2}\right)}} \tag{7.6}$$

In the aforementioned equation, β is the Prandtl-Glauert Mach correction, equal to $\sqrt{1 - M^2}$.

$C_{L_{\alpha_{A-h}}}$ is the lift slope of the aircraft without the tail. It is determined using equation 7.7.

$$C_{L_{\alpha_{A-h}}} = C_{L\alpha_w} \cdot \left(1 + 2.15 \cdot \frac{b_f}{b}\right) \cdot \frac{S_{net}}{S} + \frac{\pi}{2} \cdot \frac{b_f^2}{S} \tag{7.7}$$

$\frac{d\epsilon}{d\alpha}$ is a factor accounting for downwash, determined using another formula, also following the guidelines from System Engineering and Aerospace Design [32].

All inputs are given in table 7.3. Some inputs are also outputs of the stability and control process, hence the process is iterative. For the first iteration, they were assumed from reference aircraft.

Table 7.3: Stability inputs.

Parameter:	Value:
A_h [-]	5.650
M [-]	0.772
$\Lambda_{0.5c_h}$ $[rad]$	0.407
$C_{L_{\alpha_h}}$ $[1/rad]$	5.082
$C_{L_{\alpha_{A-h}}}$ $[1/rad]$	5.745
$\frac{d\epsilon}{d\alpha}$ [-]	0.364
l_h $[m]$	11.0
$\bar{c}$ $[m]$	3.137
$\bar{x}_{ac}$ $[m]$	0.208

With the relation for stability defined, the same has to be done for the controllability. The critical equation for controllability, for $\frac{S_h}{S}$ as function of x_{cg}, is given in equation 7.8. Controllability is most critical in landing. Therefore, all inputs such as lift coefficient and Mach number are taken for the landing condition.

$$\frac{S_h}{S} = \frac{1}{\frac{C_{L_h}}{C_{L_{A-h}}} \cdot \frac{l_h}{\bar{c}} \cdot \left(\frac{V_h}{V}\right)^2} \cdot \bar{x}_{cg} - \frac{\frac{C_{m_{ac}}}{C_{L_{A-h}}} \cdot \bar{x}_{ac}}{\frac{C_{L_h}}{C_{L_{A-h}}} \cdot \frac{l_h}{\bar{c}} \cdot \left(\frac{V_h}{V}\right)^2} \tag{7.8}$$

For an adjustable horizontal tail, C_{L_h} is equal to -0.8 [32]. The moment coefficient around the aerodynamic centre is determined by adding the wing moment coefficient and the contribution to the moment by flaps, fuselage and engine nacelles, as in equation 7.9.

$$C_{m_{ac}} = C_{m_{ac_w}} + \Delta_{flaps} C_{m_{ac}} + \Delta_{fus} C_{m_{ac}} + \Delta_{nac} C_{m_{ac}} \tag{7.9}$$

In this equation:

$$C_{m_{ac_w}} = C_{m_{0_{airfoil}}} \cdot \left(\frac{A \cdot \cos\Lambda^2}{A + 2 \cdot \cos\Lambda}\right) \tag{7.10}$$

$\Delta_{nac} C_{m_{ac}}$ can be assumed to be equal to -0.05 for wing-mounted engines [32].

$$\Delta_{fus} C_{m_{ac}} = -1.8 \cdot \left(1 - \frac{2.5 \cdot b_f}{l_f}\right) \cdot \frac{\pi \cdot b_f \cdot h_f \cdot l_f}{4 \cdot S \cdot \bar{c} \cdot \frac{C_{L_0}}{C_{L_{\alpha_{A-h}}}}} \tag{7.11}$$

In equation 7.11, b_f is the fuselage width, h_f the fuselage height and l_f the length of the fuselage, as determined in section 14.1. $C_{L_{\alpha_{A-h}}}$ is calculated following equation 7.7.

The effect of flaps on the position of centre of gravity is the most complex to determine. It is found using formula 7.12.

$$\Delta C_{m_{1/4}} = \mu_2 \cdot \left(-\mu_1 \cdot \Delta C_{l_{max}} \cdot \frac{c'}{c} - \left(C_L + \Delta C_{l_{max}} \cdot \left(1 - \frac{S_{wf}}{S}\right)\right) \cdot \frac{1}{8} \cdot \frac{c'}{c} \cdot \left(\frac{c'}{c} - 1\right)\right) + 0.7 \cdot \frac{A}{1 + 2/A} \cdot \mu_3 \cdot \Delta C_{l_{max}} \cdot \tan\Lambda_{1/4} \tag{7.12}$$

μ_1, μ_2 and μ_3 are constants from empirical relationships with as input flap chord length, type of flap and deflection. $\Delta C_{l_{max}}$ is the increase in airfoil C_l generated by the flaps at landing setting. C_L in this equation is at landing. S_{wf}/S is the ratio between flapped wing area and reference area, while c'/c is the ratio between the airfoil chord with extended flap and in clean configuration. It has to be noted that equation 7.12 gives the difference in moment coefficient around one quarter of the aerodynamic chord. In order to convert, equation 7.13 is used.

$$C_{m_{1/4}} = C_{m_{ac}} + C_L \cdot \left(0.25 - \frac{x_{ac}}{\bar{c}}\right) \tag{7.13}$$

Every parameter can now be determined in order to find the controllability relation.

A table with all inputs required for equation 7.8 is given in table 7.4.

Table 7.4: Controllability inputs.

Parameter:	Value:
M [-]	0.2
$C_{m_{ac}}$ $[rad]$	-0.471
C_{L_h} $[1/rad]$	-0.8
$C_{L_{A-h}}$ $[1/rad]$	2.6
l_h $[m]$	11
$\bar{c}$ $[m]$	3.137
$\bar{x}_{ac}$ $[m]$	0.208

Filling in all values, two lines can be plotted, one for stability and one for controllability. This so called scissor plot is presented in figure 7.3.

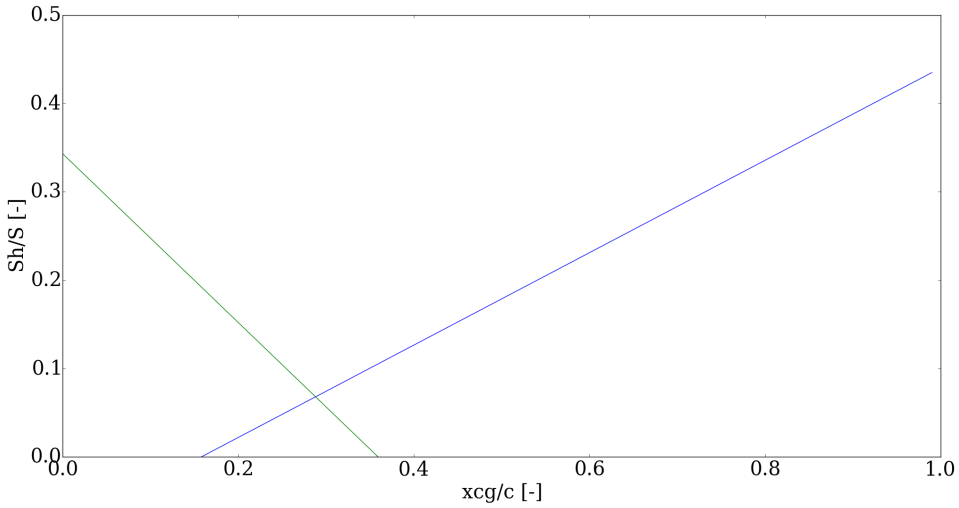

Figure 7.3: Scissor plot highlighting the stability and control of the SRJ110. The line with positive slope is the stability relation, the other one is for controllability.

7.5 Optimal Tail Sizing

By combining the centre of gravity range diagram with the scissor plot, the optimal tail surface area can be selected. Particular attention to the axis scale has been drawn when superimposing the diagrams. The horizontal axis represents in both cases the position of the centre of gravity expressed in percentage of MAC, x_{cg}/MAC, and therefore a perfect alignment of the axes has to be ensured. From figure 7.4, a value of 0.14 is found for the ratio $\frac{S_h}{S}$. The wing surface area being fixed at this stage of the design process and equal to 87.824 m^2, the horizontal tail surface area is determined to be 12.30 m^2. This value is rather small compared to reference aircraft with an horizontal stabiliser area varying between 15 and 20 m^2. However, in case of a T-tail design it is recommended to increase the obtained tail area by 20% [32]. This is done to account for deep stall resulting from the wing wake on the horizontal stabiliser especially at high angle of attack. Therefore, this results in an horizontal tail surface area of 14.75 m^2. The optimal horizontal tail size is obtained for the wing positioning such that X_{LEMAC}/l_{fus} equals 0.38. With a known aircraft length of 36 m, the position of the leading edge of the MAC is at 13.74 m.

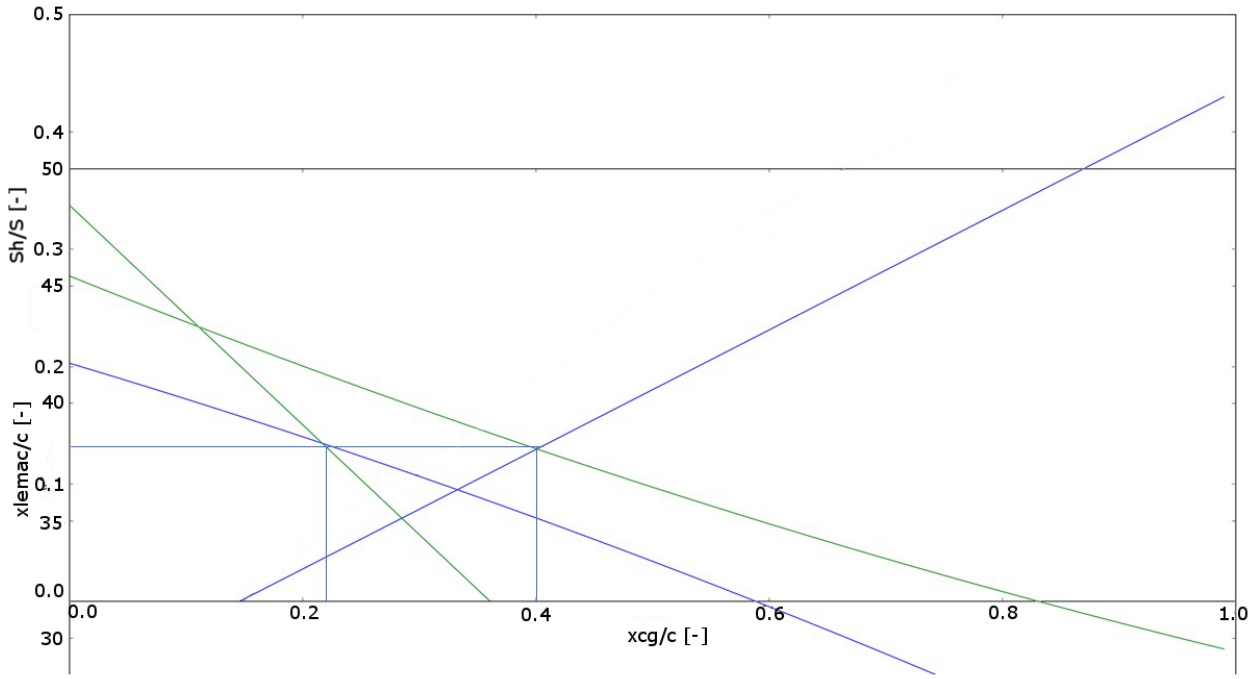

Figure 7.4: Plots matching, highlighting the optimal $\frac{S_h}{S}$ ratio, X_{LEMAC}/l_{fus} and the corresponding centre of gravity range.

Other parameters interesting to evaluate in terms of stability and control, which directly result from the tail area analysis, are the tail arms. The tail arms are defined as the distance between the mean aerodynamic quarter chord of the wing and the quarter chord of the vertical and horizontal stabilisers. In order to determine these distances, a closer look at the tail volumes of reference aircraft is required. The horizontal and vertical tail volume coefficients are defined as in equations 7.14 and 7.15.

$$V_h = \frac{S_h \cdot l_h}{S \cdot MAC} \tag{7.14}$$

$$V_v = \frac{S_v \cdot l_v}{S \cdot b} \tag{7.15}$$

It is known that aircraft with a similar tail and engine configuration have comparable tail volume coefficients. Investigation has then been carried out to determine the tail volume coefficients of previously identified reference aircraft. This task revealed to be rather difficult due to the lack of available data. Furthermore, discrepancies between the results obtained for aircraft with identical tail configuration, namely a T-tail, have been observed. This is probably due to the different propulsion technologies and the engine location. Typical values for jet transport aircraft have been found in SEAD lecture notes and online available data [32, 44]. However, the horizontal tail arm is evaluated looking at the tail volume coefficient of the Avro RJ100 since the surface area is close to the one previously obtained, namely 15.61 m^2 [34]. Using a horizontal tail volume coefficient of 0.857, an horizontal tail arm of 17.918 m is derived. For the vertical stabiliser, S_v is evaluated from reference aircraft to be 14.59 m^2. Using a value of 0.0918 for the vertical tail volume coefficient, a tail arm of 15.471 m is derived. In order to verify this result, basic trigonometric manipulations have been performed. From this, a distance of 2.5 m is found for the difference between the vertical and horizontal tail arm, which confirms the validity of the obtained results which have a difference of 2.448 m. Furthermore, the vertical tail arm is smaller than the horizontal one, which was expected prior to the analysis.

In table 7.5, updated values of the horizontal tail surface area and the tail arms are provided. The sweep at quarter chord, the taper ratio and the aspect ratio are not altered with respect to the values presented in section 7.1. It is important to keep in mind this analysis has a highly iterative character. In this section, only the final results are presented while several iterations have been performed. As a matter of fact, a change in horizontal tail surface area and tail arms length influences the weight as computed in chapter 6.

Table 7.5: Updated tail surfaces and tail arms of the SRJ110.

Parameter:	Value:
S_h $[m^2]$	14.75
l_h $[m]$	17.89
S_v $[m^2]$	14.59
l_v $[m]$	15.39
X_{LEMAC} $[m]$	13.74

In order to check the technical feasibility of the T-tail configuration selected for the SRJ110, a closer look at the horizontal and vertical tails is necessary. The location of the horizontal stabiliser with respect to the fuselage edge is dependent on the available space for the horizontal stabiliser root chord on the vertical stabiliser. If the root chord of the horizontal stabiliser is larger than the local chord of the vertical tail, the horizontal stabiliser would not fit from that point on, assuming the vertical stabiliser has a taper ratio less than 1. If this is the case, a similar configuration as the Sud Aviation Caravelle is needed. An example of this configuration is shown in figure 7.5. Assuming that both the vertical and horizontal tail are trapezoidal wings, the formula found in the Aerospace Engineering and Systems Engineering lecture slides for trapezoidal wings are applied to find the root chord and tip chord of the horizontal and vertical stabiliser, respectively [45]. The tip of the vertical stabiliser is found to be 3.00 m and the root of the horizontal stabiliser 2.34 m. Hence, the horizontal stabiliser fits at any spanwise location of the vertical stabiliser and a conventional T-tail, all the way at the tip, is chosen to minimise the effect of downwash. As a matter of fact, it is preferred to have as much fuselage clearance as possible to minimise downwash effects.

Figure 7.5: An example of the analysed stabiliser configuration, applied at the Sud Aviation Caravelle. *commons.wikimedia.org*

7.6 Landing Gear Positioning

In the Mid-term Report, a tricycle landing gear configuration was chosen after evaluation of the different options [31]. Now the general aircraft stability has been treated, and the wing location is fixed, the landing gear characteristics can be sized according to the methods from *Sadraey* [46]. This is important for stability and controllability on the ground. The wheelbase is an important parameter for the weight division on the landing gear and will be treated in subsection 7.6.1. The height of the landing gear is calculated in subsection 7.6.2, based on the required ground clearance on the ground and during rotation. The landing gear height is also an important source of aerodynamic noise, hence minimising its size is paramount. Furthermore, the wheeltrack - the distance between the main landing gear struts - is important for the lateral stability of the aircraft and handling on the ground. This will be assessed in subsection 7.6.3. To complete the sizing, the strut diameter is determined in subsection 7.6.4 followed by the final configuration in subsection 7.6.5.

7.6.1 Wheelbase

The wheelbase B is defined as the longitudinal distance between the nose and main landing gear, as shown in figure 7.6 [46]. This distance affects the static loads on each gear and can therefore be determined using moment equations. The load on the nose gear should be higher than 8% of the $MTOM$ to facilitate effective control and stability on the ground [32]. However, the load may not exceed 15% of the $MTOM$ for braking efficiency and steering characteristics.

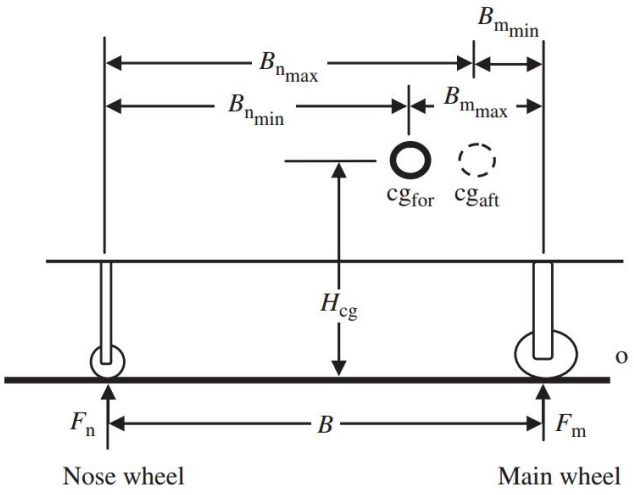

Figure 7.6: Schematic showing the different parameters for the wheelbase B.

A moment balance has been performed to comply with the target range. The position of the main gear and nose gear has been varied to yield an optimal configuration. This results in a wheelbase of 11.35 m. $B_{m_{min}}$ and $B_{m_{max}}$, as defined in figure 7.6, equal 8% and 13.4% of B, respectively. This satisfies the requirements for ground controllability where $B_{m_{min}}$ should exceed 5% and $B_{m_{max}}$ should be lower than 20% of B, according to *Sadraey* [46]. With a nose gear location at 4.7 m, it follows the main landing gear is located at 16.05 m from the nose. This gives sufficient clearance from the trailing edge and allows for storage.

7.6.2 Landing Gear Height

The engine on top configuration allows for a smaller landing gear height, which is beneficial for aerodynamic noise. Still, a sufficient clearance is required on the ground, and in particular during rotation. This is demonstrated in figure 7.7.

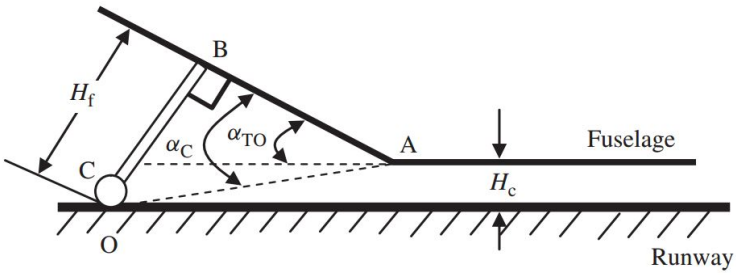

Figure 7.7: Image showing the relevant parameters for the gear height during rotation.

In order to prevent a tailstrike, $\alpha_c > \alpha_{TO}$. The clearance angle α_c follows from equation 7.16.

$$\alpha_c = \text{atan}\left(\frac{H_f}{AB}\right) \tag{7.16}$$

In this equation, H_f is the landing gear height. The length AB follows from the wing position and the onset of the 'kink' in the fuselage, 24.5 m from the nose. Hence AB equals 8.45 m. Based on a typical maximum

angle of attack at rotation α_{TO} of 10°, a main landing gear height of 1.49 m is required. The rear fuselage normally has a clearance H_c of 0.2-0.5 m during rotation [46]. In order to allow for a minimum 0.2 m margin, the total main landing gear height is calculated to be 1.7 m. Depending on the exact attachment point on the wing, additional length may have to be added to account for the vertical distance with respect to the bottom fuselage. Compared with aircraft such as the Bombardier C Series, Sukhoi Superjet and Embraer E-jets, this height is a couple decimeters shorter. For the nose landing gear, the same dimension is opted for in this stage.

7.6.3 Wheeltrack

The wheeltrack T is the lateral distance between the two main gears, as is shown in figure 7.8.

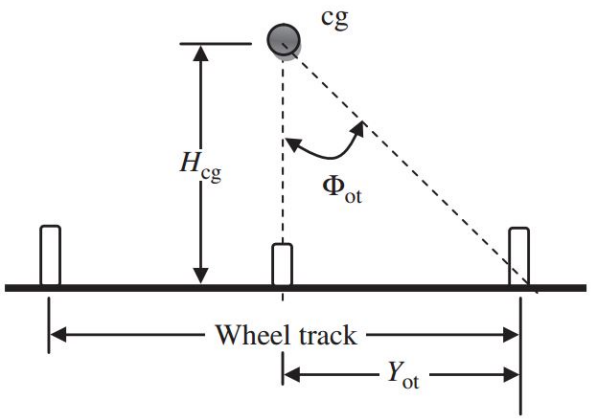

Figure 7.8: Schematic showing the wheeltrack and relevant parameters.

For the wheeltrack determination, there are three main requirements; lateral controllability and stability on the ground and structural integrity [46]. First of all, the aircraft should not roll over when making a turn. In order to satisfy this requirement, the overturn angle Φ_{ot} must not be exceeded. This angle depends on the centripetal acceleration when making a turn, and can be calculated using equation 7.17.

$$\Phi_{ot} > \text{atan}\left(\frac{V^2}{g \cdot R}\right) \tag{7.17}$$

In this equation, V is the ground speed which is assumed to be 15.4 m/s, the equivalent of 30 knots. R is the turn radius, and is taken as 18 m based on comparable aircraft [34].

It follows that Φ_{ot} equals 30.9°. This exceeds the minimum value of 25° from *Sadraey*.

Using a main landing gear height of 1.7 m as computed in section 7.6.2 and a vertical centre of gravity assumed to be in the middle of the fuselage, Y_{ot} equals 2.22 m according to equation 7.18.

$$Y_{ot} = \tan\left(\Phi_{ot}\right) \cdot H_{cg} \tag{7.18}$$

The wheeltrack T is greater than or equal to $2 \cdot Y_{ot}$, hence a value of 4.44 m follows. This is about 0.7 m outboard from the fuselage. It is also verified if this distance allows for storing of the landing gear laterally. Twice the landing gear height equals 3.4 m, giving a margin over 1 m.

7.6.4 Strut Diameter

In order to size the diameter of the landing gear strut, equation 7.19 is used [47].

$$d_s = 0.041 + 0.0025 \cdot P_m^{1/2} \tag{7.19}$$

P_m is the maximum static load on each of the main gears. This equals 51,400 N. The resulting strut diameter is 0.176 m for the main gear. The same equation has been adapted to find the required diameter for the nose gear for maximums static load. A value of 0.08 m resulted.

7.6.5 Landing Gear Configuration

Based on the landing gear height and wheeltrack determined in sections 7.6.2 and 7.6.3, respectively, the landing gear placement can be elaborated. The wheeltrack exceeds the fuselage diameter and the landing height is also large compared to the fuselage dimensions. Hence it will not be possible to embed the gear entirely in the fuselage as in for example the Piaggio Avanti. Hence a typical configuration is chosen where the gear is attached on the wing but mainly stored in the fuselage, as in for instance the Bombardier C Series shown in figure 7.9.

Figure 7.9: Image showing the landing gear configuration on the Bombardier C Series. *flickr.com*

8 Aerodynamic Analysis

The focus of this chapter is on the evaluation of the aerodynamic characteristics of the SRJ110. The aircraft component mainly driving this analysis is the wing, whose design is investigated in depth in the following chapter. However first, the airfoil selection process, as well as the selected airfoil is discussed in section 8.1. The subsequent wing configuration of the SRJ110 is provided in section 8.2. Section 8.3 investigates the winglet design to be implemented on the wing in order to enhance the aerodynamic performance of the aircraft. Once the wing configuration is fixed the aerodynamic analysis of the SRJ110 is carried out in section 8.4. High lift devices and control surfaces are sized in sections 8.5 and 8.6, respectively.

8.1 Airfoil Selection

The first step in the design of a wing is the selection of appropriate airfoils. An airfoil is the profile or cross-section of a wing. The shape of this cross-section defines for the most part the aerodynamic behaviour of the wing. Lift, drag, moment, critical Mach number are some of the many parameters defined by the chosen airfoil. For the SRJ110, not one but three airfoils will be selected, a common practice for the wing design of passenger aircraft. The reason for doing so is related with the airfoil's critical and drag divergence Mach number. When an aircraft reaches speeds in excess of about Mach 0.7, at certain locations on the airfoil airflow will reach the speed of sound because the wing accelerates the flow. This can cause shock waves over the wing surface and result in loss of lift. Loss of lift is to be avoided on parts of the wing where control surfaces are located: generally near the tip of the wing. On top of that, when lift is lost at the tip of a swept-wing aircraft, an upward moment will be created, which can be dangerous for the stability of the airplane. For these two reasons, as well as for down-wash and better lift distribution, the airfoil at the tip of the wing is generally smaller than at the root as a thinner airfoil has a higher critical and drag divergence Mach number.

The process connected to choosing the right airfoil is rather manual. First, a selection of suitable airfoils is made. Based on the requirements set by the design space and the weight estimation, the possible airfoils are analysed using *JavaFoil*. *JavaFoil* for was selected for this trade-off, as it is intuitive to use and as its result are relatively good enough for means of comparing. *JavaFoil* has its disadvantages, as will be mentioned later, but the trade-off will not be affected by them.

The first selection of possible airfoils is based on the required characteristics of the airfoil. Table 8.1 lists the relevant data from the wing and thrust loading diagrams and conceptual sizing from the Mid-term Report, as well as from the weight estimation [31].

Table 8.1: Input parameters.

Parameter:	Value:
S $[m^2]$	87.82
b $[m]$	28.00
$\Lambda_{1/4c}$ [°]	25
A [-]	8.925
W_{bc} $[kg]$	43,929
W_{ec} $[kg]$	39,609
h_{cruise} $[ft]$	35,000
M_{cruise} [-]	0.77
V_{cruise} $[m/s]$	229
$C_{L_{max}}$ [-]	1.4

As the aircraft will spend most of its operational life in the cruise phase, it is important to select an airfoil that is optimised for that condition. In order to do so, first the design lift coefficient has to be found. The design lift coefficient for the wing can be calculated using formula 8.1. The lift is assumed to be equal to 1.1 times the weight. In other words, a 10% safety margin is applied. In order to design for the optimal condition, the average between the weight at the start and at the end of cruise is taken.

$$C_{L_{des}} = \frac{1.1}{\frac{1}{2} \cdot \rho \cdot V^2} \cdot \left(\left(\frac{W}{S} \right)_{bc} + \left(\frac{W}{S} \right)_{ec} \right) \tag{8.1}$$

The resulting design lift coefficient is equal to 0.5078. This is the required coefficient for the entire wing. For the purpose of choosing an airfoil, the airfoil design lift coefficient has to be determined. This airfoil design lift coefficient - $C_{l_{des}}$ - is computed by dividing the wing design lift coefficient by the second power of the cosine of the sweep of the wing. At this point, a quarter-chord sweep of 25° was assumed, as defined in the preliminary design in the Mid-term Report [31]. The resulting lift coefficient, for which the airfoil should be optimised, is equal to 0.6181.

With $C_{l_{des}}$ known, preliminary analysis of feasible airfoils can be performed. A broad range of airfoils was taken into consideration. While NACA 4-series airfoils are omitted regarding their age and primitive design, NACA 6- and 7-series were among the airfoils investigated in this analysis. NACA 6-series airfoils are focused on creating a region with a maximised laminar flow, optimising performance. The 6-series airfoils are labelled with a number code, containing thickness, thickness location and design lift coefficient. Firstly, some parameters were varied in order to narrow down the selection. After a first analysis, a location of maximum thickness of 30% of the chord is determined to be optimal. Finally, the NACA 6-series airfoils taken into consideration for the analysis and trade-off are from the NACA 63A-6XX group. The 'XX' stands for the thickness of the airfoil, in percentage of the chord length. It is undefined here with a reason: different thicknesses - 10%, 12% and 14% - were considered. Analysing different thicknesses not only serves the purpose of directly comparing them and choosing one: as stated before, the SRJ100 requires the application of several airfoils over the length of the span. NACA 7-series is a more modern series of airfoils, further developed in order to maximise laminar flow. NACA 07-6XX, with thickness 10%, 12% and 14% were taken into the trade-off. Furthermore, NASA supercritical airfoils are considered. More specifically, NASA SC(2)-06XX series, again with thicknesses of 10%, 12% and 14%. Some of the defining outputs of the airfoils are given in table 8.2

Table 8.2: Airfoil trade-off.

Parameter:	**NACA 63A-610/12/14:**	**NACA 07-610/12/14:**	**NASA SC(2)-0610/12/14**
t/c [-]	10%/12%/14%	10%/12%/14%	10%/12%/14%
$C_{d_{cr}}$ [-]	0.00588/0.00596/0.00609	0.00715/0.00605/0.00591	0.01227/0.01368/0.01496
$C_{l_{max}}$ [-]	1.35/1.486/1.611	1.316/1.454/1.594	1.263/1.464/1.601
α_{stall} [°]	8.7/10.0/11.2	8.0/9.2/10.4	10.5/13.0/15.1
α_{cruise} [°]	0.5/0.4/0.3	-0.3/-0.4/-0.5	1.3/1.0/0.8
$C_{m_{cruise}}$ [-]	-0.118/-0.119/-0.120	-0.144/-0.146/-0.148	-0.107/-0.113/-0.119

For the selection of an airfoil the following holds: a lower drag at $C_{l_{des}}$ is preferred, a higher $C_{l_{max}}$ is better as well as a lower C_m. Overall, it is clear that the three classes of airfoils do not differ significantly. In terms of maximum lift coefficient, the NACA 6-series comes first, followed by the supercritical airfoils. The margin between the 6- and 7-series is still only 2% on average. In terms of moment coefficient, the values are similar too. While a lower moment coefficient is deemed better, it is not a defining factor in the airfoil selection. Finally, in terms of drag, from the analysis with *JavaFoil* the NACA 6- and NACA 7-series are similar. The supercritical airfoil seems to have high drag though; more than double the value of the other two. However, this value should not be taken as true. *JavaFoil* only works for low Mach numbers, as the drag it models is purely friction and pressure drag. At high Mach numbers, wave drag occurs as well which is a very dominant part of drag. Using formula 8.2 the M_{DD} is determined for a NACA-6/-7 series and supercritical airfoil.

$$M_{DD} = \frac{k_a}{\cos\Lambda} - \frac{t/c}{\cos^2\Lambda} - \frac{C_L}{10\cdot\cos^3\Lambda} \tag{8.2}$$

The technology factor k_a is the defining feature here, making the difference between the regular and the supercritical airfoils. For the 6- and 7-series, the technology factor is equal to 0.87. For supercritical, this same parameter is 0.935 [45]. From this formula, M_{DD} for the 6- and 7-series is equal to 0.7456, while it is 0.8174 for the SC(2) series. Already, it can be observed that the drag divergence Mach of the 6- and 7-series is lower than the cruise speed, which is poor. Using formulas 8.3 (if $M_{cr} \leq M_{cruise} \leq M_{DD}$) and 8.4 (if $M_{DD} < M_{cruise}$), an estimation of wave drag is made.

$$\Delta C_D = 0.002 \cdot \left(1 + 2.5 \cdot \frac{M_{DD} - M_{cruise}}{0.05}\right)^{-1} \tag{8.3}$$

$$\Delta C_D = 0.002 \cdot \left(1 + 2.5 \cdot \frac{M_{cruise} - M_{DD}}{0.05}\right)^{2.5} \tag{8.4}$$

Finally, it can be seen that the wave drag for the 6-series and 7-series NACA aifoils is equal to 0.0146, while for the supercritical airfoil, it is equal to 0.00059 only. Overall, the drag of the supercritical airfoil is significantly smaller. An expert at the aerospace faculty was consulted who strongly advised to select a supercritical airfoil.

While $C_{L_{max}}$ looks to be lower than the 1.5 defined by the design space in *JavaFoil*, the same expert mentioned *JavaFoil* consistently underestimates C_L significantly, and assured the supercritical airfoil meets the requirements. This was confirmed by the more in-depth analysis using *XFLR5*, following later in this chapter.

The NASA SC(2)-0614 airfoil was selected at the root of the wing. Around the kink, defined in the planform design in section 14.2, the SC(2)-0612 is used. Towards the tip, the airfoil gets smaller until it reaches the SC(2)-0610 airfoil. The airfoils are shown in figure 8.1.

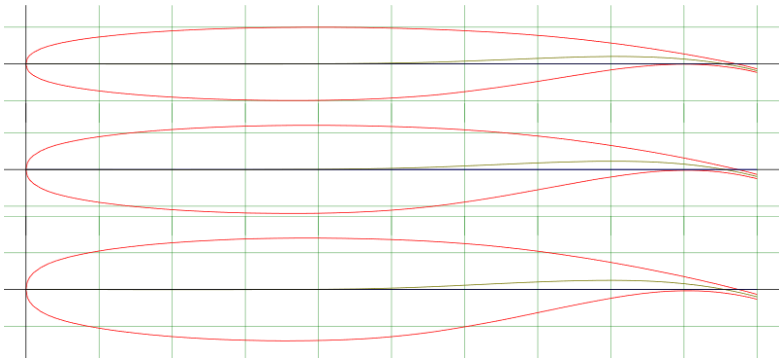

Figure 8.1: Visualisation of the three selected airfoils. The top airfoil is at the tip, the bottom at the root.

8.2 Wing Design

Based on the analysis performed in chapter 6, the value of W/S has been revised. In the Mid-term Report, W/S was estimated to be 4,109 [31]. A new value of 5,107 has been found and is considered from now on. Consequences of this design change are numerous, in particular on the aircraft performance and the wing design. The wing surface area and the wingspan have been updated as already seen in table 8.1. The wing surface area is now evaluated to be 87.82 m^2. Solving equation 8.5, a wingspan of 28 m follows. On the other hand, the aspect ratio remains unchanged.

$$b = \sqrt{A \cdot S} \tag{8.5}$$

Evaluation of the other wing parameters follows the same method as the one presented in the Mid-term Report [31]. These notably include the wing sweep, the taper ratio, the root and the tip chord.

From reference aircraft, a quarter chord sweep of 25° has been assumed for the current wing design. The validity of this value has been checked using equation 8.6.

$$M_{des} \cdot \cos(\Lambda) \leq M_{cr} \tag{8.6}$$

M_{des} is the Mach number for which the SRJ110 is designed; 0.77 at an altitude of 35,000 ft 10.1. M_{cr} is the critical Mach number of the aircraft and has been evaluated in the performance analysis to be 0.71. Solving equation 8.6, a minimum sweep of 23.23° is required in order to avoid the formation of sonic flow pockets on the wing surface [45]. Therefore, the previously assumed 25° sweep is still acceptable for the wing design of the SRJ110.

Using equation 8.7, the sweep at any chordwise location can be derived [45].

$$\tan\left(\Lambda_{x/c}\right) = \tan\left(\Lambda_{LE}\right) - \frac{x}{c} \cdot \frac{2 \cdot c_r}{b} \cdot \left(1 - \lambda\right) \tag{8.7}$$

Using a value of 0.25 for the taper ratio as fixed in the Mid-term Report, a leading edge and a half chord sweep of 28.08 and 21.76° have been found, respectively.

The next step determines the root chord and tip chord of the wing. Computing equation 8.8 with the appropriate inputs and manipulating equation 8.9, a root chord and tip chord of 5.02 and 1.25 m are derived.

$$c_r = \frac{2 \cdot b}{A \cdot (1+\lambda)} \tag{8.8}$$

$$\lambda = \frac{c_r}{c_t} \tag{8.9}$$

Another wing parameter to evaluate is the mean aerodynamic chord. As a matter of fact, the MAC is an important reference length often used in Aerodynamic, Stability and Control and Structural analyses. The value of MAC can be determined using equation 8.10, while its lateral position measured from the aircraft centre line is found from equation 8.11.

$$MAC = \frac{2 \cdot c_r}{3} \cdot \frac{\lambda^2 + \lambda + 1}{\lambda + 1} \tag{8.10}$$

$$\bar{Y} = \frac{b}{6} \cdot \frac{1 + 2 \cdot \lambda}{1 + \lambda} \tag{8.11}$$

Solving the above two equations, a MAC of 3.513 m is found, located at 5.6 m from the aircraft centre line.

The orientation of the wing with respect to the fuselage can now be determined. This is defined by two main parameters, namely the dihedral angle and the incidence angle. A positive dihedral angle is used to enhance lateral stability, emphasising the effect of the sweep angle on the overall stability of the aircraft as mentioned in the Mid-term Report. For a low wing aircraft configuration with a quarter-chord sweep less than 30°, a dihedral of 3° is found to be optimal [39].

The incidence angle of a wing is the angle between the wing chord and the fuselage axis. In other words, if the fuselage has an angle of attack of zero degrees, the angle of attack of the wing will be equal to its incidence angle. Aircraft wings have an incidence angle in order to make it fly at its cruise lift coefficient without having to angle the fuselage. An angled fuselage generates more drag, as the frontal area that is exposed to the air flow is larger. On top of that, an angled fuselage is to be avoided in passenger aircraft for purely practical reasons: an angled cabin is less convenient for passengers and in particular a sloped aisle might be problematic for cabin crew and their carts. In reality, the incidence angle might not be designed for a completely level fuselage at cruise conditions as angling the fuselage contributes positively to the fuselage lift. There is an optimum between having a small advantage of the fuselage lift and a not too large disadvantage of increased drag. Because accurately modelling the contribution of the fuselage to the lift is beyond the scope of this project, the incidence angle is designed for a minimum fuselage drag; so in order to make the wing generate lift needed at the average cruise condition while keeping the fuselage levelled. This is done by using the results of the full wing analysis later presented in section 8.4.1. From the outputs of that section, the angle of attack at cruise is determined to be 2.5°. Therefore, the incidence angle of the wing is taken equal to 2.5°.

The final design consideration concerns the wing planform design of the SRJ110. Initially, the wing planform has been assumed trapezoidal, with constant leading edge and trailing edge sweep. However, studies have proven evidence that modifying the wing planform, keeping the above wing parameters constant, results in enhanced aerodynamic and structural characteristics [48]. One of the advantages of modifying the trailing edge sweep near the fuselage is the improved flap effectiveness. As expected, the flap efficiency is proportional to the cosine of the hinge line sweep. Furthermore, a cranked trailing edge section next to the fuselage positively modifies the lift distribution around the wing surface by moving the centre of lift closer to the centre line of the aircraft. The consequence is the approximation of an elliptical lift distribution around the wing surface, which results in a lighter wing structure. Moreover, the root chord is increased allowing the implementation of higher spars. Since the airfoil remains unchanged, the thickness-to-chord ratio is constant. Higher spars are more efficient which results in a more lightweight structure. The last consideration with respect to the design of a straight trailing edge section consists of the storage of the landing gear and the engine placement. As preliminary estimate, the straight trailing edge section length is defined to be 35% of the semi-wingspan. The root chord is increased by 25%. Using simple trigonometric functions and knowing the trailing edge sweep to be 14.82 °, the added surface area equals 2.975 m^2. Since the total wing surface area remains unchanged, the removed area near the airfoil tip also equals 2.975 m^2. The updated wing planform is presented in figure 8.2.

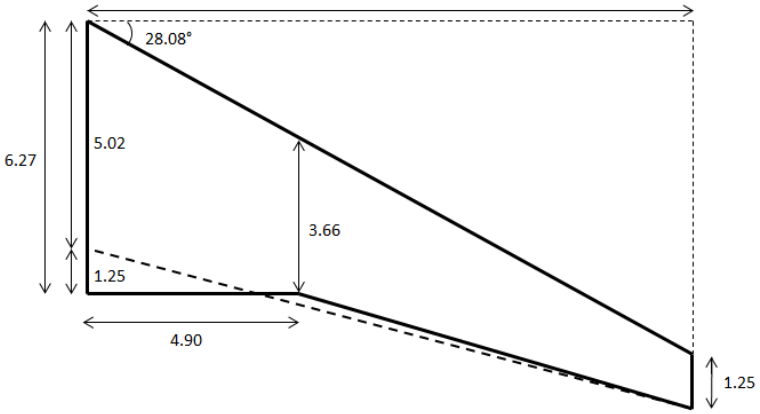

Figure 8.2: Wing planform of the SRJ110. Dimensions are expressed in m.

In this case, the length of the straight trailing edge segment is such that storage of the landing gear is ensured. The landing gear configuration has been investigated in section 7.6, and a longitudinal margin of 1 m from the landing gear position and the wing trailing edge is obtained. This allows the landing gear retraction mechanism to function and to be stored properly. Furthermore, the planform design is important for the lateral placement of the engine, as further treated in subsection 13.2.4. As a matter of fact, part of the wing can be used to shield radiating engine noise, however the sound levels in the cabin must be considered as well, as explained in subsection 13.2.3.

In addition to the undercarriage and engine position, a close look at the to be implemented flaps on this section of the wing is primordial. This is elaborated on in section 8.5.

Finally, the wing parameters previously derived are presented in table 8.3. The wing configuration is now fixed and the clean wing design of the SRJ110 concluded.

Table 8.3: Wing parameters of the SRJ110.

Parameter:	**Value:**
Aspect ratio A [-]	8.925
Wing surface area S [m^2]	87.82
Wingspan b [m]	28.00
Leading edge sweep angle Λ_{LE} [°]	28.08
Quarter chord sweep angle $\Lambda_{1/4c}$ [°]	25
Half chord sweep angle $\Lambda_{1/2c}$ [°]	21.76
Taper ratio λ [-]	0.25
Root chord c_r [m]	6.27
Tip chord c_t [m]	1.25
Average thickness-to-chord ratio t/c [-]	0.12
Dihedral Γ [°]	3
Mean aerodynamic chord MAC [m]	3.51
Spanwise location of the MAC $\bar{Y}$ [m]	5.60
Airfoil lift design coefficient $C_{l_{des}}$ [-]	0.6182
Wing lift design coefficient $C_{L_{des}}$ [-]	0.5078
Wing incidence angle i_w [°]	2.5
Airfoil	SC(2)-0610/12/14

8.3 Wing Tip Design

The main idea behind the design of winglets is to reduce the induced drag generated by the wings. This is achieved by deflecting the air flowing around the wing surfaces. Being able to quantify the drag reduction is important for the customer since this can result in additional payload or enhanced take-off performance with respect to the original aircraft configuration. The range can also be increased and the fuel efficiency is enhanced.

However, prior to investigating the most suitable design solution for the wing tips of the SRJ110, a clear understanding of the air flow behaviour around the wing tips is required. Resulting from the difference in

flow velocities on the upper and lower surface of the wings, wing vortices are induced at the tips. This phenomenon affects the lift distribution of the wing and therefore, directly influences the induced drag which is proportional to the lift around the wing. As can be seen in equation 8.12, the induced drag coefficient mainly depends on the wing lift coefficient, the aspect ratio and the Oswald efficiency factor. Also, the induced drag decreases as the airspeed increases. Therefore, the most critical situation in terms of drag generation occurs during landing and take-off.

$$C_{D_i} = \frac{C_L^2}{\pi \cdot A \cdot e} \tag{8.12}$$

By adding winglets to the wing, the effective aspect ratio is increased, while the wingspan remains unchanged. As a result, the wing surface area is also altered. Increasing the effective aspect ratio of the wing results in a reduced amount of induced drag as illustrated by equation 8.12. The impact on the effective aspect ratio and the effective wing surface area due to the implementation of winglets to the SRJ110 wing design is discussed at the end of this section when the winglet dimensions are fixed.

Another way to reduce the lift induced drag could be by extending the wing tip. However, this also induces parasitic drag. Furthermore, increasing the wingspan has structural drawbacks and ground handling limitations. Optimisation of the winglet design and selection of the most suited geometry is therefore crucial in order to lower the drag, and therefore the fuel consumption and pollutant emissions.

In figure 8.3, possible design solutions for the wing tip devices of the SRJ110 are presented [49]. Investigation of their respective advantages and disadvantages has been carried out and the main characteristics are provided hereafter. Discussion about their feasibility for the design of the SRJ110 wing tips is also undertaken.

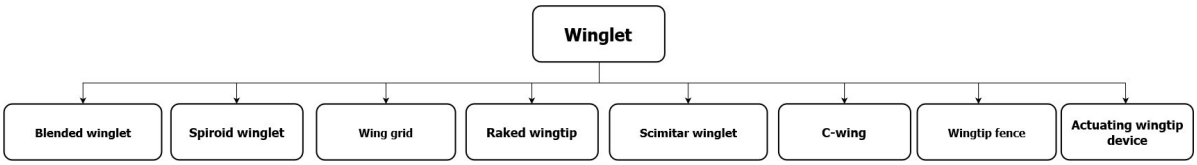

Figure 8.3: Design option tree for the wing tip devices of the SRJ110.

- Blended winglet: This is a type of winglet characterised by a smooth intersection between the wing and the winglet. This setup provides a solution for the interference drag experienced between the wing surface and the winglet at the connection location. In comparison with the wing tip extension, the bending moment is lower which is beneficial for the wing structure [50]. Less stiffening components are required to ensure the structural integrity of the wing, and therefore the wing weight is more or less kept constant with respect to the original wing configuration.

- Spiroid winglet: The spiroid winglet is a closed curved shape device positioned at the tip of the wing. As the other winglets, its main function is to reduce the induced drag by dispersing the tip vortices. This winglet configuration however introduces structural challenges.

- Wing-grid: Compared to the wingspan extension, the induced drag reduction achieved with a wing-grid is larger.

- Raked wing tip: This wing tip is installed on the B787, among others. It is characterised by a larger leading sweep angle near the tip of the wing. It is claimed to have better fuel efficiency than regular winglets [51]. Furthermore, the drag reduction is also more significant. Drawbacks are the sligthly decreased lift and the larger bending force affecting the wing structural design.

- Scimitar winglet, C-wing and wingtip fence: These wing tip devices display a more complicated configuration. For this particular reason, these design solutions are discarded for the winglet design of the SRJ110.

- Actuating wing tip devices: These devices allows the wing tip configuration to be modified during the flight such that optimal configurations can be achieved at any time, minimising the maximum bending moment at the wing root [52]. As a matter of fact, the other wing tip devices are only designed for one specific flight condition. However, this design is still under investigation and has not yet been implemented to any aircraft. This has therefore been judged unfeasible for the SRJ110.

The design of the winglet has to be carefully executed since the skin friction is likely to increase by adding excrescence to the wing design. A compromise therefore needs to be made between the induced drag reduction and the increase of friction drag. Moreover, a trade-off between weight addition and drag reduction needs to be kept in mind as will be explained later. Using the guidelines provided by *Raymer*, the winglet design of the SRJ110 has been fixed [53]. The design procedure introduced in *Raymer* is based on the original winglet developed by *Whitcomb*. This winglet consists of an upper and lower panel. However, it has been demonstrated that the winglet bottom part does not considerably contribute to the drag reduction. Therefore, this design characteristic has been left out to design the SRJ110.

The winglet design of the SRJ110 is an harmonious combination of a raked wing tip and a blended winglet. For illustrative purposes, picture of the the raked wing tip of the Boeing 787-10 and the blended winglet of the Mitsubishi MRJ90 are provided in figures 8.4a and 8.4b respectively.

(a) Raked wing tip of the B787-10.

(b) Blended winglet of the MRJ90.

Figure 8.4: Example of a raked wing tip and blended winglet configuration implemented on current aircraft.

This hybrid design is expected to lead to great aerodynamic efficiency. Although different from the classical configuration, guidelines from *Raymer* have been followed. Hereafter, the procedure undertaken to design the winglets of the SRJ110 and the reasoning of the specific design choices are discussed.

- It is assumed that the winglet starts at the location of maximum thickness of the wing tip, namely at 38.38% of the tip chord as found when analysing the tip airfoil of the SRJ110. It is mainly for this reason that a raked wing tip has been chosen. A change of leading edge sweep of 20° has been taken into account, leading to a trailing edge sweep at the wing tip of 68.08%.

- The sweep of the winglet approximates the sweep of the wing, namely 28.08°. Increasing the sweep lowers the winglet height which decreases the drag reduction as explained in the next paragraph. Lowering the sweep has also been considered. However, the drag reduction achieved with a sweep of 28.08° already leads to a drag reduction of 3.25%. Realistic values vary between 3 and 5% as found in literature [49]. The sweep of the winglet is then set equal to the sweep of the wing.

- The winglet height should not be lower than the tip chord length, namely 1.25 m. As a matter of fact, increasing the winglet height is more beneficial since the drag reduction is proportional to the winglet height. As previously explained, the winglet sweep, height and drag reduction are linked and a height of 1.431 m is found for a sweep angle of 28.08°. Using equation 8.22 later introduced in section 8.4.2, an effective aspect ratio of 9.8 is derived, resulting in an effective wing surface area of 80.46 m^2, when the wingspan is kept constant.

- A taper ratio of 0.327 is selected from *Raymer*.

- The winglet camber should be at least equals to the wing camber, namely 1.13% of the tip chord.

- It is recommended to have a 4° leading-edge-out incidence angle to increase the magnitude of the forward lift component.

- A typical thickness-to-chord ratio for a winglet is 8%.

- The sideway inclination of the winglet is assumed to be 15%. As a matter of fact, the more vertical the winglet with respect to the wing planform, the more effective it is. In contradiction with the illustration presented in figure 8.5, the winglet is blended which means that the intersection between the wing tip and the winglet is smoother and curved. Another subsidiary character of the winglet vertical inclination - often appreciated by the operator - is the visibility of the winglet for advertising and marketing purposes if needed.

The final winglet design is presented in figure 8.5.

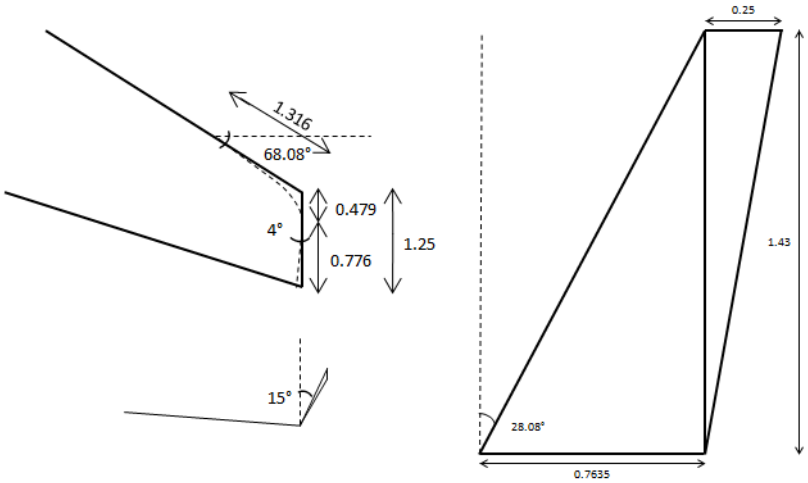

Figure 8.5: Top, front and side view of the wing tip final design of the SRJ110. Dimensions are expressed in m.

Next to the aerodynamic advantages the winglets provide, drawbacks need to be taken into consideration. The most important one is the weight increase resulting from the implementation of winglets on the wing. A first estimate for the weight of the winglets of the SRJ110 is 136 kg [54]. This small weight increase has been neglected in the Stability & Control analysis, however, influencing the centre of gravity location. Winglets also reduce the manoeuvrability of the aircraft to a certain extent and structure stiffening might be required to ensure the structural integrity of the wing in any circumstances.

8.4 Aerodynamic Characteristics Estimate

This section elaborates on the aerodynamic model used to analyse the wing performance of the SRJ110. This analysis is presented in subsection 8.4.1. Furthermore, a detailed drag breakdown of the SRJ110 is provided in subsection 8.4.2.

8.4.1 Full Wing Analysis

With the airfoil and the planform fixed, the entire wing can be modelled and analysed. Bases on advice from an expert in the field of wing design, *XFLR5* was chosen for this purpose. Using the wing dimensions determined in section 8.2, the wing planform can be modelled in *XFLR5*. NASA SC(2)-0610/-12/-14 airfoils were defined at tip, kink and wing root, respectively. The visual representation of the wing in *XFLR5* is presented in figure 8.6.

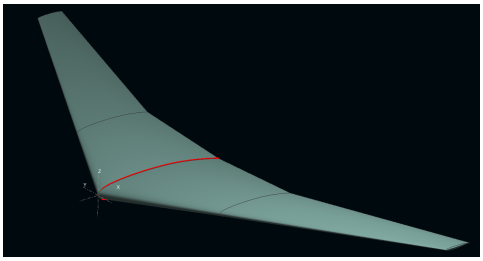

Figure 8.6: Wing visualisation from *XFLR5*.

Firstly, the 2D characteristics of all three airfoils are determined for a range of angles of attack and Reynolds numbers. Figure 8.7 provides the C_{l_α} plot for the middle airfoil, the SC(2)-0612, at a Reynolds number of sixteen million and a speed of approximately Mach 0.2.

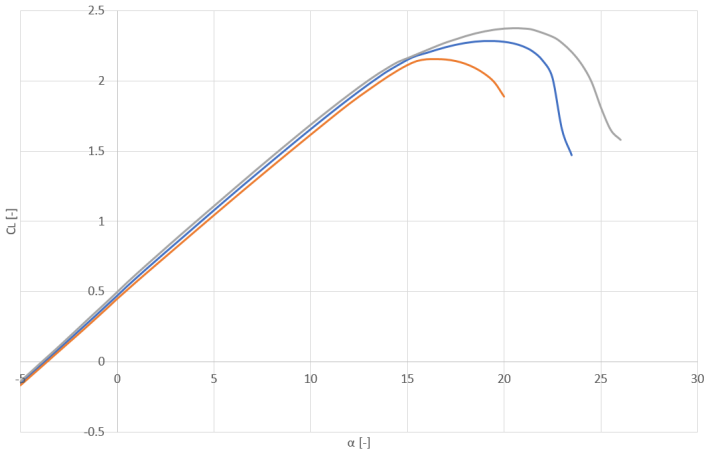

Figure 8.7: C_{l_α} curve for SC(2)-0612 airfoil at Re = 16,000,000.

It is clear that the results coming from *XFOIL* - the tool *XFLR5* uses for 2D analysis - in figure 8.7 differs significantly from the results that were previously found using *JavaFoil*. This observation was predicted, following the comment of a faculty expert, as mentioned earlier. *XFLR5* and *XFOIL* are good models, and while *JavaFoil* is easier to use for the purpose of selecting an airfoil for example, *XFLR5* offers a more detailed quantitative analysis. Some important parameters are given in table 8.4.

Table 8.4: SC(2)-06XX characteristics.

Parameter:	**SC(2)-0610**	**SC(2)-0612**	**SC(2)-0614**
$C_{d_{cruise}}$ [-]	0.00619	0.00633	0.00665
$C_{l_{max}}$ [-]	2.155	2.2825	2.3773
C_{l_α} [1/°]	0.1193	0.1208	0.1221
α_{stall} [°]	16.5	19	20.5
α_{cruise} [°]	1.5	1	1
$C_{m_{cruise}}$ [-]	-0.112	-0.1183	-0.1247
C_{l_0} [-]	0.4473	0.4721	0.499

After performing all the airfoil analyses and the planform definition, the entire planform can be analysed. The full wing geometry was modelled using the programme, as previously described and as illustrated in figure 8.6.

The 3D analysis was performed at a speed of 100 m/s - approximately Mach 0.3 at sea level. *XFLR5* is unable to accurately model at higher Mach numbers. For the lift, this can be considered as a conservative estimate, as lift increases with Mach number. The drag from the model does not account for wave drag. For this reason, a more detailed drag estimation following book methods is given in subsection 8.4.2. For the *XFLR5* analysis, the 3D panel method was selected, as it is an accurate method to model aerodynamics of complex three dimensional shapes.

The analysis outputs rough data in the form of numbers in a text file. After refining using *Excel*, relations such as C_L-α, a C_L-C_D, a C_m-α and a C_L/C_D-α curves can be found and plotted.

A graphic representation for lift coefficient in function of angle of attack is given in figure 8.8.

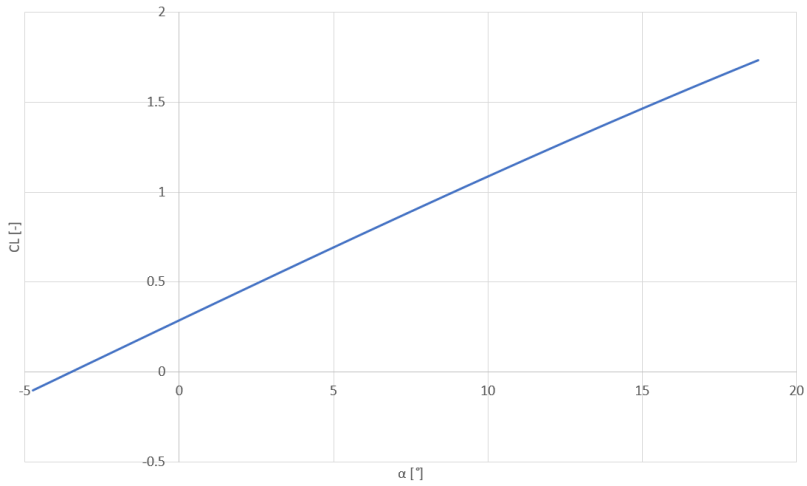

Figure 8.8: C_{L_α} curve for the entire wing planform.

XFLR5 is not good at modelling the behaviour of the airfoil close to stall. Instead of creating the round peak that can be seen in the 2D graphs, the lift coefficient keeps increasing linearly until stall. This was verified and accepted as normal. The resulting maximum wing lift coefficient in clean configuration is equal to 1.7316. It is reached at an angle of 18.75°. The lift slope, C_{L_α} is equal to 0.0784/° or $4.4920/rad$.

In figure 8.9, the lift-over-drag polar is plotted as function of the lift coefficient.

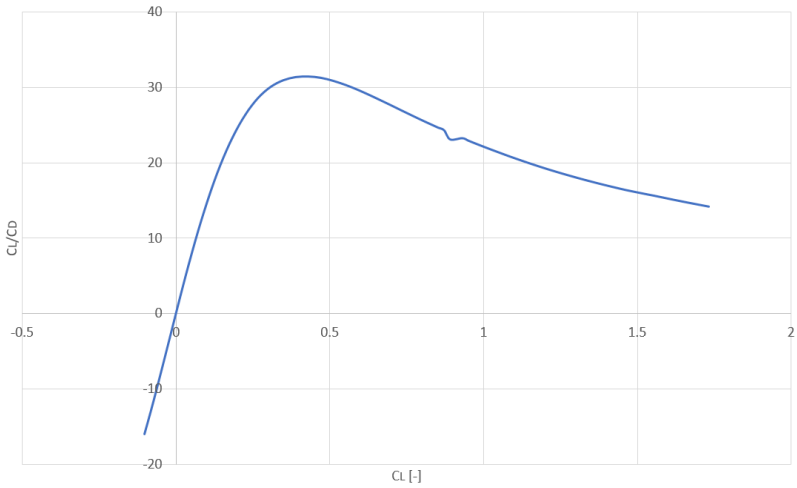

Figure 8.9: $C_L/C_D - C_L$ curve for the entire wing planform.

It can be seen from figure 8.9 that the maximum lift-over-drag of the wing is equal to 31.5. This optimal lift-over-drag ratio is achieved at a lift coefficient of 0.43, according to the analysis of *XFLR5*. This is close to the design coefficient of 0.5078 that was calculated earlier. Indeed, it can be concluded that the airfoil and wing are optimised for the cruise phase of this particular aircraft.

Major final outputs of the wing analysis are given in table 8.5.

Table 8.5: Wing analysis of the SRJ110.

Parameter:	**Value:**
$C_{D_{cruise}}$ [-]	0.01578
C_{L_0} [-]	0.2877
$C_{L_{max}}$ [-]	1.7316
α_{stall} [°]	18.75
α_{cruise} [°]	2.5
α_{0L} [°]	-3.5
$C_{m_{cruise}}$ [-]	-0.6068

8.4.2 Drag Estimation

An important parameter to consider when analysing the aerodynamics of the SRJ110 is the drag. As presented in the Mid-term Report, the drag mainly consists of two parts; the induced drag and the zero-lift drag [31].

In the Mid-term Report, equation 8.13 has been used to evaluate the total drag of the clean aircraft configuration. This equation takes into account the camber of the wing. High lift devices are neglected in the following analysis.

$$C_D = C_{D_{min}} + \frac{(C_L - C_{L_{mindrag}})^2}{\pi \cdot A \cdot e} \tag{8.13}$$

However, the average wing camber of the SRJ110 is 1.13% of the chord, from the airfoil analysis. The $C_{L_{mindrag}}$ associated to a moderate cambered wing profile is usually small and therefore equation 8.14 can be considered instead of equation 8.13 to determine the total drag coefficient of the aircraft in clean configuration [55].

$$C_D = C_{D_0} + C_{D_i} = C_{D_0} + \frac{C_L^2}{\pi \cdot A \cdot e} \tag{8.14}$$

In equation 8.14, the first terms consists of the zero-lift drag coefficient and the second terms represents the drag associated to the lift production, namely the induced drag coefficient. C_{D_0} is estimated using equation 8.15 [55].

$$C_{D_0} = \frac{1}{S_{ref}} \cdot \left(0.003 \cdot S_{w_{wet}} + 0.0024 \cdot S_{fus_{wet}} + 0.006 \cdot S_{eng_{wet}} + 0.0025 \cdot (S_{h_{wet}} + S_{v_{wet}})\right) + C_{D_{int}} \tag{8.15}$$

The last term of equation 8.15 accounts for interference, roughness and excrescence of the design and is estimated to be 10% of the zero-lift drag coefficient. To solve this equation, the wetted surface area of the wing, the fuselage, the engine nacelles and the stabilisers first need to be computed. Basic approximations can be used as shown in equations 8.16 to 8.19.

$$S_{w_{wet}} = 1.07 \cdot 2 \cdot S_{ref} \tag{8.16}$$

$$S_{fus_{wet}} = \frac{\pi \cdot d}{4} \cdot \left(\frac{1}{3 \cdot L_1^2} \cdot \left[\left(4 \cdot L_1^2 + \frac{d^2}{4}\right)^{1.5} - \frac{d^3}{8}\right] - d + 4 \cdot L_2 + 2 \cdot \sqrt{L_3^2 + \frac{d^2}{4}}\right) \tag{8.17}$$

$$S_{eng_{wet}} = 2 \cdot l_n \cdot d_n \tag{8.18}$$

$$S_{h_{wet}} + S_{v_{wet}} = 1.05 \cdot 2 \cdot (S_h + S_v) \tag{8.19}$$

In equation 8.17, the length L_1, L_2 and L_3 are respectively 3.7, 26.3 and 6 m. L_1 is the total length of the nose cone and the cockpit section, L_2 is the cabin length and L_3 represents the tail cone length of the fuselage. Finally, by solving equation 8.15, a C_{D_0} of 0.02 is found. Furthermore, table 8.6 shows the zero-lift drag breakdown between the various aircraft components. The percentage as a function of the total zero-lift drag is also provided. In this way, the most contributing components to the zero-lift drag can be identified. To keep in mind when analysing these results is the contingency factor defined during the baseline development phase [29]. Due to the current design maturity of the SRJ110, a 5% variation is to take into account for safe design.

Table 8.6: Zero-lift drag breakdown.

Parameter:	Value:	%
$C_{D_{0_w}}$ [-]	0.00642	32
$C_{D_{0_{fus}}}$ [-]	0.00813	41
$C_{D_{0_{eng}}}$ [-]	0.00189	9
$C_{D_{0_{h+v}}}$ [-]	0.00175	9
$C_{D_{int}}$ [-]	0.00182	9
$C_{D_{0_{TOT}}}$ [-]	0.02000	100

The next step is to compute the induced drag coefficient. First, the Oswald efficiency factor needs to be determined. Since the sweep of the SRJ110 is smaller than 30°, equation 8.20 can be used [55].

$$e = 1.78 \cdot (1 - 0.045 \cdot A^{0.68}) - 0.64 \tag{8.20}$$

Furthermore, a drag increment has to be taken into account due to compressibility. This drag component is known as the wave drag. To estimate the wave drag, the cruise Mach number and the critical Mach number are required to solve equation 8.21 [56].

$$C_{D_w} = 20 \cdot (M_{cruise} - M_{cr})^4 \tag{8.21}$$

Now, the total drag of the aircraft in clean configuration can be evaluated, taking into account the additional drag component due to compressibility. A value of 0.032 is finally found. When evaluating the induced drag coefficient, the effects of wing twist and ground effect have been neglected. At cruise, a corresponding lift-over-drag ratio of 15.85 is found.

When taking into account the effects of the winglets, equation 8.22 is referred to. This equation evaluates the effective aspect ratio obtained when winglets are added to the wing design. Increasing the aspect ratio without modifying the wingspan leads to a reduction of the induced drag since this is inversely proportional to the aspect ratio.

$$A_{eff} = A + 1.9 \cdot A \cdot \left(\frac{h_{winglet}}{b}\right) \tag{8.22}$$

In which h is the height of the winglet as defined in section 8.3.
With a new value for the induced drag coefficient of 0.01068, a total drag coefficient of 0.031 is found. This corresponds to a 3.245% decrease compared to the initial situation. The L/D ratio is now determined to be 16.385, which is 3.346% higher than before. This approach is rather conservative since it does not take into account the lift increase at the wing tip. Furthermore, *Raymer* claims that the *Withcomb* winglet design has the potential to increase the lift-over-drag ratio by 20% [53].

The above drag analysis is summarised in table 8.7, together with a drag breakdown and the percentage difference of the induced drag, total drag and L/D when winglets are added to the wing design compared to the original configuration.

Table 8.7: Drag breakdown of the SRJ110 clean configuration with and without winglets.

Clean wing:			**Clean wing + winglet:**			
Parameter:	**Value:**	**%:**	**Parameter:**	**Value:**	**%:**	**% Difference:**
C_{D_0} [-]	0.02	62.5	C_{D_0} [-]	0.02	64.5	-
C_{D_w} [-]	0.0003	0.9	C_{D_w} [-]	0.0003	1	-
C_{D_i} [-]	0.0117	36.6	C_{D_i} [-]	0.0107	34.5	8.85
C_D [-]	0.032	100	C_D [-]	0.031	100	3.245
L/D [-]	15.85	-	L/D [-]	16.38	-	3.35

8.5 High Lift Devices

The airfoil and wing are designed to be as efficient as possible during cruise condition, where drag should be minimised. In this condition, the aircraft is flying at a high speed and, thus, a smaller lift coefficient is required. During take-off and landing, however, the aircraft's velocity is significantly lower. In order to reach take-off lift within a limited amount of runway and to land safely at a low enough speed, a higher lift coefficient is required. The difference between the maximum lift coefficient of the clean wing, $C_{L_{max,clean}}$, and the required value is denoted by ΔC_{Lmax}. For take-off and landing the values are 0.1 and 0.9, respectively, following from subsections 6.3.1 and 8.4.1. The increase in lift can be generated by the addition of high lift devices on the leading or trailing edge. For the take-off phase, the difference in extra lift required is small, however $C_{L_{max,clean}}$ is attained at a high angle of attack of 17.5°. This is not a realistic value for airline operations and hence requires modification. In order to reduce the angle for maximum lift, the lift curve slope C_{L_α} can also be increased using high lift devices. To evaluate the additional lift coefficient from the various high lift devices, equation 8.23 can be used [45].

$$\Delta C_{L_{max}} = 0.9 \cdot \frac{S_{wf}}{S} \cdot \Delta C_{l_{max}} \cos \Lambda_{hinge} \tag{8.23}$$

S_{wf} is the area of the wing affected by a high lift device, as shown in figure 8.10.

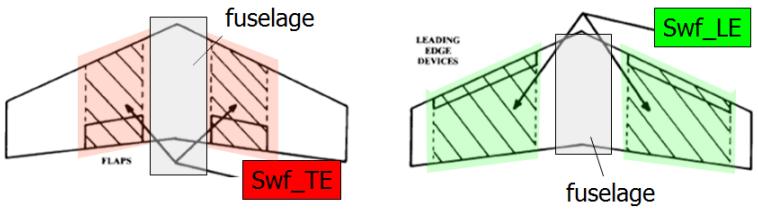

Figure 8.10: Schematic showing the definition of S_{wf} for leading edge and trailing edge high lift devices [45].

The value for $\Delta C_{l_{max}}$ is dependent on the type of high lift device and the ratio of chords c'/c when flaps are extended. In the Mid-term Report, the various types of high lift devices were investigated [31]. Based on weight, complexity, noise and drag, multiple options were eliminated. For trailing edge devices, the single and double slotted and Fowler flaps remain. These are shown in figure 8.11. For the leading edge devices, only slots and slats are considered. The respective $\Delta C_{l_{max}}$ values for each device is listed in table 8.8 [45].

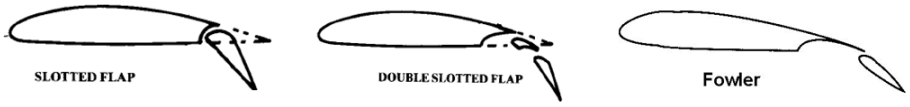

Figure 8.11: Image showing schematics of the flap types considered [45].

Table 8.8: Wing parameters of the SRJ110.

TE device:	$\Delta C_{l_{max}}$ [-]
Single slotted flap	1.3
Double slotted flap	1.6 c'/c
Fowler flap	1.3 c'/c
LE device:	$\Delta C_{l_{max}}$ [-]
Slot	0.2
Slat	0.4 c'/c

The coefficients are valid when the devices are fully deployed. During take-off this is not the case. To take into account the partial deployment, values of 80% of the tabulated coefficients are used. For the double slotted and Fowler flap, and the slat, the c'/c ratio accounts for the extension of the wing area. This is dependent on the deflection of the devices. Based on typical values and data found in *Torenbeek*, the ratio's have been computed. These are presented in table 8.9.

Table 8.9: Table showing the ratio of c'/c for various TE flap devices.

Device:	c'/c **take-off [-]:**	c'/c **landing [-] :**
Double slotted flap	1.0875	1.16
Single slotted Fowler flap	1.1325	1.16
Double slotted Fowler flap	1.1425	1.205

The addition of high lift devices also changes the lift curve slope, by influencing the gradient C_{L_α} and angle of zero lift α_{0L}.

For trailing edge devices which do not increase the wing surface area, the lift curve slope is the same as in clean condition. If the flap type extends the wing surface area, the lift curve slope follows from equation 8.24 [45].

$$C_{L_{\alpha,flapped}} = \frac{S'}{S} \cdot C_{L_{\alpha,clean}} \tag{8.24}$$

S' is the wing area including flap extension and can be approximated by equation 8.25 [45].

$$\frac{S'}{S} = 1 + \frac{S_{wf}}{S} \cdot \left(\frac{c'}{c} - 1\right) \tag{8.25}$$

It follows the increase in gradient is different for take-off and landing due to the varying c'/c ratio. The shift in angle of attack of zero lift can be computed using equation 8.26.

$$\Delta\alpha_{0L} = (\Delta\alpha_{0L})_{airfoil} \cdot \frac{S_{wf}}{S} \cdot \cos\Lambda_{hingeline} \tag{8.26}$$

$(\Delta\alpha_{0L})_{airfoil}$ equals -15° at landing and -10° at take-off. Typical limits for the angle of attack during take-off and landing for commercial airliners are 10-14 degrees.

Taking all these considerations into account, and the wing planform with the engine attached, the high lift devices have been chosen and sized. The explanation of the engine location will follow in subsection 13.2.4. Considering the C_L deficits, the devices were designed to satisfy the landing lift coefficient. For the wing area between the fuselage and the engine, double slotted flaps have been chosen. Because of the straight trailing edge, high lift devices are most efficient here. The double slotted flaps offered the most optimum $\Delta C_{l_{max}}$ of the available options while taking into account complexity and weight. The available flapped area was 17.53 m^2 of both wings combined, with a 0.1 m margin between both the flaps and the fuselage and flaps and engine. This yields a $\Delta C_{L_{max}}$ of 0.22 in the landing configuration with a flap deflection of 45 °. Secondly slats are added. Based on reference aircraft, it is common practice to have slats on almost the entire leading edge. Spanwise, the slats are placed with a margin of 0.5 m from both the wing tip and the fuselage. This yields a flapped area of 67.68 m^2. Although the resulting S_{wf}/S ratio is large, the $\Delta C_{l_{max}}$ is small and the additional lift coefficient is 0.1645. After the kink, there is a 0.1 m margin after which a flaperon is placed to provide controllability at high speed. This is a combination of an aileron and simple slotted flap. The spanwise size is 1.5 m, yielding a flapped area of 10.24 m^2 and a lift contribution of 0.13. After another 0.1 m margin, single slotted Fowler flaps are added to compensate the remaining lift deficit. It has been calculated a spanwise length of 4 m was required with a total flapped area of 20.91 m on both wings combined. This leaves another 3.4 m spanwise to the tip for the addition of ailerons, which will be covered in section 8.6. The final planform with high lift devices will be presented in figure 8.13.

After sizing the flaps for the landing condition, the values for the take-off phase have been computed. The requirement is more than satisfied, with a possible 2.5 $C_{L_{max,TO}}$.

Using equations 8.24 and 8.26, and the high lift devices configuration, the resulting C_{L_α} curves for clean wing, take-off and landing configuration have been plotted in figure 8.12. Because of the viscous limitations to model a stall on a 3D-wing in *XFLR*, only the linear part has been modelled.

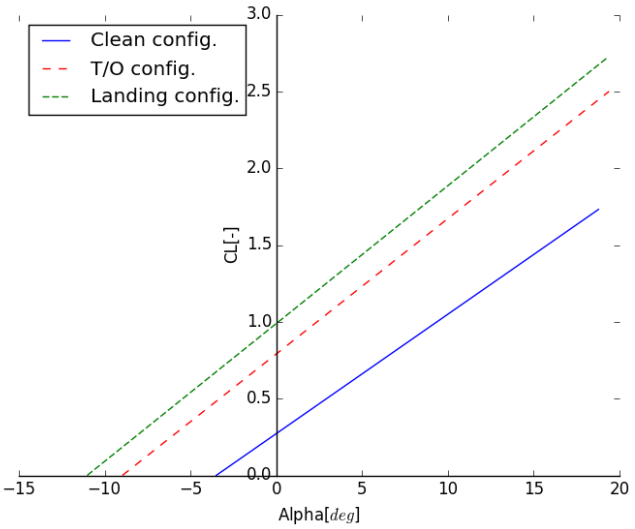

Figure 8.12: Graph showing the lift coefficient vs. angle of attack for clean, take-off and landing configuration.

For the landing configuration, the maximum lift coefficient slightly exceeds the requirement with a value of 2.71. This is attained at a rather high angle of attack. However it has been calculated the lift coefficient at the minimum approach speed set by certification standards, at maximum landing weight, is 1.72 [11]. This

value is attained at an angle of attack of around 8°. Hence there is a sufficient margin in terms of increase in angle of attack and lift coefficient for other possible flight conditions. The maximum required lift coefficient for take-off can be attained at around 12° angle of attack, which is within the limitations.

8.6 Aileron, Elevator and Rudder

This section elaborates on the design of the control surfaces of the SRJ110. The ailerons have been designed in order to comply with predefined roll performance as later explained. The rudder and the elevator have been sized based on statistics.

Properly designing the ailerons of the aircraft is crucial in order to provide roll control. Sizing the ailerons has been conducted in parallel with the design of the high lift devices discussed in section 8.5. The main reason behind this way of proceeding is the division of the wing planform between various systems. At the end, verification of the proper intertwining of all wing movables needs to be ensured.

First, the roll performance defined by the regulations has to be found. The SRJ110, being a heavy transport aircraft with a low-to-medium manoeuvrability, is included in the Class III aircraft category. A roll angle of 30° in 1.5 s then needs to be satisfied, which gives a roll rate of 0.35 rad/s. The aileron design is primarily characterised by the spanwise and chordwise location of the aileron, as well as the maximum deflection angle. From reference aircraft, a maximum upward and downward aileron deflection of 25 and 20° are assumed, respectively. Furthermore, due to the flaps design presented in section 8.5, a distance of 3.4 m is available for the implementation of the ailerons on both sides of the wing. A check has to be performed to make sure this distance is sufficient to comply with the roll performance, including clearance margins on both sides of the aileron. Moreover, the aileron taper is the same as the wing taper such that the ailerons can be attached to a straight spar.

Plain flap ailerons have been selected for the SRJ110. These ailerons are the most common control devices nowadays used in civil aviation as well as for military planes. Plain flap ailerons are characterised by a high effectiveness and a low manufacturing cost. Typical aileron location is near the tip of the wing such that the roll arm is increased, making the ailerons more efficient. However, another important phenomenon to keep in mind when designing the control surfaces of the SRJ110 is the aileron reversal occurring at high speed. Therefore, additionally to the plain flap ailerons located near the wing tips, flaperons and spoilerons are required during cruise. A flaperon is a combination of flap and aileron located, in this case, outboard next to the kink. Along the straight trailing edge of the wing, spoilerons are used. Design of the flaperons and the spoilerons has been incorporated in section 8.5. Sum of their length should be at least equal to the total length of the plain flap ailerons. Moreover, when the flaperons and spoilerons are active, the outboard ailerons are hold fixed.

The design procedure is discussed hereafter [57]. Final values are summarised in table 8.10 once compliance of the aileron design with the roll performance is ensured. The first step consists of determining the aileron length. Since 3.4 m is available, and including 0.3 m clearance between the flap and the aileron as well as at the wing tip, the room left for the implementation of the ailerons is 2.8 m. Furthermore, an aileron chord of 15% of the wing chord is assumed, which fits behind the rear spar located at 60% [58]. To check if the aileron length of 2.8 m is sufficient, the time required to achieve the mentioned bank angle needs to be calculated. The obtained value should be equal or lower than the time specified in the regulations as illustrated by equation 8.27.

$$\frac{\Delta_\phi}{P} \leq 1.5 \tag{8.27}$$

In equation 8.27, P is the aircraft roll rate with maximum aileron deflection. An average value of 22.5° has been assumed for the maximum aileron deflection to solve equation 8.28.

$$P = -\frac{C_{l_{\delta_a}}}{C_{l_p}} \cdot \delta_{a_{max}} \cdot \left(\frac{2 \cdot V}{b}\right) \tag{8.28}$$

$C_{l_{\delta_a}}$ and C_{l_p} are defined as the aileron control derivative and the roll damping derivative, and can be evaluated using equations 8.29 and 8.30, respectively.

$$C_{l_{\delta_a}} = \frac{2 \cdot C_{L_\alpha} \cdot \tau \cdot C_r}{S \cdot b} \cdot \left[\frac{(b_2 - b_1)^2}{2} + \frac{2}{3} \cdot \left(\frac{\lambda - 1}{b}\right) \cdot (b_2 - b_1)^3\right] \tag{8.29}$$

$$C_{l_p} = -\frac{(C_{L_\alpha} + C_{D_0})}{24 \cdot S} \cdot c_r \cdot b \cdot (1 + 3 \cdot \lambda) \tag{8.30}$$

In equation 8.30, τ is an effectiveness parameter. For a control surface-to-lifting surface a chord ratio of 15%, a τ value of 0.35 is found from the relation presented in [46]. b_1 and b_2 are the inner and outer spanwise location of the aileron, respectively.

Solving equation 8.27, the 2.8 m previously defined is determined to be sufficient for providing roll control to the aircraft. Final values are presented in table 8.10.

Table 8.10: Aileron design of the SRJ110.

Parameter:	Value:	Parameter:	Value:
Roll angle (regulations) [°]	30	$D_{max_{up}}$ [°]	25
Time (regulations) [s]	1.5	$D_{max_{down}}$ [°]	20
Rate (regulations) [$1/rad$]	0.35	$C_{l_{\delta_a}}$ [$1/rad$]	0.0228
b_1 [$\%b/2$]	0.778	C_{l_p} [$1/rad$]	-0.526
b_2 [$\%b/2$]	0.9786	P [rad/s]	0.278
Aileron length [m]	2.8	Δ_ϕ/P [s]	1.256

In figure 8.13, the final wing planform is presented with all the wing movables included.

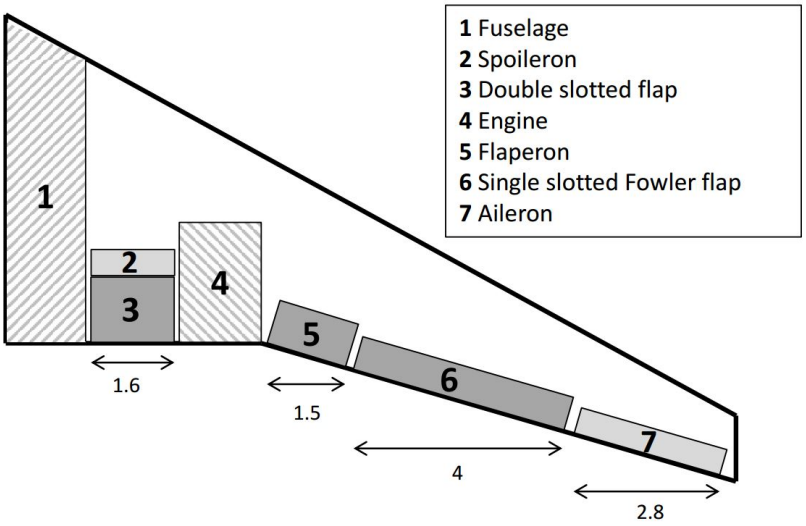

Figure 8.13: Schematic drawing showing the wing planform with fuselage, engine, high lift devices and control surfaces. Dimensions are expressed in m.

Finally, the design of the rudder and the elevator is analysed. From literature, the chord of the rudder and the elevator of the aircraft is respectively 30 and 28% of the vertical and horizontal stabiliser chord [46].

9 Structural Analysis

In this chapter the SRJ110 will be structurally designed. First, different aerospace materials are compared to each other in section 9.1. Afterwards the wing structure is determined in section 9.2. Next, the fuselage structure is specified in section 9.3. Lastly, in section 9.4, the engine mount is designed.

9.1 Material Choice

The main material for aircraft has always been aluminium. Lately the use of composites is rising, with the prime reason being weight saving over aluminium. In this section three materials, all known for their application in the aerospace industry, are investigated and compared. For aluminium, the alloy 7075 is opted for as its properties are much better than the more common 2024 alloy. Originally it was chosen for the alloy 7085, used in the Boeing 787, however no properties could be find for this alloy. As the alloy 7075 has similar properties, it would do for this design phase [59]. The tensile and compression strength for aluminium are assumed equal [60]. Furthermore the glass fibre composite Glare is compared in this section, as it is used in current aircraft such as the Airbus A380. For carbon fibre reinforced polymer, CFRP T800H is chosen in this section. Firstly the specific weight of the materials is discussed. Subsequently the ease of manufacturing and maintenance of the three materials is compared. Next, the total cost to use these materials is investigated. Lastly, the sustainability of these products is discussed.

9.1.1 Weight

In table 9.1 the characteristics of the three investigated materials are listed [61–64]. Glare 1 is a unidirectional composite as it has better properties in comparison to the other Glare composites. For this composite no shear strength could be found. However the matrix of a composite is responsible for carrying the shear loads. The alloy used in Glare 1, aluminium 7475-T76, has a shear strength of 310 MPa. Hence it is assumed that the shear strength of the Glare 1 is between 200-300 MPa [65]. For every property, the second column represents the specific value, in other words the parameter value divided by the density. When looking at the non-specific values, CFRP is the strongest in tensile and compression. For shear, aluminium or Glare is the best option. CFRP is obviously the stiffest and lightest material, according to the Young's Modulus and density. However when using a material, the weight is relative to the other properties. Hence, the properties such as Young's Modulus are divided by the density in order to compare equally.

Table 9.1: Characteristics of Aluminium 7075-T6, Glare 1 and CFRP T800H.

	Tensile Strength:		**Compressive Strength:**		**Shear Strength:**		**Young's Modulus:**		**Density:**
	$[MPa]$	$[\frac{MPa}{kg/m^3}]$	$[MPa]$	$[\frac{MPa}{kg/m^3}]$	$[MPa]$	$[\frac{MPa}{kg/m^3}]$	$[GPa]$	$[\frac{GPa}{kg/m^3}]$	$[kg/m^3]$
Aluminium 7075-T6	503	0.179	503	0.179	330	0.117	71	0.025	2810
Glare 1	545	0.216	447	0.177	200-300	0.079-0.119	65	0.026	2520
CFRP T800H	2840	1.893	1570	1.047	80	0.053	160	0.107	1500

To investigate which material will result in the lightest structure, the specific properties in table 9.1 need to be taken into account. The highest specific value means that when using the same quantity of mass, that material is stronger. For tensile and compressive strength, CFRP clearly wins with a specific value almost ten times higher than aluminium and Glare. Aluminium is definitely better in managing a high shear strength, with respect to weight, than CFRP. The specific shear strength of Glare is equal or smaller than aluminium, but still clearly better than CFRP. If a very stiff material is needed, CFRP is almost five times stiffer than the other two materials. Looking at the properties, using only CFRP will not be an option as it has poor shear properties. Moreover, predicting the exact properties of composites is difficult, hence safety factors need to be used. This will result in the composites being heavier than shown in the table, since more material needs to be used. However, CFRP will still be the lightest applicable material. An example of a successful weight saving would be the Boeing 787, with a structure that consists for 50% of T800H, leading to a weight decrease of 20% [66].

To conclude the comparison for strength and weight, if a high shear strength is not required, CFRP comes out as the most optimal material. Even though Glare has a lower density than aluminium 7075, its properties are quite comparable. If in particular sections of the aircraft such a high properties are not needed, Glare is a better choice than aluminium regarding the weight.

9.1.2 Manufacturing

The ease of manufacturing is not only important for cost, but also for the feasibility of a design. If a component is very difficult to manufacture using a certain material, mass production is nearly impossible. Since the three materials discussed in this section are investigated for being a main material of the aircraft, this is a crucial parameter. Furthermore the difficulty to manufacture could lie in the uncertainties or the likelihood of making mistakes. If the properties of a material cannot be determined within a certain range, it will have a negative impact on the overall design. As aluminium is already commonly used, it has a large advantage. Not only are the manufacturing methods clearly established, the characteristics of aluminium are isotropic and easy to compute. Composites are very dependent on the fibre fabric, the direction of the fibres and the matrix material [67]. It is crucial the fibres are placed in the correct direction. Even a small misalignment will strongly reduce the properties in the necessary direction. Moreover, properties rely on the method of layer attachment. Unfortunately, no method exists for predicting the adhesive strength [68]. Even though aluminium is clearly the easiest to manufacture, composites are relative new in the industry, so it is expected the ability to predict properties will increase in the near future, improving manufacturability and design uncertainties.

9.1.3 Maintenance

Maintenance exists of two parts: firstly the detection of defects and secondly the repair of defects. It is preferred that detection and reparation can be done in a conventional way, which unfortunately is not always possible. The most prominent problem for composites is the presence of cracks, which can result in delamination. Cracks in composites are not visible without special equipment, e.g. ultrasound systems [68]. The most common detection method for cracks in CFRP is Eddy Current Testing (ECT) [69]. This method is rapidly advancing, as it is a non-contact and non-destructive method for conductive materials. The conventional riveted repair on Glare is just as easy as on aluminium. Nevertheless, there is a better way, namely using adhesive bonding. This method proved to be more resistant to fatigue, since the loads will be transferred more uniformly and efficiently [70]. As mentioned before, aluminium is extensively used for aircraft. Maintenance methods are already in place, thus it makes aluminium the most easy to maintain.

9.1.4 Cost

Cost is one of the most determining factors in the aircraft industry. The cost of CFRP is about 80-90 USD/kg. This is significantly higher than aluminium 7075, which has a cost of about 2-2.5 USD/kg [71]. However it is expected that the prices of carbon composite will decrease drastically in the coming years; by 50%-70% [72]. Glare costs about 4-5.5 USD/kg, hence it is comparable to aluminium. These figures are however excluding the manufacturing costs. Looking at situations in which tensile and compression strength are crucial, CFRP is the lightest material. Even though CFRP will still be more costly, a significant amount of weight and thus fuel will be saved using this lighter material. So using CFRP will increase the unit cost, but decrease the operational cost. Glare is more costly than aluminium, while its specific properties are not sufficiently better. Hence, it is not recommended to use Glare as it will increase both the unit cost and the operational cost. Aluminium is not only cheaper regarding purchase price, its also the cheapest considering manufacturing and maintenance. As mentioned before, the production and repair techniques are already largely developed for aluminium. This is not the case for composites, whose use in aircraft is still relatively new. Even though currently using composites is more expensive than aluminium, the sales price will lower due to the decreasing material cost. Furthermore the maintenance cost will reduce, when the material becomes more commonly applied in aviation.

9.1.5 Sustainability

Last but not least, the materials used should be sustainable in multiple ways. The manufacturer should have a progressive policy on sustainability and environmental effects. Besides that, the factory should not be too far from the aircraft assembly plant, saving on transportation cost and thus fuel. Furthermore, the material itself should be recyclable. Metals, as for instance aluminium, can easily be recycled by melting and forming it again. The process of melting scrap metal only uses 5% of the energy used in the original process. Although

aluminium 7075 is not a pure metal, as long as the correct sequence of every metal in the alloy is known, it would have no significant throwbacks [73]. Glare is also easily recyclable and has economical benefits. By cooling the material down significantly, Glare becomes brittle and the glass and aluminium will separate. Even though the aluminium will not be perfectly separated, it can be sold for a higher price than the recycle cost [74]. The recycling of the carbon composite is especially developed for dealing with the fibres. It has been proven that, after the fibres and resin are separated, the characteristics of the fibres are comparable to that of new fibre [75]. Nevertheless the most profound environmental problem of carbon composite does not concern recycling, but a post-crash fire. A toxic smoke will be formed when the carbon fibres catch fire. However after testing the Boeing 787, the toxicity level of the carbon skin panels were not worse than of an aluminium fuselage [76]. Still, for all incidents involving carbon fire, a full decontamination procedures needs to be put in place.

It can be said that the materials discussed in this section are all suitable for the sustainability policy of this project. However, when using CFRP the emergency response in particular should be adapted accordingly. Only the manufacturer should be carefully chosen.

After this investigation, it was decided that Glare 1 will probably not be included in the SRJ110. Its higher cost is not sufficiently offset by the marginal increase in mechanical properties compared with the aluminium. Aluminium 7075 came out as the best material to use on the SRJ110, due to its excellent properties and low cost. However, CFRP T800H will also be included in the design, especially in parts that need high tensile or compressive strength. It is believed that, even though the unit cost will increase, the operational cost will decrease. Moreover, being lighter means less fuel is required, which is also beneficial for the environment.

9.2 Wing Structure

The wing design is of paramount importance in the design of any airplane. It is not only responsible for lift generation, but in most cases also for the storage of fuel, landing gear, control surfaces and high lift devices. The internal structure of the wing, the wing box, should be able to withstand all loads and stresses induced on the aircraft on the ground and in-flight, while taking into account the airfoil geometry and other attachments. In this section, a preliminary sizing of the wing box is presented. To start, wing loading diagrams are generated based on the possible loads the aircraft may encounter. Results are presented in subsection 9.2.1. This is followed by the design considerations for the wing box in subsection 9.2.2. At this stage, the sizing is performed to withstand bending stress and shear stress. Finally, in subsection 9.2.5, the final lay-out of the wing box is introduced.

9.2.1 Wing Loading Diagrams

The lift acting on the aircraft wing induces internal forces and moments resulting in stresses. In order to design a structure that is able to cope with these stresses, it is important to identify and quantify the internal loading on the wing. The lift of the aircraft is distributed along the wingspan. For the generation of the distributed load, shear and moment diagrams, a method from *MIT* has been used [77]. The net wing load distribution q is a function of location along the span y according to equation 9.1.

$$q(y) = L'(y) - n \cdot g \cdot m'(y) \tag{9.1}$$

In this equation L' and m' are the lift and mass as function of the span, respectively, and n is the load factor. g is the gravitational acceleration of 9.81 m^2/s. An approximation can be made where the net aerodynamic and weight loading is proportional to the local chord, as in equation 9.2.

$$q(y) \simeq K_q \cdot c(y) \tag{9.2}$$

The constant K_q can be evaluated using equation 9.3.

$$K_q = \frac{L - n \cdot W_{wing}}{S_{wing}} = \frac{n \cdot W_{fus}}{S_{wing}} \tag{9.3}$$

For the load factor, the most critical case in-flight has been chosen based on the $V-n$ diagrams from subsection 6.3.2. This limit load factor is equal to 2.5 in cruise condition. A safety factor of 1.5 has been applied to arrive at the ultimate load factor. W_{fus} is the aircraft weight, excluding the wing. The weight at begin of cruise has been chosen to evaluate the wing. This corresponds with the maximum load factor and is also the most critical case.

In *Python*, a function has been written to generate the chord as a function of the span in N intervals for evaluation of $q(y)$. Consequently, the value for q at 768 locations along the span has been computed.

From the distributed load, the shear can be calculated by integrating along the span according to equation 9.4. Subsequently, the moment can be obtained by integrating the shear, again, along the span as in equation 9.5.

$$S(y) = \int q(y) \cdot dy \tag{9.4}$$

$$M(y) = \int S(y) \cdot dy \tag{9.5}$$

Python is used to compute a range of values for the shear and moment as function of the spanwise position. The corresponding loading diagrams are plotted in figure 9.1.

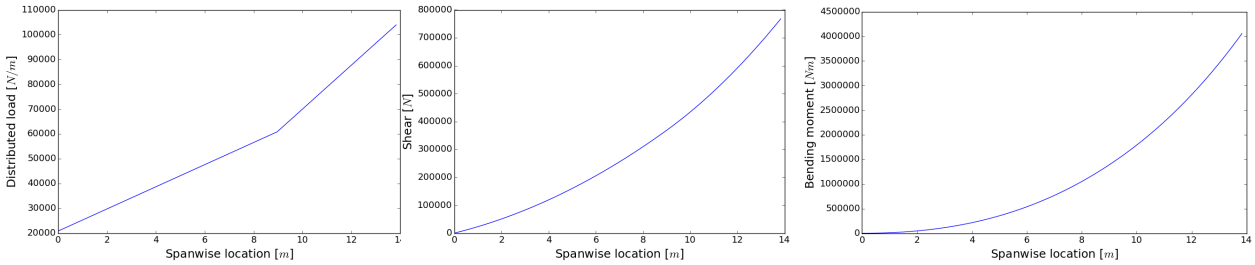

(a) Graph showing the spanwise distributed load.

(b) Graph showing the spanwise shear force.

(c) Graph showing the spanwise bending moment distribution.

Figure 9.1: Loading diagram for a half wing.

9.2.2 Wing Box Design

The wing of the aircraft will be subjected to a whole range of aerodynamic loads during flight, so it is of utmost importance that the wing contains a wing box which is able to cope with these forces. The wing box is located in the wing as depicted in figure 9.2. As one can see, the wing can be divided into two sections, namely the first section from the tip to the kink and the second section from the kink to the root. The chord increases linearly within each of these sections, however at a different rate in each section. This automatically implies that the thickness of the airfoil follows the same linearly increasing characteristics as the chord.

A wing box consists of two vertical units, the spars and two horizontal units, the webs. In reality, the wing skin is mostly taking up the task of the web. To be able to start analysing the design of the wing box, the spar locations need to be known. Usually the front spar is located at about 15% of the chord length and the rear spar is about 60% of the chord length [45]. These dimensions allow the wing to have enough room to account for the high lift devices, which should be about 40% chord. Since there is a change in the increase in chord length at the tip, keeping 15% and 60% at every spanwise location is not possible. That is why the front spar has been fixed at the tip and the root and the rear spar at the tip and the kink, in order to satisfy the minimum area needed for the high lift devices. The exact spar locations can be seen in table 9.2.

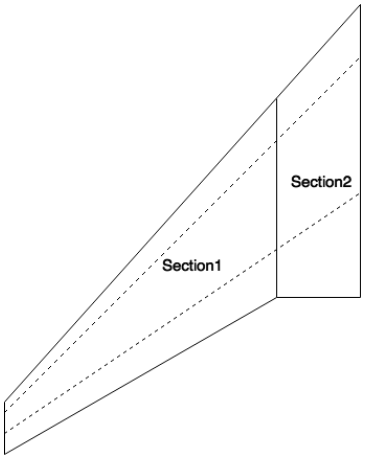

Figure 9.2: Spanwise location of the spars in the wing illustrated by the dashed lines. Note: not to scale.

Table 9.2: Location of front and rear spar in % chord.

	Tip:	Kink:	Root:
Front spar [%c]	15	17.5	15
Rear spar [%c]	60	60	50

Table 9.3: Actual spar heights in m at tip, kink and root.

	Tip:	Kink:	Root:
Front spar [m]	0.1048	0.3861	0.6472
Rear spar [m]	0.1043	0.3605	0.7226

Since now the location of each spar and thickness of the airfoil is known at every spanwise location, the height of the spars and thus the wing box can be determined. However, from the analysis it becomes obvious that the front and rear spar do not have the same heights, so for the purpose of analysis at this early stage of design, the spar heights are assumed equal by taking the average height. This assumption will simplify the problem to the analysis of a rectangular box. The determination of the chord and the spar heights along the span was done using a *Python* script. A schematic drawing of the wing box in the airfoil is shown in figure 9.3.

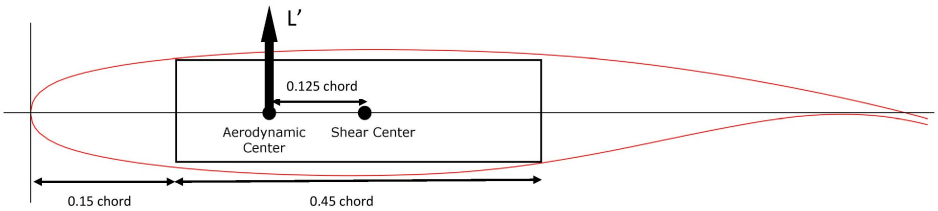

Figure 9.3: Schematic drawing of the wing box cross section.

9.2.3 Shear Stress Sizing

The shear force generated by the aerodynamic loads introduces a shear flow and a shear stress in the wing box cross section according to equations 9.6 and 9.7.

$$q = \frac{V' \cdot Q}{I} \tag{9.6}$$

$$\tau = q \cdot t \tag{9.7}$$

In these equations, V' represents the shear force at a single spanwise location, Q is the first moment of area, I is the moment of inertia, q is the shear flow and t the thickness. As can be see in figure 9.3, the shear centre is assumed in the centre of the box, implying that the shear flow is caused by the assumption of the shear force acting at that centre point, in combination with a torsion moment, see figure 9.4a. The shear flow in the cross section is represented in figure 9.4b. From this diagram, one can clearly see that the maximum shear flow is located in the middle of the spars, or at half the wing box height.

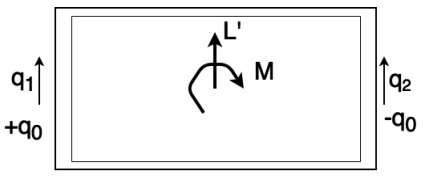

(a) Contribution of shear force and torsion moment in the wing box cross section.

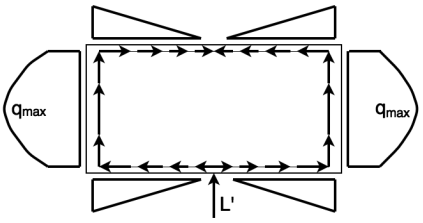

(b) The shear flow distribution in the wing box cross section.

Figure 9.4: Shear in the wing box cross section.

The shear flows q_1 and q_2 in the spars are the result of the shear force, whereas the q_0 is the result of the torsion. As one can see from the direction of the torsion moment M, q_0 will be added to q_1 and subtracted from q_2. The formula for determining q_0 can be seen in equation 9.8.

$$q_0 = \frac{T}{2 \cdot A} = \frac{0.125 \cdot c' \cdot V'}{2 \cdot A} \tag{9.8}$$

c' is the local chord length, A is the enclosed area of the wing box and T is the torsion. In order to withstand the maximum shear stress, the maximum total shear flow is divided by the local thickness. This value should be lower than the maximum shear strength as follows from equation 9.9.

$$\frac{q_{max}}{t_{spar}} < \tau_{max} \tag{9.9}$$

9.2.4 Bending Stress Sizing

The aerodynamic bending moment causes a normal stress in the wing box cross section according to equation 9.10.

$$\sigma = \frac{M' \cdot y}{I} \tag{9.10}$$

Here, y is the distance from the neutral axis to the location of the stress and M' is the bending moment at a certain location along the span. In flight, the upward lift force causes a tensile stress in the bottom part of the wing and a compressive stress in the top part. y is maximum in both the top and bottom part - and equal to half the spar height - hence these locations will be examined for normal stress.

9.2.5 Final Wing Box Lay-out

For simplicity, it has been chosen to design the wing box cross section at five spanwise locations. Because of the amount of variables, it was not possible at this stage to optimise for a continuously changing cross section. In section 1 from figure 9.2, there will be two design segments while in section 2 there will be three segments because this part takes up the majority of the loads. The length of each piece is equally divided. Because the loads increase towards the root, for the design of the wing box the most inboard loads for each section will be used while the most outboard, smallest and therefore limiting, dimensions are used. The relevant parameters are listed in table 9.4.

Table 9.4: Table showing the dimensions, forces and moments for the five wing box design sections.

Wing box:	**Spanwise position from tip [m]:**	**Spar height [m]:**	**Chord length [m]:**	**Max. shear force [N]:**	**Max. bending moment [Nm]:**
1	0-4.55	0.105	1.25	141,899	289,900
2	4.55-9.10	0.228	2.54	375,869	1,434,596
3	9.10-10.73	0.373	3.66	489,769	2,141,228
4	10.73-12.37	0.512	4.53	627,427	3,054,068
5	12.37-14.00	0.685	5.40	767,839	4,056,040

For the wing box structure, a carbon fibre composite was opted for. This is the most common material used for the wing section in modern aircraft and it also offers the possibility to cope with the loads without stringers. The properties are equal to those listed for CFRP T800H in table 9.1; a tensile strength of 2,840 MPa, a compressive strength of 1,570 MPa and a shear strength of 80 MPa. In order to design for the most optimum load carrying, the fibres in the top and bottom skin are aligned mostly unidirectionally along the span. In the spars, the fibres are placed at +/- 45° to carry the shear. This is depicted in figure 9.5.

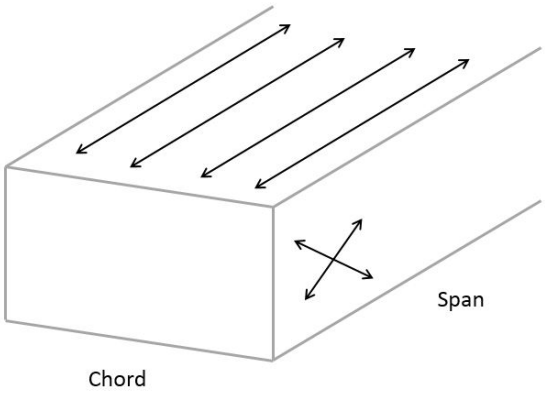

Figure 9.5: Schematic drawing showing the general fibre direction in the wing box.

In a *Python* script, the shear flow and normal stress due to bending are calculated based on the geometry and load inputs of table 9.4, together with thickness values for the spar and top and bottom skin. The script calculates the inertia and maximum bending stress and shear stress. These values are compared with the maximum allowable values. The thicknesses are manually adapted until the highest structural stresses fall below the maximum material strengths. For each of the five sections, the resulting values for the thicknesses are listed in table 9.5.

Table 9.5: Table showing the skin and spar thicknesses for the 5 wing box sections.

Section:	**Spar thickness [m]:**	**Top skin thickness [m]:**	**Bottom skin thickness [m]:**
1	0.009	0.005	0.004
2	0.014	0.008	0.008
3	0.013	0.007	0.007
4	0.013	0.007	0.007
5	0.013	0.007	0.007

It can be noted that the values increase from section 1 to 2 and then decrease again and stay constant for section 3-5. Although the loads increase closer to the root, so do the spar height and chord length, especially from the kink to the root. Also, the t/c ratio changes twice along the span. This in turn automatically increases the inertia, and an increase in thickness is not necessarily required to cope with the increase in load. Because of the high values for tensile and compressive strength of the carbon fibre composite, the normal stress due to the bending moment is not the limiting case. The maximum shear stress in the spar is critical for the thickness determination. It is hypothesised that the increase in wing box dimensions with a constant thickness results in an inertia increment at equal rate as the shear force rise, therefore offsetting the higher shear stress and no additional material is required.

Besides the composite skin, a honeycomb structure is opted for around the entire wing box, made out of Nomex [78]. This acts as a sandwich structure between two composite plates, attached by an adhesive as is shown in figure 9.6. Although this material does not really contribute to carrying shear or normal stress, and the addition to the moment of inertia is negligible, the honeycomb structure counters buckling and warping at a relative low weight. These phenomena are not studied in this stage and the sizing of the honeycomb layer will be part of a detailed design phase.

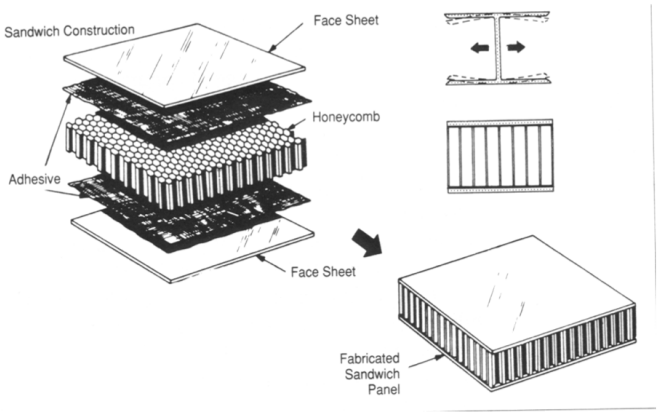

Figure 9.6: Combination of composite skin and honeycomb structure [79].

Further optimisation of the wing box is also possible in the detailed design phase. Usually, the front spar requires more thickness than the back spar due to addition of the shear flow due to torque. For the top and bottom skin, the top skin is usually thicker as the compressive strength is lower compared to the tensile strength for the bottom. The number of sections can also be increased for less overdesigning. For this optimisation, significant computation power is required due to the number of variables.

9.3 Fuselage Structure

The fuselage has to endure a lot of stress during operation, ranging from stresses caused by touch-down to pressurisation stresses. In this section the most critical load case for the fuselage will be discussed and

analysed. Using this stress analysis, the fuselage skin and stringers can be sized and finally the fuselage's structural weight can be determined. The method used for this analysis is a numerical method, partially taken from the TU Delft course Simulation, Verification & Validation (*SVV*) [80–82]. For a more elaborate explanation on the whole fuselage structural analysis, please consult these reports. Firstly, in subsection 9.3.1 it will be explained which material is chosen for the structural analysis of the fuselage. Next, in subsection 9.3.2, all the assumptions are listed. The governing equations and booms are set up in subsections 9.3.3 and 9.3.4 respectively. Subsequently, the stress calculation is done in subsection 9.3.5. Hoop stress and fatigue are checked on in subsections 9.3.6 and 9.3.7, respectively. Finally, a conclusion will be drawn in subsection 9.3.8.

9.3.1 Aluminium versus Composites

As concluded in section 9.1, carbon composites have a much lower density and better material characteristics compared to aluminium. Therefore, doing the fuselage structural analysis for both aluminium and composite would be ideal. However, since it would be too time-demanding to do a composite structural analysis, it was decided to only analyse for Aluminium 7075-T6. Yet, this does not form a problem: it is known that a carbon composite fuselage weighs about 20% less compared to aluminium and thus the structural weight of the carbon fuselage can be determined [83]. This weight reduction could be extremely useful for compensating the innovative noise mitigation measures proposed in chapter 13, especially since these measures are not yet taken into account in the component weight estimation described in chapter 6 The skin and stringer dimensions of a possible carbon fuselage will be determined in a later design stage.

9.3.2 Assumptions

- A hard landing is more critical for the fuselage than cruise, as during a hard landing the fuselage endures bending and reaction forces from the landing gears. The load during landing mostly lies around 2.5 g, however for the calculations a standard safety factor of 1.5 is applied [84]. In other words, the fuselage will be designed for a landing with a load case of 3.75 g. Furthermore, a strong crosswind of 30 knots is acting on the tail. This is in compliance with CS25 regulations [11].
- The fuselage during landing is considered a static problem with the front and rear landing gear touching down at the same time, however this reduces the actual stress introduced by the rear landing gear.
- The forces on the landing gear are point loads and the weight of the structure is a uniformly distributed load. This does not have a significant impact on the results.
- The windows and the wing are not taken into account, making the necessary skin and stringer thickness in this computation thinner than required.
- No forces act in the z-direction since the landing gear is taken as a roller support (see figure 9.7).
- To simplify calculations, only the pressurised fuselage is taken into consideration, i.e. from bulkhead to bulkhead. This part of the fuselage is assumed to be perfectly cylindrical.
- All attachments are infinitely stiff so no deformations occur. However since the fuselage is modelled as a beam, it can have very small deflections that are thus not accounted for.
- Thin-walled assumptions are valid for the skin and stringers and are applied to compute the properties of the cross section.
- To calculate the stresses, the skin, the stringers and the floor are modelled as booms.
- The fuselage is discretised per 10 cm along the z-axis to be able to keep the computations within a reasonable time.
- It was decided to stick to a number of 36 stringers (one per 10°) and a number of 11 booms for the floor. Because of this decision, large parts of the SVV code could be used and a lot of time was saved.

9.3.3 Governing Equations

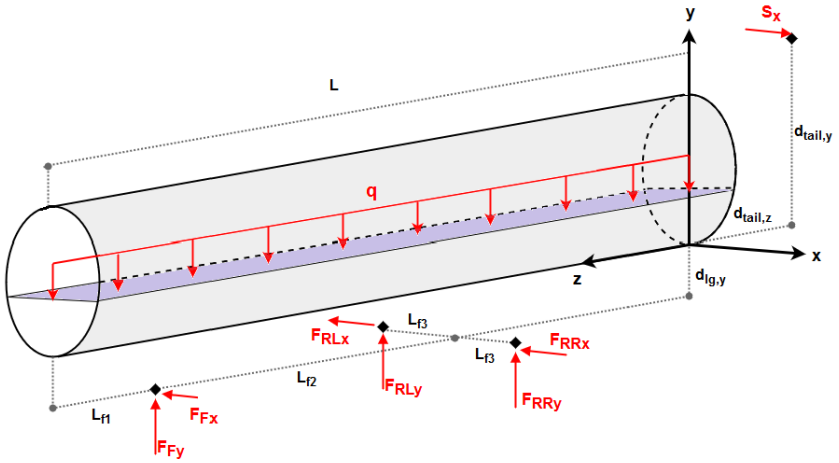

Figure 9.7: Free body diagram of the fuselage during a hard landing with crosswind.

Before the stress calculations can be performed, the governing equations have to be set up. These equations can subsequently be used to calculate the introduced shear forces and bending moments. First a free body diagram was made, as can be seen in figure 9.7. Note that the origin of the reference frame is located at the aft of the pressurised fuselage. The maximum crosswind force S_x on the vertical tail is just over 2,700 N. The force of the crosswind depends on the area of the vertical tail, the pressure at sea level, the maximum speed of the crosswind and the drag coefficient of the tail's side panel. To calculate the latter, the vertical tail was assumed a flat plate [85]. The equilibrium equations were solved using a *Python* script. Afterwards the shear and moment diagrams were plotted to determine the location of the maximum moment and shear. These diagrams are shown in figure 9.8. As can be seen, the maximum shear and moment occur at approximately 14 m from the aft fuselage; this is where the main landing gear is located.

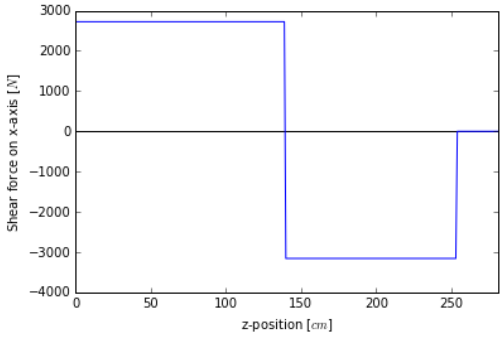

(a) Shear force diagram in x-axis.

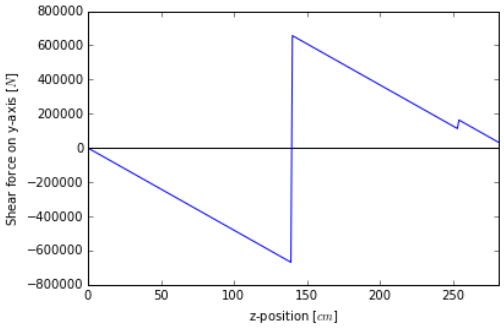

(b) Shear force diagram in y-axis.

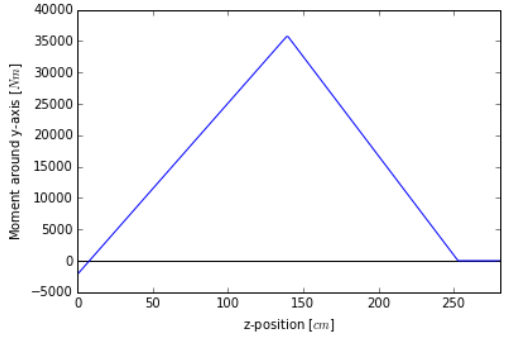

(c) Moment diagram around y-axis.

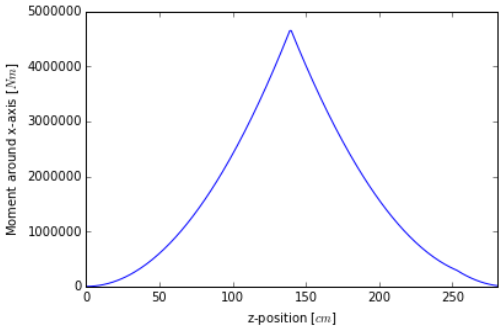

(d) Moment diagram around x-axis.

Figure 9.8: Shear and moment diagrams along the fuselage z-axis.

9.3.4 Boom Placement

Next the booms required placement. 36 booms for the fuselage skin and stringers and 11 to represent the floor were decided on. As mentioned before, these values were chosen for simplified calculations. A representation of the boom placement can be seen in figure 9.9. The starting values for skin thickness and stringer thickness, width and height were 2 mm, 12 mm, 20 mm and 15 mm, respectively. The floor thickness was fixed to 20 mm to simplify later iterations. The boom areas were determined using equation 9.11, where t_D is the thickness of the floor or the skin, b the distance between two consecutive booms, σ the normal stress and $A_{stringer}$ the area of the stringer [86].

$$B = \frac{t_D \cdot b}{6} \cdot \left(2 + \frac{\sigma_2}{\sigma_1}\right) + A_{stringer} \tag{9.11}$$

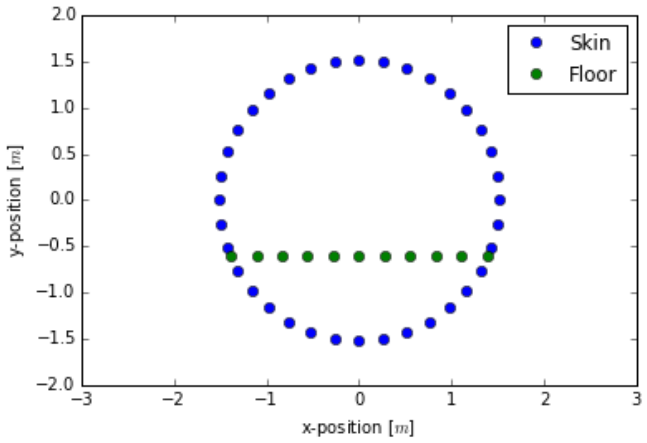

Figure 9.9: Placement of the booms in the x-y plane.

9.3.5 Stress Calculation

In order to calculate the stresses and shear flow, the moment of inertia of the cross section was determined as well as the centroid. After this, the normal and shear stress could be calculated at each boom and along the whole z-axis. The von Mises yield criterion was used to determine the location of the maximum stress. The maximum von Mises stress is also located at the main landing gear position, since there the shear and moment stresses are the highest. This can be seen in figure 9.10.

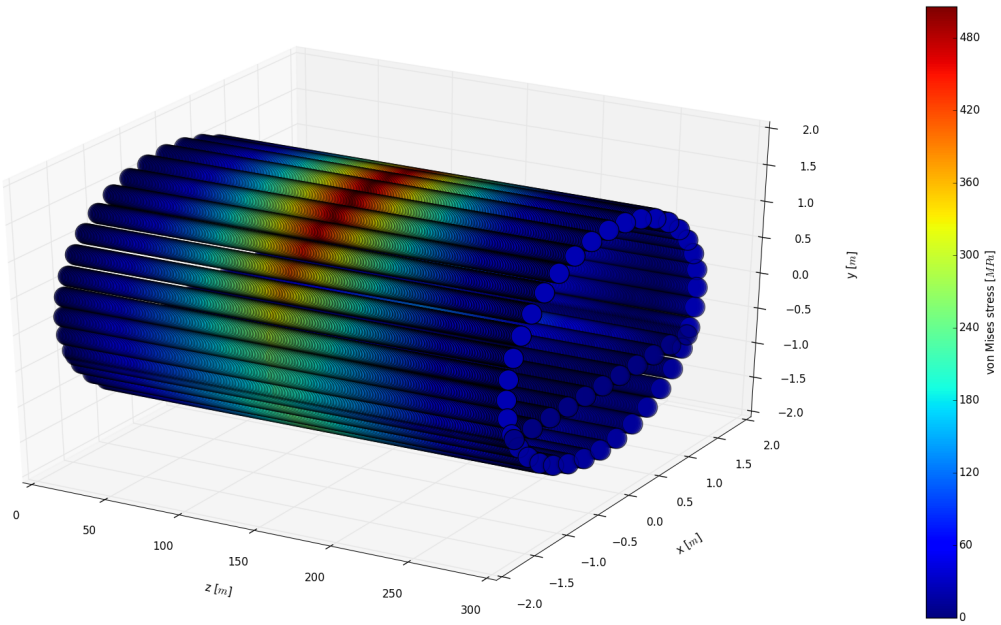

Figure 9.10: Von Mises stress along the fuselage.

Using these normal stress, shear stress and von Mises stress, the iteration was started to find the optimal skin thickness and stringer dimensions. The goal was to find dimensions such that the loads could be carried without any yielding or buckling whilst minimising the structural weight. This was done for Aluminium 7075-T6. The final dimensions can be found in table 9.6. The maximum stresses acting on the fuselage, as well as the pressurised fuselage's structural mass, are shown in table 9.7. As stated before, a composite fuselage would reduce the mass by 20%, resulting in a mass of 3,693 kg. It is important to note that there is a discrepancy between the fuselage's mass calculated here and the one calculated in the Class II weight estimation. This is because the Class II estimation approaches the fuselage differently: the weight given here is only about the pressurised fuselage, whilst the Class II estimation takes into account the nose and tail cone too.

Table 9.6: Final dimensions for the fuselage structure.

Property:	Al 7075-T6:
t_{skin} $[mm]$	1.2
t_{st} $[mm]$	1.4
h_{st} $[mm]$	15.0
w_{st} $[mm]$	16.0

Table 9.7: Stress and mass properties of the pressurised fuselage structure during hard crosswind landing.

Property:	Al 7075-T6:
$\sigma_{t_{max}}$ $[MPa]$	499.6
$\sigma_{c_{max}}$ $[MPa]$	255.2
τ_{max} $[MPa]$	131.6
$\sigma_{vM_{max}}$ $[MPa]$	505.7
m_{fus} $[kg]$	4616.0

9.3.6 Hoop Stress

After the determination of the fuselage structural dimensions, it was checked whether the fuselage was able to withstand stresses caused by pressurisation. These stresses, so-called hoop stresses, are caused by a pressure difference between the inside and outside of the fuselage. The stress is given by equation 9.12, with ΔP the pressure difference, r the fuselage radius and t_{skin} the skin thickness [86]. For the calculation of the pressure difference, it was assumed that the cabin altitude was held at 6,000 ft. This altitude is very comfortable for passengers and is also used in the Boeing 787 [87].

$$\sigma_{hoop} = \frac{\Delta P \cdot r}{2 \cdot t_{skin}} \tag{9.12}$$

Filling in the values resulted in a hoop stress of 72.4 MPa for Aluminium 7075-T6. This implies that the hoop stress does not exceed the stresses caused by a hard cross-wind landing. Upon recommendation of a structural expert, the hoop stress was also calculated for a negative pressure difference, i.e. when the pressure outside of the fuselage is higher than inside the fuselage. This can happen in case of an emergency descent, where the cabin altitude is kept at 6,000 ft and the aircraft descends to sea level. Also for this case, the negative hoop stress does not exceed the stresses in the landing situation. Therefore, the fuselage dimensions remain the same. However, a major consequence of the pressurisation is the increased risk of fatigue. This is discussed in the next subsection.

9.3.7 Fatigue

As the aircraft is pressurised during each flight, fatigue will occur due to the repeatedly applied loads. To see after how many flights (or cycles) the aluminium will fail, the S-N curve for Al 7075-T6 can be used from figure 9.11a. This curve relates the applied stress to the number of cycles before the material fails. With the hoop stress calculated in subsection 9.3.6, one can see that it is clearly below the fatigue limit. This means the pressurisation will not have any critical effect on the aluminium 7075-T6. Yet, it is known that small cracks form in aircraft fuselages due to pressurisation. This is however not catastrophic and is mainly caused due to geometrical discontinuities, such as cut-outs for windows and rivets [88].

For composites, fatigue is considered even less of a problem than aluminium. Composites are known for there good fatigue characteristics, as can be seen in the S-N curve in figure 9.11b. The only drawbacks for composite fatigue is the larger scatter in failure stress and the fact that the stiffness degrades throughout stress cycles [89].

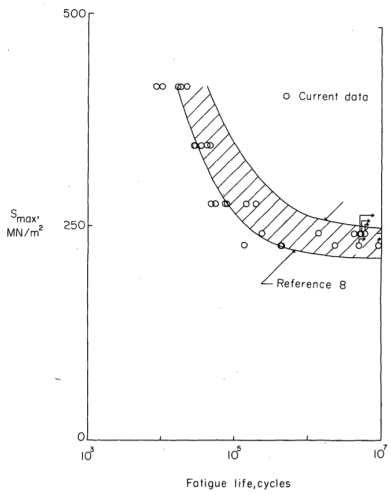

(a) S-N curve for aluminium 7075-T6 [90].

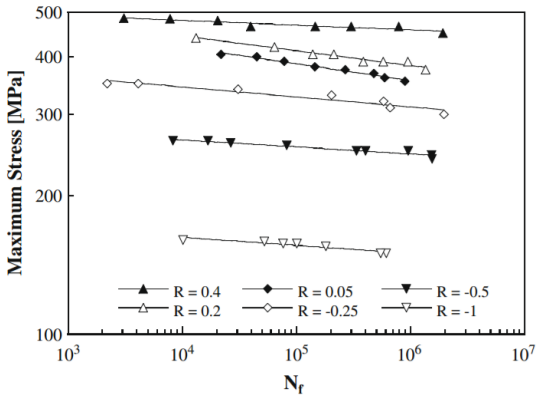

(b) S-N curve for CFRPs [91].

Figure 9.11: S-N curves for aluminium and CFRP.

9.3.8 Conclusive Statement

To conclude the fuselage's structural design, the choice has to be made between an aluminium or composite fuselage. As described in section 9.1, CFRP has significantly better characteristics than aluminium. It performs better in tension and compression, has a higher Young's modulus hence stiffness at a significantly lower weight. Although there is a price increase when choosing CFRP over aluminium, it was decided to embrace the use of carbon composites for the SRJ110 due to its better characteristics and positive future outlook. Furthermore, the 20% weight saving would decrease the fuel cost considerably as fuel prices continue to rise. However, at this stage of the design this weight reduction is not implemented yet. This decision was made for several reasons. Firstly, the estimation, 20%, is rather rough and therefore not deemed as completely reliable. Secondly, the mass of multiple noise mitigation measures, discussed in a chapter 13, are neglected at this stage, due to lacking data. Thirdly, the weight is subject to change as more detailed analyses should be performed, hence a conservative estimate is preferred. The possible use of Glare 1 has been discarded since there is no convincing difference when compared to aluminium, in both material characteristics as well as weight.

9.4 Engine Mount Design

As a final part in the structural design, the engine mount is discussed. As can be seen in figure 9.12, it is clear that the engine is mounted on top of the wing with a pylon (or strut). A pylon is chosen above a wing-embedded engine because the latter would create a lot of high-speed drag. Using a pylon can create strong shock waves, however there is an optimal position where the shock wave is minimised and a favourable interference between nacelle and wing is reached [92]. This pylon needs to carry and transfer the loads from the engine to the wing. The loads consist of vertical, side, torsional and thrust loads [93]. As mentioned in the Mid-term Report, the strut also has to be designed in such a way that the engine does not tear the wing apart and does not hit the tail in case of an engine separation [31]. This will be done by designing the attachment pins in such a way that the engine separates in the right direction when the pins break under an excessive force.

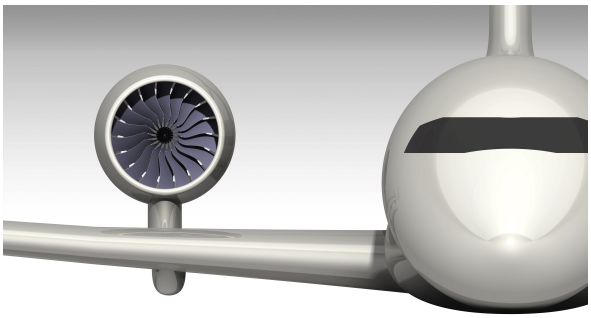

Figure 9.12: Render of the engine with pylon.

10 Flight Performance

This chapter will deal with analysing the performance of the aircraft. First of, all the optimum cruise speed and cruise altitude will be determined by analysing the most efficient combination with respect to fuel consumption in section 10.1. Next, the climb performance of the aircraft is analysed in section 10.2 by determining the possible climb rates and climb gradients. Last, but not least, an elaborate analysis of the airfield performance will be provided in section 10.3. This comprises the required take-off distance, landing distance as well as the balanced field length.

10.1 Cruise Altitude, Cruise Speed and Fuel Consumption

Primordial for the to be designed airliner is its performance with respect to cruise speed, cruise altitude and the fuel consumption. Cruise speed is important for the simple reason that limiting the time it takes to reach a set destination introduces the possibility conduct more flights in the same period of time, offering increased revenue. Cruise altitude is closely related with cruise speed in the form of the Mach number. As will be shown later, the cruise Mach number has a significant influence on the last parameter that is discussed in this section: the fuel consumption. The goal of this section is to determine a combination of cruise speed and cruise altitude that provides the best fuel efficiency of the aircraft. Last but not least, a brief discussion of pollutant emissions is also provided.

In the beginning of the design phase, the following requirement was set with respect to the cruise Mach number and the corresponding altitude: Mach 0.7 at 25,000 ft. This requirement was translated to a ground speed, as the customer is interested in how long it takes for the aircraft to travel from departure to its destination. The requirement on ground speed is shown below:

- SRJ110-PERF-CRU-A1: The aircraft's true air speed, c.q. ground speed, shall exceed 216 m/s.

For the jet aircraft under consideration, flying at 25,000 ft is not an optimal condition. The reason jet aircraft generally fly higher is because of the thinner air at higher altitudes. The thinner air imposes less drag on the aircraft which in turn reduces the fuel consumption. For this model, the drag coefficient is modelled as in equation 10.1.

$$C_D = C_{D_0} + C_{D_i} + C_{D_w} \tag{10.1}$$

The construction of this drag model was conducted in close collaboration with the Aerodynamics Department. A detailed determination of the zero-lift drag coefficient C_{D_0} can be found in equation 8.15. The lift induced drag coefficient C_{D_i} is determined from the rightmost part of equation 8.14. Last but not least the wave drag coefficient C_{D_w} is modelled according to equation 8.21. From the drag coefficient the total aircraft drag follows naturally from 10.2. The aircraft drag is of prime importance in determining the aircraft fuel consumption.

$$D = C_D \cdot \frac{1}{2} \cdot \rho \cdot V^2 \cdot S \tag{10.2}$$

This drag should be overcome by the engine thrust. For steady flight, the thrust should equal the drag. Once the drag (thus thrust) has been determined, the fuel flow can be determined from the specific fuel consumption (SFC) of the engine. SFC is a constant value which equals the amount of fuel used per unit thrust per hour. The most common unit for this parameter is $lb/lbf/hr$. Determining the exact value of this parameter however is not as easy as expected. Engine manufacturers are reluctant to make this value available to the general public, especially for recently developed engines. Therefore a different approach is followed based on the expected trend in engine development. When looking at figure 10.1, the expected value for the SFC in cruise equals approximately 14 $mg/N/s$. This corresponds to a value of 0.5 $lb/lbf/hr$. In agreement with an expert in the field of aircraft propulsion, this value was determined to be accurate with respect to current developments. As a result, this value will be used in subsequent calculations with respect to fuel efficiency.

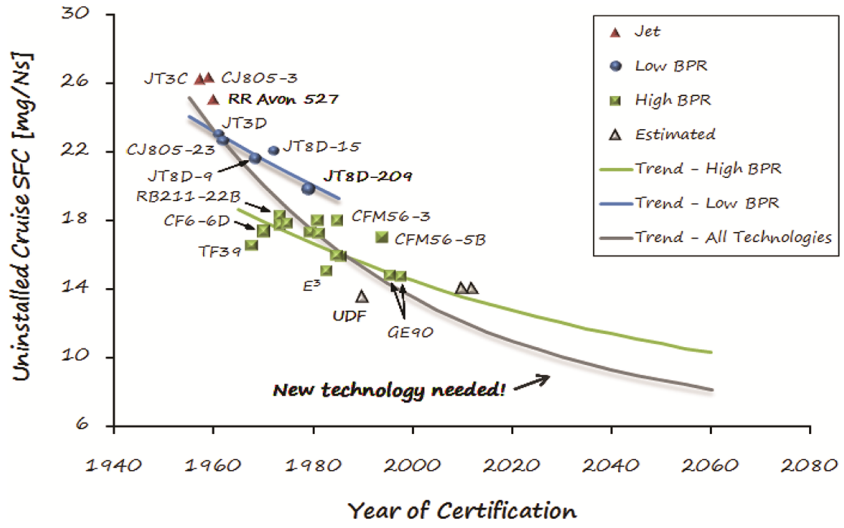

Figure 10.1: Historic and projected trends in SFC of jet engines [94].

By converting the drag calculated from N to lbf, the fuel flow in cruise can be determined. Then, by multiplying the fuel flow by the amount of time required to reach set destination, the total amount of fuel used during the cruise phase can be calculated. Dividing the fuel used by the amount of passengers in the aircraft and the distance travelled, yields the typical measurement unit for fuel consumption: $kg/PAX/NM$. For the cruise segment of flight, a distance of 1,400 NM was assumed. This takes into account a 100 NM sector for the climb, descent and approach phases of the journey, making the total flight distance equal to 1,500 NM.

Even though the cruise phase is the most fuel intensive stage of flight, ignoring the fuel burned in the other phases of flight would yield an underestimation of the actual fuel efficiency of the aircraft. In order to compensate for this, fuel used during the taxi, climb, descent and approach phases was added. For the taxi phase, an estimate of 155 kg fuel was determined to be a valid quantity [95]. For the climb, descent and approach phases the fuel consumption is based on the PW1500G engine data found in the ICAO aircraft engine emissions database [5]. Even though the PW1500G engine is not the selected engine for the aircraft, the engine belongs to the same family as the PW1700G and has a higher rated power output. This combination should lead to a conservative estimation of the fuel used during these phases. The results of the developed model are shown in figure 10.2.

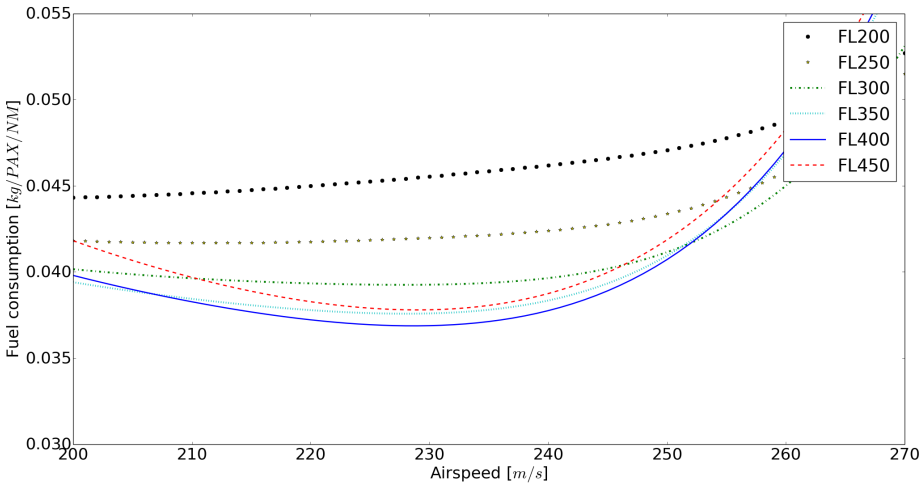

Figure 10.2: Results of the optimum cruise altitude and cruise speed analysis.

As can be observed from the figure, the optimum flight condition for cruise would be at $FL400$ with an airspeed of 230 m/s. For this case, however, there were several significant design constraints. First of all the design lift coefficient $C_{L_{des}}$ was found to be rather high, and the Aerodynamics Department experienced difficulties in finding an airfoil capable of achieving this lift coefficient at acceptable levels of angle of attack and

drag. In addition, the difference between the cruise Mach number and the drag divergence Mach number was determined to be rather small. This would mean that if the aircraft has to accelerate, for example if a Traffic Collision Avoidance System (TCAS) warning is issued, this would be extremely difficult due to the significant increase in drag. For these reasons, a cruise speed of 229 m/s at FL 350 was determined as an acceptable balance between aerodynamic performance and fuel efficiency. This would equate to a cruise Mach number of 0.77, which is a reasonable value compared to reference jet aircraft and significantly faster than the original requirement of Mach 0.7. The corresponding fuel efficiency at these flight conditions is 0.0376 $kg/PAX/NM$. This is still significantly better than the requirement which was set at 0.04263 $kg/PAX/NM$. To be exact, the fuel efficiency of the SRJ110 is almost 12% better than the set requirement.

Being efficient with respect to fuel usage is a key contributor to the profitability and the sustainability of the aircraft. A low fuel consumption saves the operator of the aircraft a significant amount in kerosene costs throughout the operational use. Additionally, less fuel burnt means less toxic emissions are expelled into the atmosphere. The customer has set constraints to the amount of toxic pollutants that the aircraft is allowed to emit:

- The pollutant emissions should be better or at least similar to the Embraer E2 currently under development.

The requirement did not specify the exact aircraft in the Embraer E2 series where the emissions should be based on. The Embraer E2 series is fitted with engines from the same PW1000G family as the SRJ110. An overview of the application of the PW1000G engine series is shown in table 10.1:

Table 10.1: PW1000G series application on aircraft.

Aircraft type:	**Engine**:	**Maximum static thrust** [kN]:
Airbus A320neo	PW1100G	160
MRJ70/90	PW1200G	67
Irkut MC-21	PW1400G	140
Bombardier CSeries	PW1500G	104
Embraer E170-E2, SRJ110	PW1700G	76
Embraer E190/195-E2	PW1900G	102

Because not all engines in the PW1000G family are certified yet, including the PW1700G, a different approach had to be taken to provide an estimate on pollutant emissions. From the PW1000G family the only certified engines are the PW1500G, which is currently in service on the Bombardier CS100, and the PW1100G, in use on the A320neo. Because the PW1100G has a significantly higher power output than the PW1500G, the latter will be chosen for the analysis of pollutant emissions.

The PW1700G is very similar to the PW1500G. It shares the same combustor; a high-tech TALON X variant specialised at slashing pollutant emissions to the fullest extent possible. In addition, the turbine stage layout is exactly the same with a two-stage high pressure turbine and a three-stage low pressure turbine. The only difference in the engine layout is the composition of the compressor stage. The PW1500G uses a geared fan, a three-stage low pressure compressor and an eight-stage high pressure compressor. The PW1700G engine has one less low pressure compressor stage compared to the PW1500G. It is however not expected that this difference causes significant changes in pollutant emissions over the PW1500G due to the fact that the most critical component, the combustor, is shared between the two. Combining the fuel efficiency of the aircraft and the emissions per kilogram fuel, the emission of pollutants per passenger per nautical mile traveled can be determined. A comparison will be made between the SRJ110's emission characteristics and the emissions corresponding to the fuel efficiency requirement set by the customer. The results are summarised in table 10.2.

Table 10.2: Pollutant emissions of the SRJ110, as well as the requirement [5, 96].

Pollutant	**Emission** [g/kg]**:**	**Emission required** [$g/PAX/NM$]**:**	**Emission obtained** [$g/PAX/NM$]**:**
Hydrocarbons (HC)	0.10	0.004263	0.003760
Carbon monoxide (CO)	0.10	0.004263	0.003760
Nitrogen oxides (NO_x)	16.7	0.7119	0.6279
Carbon dioxide (CO_2)	3150	134	118

Compared to reference aircraft, the SRJ110 scores excellently with respect to harmful emissions. The margin with respect to the CAEP 6 standards for nitrogen oxides is well over the 50% required. Emissions for nitrogen oxides are up to 52.2% lower than the CAEP 6 standard [5]. The low emissions are a direct result of the fact that the SRJ110 has superior fuel efficiency with respect to the Embraer E2 series, which is even higher than the requirement set. The results show that the SRJ110 meets the emissions requirement as stated by the customer with great deal of verve and is more than ready for the future.

10.2 Climb Performance

The climb performance of the aircraft governs how fast and efficient the aircraft can reach its cruise altitude. A high climb rate also reduces the perceived noise on the ground, simply because the distance from the measuring point increases faster. The climb rate is treat in subsection 10.2.1 while the gradient is computed in subsection 10.2.2.

10.2.1 Climb Rate

The climb rate can be determined by calculating the excess power the aircraft has available. The excess power is the difference between the available power P_a and the required power P_r, where the former is the speed multiplied with the thrust an the latter is the drag multiplied with speed. This relation is shown in equation 10.3.

$$RC = \frac{T \cdot V - D \cdot V}{W} = \frac{P_a - P_r}{W} \tag{10.3}$$

The climb rate will be calculated for various phases of flight. The first condition is the steady climb rate in a clean configuration at varying altitudes. From these results the maximum available rate of climb while cruising at a certain altitude can be deduced. For this phase the climb rates are calculated using the begin of cruise weight, so the climb rate only increases as the the cruise phase progresses. The next step is to model the engine's performance with altitude and velocity. Due to the lower air density at altitude the thrust decreases. The thrust also decreases with increasing velocity due to decrease in added momentum of the air by the turbofan. To simulate this a model has been constructed to predict the engine's performance with altitude and velocity. This model is represented by equation 10.4.

$$T_{corr} = f(h, M) \tag{10.4}$$

The amount of thrust at each altitude and airspeed can be seen in figure 10.3.

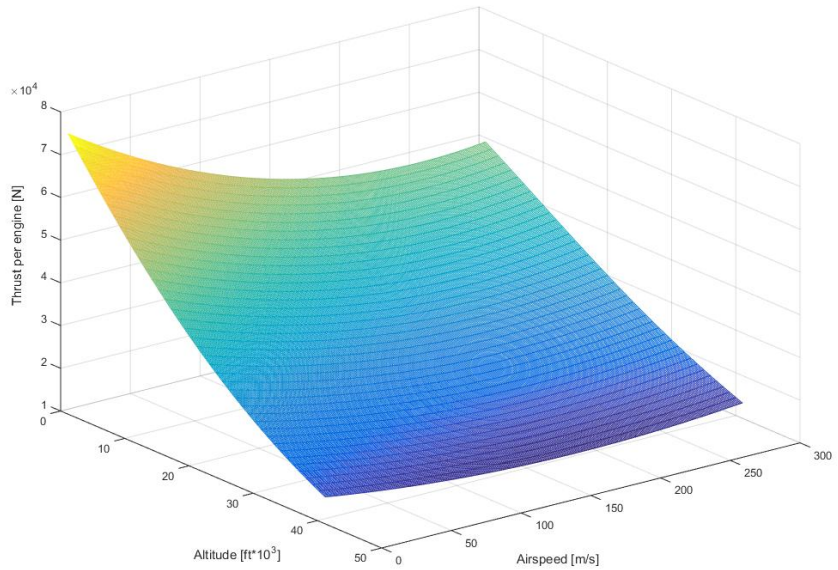

Figure 10.3: Maximum available thrust per engine per altitude and TAS of the PW1700G.

The drag polars including the wave drag have already been computed in section 8.4.2. Now every parameter for equation 10.3 is available and the results for steady rate of climb can be seen in figure 10.4. The values are taken at different flight levels, indicated in the legend. The presented climb rates are calculated with maximum available engine thrust.

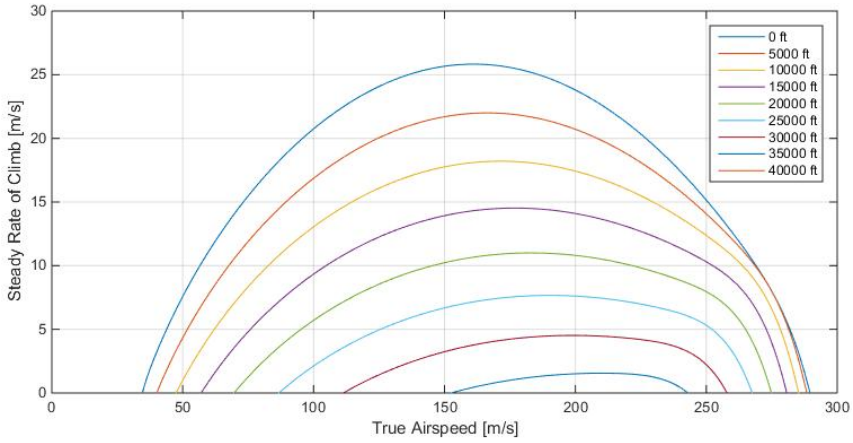

Figure 10.4: Maximum steady rate of climb of the SRJ110.

In figure 10.4 it can be seen that the service ceiling of the SRJ110, the point at which the maximum available rate of climb equals 0.5 m/s, is just over 35,000 ft at start of cruise weight.

In reality the steady rate of climb is an idealised situation. An aircraft climbs with a constant indicated airspeed which is, assuming there are no instrument errors, equal to the equivalent airspeed. The true airspeed is therefore not steady along the climb, but increasing with altitude. A correction for unsteady climb can be computed using equation 10.5 [97].

$$\frac{RC}{RC_{steady}} = \frac{1}{1 + \frac{M^2 \cdot \gamma}{2} \cdot (\frac{R}{g} \cdot \lambda_T + 1)} \tag{10.5}$$

Here γ is the rate of specifics heats for air. R is the gas constant, g is the gravitational acceleration and $lambda_T$ is the increase in temperature per altitude, equal to -0.0065 K/m. The effect this correction has on the rates of climb can be seen in figure 10.5. For example, the unsteady rate of climb at 30,000 ft and 200 m/s is about 80% of the steady rate of climb.

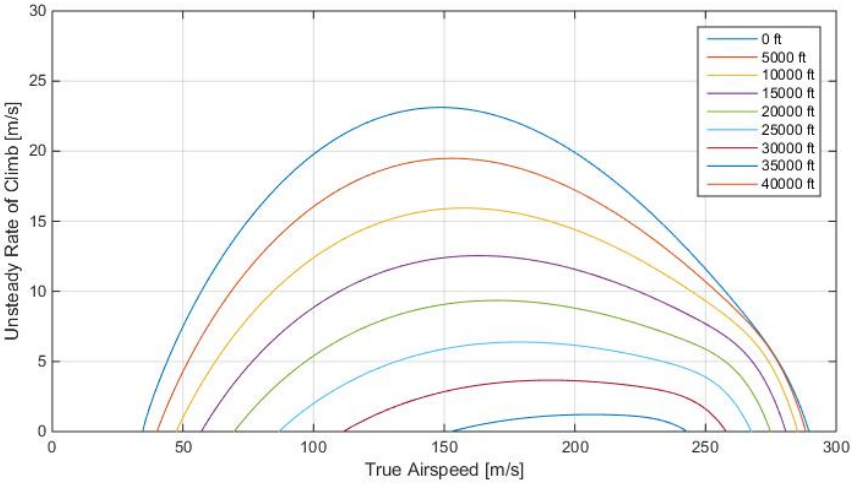

Figure 10.5: Maximum unsteady rate of climb of the SRJ110.

The next situations that will be analysed are the climb rate with take-off flaps and the climb rate with take-off flaps when an engine failure occurs on lift-off. During take-off the main difference from the earlier calculations is the fact that the flaps are extended to take-off setting. Since the landing gear is retracted almost

right after take-off, the added drag from the landing gear is not included here. The effects the landing flaps have are an increase in C_{d_0} of 0.015 and an increase in Oswald factor of 0.05 [39]. An engine failure would not only halve the available thrust but also add a windmilling drag from the failed engine. The added drag coefficient $C_{d_{windmill}}$ is assumed to be around equal to the coefficient found for the Fokker 70, which is 0.003. The rates of climb for clean configuration, take-off configuration and one engine inoperative (OEI) have been plotted in figure 10.6.

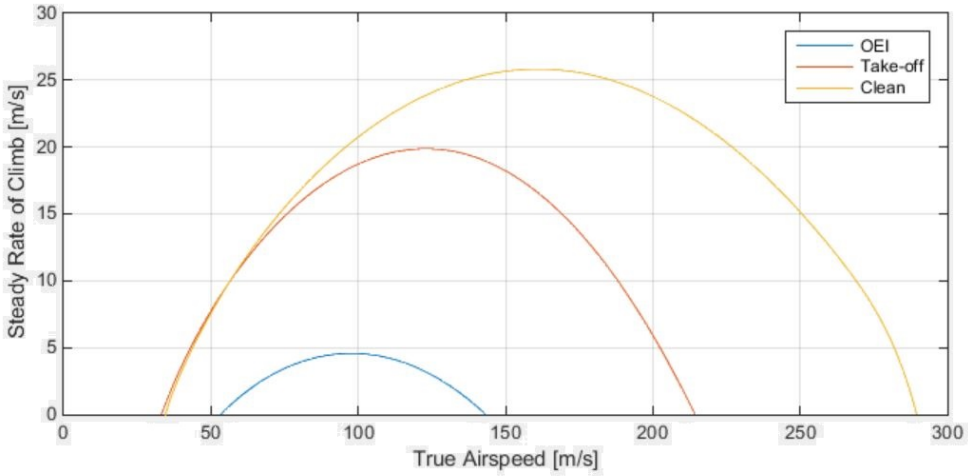

Figure 10.6: Maximum steady rate of climb during take-off with and without engine failure of the SRJ110.

The climb rate with an engine failure decreases rapidly, with the maximum climb rate in OEI conditions being 4.57 m/s at an airspeed of 98 m/s. At the most critical point, the point of rotation at around 70 m/s, the climb rate is 2.9 m/s assuming the landing gear is up. During a normal take-off the maximum climb rate after rotation is 13.7 m/s.

The last situation for which it is important to know the climb rate is at a rejected landing. During a balked landing the aircraft is flying at approach speed with full flaps extended at maximum landing weight. The approach speed for the SRJ110 is 1.3 times its landing stall speed, equal to 67 m/s. The zero-lift drag coefficient during the approach is estimated at 0.103 by extrapolating data from the Fokker 70. The maximum landing weight is estimated to be 90% of the maximum take-off weight. In figure 10.7 the maximum climb rate after a missed approach is presented.

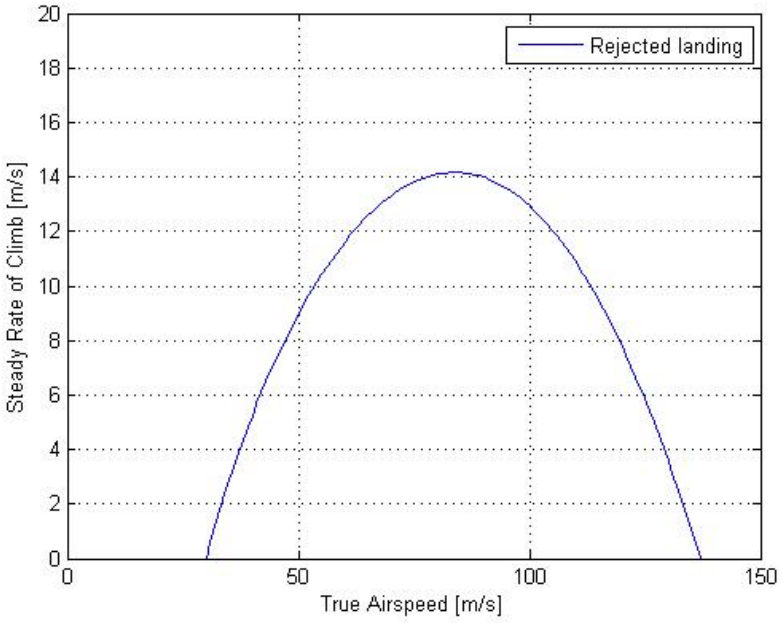

Figure 10.7: Maximum steady rate of climb during a missed approach of the SRJ110.

From this graph it can be concluded that the maximum available rate of climb at approach speed is equal to 12.9 m/s. This is assuming that the aircraft starts with a horizontal flight path and stays at constant speed during the climb. In reality during an approach the aircraft will be on a glide path and the engines will need some time to spool up to maximum thrust so the true rate of climb will be somewhat lower.

10.2.2 Climb Gradient

The climb gradient γ is the angle between the horizontal and the flight path during climb. Although the highest climb gradient does not coincide with the highest climb rate, the climb gradient does matter for e.g. obstacle clearance during take-off, or to climb when aircraft need to evade each other. The climb gradient corresponding to a climb rate can be computed by using equation 10.6.

$$\gamma = \text{asin}\left(\frac{RC}{V}\right) \tag{10.6}$$

Since the most important phase for determination of the climb gradient is during take-off, the gradients will only be determined for sea level in clean configuration, take-off configuration and one engine inoperative (OEI) take-off conditions. The gradients at other altitudes also can be calculated using equation 10.6 but are not presented in a figure.

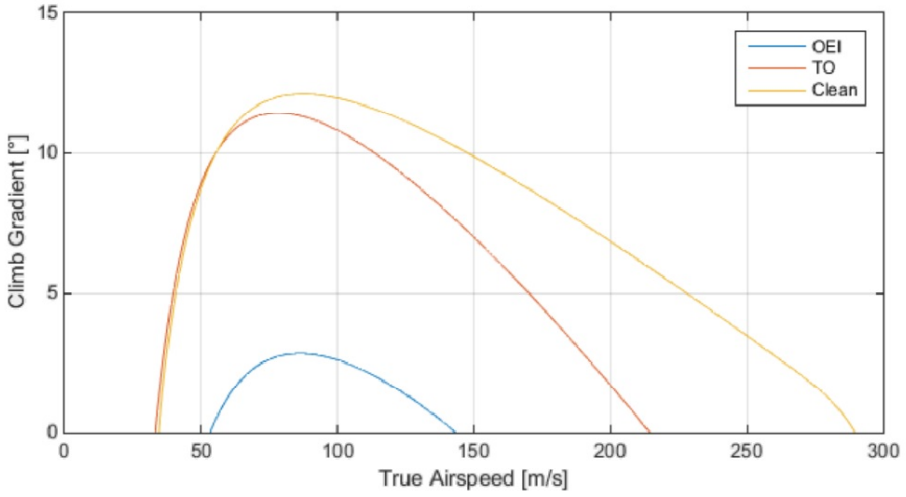

Figure 10.8: The maximum climb gradient of the SRJ110 per airspeed in take-off condition.

In the figure the same trends between the three configurations can be seen as for the climb rate in figure 10.6. The gradient after rotation for the take-off configuration is equal to 11.3°. The gradient achieved after take-off with an engine failure is critical and needs to exceed 2.4% according to CS25. The gradient at the rotation point is 2.5° and the maximum gradient during OEI equals 3° at 85 m/s. 2.5 ° translates to 4.4 %, so the OEI take-off gradient requirement is met.

In order to comply with CS25, a climb-out gradient of 2.5° should be attainable when a pilot decides to abort a landing attempt. By using the climb rates found for the rejected landing case, the climb gradients can be computed. The results are presented in figure 10.9.

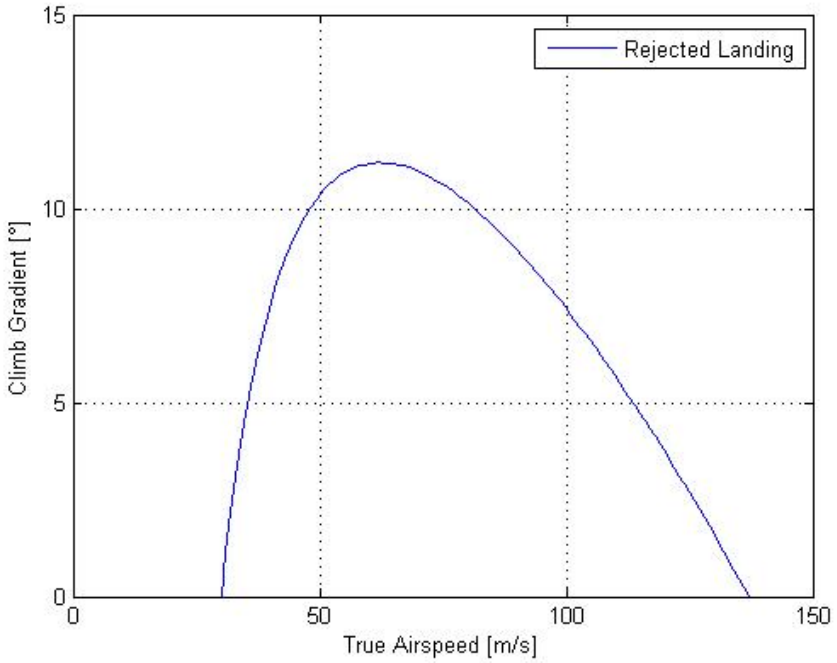

Figure 10.9: The maximum climb gradient of the SRJ110 per airspeed for landing condition.

From this figure it can be concluded that the maximum attainable climb gradient in landing configuration at an approach speed of 67 m/s equals 11°. Again it must be noted that in reality this value cannot be reached instantly after aborting the take-off attempt due to the transition from glide slope to climb and the spool up time of the engines.

10.3 Airfield Performance

One of the main requirements for the aircraft is the ability to operate to and from London city, which is a challenge due to the short runway and location in the city. In this chapter the take-off and landing distances will be analysed. As London City is the most critical for this aircraft, only the take-off from this airport will be discussed here. This means that with a load factor of 80% and a range of 1,000 NM, as per the requirement, the take-off weight used equals 42,100 kg.

10.3.1 Take-off Distance

The take-off distance of an aircraft consists of two phases. The first is the ground roll which lasts until the aircraft lifts off. The second phase is the airborne phase which lasts until the aircraft reaches the screen height of 15.2 m [97]. To solve these calculations, it is assumed that there is no headwind. Usually, an aircraft will perform take-off into the wind, which will shorten the take-off length. Firstly, the ground roll phase will be treated. The equation to estimate the ground roll distance can be seen in equation 10.7 [97].

$$S_g = \frac{V_{lof}^2 \cdot MTOW}{2 \cdot g \cdot (T_{av} - D_{av} - D_{g_{av}})} \tag{10.7}$$

In this equation, V_{lof} is the lift off speed, equal to 1.05 times the minimum speed, which is reached at the maximum lift coefficient during take-off of 1.8, as determined in chapter 8.5. In the case of the SRJ110, the lift-off speed is equal to 68 m/s. D_g is the ground drag from the aircraft wheels. The next step is to compute the average values for thrust, drag and ground drag. These are found at the point where the velocity is $V_{lof}/2$. The average velocity is then 48.4 m/s. The average thrust can be found from equation 10.4 and is found to be 13.2 kN. The average drag can then be found by using the drag polars from chapter 8, and equals 24.4 kN. The ground drag can be calculated using equation 10.8.

$$D_{g_{av}} = \mu \cdot (W - L_{av}) \tag{10.8}$$

Where the ground drag coefficient μ is estimated to be 0.02 [97]. The average ground drag is then computed to be 3.7 kN. With these parameters the ground run distance can be calculated, the result of which is 948 m.

The second phase of take-off is the aerial phase. After lift-off, it is assumed that the aircraft's trajectory follows a circular path until it reaches its climb gradient. When the aircraft reaches screen height, the take-off is complete. In this case the initial climb gradient will be 10 degrees. The aircraft can reach this gradient as demonstrated in section 10.2.2. The radius of the transition to climb gradient can be determined using equation 10.9.

$$R_{TO} = \frac{V_{lof}^2}{g \cdot n} \tag{10.9}$$

In this equation, n is the take-off load factor. In this case a load factor of 1.15 is assumed [97]. The resulting radius of curvature is then 416 m. Using trigonometry the horizontal distance can be determined and a value of 122 m is found. To find the total take-off distance only these two results need to be combined, adding up to a total take-off distance of 1,071 m. It can be concluded that the SRJ110 will be able to take off within the take-off run available (TORA) of 1,199 m in sea level conditions.

The defining characteristics of the SRJ110 are its top mounted engines, which allow the aircraft to have a wing close to the ground. This allows it to take more advantage of the ground effect. The ground effect increases the amount of lift the wing produces whilst the induced drag is reduced. Here only the decrease in induced drag will be analysed. The increase in lift is not very significant and it is lost upon rotation so it is not accounted for in this analysis. The decrease in induced drag can be computed using equation 10.10.

$$\phi = \frac{16 \cdot \frac{h}{b}^2}{1 + 16 \cdot \frac{h}{b}^2} \tag{10.10}$$

Here, ϕ is the factor by which the induced drag decreases, b is the wingspan and h is the height of the wings above the ground. In the case of the SRJ110, the wing is located 1.7 m above the ground as determined by the landing gear length set in section 14.4. ϕ can then be implemented in the drag equation in the following way as shown in equation 10.11.

$$C_{D_{ge}} = C_{D0_{TO}} + \frac{C_L^2 \cdot \phi}{\pi \cdot A \cdot e_t} \tag{10.11}$$

From this equation, a drag coefficient of 0.177 is estimated. For comparison, the drag coefficient without ground effect in the same conditions is 0.193. Feeding this back into equation 10.7 results in a ground distance of 1,054 m. The total take-off distance when taking the ground effect into account is then around 17 m shorter in comparison to when it is not taken into account. It can be concluded that the ground effect does not have a very large impact on the take-off roll. Before the technical analysis it was assumed that the landing gear could be short since no engine clearance needed to be accounted for. In the end it was found that tail strike clearance was still a considerable limit. Therefore the ground effect could not be utilised as effectively as was predicted.

On a hot day in Arizona, temperatures could rise to as much as 50°C with an air pressure of 100,609 Pa. Using the ideal gas law, the air density is then 1.085 kg/m^3. If the engine thrust and the lift produced by the wings are adapted using air density from those conditions and subsequently imposed on London City, the aircraft would have a take-off distance of 1,293 m with a ground roll of 1,166 m, both excluding ground effect. So in this case, the take-off cannot be completed within the take-off run available (TORA). However, the ground roll distance still fits within the TORA. The take-off distance available (TODA), which includes the TORA and the clearways at London City is 1,319 m. So if the clearways are used for the climb phase the aircraft is still able to take-off at these 'hot and high' conditions. It should be noted that the highest temperature ever measured in the United Kingdom is 38.5 °C [98]. An analysis of other important hot and high airfields would be an interesting subject to investigate during the post-DSE design stage.

10.3.2 Landing Distance

Landing at London City also introduces challenges. Most notable is its short runway. Additionally, due the location of the airport in the middle of a metropolis, the glide slope for London City is set at 5.5°. In order to comply with CS25 Appendix Q regulations, a 6.5° approach needs to be attainable [11]. In this analysis the most stringent scenario of 6.5° will be used. Some further assumptions are that the maximum lift coefficient

is 2.6, the maximum landing weight is estimated at $0.9 \cdot MTOW$, the landing load factor equals 1.1 and the Oswald factor increases by 0.1 due to landing flaps [39, 97].

The landing phase exists of of the airborne phase, which starts at a screen height of 15.2 m, and a ground phase. Firstly, the airborne distance will be computed. Using equation 10.9 with the load factor for landing, the radius of curvature for the flare is found to be 415 m. Using trigonometry the horizontal distance travelled during the airborne phase is found to be 48.5 m. For the ground roll distance some assumptions needed to be made. It is assumed that the average lift coefficient with lift dumpers extended equals 0.5 based on data from the Fokker 70. Furthermore it is assumed that the average reverse thrust available is half the average take-off thrust. Additionally the braking coefficient μ_{la} is assumed to be 0.5 [97]. In order to find the average values for reverse thrust and drag, first the average speed during landing needs to be computed. The average landing speed is defined as the approach speed divided by square root of two. This can be seen in equation 10.12.

$$V_{L_{av}} = \frac{1.15 \cdot \sqrt{\frac{W}{S} \cdot \frac{2}{\rho} \cdot \frac{1}{C_{L_{max,land}}}}}{\sqrt{2}} \tag{10.12}$$

The zero-lift drag coefficient during landing, with extended spoilers, deployed landing gear and landing flaps is estimated to be 0.103 by extrapolating data from the Fokker 70. Using the above values, the magnitudes of the average drag D_{av}, average reverse thrust $T_{av_{rev}}$, and average brake drag $\mu \cdot (W - L_{av})$ can be determined. Subsequently, equation 10.13 can be used to determine the landing ground roll distance.

$$S_{brake} = \frac{W^2}{2 \cdot g \cdot S} \cdot \frac{2}{\rho} \cdot \frac{1.3^2}{C_{L_{max}}} \cdot \frac{1}{T_{av_{rev}} + D_{av} + \mu \cdot (W - L_{av})} \tag{10.13}$$

The resulting brake distance is then found to be 501 m. One second of reaction time before applying the brakes is added as an additional safety factor. This gives a final total landing distance of 617 m. FAR regulations require an additional safety factor to account for pilot skill of 1.67 [53]. Taking this into account the certified landing distance is 925 m. This is well within the available landing distance of 1,199 m.

On a wet runway, the brake coefficient μ decreases significantly, even more so with snow on the runway. In order to check compliance with landing on a wet runway, the braking coefficient for a wet runway has been estimated at 0.25 [97]. Using this new brake coefficient the landing distance can be calculated again for a wet runway. The result of this analysis is a FAR certified landing distance of 1,112 m at a London City operation maximum landing weight.

10.3.3 Balanced Field Length

The balanced field length is the distance at which during a take-off run the braking distance is equal to the distance remaining until rotation. The speed at this point is called V_1, or the decision speed since at this point the pilot needs to decide whether to continue the take-off or abort in case of an emergency. The total ground run required at London City has already been determined in section 10.3.1. Since the average acceleration is known and assumed constant, the distance until rotation can computed for every speed using equation 10.14.

$$S_{rem} = S_{rot} - \frac{0.5 \cdot V_{rot}^2}{a_{av}} \tag{10.14}$$

Where S_{rem} is the remaining time until take-off. The required braking distance at each speed can be calculated in a similar way. For the braking, it is assumed reverse thrust is not used and the engines produce no thrust. Furthermore, the braking coefficient μ is taken from section 10.3.2 on a dry runway. The average deceleration per speed can be found using equations 10.8, the drag polar of the aircraft and the fact that $F = m \cdot a$. The braking distance per speed can then be computed using equation 10.15.

$$S_{rem,brake} = \frac{0.5 \cdot V_{rot}^2}{a_{av,dec}} \tag{10.15}$$

In this equation, $S_{rem_{brake}}$ is the brake distance required at each speed and $a_{av_{dec}}$ is the average deceleration. The balanced field length for a dry runway is presented in figure 10.10.

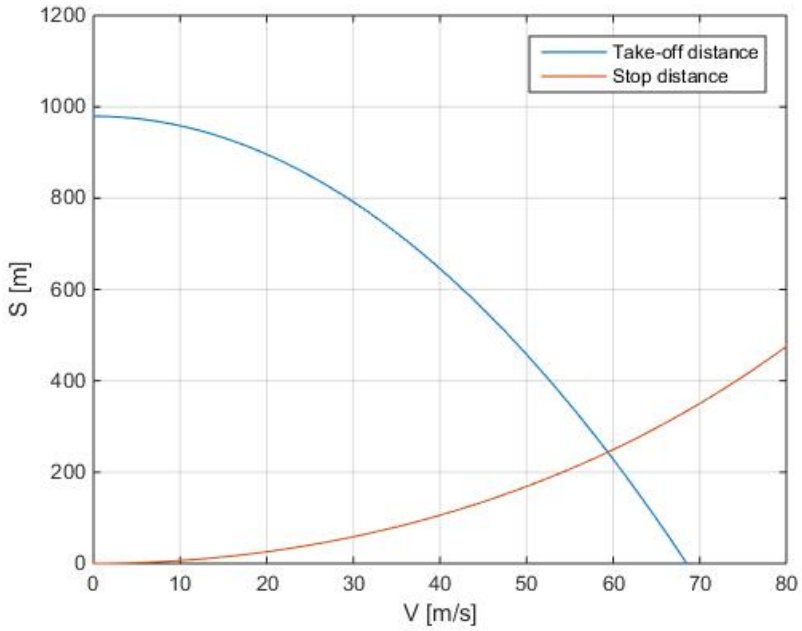

Figure 10.10: Balanced Field Length for a London City take-off.

From figure 10.10, it can be concluded that the decision speed for a dry runway with the maximum take-off weight at London City is equal to 59 m/s.

11 Subsystem Design

With the major systems in place, it is possible to design several subsystems. These subsystems play a crucial role in the safe and efficient operations of the aircraft. Without their proper functioning, the aircraft is inoperable. The to be designed subsystems are the fuel system, hydraulic system, weather hazard protection system and electrical system. These are discussed in sections 11.1, 11.2, 11.3 and 11.4 respectively.

11.1 Fuel System Design

The fuel system of an aircraft consists of numerous components, fusing together as one complicated system. Since all these components rely on one another, they have to be able to function independently in case of failure. Hence, the fuel system has to be designed with sufficient detail. First, all fuel system components are discussed, after which the fuel tanks are examined in more detail and finally, the integrated fuel system itself is presented [45].

11.1.1 Fuel System Components

The various components of the fuel system are treated hereafter separately.

Fuel Tank

The largest component of the fuel system is the fuel tank. For medium-range aircraft such as the project aircraft, the tanks are mostly integrated in the wings and fuselage, sealed with ribs and spars. The wing is a suitable storage location, since there is a lot of unused space available in the wing box. Additionally, in the wing the fuel introduces wing bending relief, which is beneficial for the structural design. Furthermore, the tank can be divided into multiple segments for a more optimal fuel and weight distribution. However, for roll manoeuvres the wing tank is less convenient. A possible solution for this issue could be anti-slosh baffles. These are valves that prevent the fuel from flowing freely between the root and tip.

An interesting feature to add to the fuel tank is the *self sealing* technology. To prevent an explosion of the fuel, the tanks are filled with an inert foam. The gas space above the remaining fuel is divided into thousands of small spaces which do not contain sufficient vapour to support ignition [99].

Pumps and Vents

Pumps and vents need to be incorporated in the fuel system for the fuel to be able to flow and to be pressurised. There are two main types of pumps used in the aerospace industry, namely booster pumps and transfer pumps. The booster pumps are suited to send the fuel to the engines at a requested fuel flow rate with a suitable pressure, whereas the transfer pumps are utilised for transfer fuel between tanks.

Piping and Valves

A complicated network of pipes and valves interconnects every single fuel-related component with one another, distributing the fuel to wherever it is needed. However, since all fuel systems are interconnected, it is recommended that parts of the network should be able to be isolated in case of emergency situations or fuel rate variations. Valves are the mechanisms which are supposed to fulfil this task of shutting off fuel pipes, preventing fuel from flowing through them.

Crossfeed

A crossfeed is essential for the fuel system, since the engines need to be provided with fuel at all times. If, for any reason, a section of the fuel system is isolated by the valves and one engine is not provided with fuel anymore, the crossfeed will come into force. One booster pump will then be providing multiple engines with fuel. To prevent head losses in the pipes, the crossfeed has to be installed as close as possible to the tanks and pumps.

Emergency Fuel Dump

In emergency situations where fuel is crucial, fuel will possibly needed to be dumped. If the aircraft has just taken off with maximum fuel and needs to make an emergency landing, it will dump fuel until a lower weight is reached. If a crash landing is expected, the amount of fuel needs to be reduced to a minimum to prevent

fuel ignition on impact. However, in most current regional or medium range jets a fuel dump system is not present. For this reason, it is chosen as an option for the aircraft. The dumping is done by a separate set of pumps, jettisoning the excess fuel.

Measuring Equipment
The amount of fuel present inside the tanks should be known at any time and should be provided to the pilots. This is done by measuring equipment. Typical equipment for modern day airliners are ultrasound and capacitance probes. A more classical, but less reliable, method is a flotation device attached to a probe, floating on the fuel surface.

11.1.2 Fuel Tank Volume

The fuel tank volume will be estimated in this subsection. The fuel tank is located in the wing box and in the fuselage at the wing-fuselage integration. The formula to calculate the volume is presented in equation 11.1. Please consult figure 11.1 for the clarification of the equation.

$$V = \frac{L}{3} \cdot (S_1 + S_2 + \sqrt{S_1 \cdot S_2}) \tag{11.1}$$

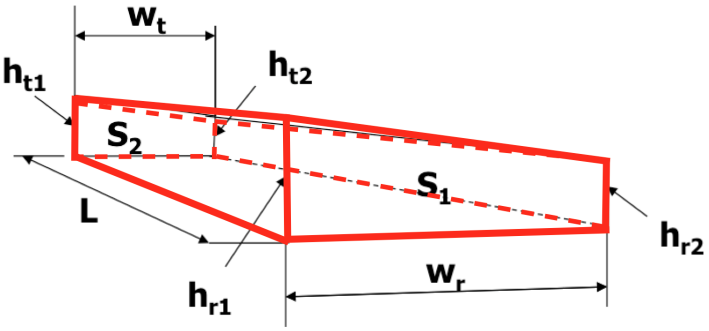

Figure 11.1: The wing box depicted as fuel tank with dimensions, corresponding to equation 11.1 [45].

The wing box layout and the spar location and spar height were explained in the section 9.2. Using the exact box dimensions, the result for the wing tank volume is $V_w = 12.5 m^3$. The fuselage also contains a centre tank, which holds the volume $V_c = 4 m^3$. This brings the total volume carrying capacity to a volume of V_t equal to 16.50 m^3. This is more than sufficient, since the required tank volume is 10.56 m^3, which follows from chapter 6. The required tank volume was calculated by dividing the maximum fuel weight by the density of jet fuel. However, since other systems and structure are present in the wing box, some of the space calculated is not available for fuel. Therefore, about 1.5 m^3 is subtracted from the previously calculated volume, which leaves 14 m^3 for fuel.

11.1.3 Integrated Fuel System

The final integrated fuel system design is presented in figure 11.2. Names of the components of the system are presented in the legend. The wing tanks were divided into three compartments, for optimal fuel and weight distribution, as stated before. Three different fuel flows can be distinguished, namely the engine feed flow in red, the transfer flow in yellow and the fuel dump flow in green. The engine feed system is characterised by the booster pumps, which are connected to each tank. In every tank at least 2 booster pumps are active for redundancy. Furthermore, the transfer system connects all seven tanks to ensure that fuel is able to flow from one tank to another. Next, the optional dump system has a valve in each tank to make sure fuel is able to be dumped when requested. The refuelling valves are located in the tip tanks, since the tanks will be filled from the tip to the root in order to obtain maximum bending relief. Lastly, in every tank measuring equipment is installed on two locations to have a reliable fuel estimation.

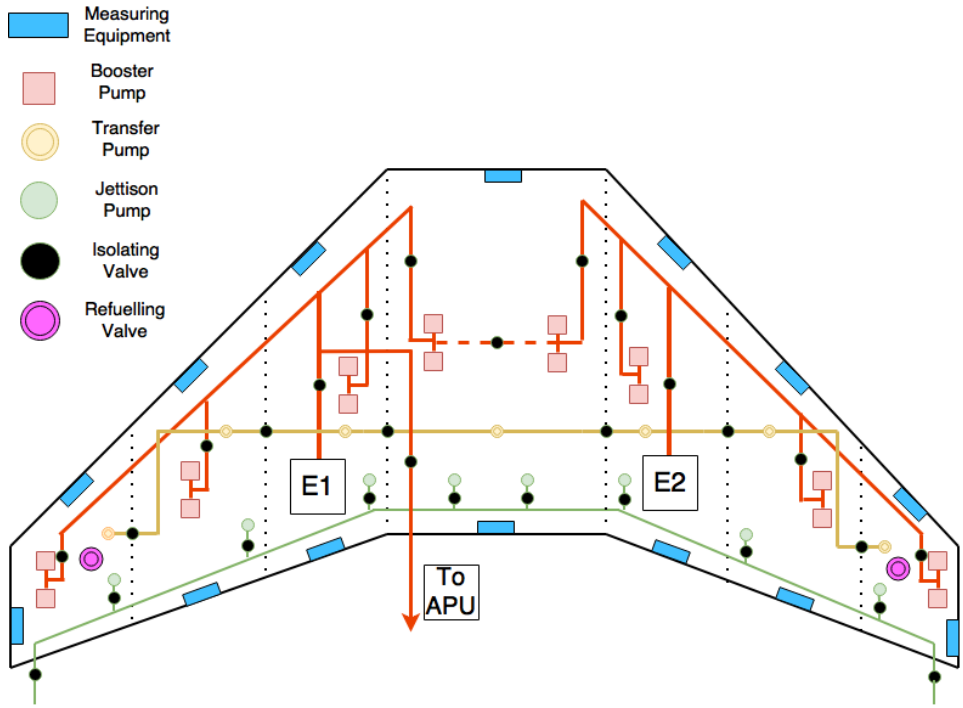

Figure 11.2: A schematic of the complete fuel system with all components integrated [45].

11.2 Hydraulic System

The hydraulic system of the aircraft powers all vital systems and actuators, such as the flight controls, high lift devices, landing gear, breaks, thrust reversers, etc. The fluid used in hydraulic systems is almost incompressible and is able to withstand and deliver high pressures. This is the reason why these systems are very reliable. There are three types of hydraulic fluid in use nowadays; vegetable, mineral and synthetic fluids. The vegetable fluid, which can cause sludge and corrosion, is mostly used in older aircraft with natural rubber seals. The mineral fluid is a more attractive product. It has good lubricating properties and inhibits corrosion and foaming. It is also stable and has a low viscosity change with temperature changes. However, this fluid does have a downside, namely it being very flammable. Lastly, the synthetic fluid is discussed. This fluid is less flammable than the mineral one, however it tends to attract moisture and corrodes certain plastics and paint [100]. To conclude, the most attractive solution that will be used in the aircraft hydraulic system is the mineral fluid, because of the many advantages.

The aircraft will be equipped with three independent hydraulic systems, since having hydraulic control at all time is of utmost importance. The most important flight controls, namely the elevators and the rudder, are placed in such a way that any of the three hydraulic systems can power them at any time. This is done because the aircraft always needs to have adequate controllability. Furthermore, the elevator feel, stabiliser trim, ailerons and yaw damper are fed with two systems. The other systems are fed with just one hydraulic system. One engine pump and one electric pump each power both the left and right system, whereas the centre system is powered by two electric pumps. A Ram Air Turbine (RAT) is also present to power the flight controls section of the centre hydraulic system if necessary. Please note that the air conditioning system will not be powered by the engine via the hydraulic system, but will be powered electrically. Please consult figure 11.3 for the detailed schematic. This is a schematic of a typical hydraulic system that will be implemented on this aircraft [101].

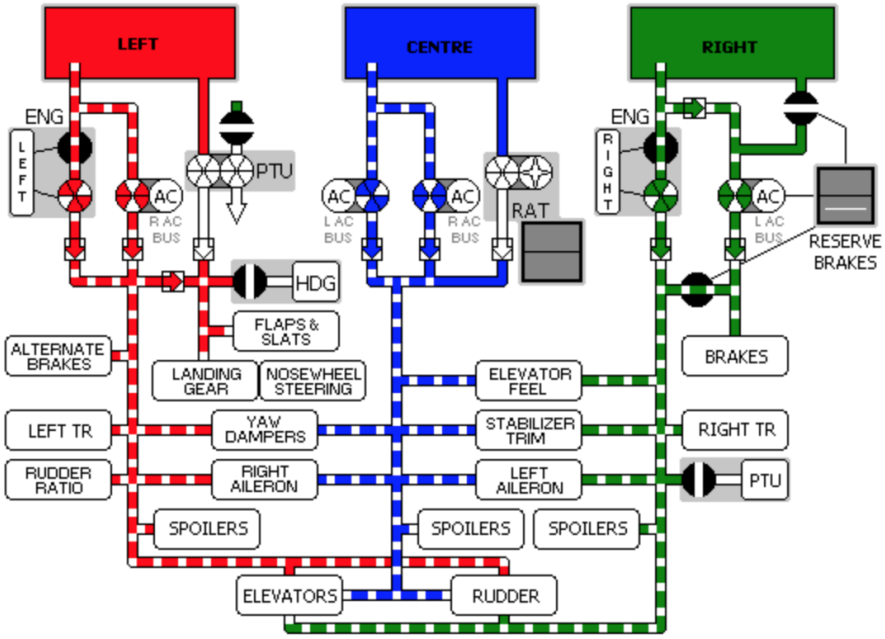

Figure 11.3: The hydraulic system of the SRJ110 [101].

11.3 Weather Hazards and Protection Systems

The most prominent weather hazard protection system is the de-icing system. Ice build-up is especially intense on the leading edge at the stagnation area. This translates to the leading edges of wing and tail surfaces. The ice deteriorates aerodynamic efficiency, can cause jamming of control surfaces, contaminates the engine intake with possible ice ingestion and clogs the intake of measuring instruments. The ice can be prevented by anti-icing on the ground and de-icing during flight.

For the system, three options are available. The first option is a heating duct in the surface leading edge, the second option are pneumatic boots and the third option is electric de-icing. The heating duct consists of heating elements located in the wing and tail leading edge. These elements produce and radiate heat. This heat prevents water in the air from forming ice build-up in the leading edges of the the wings and the tail and melt the ice already formed. The pneumatic boots are small cushions located on the leading edge that can inflate and break the ice present. Lastly, the electric de-icing consists of filaments that are heated, followed by the heating of resistor plates, separating the ice from the surface. The heating is done by using sending a current through the filaments and resistor plates. Figures 11.4a, 11.4b and 11.4c provide a visual description of the de-icing systems [45].

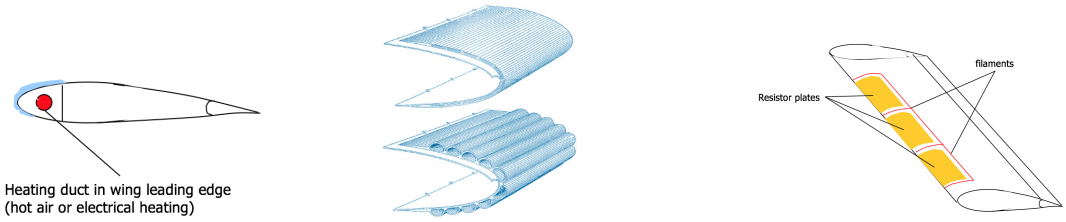

(a) De-icing system using a heating duct [45].

(b) De-icing system using pneumatic boots [45].

(c) Electrical de-icing system with filaments and resistor plates [45].

Figure 11.4: Various de-icing system configurations.

The most optimal solution for a medium-range sized aircraft is the widely used heat duct. Pneumatic boots are rarely used on modern day jet aircraft. The electrical de-icing system is also less feasible, due to its complexity.

Furthermore, lighting poses a threat to the well-being of the aircraft as well, even though aircraft accidents due to lightning strikes are very rare. For that reason, the aircraft should be able to withstand lighting strikes, without compromising the safety of the passengers and aircraft structure in general. In general, most aircraft are made from e.g. aluminium. Since it is a metal, its conducting properties are ideal for lighting protection as the aircraft behaves like a cage of Faraday. The beam will hit the aircraft, travel throughout the fuselage to the back and exit again. Since this aircraft will be made out of composites, these properties are not valid anymore, since this material is a lot less conductive compared to aluminium. To cope with this conduction deficiency, the composites are equipped with an embedded layer of conductive fibres or screens, such as a copper mesh, designed to carry lightning currents. These designs are thoroughly tested before they are incorporated in an aircraft [45]. The extremities of the aircraft will also be equipped with very small vanes in order to let some of the static electricity, generated by friction, escape.

Another vulnerable part of the aircraft is the fuel tank. A single tiny spark could be enough to set the entire aircraft on fire. Therefore, extreme precautions are taken to assure that no lightning current can cause a spark near the fuel system of the aircraft. The tank skin must be thick enough, joints and fasteners must be tightly designed, access doors and fuel filler caps must be designed and tested to withstand lightning, etc.

11.4 Electrical System

All systems that require electric power in the aircraft will be powered by the electrical system. In this subsection, this system will be described.

The system consists of four main parts, namely a generating, storing, distributing and controlling, and applying part. The energy is used by different aircraft systems, such as vital flight control systems and instruments, such as navigational and communicative systems, and passenger services, such as air conditioning, in-flight entertainment, lights, etc. Figure 11.5 presents the electric block diagram.

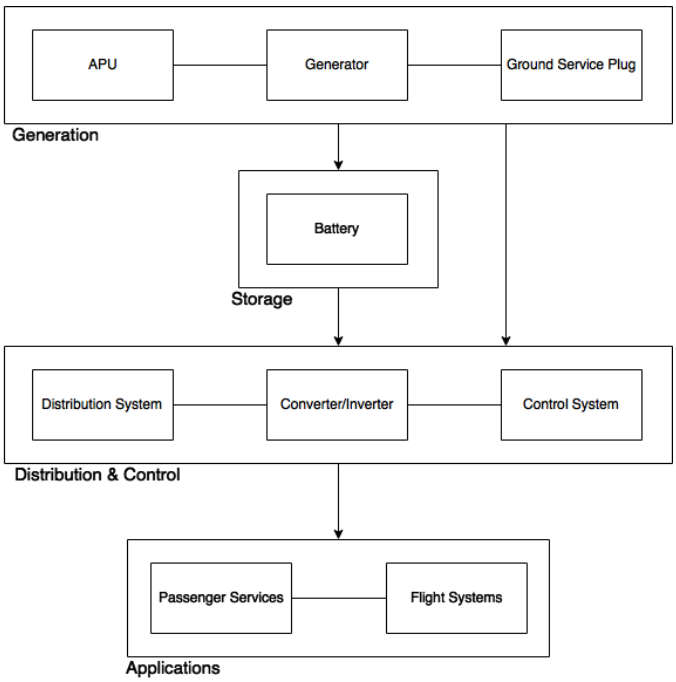

Figure 11.5: Electrical block diagram.

As can be seen in figure 11.5, the system consists of four main blocks. In the generation block, three main components are present. First of all, there is the generator, generating electricity at the engine. Secondly, there is the Auxiliary Power Unit (APU), which should be able to supply the aircraft with sufficient power if the engines are switched off. Thirdly, when the aircraft is standing on the ground, it can be connected to the grid of the airport.

The second main block is the storage block, with the batteries. Excess energy can be stored in the batteries and they can provide the aircraft with extra energy when requested or when there is no energy being generated.

The third block is the system management block. Distribution and control is performed here. The electrical energy is distributed over all wires in the powergrid of the aircraft. Also, the different parts of the electrical system are connected by fuses and circuit breakers, preventing the net from an electrical overload. and controlled, as well as converted or inverted to AC (alternating current) or DC (direct current) if necessary.

The fourth block is the applications block. As previously mentioned, it contains the passenger services such as air conditioning or lighting, as well as flight instruments and communicative systems.

11.5 Flight Control System

The flight control system is the last system to be discussed in this subsystem chapter. This system is responsible for the control of the aircraft and more specific its control surfaces and engines. It contains the software controlling the aircraft and the hardware parts actuating and performing the control manoeuvres. Its main components are the autopilots, flight computer, flight control unit (FCU), flight management system (FMS), sensors, throttle lever and stick.

First, the loop starts with the pilots. They can engage the autopilot and/or the auto-throttle to fly the plane, or operate the controls manually. Any output from these commands, done either manually or by the autopilot, is used as input in the flight computer. The computer sends a command to the flight control mechanisms. The control surfaces, e.g. ailerons and elevators, will deflect and the engines will provide thrust if required. The aircraft responds to the controls or engine input by rolling, pitching up, accelerating, etc. Sensors such as gyroscopes or accelerometers detect the changes and report back to the flight management system or show the changes via the cockpit instruments to the pilots. They can either give a new input manually via the stick or throttle, or, if the autopilots are selected, the flight management system manages the response. The autopilots, of which two are present for redundancy, receive their input from the FCU. This unit can have two modes, namely the manual mode, in which the pilots decide on the inputs for the auto pilot. The other mode is the managed mode, in which the flight management system determines the input for the FCU. The block diagram for the flight control system is provided in figure 11.6.

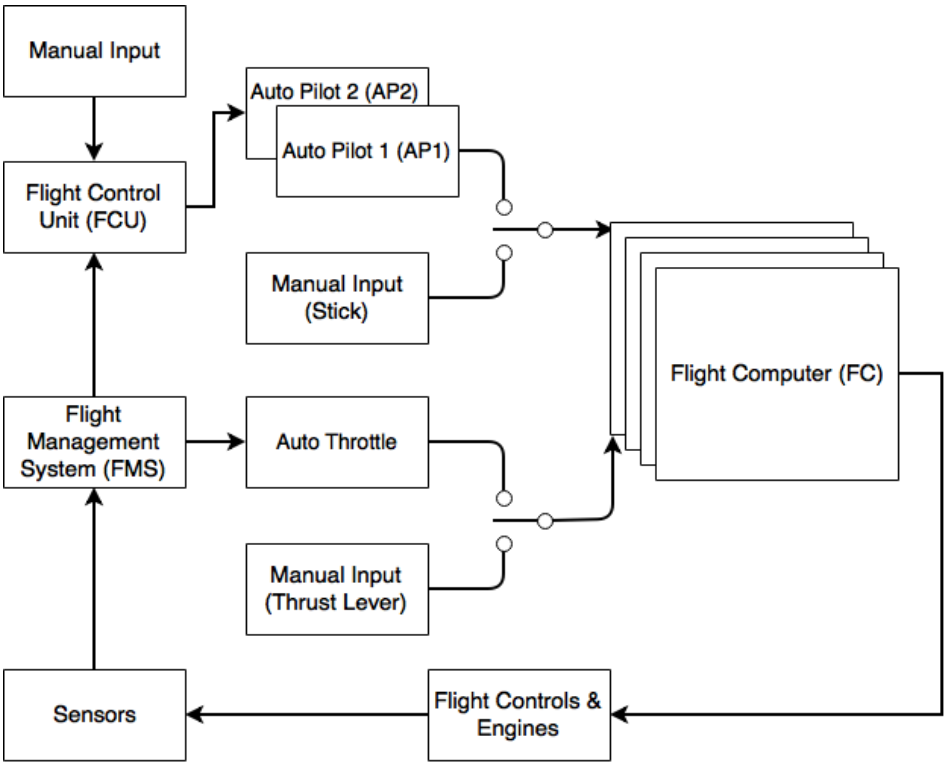

Figure 11.6: Block diagram of the flight control system of the SRJ110.

12 Noise Concept & Regulations

In this chapter, an introduction into aircraft noise is provided. Firstly, some general concepts of sound and noise are explained in section 12.1, together with the various methods used to measure aviation noise. This is followed by a general breakdown of the aircraft components that contribute to noise in section 12.2. Subsequently in section 12.3, the noise regulations and standards are elaborated on. Also, the certification method is explained. In section 12.4, the noise emission of comparable aircraft is presented and the design goal is determined. Finally, the noise contours are treated in section 12.5.

12.1 Noise Concept

Noise is defined as undesirable sound [102]. Sound is a disturbance in the air which is produced by a source, and heard by an observer. Sound propagates through the air as a wave, by transmitting acoustic energy to air particles. This energy causes particles to vibrate, which in turn induces pressure changes.

Sound is usually expressed in decibels dB, a logarithmic scale. For quantifying sound, in general a reference value denoted by subscript '0' is required. There are various measures to express sound. For instance, the Sound Pressure Level SPL uses the effective pressure p_e according to equation 12.1.

$$SPL = 10 \cdot \log_{10}\left(\frac{p_e^2}{p_{e_0}^2}\right) \tag{12.1}$$

Frequency is also a major factor for the human ability to observe sound. The SPL in dB for both the threshold of hearing and pain are dependent on the frequency. This is illustrated in figure 12.1.

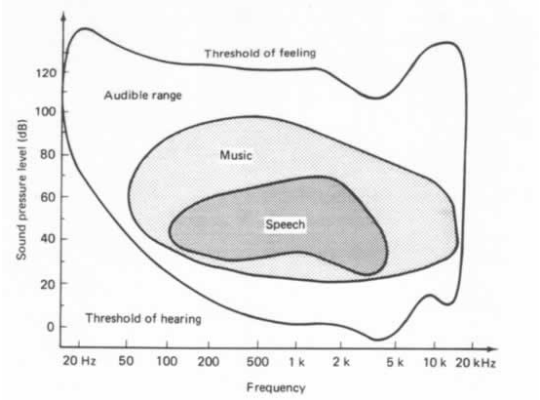

Figure 12.1: Graph showing the audible range in SPL as function of frequency [102].

The relative loudness at various frequencies can be included in the SPL using the A-weighting system. In general, the human ear experiences higher frequencies as louder, as can be seen in figure 12.2. Correction factors are applied to account for this in the weighted SPL, SPL_A, which is expressed in dBA.

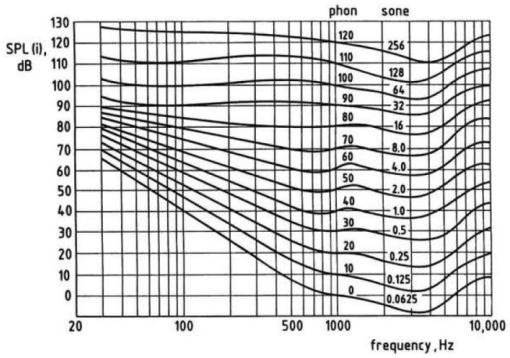

Figure 12.2: Graph showing the equal loudness lines for various tones [102].

Another important descriptor incorporates duration of the noise. The Sound Exposure Level SEL is the time integration of the sound pressure squared, according to equation 12.2. This is normalised to one second [103].

$$L_E = 10 \cdot \log_{10}\left(\frac{E}{E_0}\right) \tag{12.2}$$

Here, the Sound Exposure Level is denoted by L_E and is expressed in dB and E is the sound exposure which follows from equation 12.3.

$$E = \int_{t_0}^{t_1} p(t)^2 dt \tag{12.3}$$

Another way to quantify the environmental impact of noise and the time exposure, specifically caused by aircraft, is by using the Effective Perceived Noise Level ($EPNL$), measured in $EPNdB$. $EPNL$ takes into account the annoyance experienced by the human sense based on the perceived tones and duration [103]. The measure represents the time integration of loudness over the period where the noise is within 10 dB of the maximum value, as can be seen in figure 12.3. $EPNdB$ is the most common way to express aircraft noise and it is also used in regulatory documents and certification criteria. The computation of the $EPNL$ value however is lengthy and depends on frequency and time.

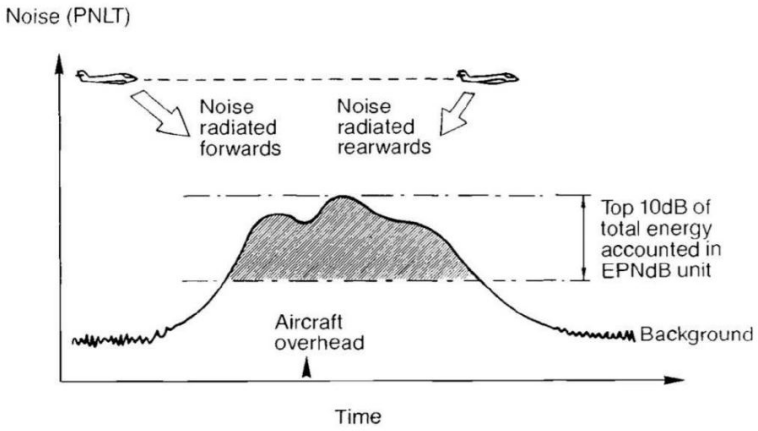

Figure 12.3: Image showing the $EPNL$ noise measurement [104].

For the purpose of this report, integration over time and the frequency weighting are neglected. Furthermore, a change in decibels is considered the same irrespective if it is noted in dB, dBA or $EPNdB$.

12.2 Noise Sources

Aircraft noise can be divided into two major categories: airframe noise and engine noise. Within these categories, multiple sources can be identified further [103]. Airframe noise consists of:

- Aerodynamic surfaces
  - Slats
  - Flaps
  - Wing
  - Stabiliser
- Landing gear
- Antennas

For a turbofan equipped aircraft, the engine noise consists of:

- Fan
- Jet
- Compressor
- Combustor
- Turbine

The contribution of airframe and engine noise to the total emission depends on the stage of the flight. During take-off when the engines are at a high thrust setting, the engine noise is dominant due to the fan and jet. During approach when the engines are set at idle, the airframe noise is about equal to the engine noise and the latter is mostly caused by the compressor and turbine. It is difficult to quantify the ratio of noise sources, as the various components also amplify or attenuate each other and because of the dependency on aircraft configuration and thrust setting. A coarse representation of the relative share for jet aircraft is depicted in figure 12.4.

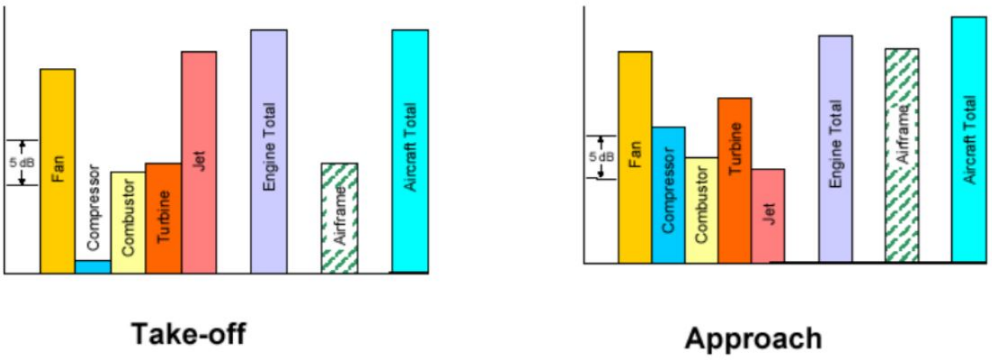

Figure 12.4: Illustration showing the relative share of airframe and engine noise during both take-off and approach [105].

12.3 Noise Regulations

One of the main stakeholder requirements is the reduction of noise emission, compared to the Avro RJ100 [29]. The derived system requirements are listed in section 2.2.4. In order to design for compliance with these requirements, more elaboration on the noise regulation and benchmark aircraft is necessary.

The Federal Aviation Regulations, FAR, are set by the US Federal Aviation Administration (FAA). The current FAA noise standards for jet and large turboprop aircraft are equivalent to the ICAO (International Civil Aviation Organisation, a UN body) Annex 16, Volume 1 standards, laid down by the Committee on Aviation Environmental Protection (CAEP) [8]. The European regulatory authority EASA (European Aviation Safety Agency) also uses the ICAO Annex 16 standards [106]. Therefore, the ICAO CAEP standards have been taken as leading to guarantee certification in the majority of the market. In the next subsections, first the noise measuring points are treated after which the emission limits and noise of comparable aircraft are listed.

12.3.1 Noise Measurement Points

For certification purposes, the aircraft noise is measured at three points: lateral, flyover and approach. These positions are illustrated in figure 12.5. Additionally, the measurements must be corrected for a reference atmosphere.

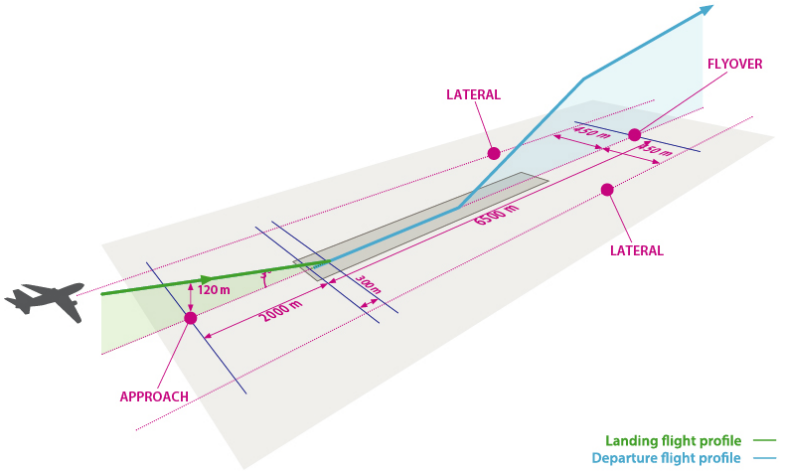

Figure 12.5: Image showing the lateral, flyover and approach measuring points [106].

Lateral Measurement The lateral measurement point, also noted as sideline, is the location where the noise level is maximum during take-off, measured on a line parallel to, and 450 m from the runway centre line. For certification purposes, sufficient measurement points have to be used to determine the maximum noise level. Additionally, these measurements must be made simultaneously at a symmetrical point at the other side of the runway [102].

Flyover Measurement For the flyover measurement, also known as community, the noise level is measured at a distance of 6,500 m from the start of the take-off roll, at a point on the extended runway centre line. The aircraft must use take-off thrust up to a certain altitude, depending on the number of engines, and must perform the measurement at maximum take-off mass. Above this altitude, the thrust may be reduced to the required value for a climb gradient of 4% or for level flight in case of one engine inoperative condition. The flight speed depends on the engine configuration. In terms of configuration, take-off settings must be used for the high lift devices until the measuring point. The landing gear may be retracted [102].

Approach Measurement The measurement on approach is conducted on the extended runway centre line, 2,000 m from the threshold. In the required configuration, the aircraft descends at a nominal glideslope of 3° with landing gear down at a speed not less than $1.3 \cdot V_{stall,land} + 10\ kts$. The height at the measurement point is 120 m. Additionally, the most critical approach setting must be used with respect to the high lift devices. The airplane mass must be the maximum landing mass [102].

12.3.2 Noise Limits

For each of the three measuring points, there are certain limits imposed by the ICAO standards. Furthermore, there is the so called cumulative margin, which is the linear summation of the three individual limits [107]. This is used for comparison purposes only and serves no physical use. The current standard for most commercial aircraft is *Chapter 4* since 2001. At the end of this year, or in 2020 depending on the aircraft mass, a new, more stringent standard becomes applicable; *Chapter 14*. This new standard will have a 7 $EPNdB$ margin compared to the cumulative limit from *Chapter 4*. The limits are a logarithmic function of the aircraft mass after a certain threshold, as can be seen in figure 12.6.

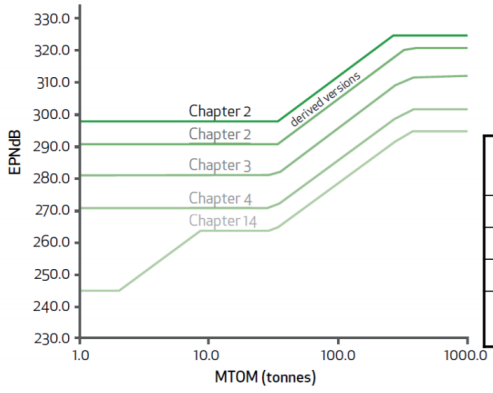

Chapter	Applicable Year	Cum Margin (EPNdB)
2	1972	Ch. 3 ~-16
3	1978	0 (Ref)
4	2006	Ch. 3 +10
14	2017 & 2020	Ch. 3 +17 (Ch. 4 +7)

Figure 12.6: Illustration showing the development of CAEP regulations [107].

The local limits, depending on the $MTOM$ in tonnes, are listed in equations 12.4 [103].

$$EPNL_{lateral} = \begin{cases} 94, & \text{for } MTOM \leq 35 \cdot 10^3\, kg \\ 80.87 + 8.51 \cdot \log_{10}(MTOM), & \text{for } 35 \leq MTOM \leq 400 \cdot 10^3\, kg \\ 106, & \text{for } MTOM \geq 400 \cdot 10^3\, kg \end{cases} \tag{12.4a}$$

$$EPNL_{fly-over} = \begin{cases} 89, & \text{for } MTOM \leq 48.1 \cdot 10^3\, kg \\ 69.65 + 13.29 \cdot \log_{10}(MTOM), & \text{for } 48.1 \leq MTOM \leq 385 \cdot 10^3\, kg \\ 106, & \text{for } MTOM \geq 385 \cdot 10^3\, kg \end{cases} \tag{12.4b}$$

$$EPNL_{approach} = \begin{cases} 98, & \text{for } MTOM \leq 35 \cdot 10^3\, kg \\ 86.03 + 7.75 \cdot \log_{10}(MTOM), & \text{for } 35 \leq MTOM \leq 280 \cdot 10^3\, kg \\ 105, & \text{for } MTOM \geq 280 \cdot 10^3\, kg \end{cases} \tag{12.4c}$$

12.4 Noise of Comparable Aircraft

In order to set the benchmark for the noise levels, the performance of current aircraft is investigated. EASA publishes the noise emission for each certified aircraft, for both jet aircraft and heavy propeller aircraft [7]. A selection of comparable aircraft is presented in table 12.1 including the engine type, $MTOM$ and individual and cumulative noise level. Per aircraft, multiple versions are certified. The values from the aircraft with the $MTOM$ closest to the design mass have been used, without any noise mitigation measures.

Table 12.1: Noise levels and characteristics of comparable aircraft [7].

Aircraft:	**Engine:**	***MTOM* [*kg*]:**	**Lateral*:**	**Flyover*:**	**Approach*:**	**Cumulative:**
Avro RJ100**	LF507-1F	46,000	88.1	86.1	97.6	271.8
Bombardier CRJ1000	CF34-8C5	41,640	90.9	84.1	93.3	268.3
Embraer E190**	CF34-10E5	46,000	91.6	82.4	92.5	270.1
Bombardier CS100	PW1524G	57,000	88.2	77.4	91.5	257.1
Design	PW1700G	45,730	83.1	81.1	92.6	256.8***

* In $EPNdB$.

** Aircraft is certified with respect to *Chapter 3*.

*** Cumulative value to meet the noise reduction with respect to the Avro RJ100.

It can be noted that the design value for the lateral measurement is lower than any of the reference aircraft performance, even the newest generation Bombardier C Series. In terms of both flyover and approach noise, the Bombardier C Series shows a significant improvement over peers despite the fact the aircraft is the heaviest in this comparison. Therefore, the new design technologies implemented in the C Series look promising for noise reduction. For the approach measurement, the CRJ1000, E190 and CS100 are closest to the design value, with the two latter aircraft already surpassing the requirement. This is important to note, as the approach emission is an indicator of the airframe noise.

Based on the $MTOM$ estimation, the cumulative certification limit is 282.9 $EPNdB$ based on *Chapter 3*. For *Chapter 14*, this value is 265.9 $EPNdB$. It can be seen that this value is lower than the requirement compared with the Avro, hence meeting the latter will automatically meet the certification standard.

12.5 Noise Contour

Besides the discrete measurement points, also the entire area affected by noise is of importance. These areas are mapped using so called noise exposure contours, of which an example is shown in figure 12.7. There are various levels used to determine the boundaries. For the customer requirement, a sound exposure level of 65 dBA is of interest. A decrease in contours means a smaller area around the airport is affected by noise. This is especially important for airfields in highly populated areas where the general public lives close to the runway.

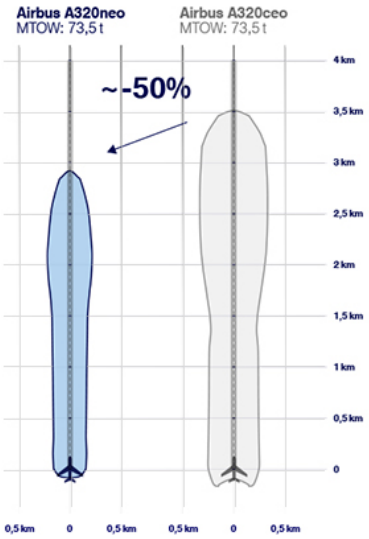

Figure 12.7: Image showing the noise contour for an A320 aircraft with current and new engine options. *lufthansagroup.com*

13 Noise Mitigation Measures

In order to meet the noise reduction requirement set by the customer, a range of mitigation measures has been explored. These are presented in the present chapter, starting with mitigation of aerodynamic noise in section 13.1. This is followed by measures to reduce power plant noise in section 13.2. A conclusion on the effect of these measures is provided in section 13.3. Finally, the noise contours are modelled in section 13.4.

13.1 Aerodynamic Noise Mitigation

This section focuses on aerodynamic and airframe noise mitigation. Airframe noise accounts for up to 69% of the total noise of an aircraft [108]. Landing gear, flaps and slats are the largest contributors to this noise source. Airframe noise is mainly caused by the vibrations caused by turbulent airflows, often due to open cavities or sharp edges. Aerodynamic noise is of particular relevance during the approach and landing phase, when the engines are at a lower thrust setting, all high lift devices are out and the landing gear is lowered. In section 13.1.1, certain measurements at wing level are discussed. In section 13.1.2, means to mitigate noise at the landing gear are considered. As previously mentioned, the main origins of aircraft noise are turbulence and friction. The goal is therefore to see how much noise could be mitigated by reducing the latter two causes, independent of aircraft configuration. Lastly in section 13.1.3, the choice of measurements for the design are discussed.

13.1.1 Wing

Wing noise, mainly coming from slats and flaps, consists of a large contribution to the total noise at approach, up to 31% [108]. In this section, some interesting mitigation measures for wing aerodynamic noise are discussed.

First of all, the flap noise mitigation methods are discussed. Flap noise can account for 6% of the total noise. This is an indicative value, not necessarily valid for every aircraft or configuration [108]. It is possible to reduce noise at the trailing edge itself by installing brushes on the trailing edge. These brushes can be made of steel or of a more flexible material, both having a comparable noise reduction. According to *Finez et al.*, brushes reduce noise due to "*the fine span wise fibres of brush [that] disorganise turbulent structures before they radiate sound*" [109]. This is one of the most promising - and tested - mitigation methods for the wing noise, with an average reduction of 3 dB on wing level. Secondly, a way to reduce flap noise even further is to close the cavity at the side of the flap. The noise from the side of the flap can be further decreased using brushes or a porous edge, or by using flap edge fences. The latter could lower flap noise by 7 dB [110]. Another method which looks promising is a flap with continuous mould line links (CML). These links make the flap blends into the wing at the edge. This reduces drag, and therefore noise. During tests, this flap configuration has demonstrated a noise reduction between 5 and 17 dB on wing level [111]. This idea is relatively new, so this concept has not been used on aircraft yet. Furthermore, it is also possible to look for different materials, for example porous material. When having a porous flap side edge, noise is reduced due to a pressure release. However, this also causes a loss in lift [112]. This method yields a noise reduction varying between 2 and 6 dB.

Slat noise also is a major point to improve, since it causes up to 25% of the total noise of aircraft [108]. Regarding leading edge noise, more specifically slat noise, three mitigation methods look promising. They all share the same principle, namely reducing the hole between the slat and the wing. Slat cove covers for example fill the cavity behind the leading edge slat. NASA has created a deployable and stowable mechanical design, reducing noise with 4 dB on wing level [113, 114]. Next to the slat cove cover, attachment of seals on the top and bottom of the slat can also be used, so that there is no gap between wing and slat when extended. Similar to the trailing edge brushes previously discussed, brushes can be applied at the trailing edge of the slat and/or at the leading edge of the wing, between wing and slat. This option is not great, however, as it decreases the lift coefficient generated by the slat making the landing speed go up, eventually increasing noise levels. Another method to decrease the slat noise is sealing the slat-track cut-out by sealing it. Tests in which the slat-track cut-out was just sealed with tape showed a decrease of wing noise by 2 dB. Lastly, a concept still under examination is the adaptive slat. This type of slat has a longer slat chord and also needs a positive overlap in order to not leave a gap after deployment [115]. It has a promising wing noise reduction of 5 dB [116]. Optimised slats could reduce the overall aircraft noise during approach by 0.5 $EPNdB$ [117].

13.1.2 Landing Gear

The landing gear can account for 31% of the total aircraft noise [108]. There are two methods already used on some aircraft to reduce this noise. The first is the use of fairings. A fairing smoothens the structural form of

the landing gear, making it more aerodynamic. Current fairings are still rather rough. The use of even more streamlined fairings would reduce noise even more. However, at this point in time, more advanced fairings are unrealistic since it is harder to house the mechanics of the landing gear, and retraction is complicated. Fairings currently in development can reduce the noise by 2.0 to 3.5 $EPNdB$, as tested on an Airbus A340 [114]. A second method is the use of splitter plates. This entails a plate that splits the air downstream of the landing gear, slowing down the air velocity, thereby reducing noise. This does not have a significant impact - about 1-2 dB. However, it is possible to combine it with fairings. There is also another possibility that is currently being investigated; a totally new architecture of the landing gear. A noise reduction of more than 4 dB on landing gear level is predicted with this design. However, these are still in a preliminary stage and may not be applicable anytime soon. In figure 13.1, examples of brushes and landing gear fairings are provided.

(a) Landing gear fairings. *Boeing*

(b) Brushes on the landing gear doors of the MRJ90.

Figure 13.1: Examples of noise mitigation measures for the landing gear noise.

13.1.3 Mitigation Measures

After investigating the principles and causes of airframe noise, as well as some of the different possible related noise mitigation measures, actual mitigation strategies for the airframe noise of the SRJ110 can be designed.

Firstly, the flaps are looked into. Along the trailing edge of the wing, metal brushes will be installed. Metal brushes were chosen over more flexible ones because of strength and precision. Metal brushes are more sturdy and durable, and will not deform as easily as plastic ones, making design, installation and functioning more accurate, allowing for noise reduction without creating more drag from non-aligned fibres. Noise reduction potential is identical for both types of brushes.

Filling cavities between the slots of the double-slotted flaps would decrease noise. However, this is something that can not be done. The beneficial aerodynamic properties and the increase in lift offered by slotted flaps are physically caused by air flow through these gaps. There are other ways to decrease flap noise though. At the outer edge of the flaps, wing fences will be installed. They will close the cavities at the edge of the flap as well as reducing turbulent flow and vortexes at the flap edges, minimising drag and noise [110]. Noise reduction potential of flap tip edges are up to 7 dB on flap level. The design of the flap edge was based on the research by the *National Aerospace Laboratory (NLR)*. The lay-out of the flap is shown in figure 13.2.

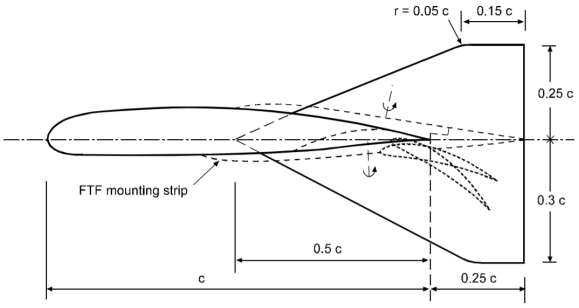

Figure 13.2: Flap tip fence design [110].

Leading edge high lift devices make up a large part of aerodynamic noise. Droop-nose flaps do not create gaps between the high lift device and the wing, something a slat does. However, the larger increase in lift that come with slats is needed for the aircraft to meet its requirements in terms of performance. Still, there is significant room for improvements concerning slat noise.

An innovative idea and concept that emerged for the SRJ110 is the use of wing fences to reduce noise. Wing fences are small vertical surfaces around the wing and more specifically wrapping around the leading edge. Historically, they have been used on high-sweep aircraft to stop air flow from flowing towards the swept tip, and eventually to avoid tip stall. A wing fence on a Caravelle is shown in figure 13.3, together with a visual representation of the design of wing fences. On each wing, two wing fences are placed, at the edges of the slat. Flexible brushes or a rubber edge make sure the connection between slat edge and wing fence is as smooth and airtight as possible. On top of that, the slat-track cut-out is sealed as much as possible.

(a) Wing fences on a Sud Aviation SE 210 Caravelle. *commons.wikimedia.org*

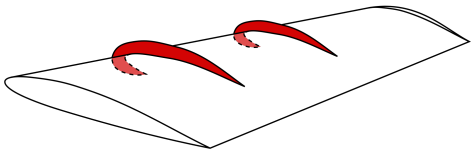

(b) Visual representation of wing fences. *commons.wikimedia.org*

Figure 13.3: Wing fences design.

The landing gear is designed as aerodynamically as possible. Fairings are used for that purpose. Nuts, bolts and holes are hidden or sealed from the outside in order to minimise flow disturbance. The landing gear bay closes and opens by means of two doors, similar to the SSJ100 for example, shown in figure 13.4. One, short plate is connected to the landing gear strut, so that when the landing gear closes inwards, the plate seals the gap by connecting to the wing - like in most aircraft of the type e.g. A320, SSJ100. The second door closes the fuselage bay where the wheels are stored from the other side, again, as can be seen in the figure. In the SRJ110, the fuselage bay door will close again after the landing gear is extended, which is nowadays rather common. By doing this, the cavity is closed and noise will be reduced. The plate attached to the gear strut itself will be aerodynamically integrated in the landing gear fairing. On top of that, the aft edge of the plate will have brushes, reducing noise once again.

Figure 13.4: Landing gear of the SSJ100. *tweetcs.com/SSJ100/*

13.2 Engine Noise Mitigation

As has become clear from figure 12.4 showing the relative noise share of aircraft components and the emission of the newest generation aircraft, the engine is the most significant component to meet the critical lateral emission limit. Within the power plant, there are two main noise sources: the jet and fan. Mitigation measures for each of these sources are presented in subsections 13.2.1 and 13.2.2, respectively. Subsequently, shielding of the engine is treated in subsection 13.2.3. Lastly, the final power plant configuration is presented in subsection 13.2.4.

13.2.1 Jet Noise Mitigation

Jet noise is caused by the exhaust of hot gasses behind the engine. When the fast flowing, hot exhaust mixes with the slow and colder ambient air, a turbulent region is introduced. The jet noise is proportional to the exhaust velocity V_e to the power of eight. Hence a decrease in this velocity can lead to a significant reduction in jet noise. In order to generate momentum, product of mass and velocity, required for propulsion, the

engine can either accelerate a small amount of mass very fast or accelerate a large amount of mass less fast. The latter is incorporated in modern turbofan engines by means of a bypass. Using this configuration, a large amount of air circumvents the core. This results in an efficiency increase as less air needs to be ignited with fuel, while sufficient momentum is still generated. A high bypass ratio also leads to a reduction in the exhaust velocity and thus jet noise. Another way to reduce jet noise is to shorten the mixing region of the exhaust gas and ambient air, or to accelerate the mixing. This can be achieved by adding serrated edges to the engine nacelle or exhaust, called chevrons, which smoothen the airflow. Chevrons are a common feature on present day aircraft such as the Boeing 787, 747-8i and 737 MAX, as shown in figure 13.5. According to *Martens*, chevrons can yield a, cumulative, noise reduction up to 5 $EPNdB$ [118].

Figure 13.5: Serrated edges, chevrons, on the rear of GEnx turbofan engines. *wired.com*

13.2.2 Fan Noise Mitigation

After the jet exhaust, the fan is the most prominent source of engine noise. Contrary to jet noise, fan noise does not significantly decrease at lower thrust settings, as can be seen in figure 12.4. The noise is mostly caused by the pressure changes in the front part of the engine where the airflow passes blades, stators and vanes. The pressure changes are required for an optimum thrust generation, hence reducing fan noise at the source offers limited possibilities. Parameters such as the blade tip clearance, blade diameter and count, and stator design influence the fan noise [119]. However, aerodynamic optimisation of the air intake is beyond the scope of this project. Up to a certain extent, it is possible to add acoustic liners to absorb radiated acoustic energy. This is a commonly used, passive method for reducing far-field noise. Because the fan, comparable with propellers, can also experience supersonic shock waves at the tip, the fan's blade diameter and RPM also have a profound effect on the noise. The size of the fans is linked with the engine efficiency and jet noise. A larger fan, and bypass, is preferred for the reduction of jet noise and efficiency. However, it is detrimental for fan noise. Hence a trade off has to be performed for the advantages and disadvantages of a larger engine blade diameter. Recent innovations in turbofan engines have focused on adding a gearbox between the fan and compressor-turbine, resulting in the geared turbofan shown in figure 13.6. Typically, the various engine components are connected by a single shaft. In this configuration, the rotational speeds of the compressor and turbine are limited by the maximum tip speed of the fan. The addition of a gearbox surmounts this limitation. When the shaft of the compressor and turbine can run at a higher rotational speed, less stages are necessary. This saves weight and increases efficiency. As the fan can spin at a lower RPM, the noise is also reduced. The disadvantages are the addition of the gearbox with is more complex and heavy, and some energy loss in the gear mechanism.

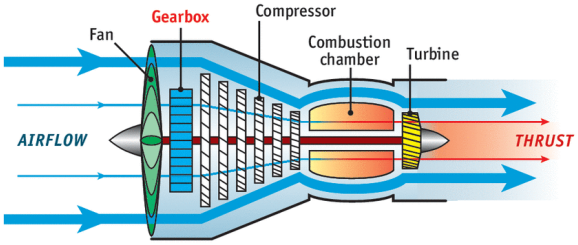

Figure 13.6: Image showing the interal lay-out of a geared turbofan engine. *economist.com*

13.2.3 Engine Noise Shielding

In subsection 12.4, it was demonstrated that new aircraft such as the Bombardier CS300 already are close to or surpass the flyover and approach noise limitations. This can be attributed to the newer, geared turbofan engines used. Only the lateral requirement is not met with a significant deficit of 5.1 dB. Hence, improvements to the engine alone are not sufficient. In order to reduce the engine noise on the lateral certification point, the engine position on top of the wing has been chosen. This way, the wing will shield part of the radiating noise. Research by the *FAA & Boeing* and *NASA* has predicted reductions specifically for lateral noise of 4.3 to 5 $EPNdB$ [120, 121]. A more recent study by *Powell, Sóbester* and *Joseph* demonstrated the effect of shielding by the wing on noise for a top mounted engine [122]. The results are shown in figure 13.7 with the sound pressure level as function of frequency, for the pure engine sound and the engine sound when the wing is there to shield it. The left graph shows the measurements of a microphone in direct line of sight from the engine, the second figure are the measurements of a microphone from whose perspective the engine is behind the wing.

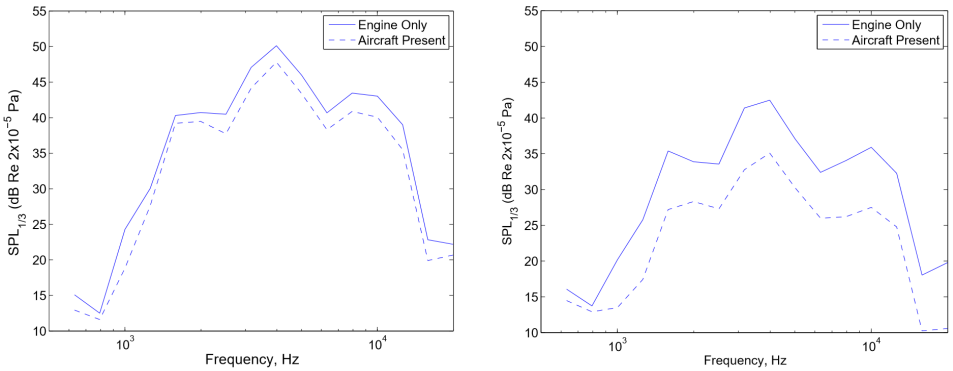

Figure 13.7: Sound pressure level of engine sound in function of frequency recorded by microphones (a) in direct line of sight of the engine and (b) in the shadow zone [122].

Although it is not possible to translate the results from the experimental measurements to the effect of a full scale aircraft where other noise sources are present, the experiment once again shows that the engine on top position can offer significant improvements to (lateral) noise.

Another effect of the engines mounted on top of the wing is the lower required ground clearance. This allows for a shorter landing gear, which is beneficial for the aerodynamic noise in approach condition. Halving the landing gear may lead to a decrease of 3 dB on component level.

An additional way to reduce noise from the engine is an enlarged nacelle on the outboard side. This can shield part of the fan noise propagating to the side. However before incorporating this measure, the aerodynamic effects should be investigated to prevent efficiency loss in the engine.

Noise propagation can also be limited by the addition of an absorptive coating on the fuselage close to the engine. This prevents reflection and can reduce the total emitted noise from the aircraft. Electrospun nanofiber is a promising new material that absorbs both low, medium and high frequency sound while still being lightweight, according to *Asmatulu, Khan* and *Yildirim*. The research focused on reducing cabin noise, hence more investigation is required to determine if the nanofiber material is beneficial for environmental noise as well, and if it is safely applicable to the outer fuselage.

Nevertheless, the cabin noise cannot be neglected considering the engine location close to the passenger compartment and the electrospun nanofibers may be incorporated regardless. Other options to reduce cabin noise are more insulating materials in the fuselage and the use of active noise cancelling by means of anti-noise. Another way to reduce cabin noise is elimination of vibrations. Bombardier has successfully implemented a system called Active Noise and Vibration Suppression (ANVS) in the Q400 [123]. Microphones in the cabin measure the noise levels and send this information to a computer together with the engine information. The processor consequently controls Active Tuned Vibration Absorbers (ATVA) in the fuselage. These devices initiate out-of-phase counter vibrations to reduce the original vibrations. Although this system has been developed for propeller aircraft, it is also implemented in the Bombardier Challenger 604. Hence, it is possible to implement this in the SRJ110. Concluding, the cabin noise will be mitigated by a combination of extra shielding, insulation and active noise control. This will ensure the sound levels will not exceed current aircraft due to the new engine placement and passenger comfort will be maintained.

13.2.4 Power Plant Configuration

As is clear from subsections 13.2.2 and 13.2.3, there is a trade-off for the fan and engine dimension for the jet and fan noise. For (fuel) efficiency, weight and required thrust reasons, a geared turbofan engine has been chosen in section 6.4; the Pratt & Whitney 1700G. This engine has a bypass ratio of 9:1 [3]. This is 25% lower than the PW1500G installed on the Bombardier CS100. This will result in a fan noise reduction compared to the CS100. This may be at the expense of some efficiency and jet noise. However for both these characteristics, there is a design margin. Furthermore, the jet noise will be mitigated by the addition of nacelle and exhaust chevrons. In order to use the shielding of the wing as much as possible, the engine should be as inboard as possible. However, there also has to be sufficient clearance between the engine and fuselage for noise and safety reasons, and to provide a clear path from the emergency exit. Therefore, it has been chosen to place the outer edge of the engine on the kink. This results in a clearance of 1.81 m between the engine and fuselage. The engine is placed at the back of the wing to increase the wing area that shields the inlet and thus fan noise. The spanwise position of the engine can be seen in figure 13.8. The longitudinal position of the engine is not performed at this stage. For optimisation, an accurate noise model is to be created in the detailed design phase.

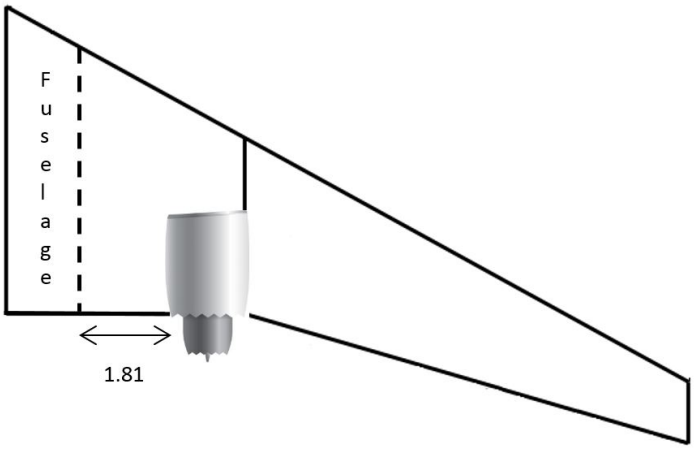

Figure 13.8: Image showing the spanwise location of the engine and the clearance with the fuselage. Dimension expressed in m.

13.3 Final Noise Reduction

Various noise mitigation measures have been presented in the previous sections, both for the aerodynamic and engine noise. Because of the complex nature of aircraft noise with attenuation and absorption of many different components and the non-linear dB scale, it is not possible to accurately quantify the total noise reduction of the aircraft with all mitigation measures implemented. This would require elaborate noise modelling of the aircraft, which is beyond the scope of this project. As explained in the Mid-term Report, even conceptual models such as *INSTANT* require a plethora of parameters which are not available in this stage [31] . E.g. for *INSTANT* over 40 specific input parameters involved, often relating to detailed engine characteristics such as jet density and pressures in the combustors [103]. Therefore, it has been decided to apply to noise mitigation measures on a comparable aircraft for an estimated noise emission. Based on the current design standards and (engine-)technology, the Bombardier CS100 has been chosen as reference aircraft. As has been explained in subsection 12.4, the lateral, fly-over and approach noise levels are 88.2, 77.4, 91.5 dB, respectively [7]. It is stressed this aircraft's $MTOM$ is 12 tonnes higher compared to the SRJ. The same aircraft design at a lower weight will most likely result in lower noise levels. The lateral noise emission is the most critical requirement to meet, as the CS100 has a deficit of 5.1 $EPNdB$ compared to the design requirement. As explained in subsection 13.2.3, multiple research studies have predicted a decrease of 4.3 to 5 $EPNdB$, specifically for lateral noise, for an engine on top configuration. Taking a the most conservative value, this measure would result in a noise emission of 83.9 $EPNdB$. The chevrons, additional acoustic liners, fairings and wing fences and absorbing layer on the fuselage yield an additional noise reduction. For flyover noise, the same mitigation measures will ensure compliance with the design requirements. Additionally, some operational procedures can reduce noise on this measurement location. These methods are explained in section 17.3.

For the approach noise, generally engine noise reduction is less effective due to the low thrust setting.

However, as has been explained previously, the fan noise does not significantly decrease in this flight phase. Hence the shielding and absorption will offer some noise reduction. The aerodynamic noise is the most profound and it must be stressed that the baseline value of 91.5 dB from the CS100 is an overestimation compared the SRJ110. The Bombardier has a MLM about 8 tonnes heavier and a wing area which is 28% larger than the SRJ [7, 124]. More weight and area results in more noise. Together with the slightly smaller landing gear, fairings, wing fence and brushes the approach limit will be easily met.

In conclusion, the noise emission requirements for the lateral, fly-over and approach measurement points will be met and exceeded with the proposed design additions. Considering all the modifications and baseline values of the heavier and larger reference aircraft, a respectable margin is attained for the noise reduction. Simulations are to be performed in a later design stage, followed by full scale testing to determine the final noise emission.

13.4 Integrated Noise Model Analysis

In order to determine extent to which the requirement on the reduced noise exposure area is met, an analysis has been conducted using the Integrated Noise Model (*INM*). *INM* is an internationally acknowledged tool for modelling noise impacts around airports. Using this tool, noise decay can be visualised and the exposed area to noise levels larger than 65 dBA can be determined. First of all, in subsection 13.4.1, the way the model is applied is highlighted. Next, in subsection 13.4.2, the results of the analysis are discussed and compliance with the requirements checked.

13.4.1 Model Explanation

INM requires two main input documents. First of all, a trajectory file is required. The trajectory file should provide the x, y and z coordinates of the aircraft during the approach, ground roll and take-off phases, as well as the corresponding net corrected thrust per engine at each data point. It is made sure that the trajectory is in compliance with that of the noise certification measurements as shown in figure 12.5. The exact trajectory of the SRJ110 was built based on the performance analysis parameters presented in sections 10.3.2 and 10.3.3. For the Avro RJ85, a different approach was required due to the lack of input data. Based on *FlightRadar24* data, some preliminary estimates on the aircraft performance parameters such as drag and thrust setting were made. By determining the rate of climb and airspeed from *FlightRadar24*, the total drag of the aircraft could be estimated during the initial climb-out after take-off by using the rate of climb equation 10.3. To use the equation, an estimate of the aircraft weight had to be made and the thrust had to be predicted using the thrust correction equation 10.4 and corrected for air density effects. The predicted zero-lift drag coefficient for the Avro using this approach is found to be 0.056, only slightly higher than the SRJ110. The model for the Avro RJ85 has been tweaked by an expert in the field of aircraft noise to obtain as reliable reference data as possible by matching the noise levels of the *INM* analysis with those determined in the noise certification database [7]. The trajectories are a rudimentary estimate of a take-off and landing path, assuming a constant rate of climb and descent. For approach certification, the aircraft needs to fly at a glide slope of 3°, and the approach trajectories are therefore along the same flight path. The corrected net thrust and the airspeed are still different. The flight trajectories are visualised in figure 13.9.

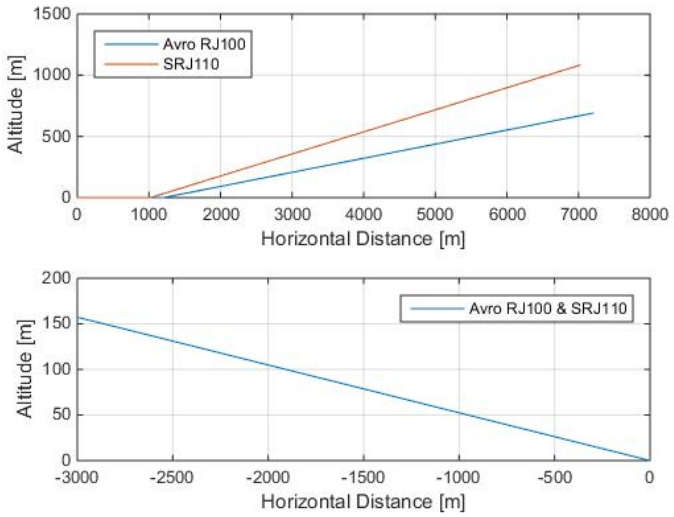

Figure 13.9: The projected trajectories used for noise modelling for the Avro and the SRJ110 during take-off and approach.

The top figure represents a crude take-off ground run and climb-out. The lower figure shows the three degree glide slope. It can be seen that the SRJ110 has a higher climb rate than the Avro. This can have a significant impact on the measured noise due to the increased distance from the measuring points on the ground.

The second input file required for *INM* is a table with measured noise levels for different aircraft configurations and thrust setting. For the Avro RJ85, the available data of the BAe 146-200 has been used as reference noise data. For the SRJ110 however, because the aircraft is still in development, such detailed noise measurement tables do not yet exist. Therefore, the noise levels of the SRJ110 were estimated by altering the tables that were available for an Embraer E190. Although it was not possible to accurately quantify the final noise reduction, as explained in section 13.3, a conservative and rough estimation was made for use in the model.

For flyover noise, the noise reduction compared to the Embraer E190 was taken as 3 dB. The PW1700G claim a noise reduction of 3 dB at engine level compared to engines that are currently in use [41]. Together with the added chevrons and increased acoustic liners, a 3 dB reduction on aircraft level seems feasible. The aerodynamic improvements are expected to contribute another 1 dB in noise reduction, resulting in a total reduction compared to the E190 of 4 dB. This is quite a conservative value as the noise certification values differ 5 dB between the Embraer and the newer CS100, another benchmark used. These values, however, often give a distorted impression as 'tricks' are applied during certification. Taking everything into account, a 4 dB noise reduction with respect to the E190 seems a valid estimate.

Aerodynamic sources are responsible for the majority of the noise generated during approach. The inclusion of the landing gear fairings, brushes and flap tip fences are assumed to yield a 2 dB reduction on aircraft level. The fan noise, which does not decrease significantly with thrust settings as explained before, has also been reduced using multiple methods such as a lower bypass and acoustic liners. Hence another 1 dB noise reduction is added, resulting in a total of 3 dB reduction. On the certification points, the Bombardier CS100 has 1 dB lower noise emission compared to the E190. However, the former aircraft is significantly heavier which places an even more important role in aerodynamic noise. Additionally, not only aerodynamic noise was mitigated but also fan noise. Hence a total reduction of 3 dB is plausible.

In addition, some alterations were made to the measured noise levels further away from the aircraft. It was ensured that the noise decay trend present in the E190 data is present in a similar manner in the SRJ110 data. Last but not least, the table has also been extended with a new entry, representing the maximum thrust setting of the SRJ110. The noise level at the source for this new, high-thrust setting has been determined by first extrapolating the relation between thrust setting and source noise for the E190 to the new thrust value. Afterwards the noise reduction values as discussed before in this section have been applied. This approach ensures that the noise tables for the SRJ110 are as accurate as possible in the current design stage.

13.4.2 Discussion of Results

With all the input data determined, the program can finally be used. First of all, the departure noise contour for the Avro RJ85 was determined. This noise contour is presented in figure 13.10a. Next to the departure noise contour of the Avro RJ85, the departure noise contour of the SRJ110 is presented in figure 13.10b. In both figures, the horizontal distance value of zero corresponds to the point of brake release on take-off roll. The lateral distance is set zero at the centre of the runway. This implies that the lateral distance should actually be read as an absolute value.

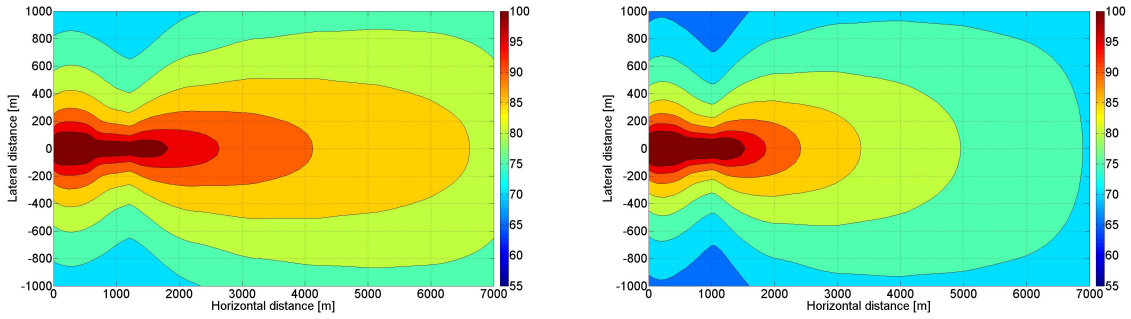

(a) Departure noise contour for the Avro RJ85 [dBA].

(b) Departure noise contour for the SRJ110 [dBA].

Figure 13.10: Take-off noise contours for both the Avro RJ85 and the SRJ110.

With respect to the departure noise contours, several remarks can be made. The SRJ110 offers a significant noise reduction over the Avro RJ85 in both the lateral as well the longitudinal direction. The lateral noise reduction is most present during the climb out phase, where the increased departure performance of the SRJ110 plays an important role. Very close to the aircraft, the noise levels of the SRJ110 are actually a bit higher than that of the Avro RJ85. It is expected that this is a direct effect of the higher thrust setting the SRJ110 uses on the take-off trajectory. The general shape of the noise contours of both aircraft is the same. This is an indication that there are no significant discrepancies between both aircraft and the model shows consistent results.

For the arrival procedure, noise contours can be created as well. The arrival noise contour for the Avro RJ85 is shown in figure 13.11a. In similar fashion, the arrival noise contour of the SRJ110 is presented next to that of the Avro RJ85, in figure 13.11b. Please note that the negative horizontal distance indicates the distance until the touchdown point on the runway is reached. The touchdown point is located at zero horizontal distance. The lateral noise axis follows from the same principle as explained in the departure noise contour.

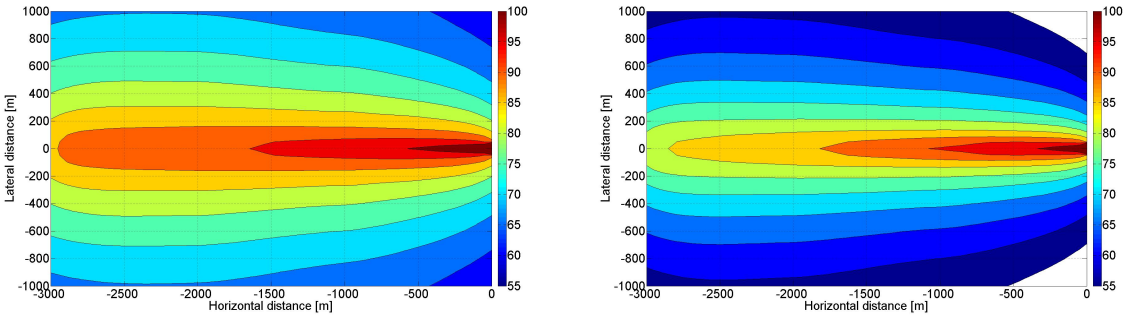

(a) Approach noise contour for the Avro [dBA].

(b) Approach noise contour for the SRJ110 [dBA].

Figure 13.11: Approach noise contours for both the Avro RJ85 and the SRJ110.

With respect to the approach noise contours the following statements can be made. The SRJ110 once again has a significant noise reduction over the Avro RJ85 in both the lateral and longitudinal direction. The general shape of the figures is again equal which indicates consistency in the application of the model.

With the noise contours displayed, the next step is to check if the exposed area to sound exposure levels greater than 65 dBA is indeed reduced by 30% as stated in the requirements. For both the Avro RJ85 as well as the SRJ110, the total area where noise levels higher than 65 dBA are measured is summed. These summed values, as well as the percentage reduction the SRJ110 offers over the Avro RJ85, are presented in table 13.1

Table 13.1: The measured noise (in dBA) exposure area for both aircraft and corresponding percentage reduction.

	Avro RJ85 noise area [km^2]:	**SRJ110 noise area [km^2]:**	**Reduction [%]:**
Departure	41.1	31.6	23.1
Approach	9.2	4.0	56.5
Total	50.3	35.6	29.2

From this table it can be concluded that the 30% area reduction is not met by only a small margin. There are however some important remarks that have to be added about how this value is constructed. The *INM* model does not take into account the fact that the wing shields some of the engine noise due to the engine location on top of the wing. According to figure 13.12, for engines placed on the wing, the shielding should decrease the flyover noise by 1.49 dB [125]. For the sideline measurement point, the aircraft wing shields only part of the engine noise due to the limited sideline angle between the aircraft engine and the noise measurement station. A conservative estimate has been made that this reduction should be in the order of approximately 1 dB. With these additional noise reduction figures, it is more than likely that this yields the additional 0.8% reduction in the noise contour area in order to satisfy the requirement. Also when taking into account the rather rough noise reduction estimation, the noise contours should be sufficiently reduced to meet the requirement.

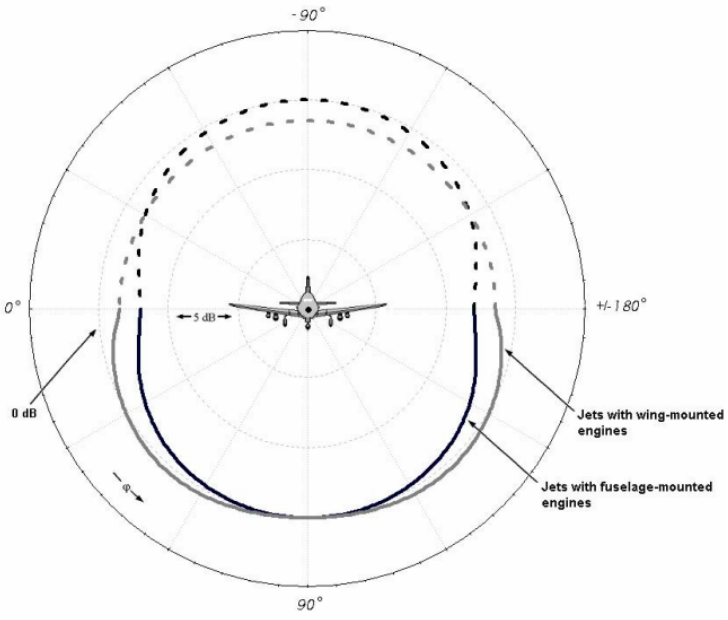

Figure 13.12: Shielding effects by alteration of engine position [125].

With the noise contours determined, a natural step would be to check the noise levels at the certification points as shown in figure 12.5. The results of the analysis are shown in table 13.2

Table 13.2: *INM* measured noise levels at the certification points.

	Avro RJ85 noise level [$EPNdB$]**:**	**SRJ110 noise level** [$EPNdB$]**:**
Approach	97.6	89.0
Sideline	88.1	82.1
Flyover	86.9	75.9

As can be observed from the table, the SRJ110 scores significantly better at the noise certification points with margins of 8.6, 6.0 and 11 $EPNdB$ to the Avro RJ85 on approach, sideline and flyover noise,+ respectively. This also means that the requirement to be 5 $EPNdB$ below the Avro RJ85 on FAR noise certification points has been met. This is of course within a certain margin of error of the model as discussed earlier. On the other hand, the effects of engine noise shielding have not been included yet. All together this estimate, given the circumstances, is the best that could possibly be made at this stage of the design. The results are very promising however and the SRJ110 seems to live up to its expectations as the best in class regional airliner available on the market.

14 Final Aircraft Design Configuration

In this chapter, the final design configuration of the SRJ110 is unveiled. The design choices are derived from the technical analyses performed in chapters 7 to 10. To come up with such an aircraft configuration, several iterations have been undertaken. Only the final design properties are hereafter presented. First, the fuselage and cabin layout are discussed in section 14.1. This is followed, in section 14.2, by a summary of the wing design previously analysed in chapter 8. As a result from the Stability & Control analysis, the tail and the landing gear design are derived. Findings are provided in sections 14.3 and 14.4, respectively. Furthermore, technical drawings are available in appendix B for a complete and detailed overview of the design lay-out.

14.1 Fuselage

The first feature of the fuselage design presented in this section consists of the internal layout of the cabin. Since the customer desires a capacity of 110 passengers at a certain comfort level, the interior is designed for at least that specific number.

Firstly, the seating configuration has to be selected. In the relevant class of aircraft, 2-2, 3-2 and 3-3 seating configurations are commonly used. The fuselage diameter plays a significant role in generating drag. Generally, a 10% increase in fuselage diameter yields a 1.5 - 3.0% increase in drag [39]. Furthermore, passengers generally prefer not to sit in a middle seat [126]. Based on those considerations, a 2-2 row configuration is chosen. A seat width of 47 cm is decided upon, which is 0.6 cm wider than in the Embraer E190 and E190-E2, equal to the Sukhoi SJ100, but 1.25 cm smaller than the "best-in-class" CS100. The aisle width is determined in compliance with the CS25 regulations, as well as favourably compared to competitors. CS25.815 states that the aisle width should be minimum 38 cm up until 64 cm above the cabin floor, and more than 51 cm from 64 cm above the floor up. An aisle width of 50 cm is chosen at the narrowest point; in between the armrests. As the armrests are located at a height of around 55-60 cm, this complies with the certifications. The aisle width is equal to that of the Embraer E-Jets, wider than in the CS100 and about 3 cm smaller than in the SSJ100. The height of the aisle is equal to 2 m.

Knowing the seat and aisle width, and choosing for the standard 5.1 cm wide armrests, the cabin width can be calculated [126, 127]. Accounting for a 5 cm margin between armrest and cabin wall at each side (as in reference aircraft), a minimum total cabin width of 279 cm at the widest point is determined. However, taking into account the curvature, the base of the seats eventually forms the most critical width requirement. From this follows a maximum widest-point width of 283 cm. From extrapolation based on reference numbers, the total horizontal outside fuselage diameter is estimated to be equal to 303 cm. For 110 passengers in a full 2-2 configuration, 28 rows are required. More specifically, the fuselage has 27 full rows and one half row, located at the back near the lavatories. A representation of the fuselage cross-section of the SRJ110 is given in figure 14.1.

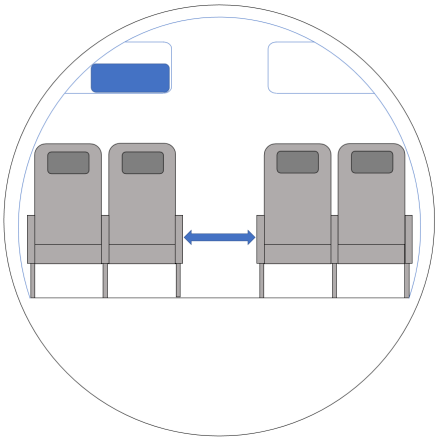

Figure 14.1: SRJ110 economy class cabin. All dimensions are to scale.

The overhead bins are required to have a capacity of at least 5 m^3. Their cross section is sized comparable to reference aircraft. On top of that, it is made sure that it is possible to store a suitcase with the maximum

dimensions most European carriers allow [128]. That suitcase, with dimensions of 56 cm x 45 cm x 25 cm, is visualised in figure 14.1 and can fit in the overhead bins even with its longest side placed in lateral direction. Then, a volume estimation was performed. By assuming the bin cross section as a triangle and a rectangle connected, a cross section area of 0.2025 m^2 was found. This area is then multiplied by the length and by two, for the two sides of the cabin. The length was corrected for partitions and lost space. A total volume of 8.1 m^3 was found, easily fulfilling the requirement. This is a major plus, as with more space, boarding will take place faster and with less complications.

For hold luggage, a volume of 12 m^3 has been determined previously as requirement, based on nominal luggage allowance and dimensions. Again, this was validated. The cross section of the cargo space was determined following the formula for the area of a circle section. This area is then multiplied by the length and corrected for tail slope, door locations and wing intersection and landing gear stowage. A volume of around 15 m^3 is found. The requirement is met with room to spare. This would allow for a bit more cargo to be taken on board, or for offering a fuselage fuel tank as an option for interested customers.

The amount and type of emergency exits have to comply with regulation article CS25.807. Following the regulations, as illustrated in figure 14.2, the aircraft should have two Type I exits and one Type III exit per side [11]. Figure 14.3 shows the layout of the cabin, with two Type I exits in the front, two Type I exits in the back and two Type III exits over the wings. Furthermore, two lavatories and two galleys are implemented, as standard with Embraer 190 layouts of for instance KLM and Air Moldova [10, 129].

Passenger seating configuration (crew member seats not included)	Emergency exits for each side of the fuselage			
	Type I	Type II	Type III	Type IV
1 to 9				1
10 to 19			1	
20 to 39		1	1	
40 to 79	1		1	
80 to 109	1		2	
110 to 139	2		1	
140 to 179	2		2	

Figure 14.2: CS25.807.

A seat pitch of 78.7 cm (31 inches) is assumed based on industry standards in *Roskam* and comparison to competitors [126]. The total length of the cabin is determined using the configuration in figure 14.3. 76 cm and 91 cm are taken for longitudinal galley and lavatory dimensions. 91 cm and 45 cm minimum clearance for Type I and Type III exits respectively are accounted for, and margins are added for the start and end of cabin. A total cabin length of 26.2 m is found [39]. This value is 44 cm larger than the Embraer 190. The estimation seems valid when taking into account that the E190 can carry 106 passengers at a 78.7 cm pitch [127].

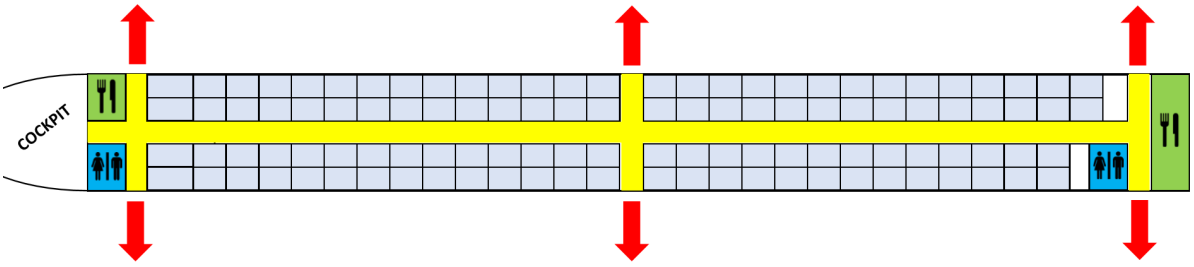

Figure 14.3: Seat plan of the SRJ110.

If the final customer wishes to either seat more people or to offer a business class, seat pitches will change in order to accommodate these changes. The tightest seat pitch Embraer offers on the E190 is 73.7 cm (29 inches) [127]. Keeping the cabin length constant would yield additional '1.87' rows, so one full extra row in practice. Extending the fuselage by 10 cm would allow for two full extra rows - eight more passengers - with a 73.7 cm (29 inches) seat pitch. If a seat pitch of 76.2 cm (30 inches)- common with carriers such as Ryanair - is selected, this would allow for '0.9' rows extra in case of the original fuselage length. In practice this does not lead to an additional row. Again, if a 10 cm longer fuselage length is opted for, decreasing the pitch from 78.7 to 76.2 cm would allow for a full extra row, or four passengers. It is therefore decided to take a cabin length of 26.3 m, allowing 110 passengers at 73.7 cm seat pitch, 114 at 76.2 cm and 118 at 78.7 cm. The flight deck length for a two-crew cockpit is equal to 2.5 meters [39]. The tail section is sized complying with regulations considering ground and rotation clearance. Tail section sizing was done following the Aerospace Design and Systems Engineering Elements lecture [39]. The tail section of the aircraft is 6 m long. The sloped end totals 11 meters and starts at the back of the cabin already. In total, the length of the fuselage is equal to 36 meters.

In order to fit three rows of first class seats - 6 seats in total - with a best-in-class seat width of 53 cm and a pitch of 96.5 cm, four rows of economy have to be removed. This will result in a total passenger number of 103, of which 97 economy class.

Industry standards by Airbus advise one flight attendant per 20 business class passengers or per 35 economy class passengers [39]. This results in four flight attendants, each requiring their own seat.

14.2 Wing

The wing design configuration of the SRJ110 has been investigated in depth in chapter 8. A summary of the main wing design criteria is provided in this section. Please refer to chapter 8 for the complete analysis. Moreover, a detailed presentation of the final wing planform, including high lift devices and control surfaces, as well as the winglet design are provided in figures 8.13 and 8.5, respectively.

In table 14.1, the final wing design parameters of the SRJ110 are introduced. The implementation of raked wing tip and blended winglets has affected the aspect ratio of the wing initially assumed from reference aircraft. An aspect ratio of 9.8 is now evaluated. Keeping the wingspan unchanged, an effective surface area of 80.46 m^2 is found. The wingspan is assumed unchanged, such as the other wing parameters.

Table 14.1: Final wing parameters of the SRJ110.

Parameter:	**Value:**
Effective aspect ratio A [-]	9.8
Effective wing surface area S [m^2]	80.46
Wingspan b [m]	28.00
Leading edge sweep angle Λ_{LE} [°]	28.08
Quarter chord sweep angle $\Lambda_{1/4c}$ [°]	25
Half chord sweep angle $\Lambda_{1/2c}$ [°]	21.76
Taper ratio λ [-]	0.25
Root chord c_r [m]	6.27
Tip chord c_t [m]	1.25
Average thickness-to-chord ratio t/c [-]	0.12
Dihedral Γ [°]	3
Mean aerodynamic chord MAC [m]	3.51
Spanwise location of the MAC $\bar{Y}$ [m]	5.60
Airfoil lift design coefficient $C_{l_{des}}$ [-]	0.6182
Wing lift design coefficient $C_{L_{des}}$ [-]	0.5078
Wing incidence angle i_w [°]	2.5
Airfoil	SC(2)-0610/12/14

As the wing is optimised for performance in cruise conditions, it could not provide sufficient lift during low speed flight phases as take-off and landing. Hence, high-lift devices were sized to compensate the lift coefficient deficit. Between the fuselage and the engine, double slotted flaps are installed to take advantage of the straight trailing edge. Right after the engine, a flaperon is installed to provide some extra lift and also lateral control at high speed. Between flaperon and wing tip, a spanwise length of 4 m is equipped with single

slotted Fowler flaps to provide the remaining required C_L. This leaves sufficient room for control surfaces as ailerons, which are typically installed as outboard as possible. On the leading edge, slats are installed to improve stall performance. Again, the final planform can be seen in figure 8.13. Besides sizing for an increase in lift coefficient, the high lift device configuration also influences the C_{L_α} value. It has been ensured that the required lift coefficients during take-off and landing can be attained at feasible angles of attack. Hence, pilot visibility is provided and a tailstrike is prevented. The lift versus angle of attack graph for the aircraft with and without high lift devices can be consulted in figure 8.12.

14.3 Tail

In this section, the final tail configuration of the SRJ110 is introduced. More detailed information about the tail design can be found in chapter 7. In table 14.2, the final values for the design of both the horizontal and vertical stabilisers are provided. To also keep in mind is the T-tail configuration selected for the stabiliser of the SRJ110.

Table 14.2: Final tail design of the SRJ110.

Parameter:	Value:
S_h [m^2]	14.75
$\Lambda_{1/4c_h}$ [°]	26.5
λ_h [-]	0.36
A_h [-]	5.65
l_h [m]	17.886
S_v [m^2]	14.59
$\Lambda_{1/4c_v}$ [°]	40.25
λ_v [-]	0.72
A_v [-]	1.13
l_v [m]	15.386
X_{LEMAC}[m]	13.74

14.4 Landing Gear

The SRJ110 is equipped with a tricycle landing gear. The wheelbase and longitudinal landing gear position are determined in compliance with maximum load requirement for nose gear and by performing a moment balance. The wheelbase is equal to 11.35 m. The front landing gear is located at 4.7 m from the nose. The main landing gear is then positioned at 16.05 m.

The height of the landing gear is constrained by clearances. While engine ground clearance is not an issue for the top-mounted engine design of the SRJ110, tail ground clearance at rotation is still a constraint. Both front and main landing gear are determined to be 1.7 m high: a couple of decimetres shorter than competing aircraft.

The weeltrack is the lateral distance between the two main gears. It is determined by controllability, stability and structures. The wheel base is equal to 4.44 m. The diameter of the strut is 0.176 m for the main gear and 0.08 m for the nose gear. The nose gear and both main landing gears all have two wheels.

The main landing gear strut is located 0.7 m outboard from the fuselage. It retracts inwards. The struts are stored in the wing and the wheels in the fuselage. The landing gears are made more aerodynamic with the addition of fairings. The fuselage doors are made as large as possible - and so the doors attached to the strut smaller. This way, the noise from the strut-attached door is lower and when the other door is closed, the total cavity is smaller. Furthermore, the strut door has brushes on its trailing edge.

15 Cost Analysis

The cost of an aircraft is of major importance to potential customers. Preferably an aircraft is as cheap as possible to purchase and operate, maximising the profit for operators at the lowest possible investment. Therefore the unit cost and direct operating cost are determined in this chapter, since it is key to the sales potential of the SRJ. The former is discussed in section 15.1 and the latter is described in section 15.2. Furthermore, the return on investment is treated in section 15.3.

15.1 Unit Cost

Even the most fuel efficient aircraft in the world would remain on the ground if the unit cost is not within the range of its competitors. It is a careful consideration made by operators to save money eventually. To determine the unit cost of the SRJ aircraft, the method from *Roskam* part VIII is applied [130]. The method is developed in the late eighties so an inflation correction is utilised to convert 1989 dollars to 2017 dollars.

According to chapter 4 from *Roskam*, the unit cost is divided over two main phases; the research, development and testing phase (RDTE), and the manufacturing phase. Firstly, the first phase, often referred to as RDTE, is analysed. The total cost is subdivided into seven categories: airframe engineering and design (AED), development support and testing cost (DST), flight test airplanes (FTA), flight test operations (FTO), test and simulation facilities (TSF) and finance cost (FIN). Equation 15.1 shows this relation.

$$C_{RDTE} = C_{AED_r} + C_{DST_r} + C_{FTA_r} + C_{FTO_r} + C_{TSF_r} + C_{FIN_r} \tag{15.1}$$

All components have been computed individually in compliance with the descriptions found. Hence, all necessary assumptions were made according to the guidelines provided by *Roskam*. The general approach was similar for every component: the estimation is a summation of the cost of required man hours, tools and materials if the component logically consisted out of these three components. As an example, the AED and FTA required all three cost components whilst FIN only had one. The results are shown in table 15.1.

Table 15.1: Breakdown of the RDTE costs.

Cost component:	**Cost [million USD]**
AED	119.21
DST	9.75
FTA	562.71
FTO	2.26
TSF	0.00
FIN	60.34
RDTE	754.27

An extensive explanation on how the above numbers are obtained would be both complicated and lengthy. Three observations however are important to clarify. First of all, the FTA cost is the most dominant contributor to the RDTE cost as it includes the number of test planes that will be produced; namely four. This number is based on the numbers of test aircraft other aircraft manufacturers have produced for similar aircraft such as the E190-E2 [131]. The research, development and production of these four testbeds is very expensive as it also requires the development of tools and facilities. Moreover, it can be noticed that the TSF cost is zero. This is because no extensive test and simulation facilities are required, at least not more extensive than other conventional aircraft.

The second phase of the cost estimation is the manufacturing phase. After research and development, the first series of four aircraft is produced and if certified the production is taken to the next step: commercial production. Consequently, the manufacturing price per aircraft is the logical follow-up such that the overall unit cost can be determined. The manufacturing cost is divided over four main costs, namely the following: airframe engineering and design (AED), airplane production (APC), flight test operations (FTO) and finance cost (FIN). Equation 15.2 illustrates this relation.

$$C_{MAN} = C_{AED_M} + C_{APC_M} + C_{FTO_M} + C_{FIN_M} \tag{15.2}$$

In contrast with the previously discussed RDTE cost, the manufacturing cost are variable with respect to the numbers of aircraft produced. As described in chapter 3, the projected number of produced aircraft equals 500. For this particular point the breakdown of the total manufacturing cost is shown in table 15.2. This results in a total a manufacturing cost of about 42.77 million USD per aircraft.

Table 15.2: Breakdown of the MAN costs.

Cost component:	**Cost [million USD]:**
AED	185.14
APC	19,415.17
FTO	75.00
FIN	1,710.90
MAN	21,386.21

The two components, RDTE and MAN, summed up yield a unit cost of 44.28 million USD if 500 aircraft are produced. As the applied method is rather rough, a safety margin (contingency factor) of 10% is added to the unit cost. This margin accounts for the rather pioneering decision for this class of airliners to apply composites for the entire structure and the innovative noise measures. The unit cost is thus estimated to be 48.71 million USD. The sales price would in this case be, adding a profit margin of 12.5% comparable to *Roskam* standards, 54.80 million USD. This production number however is not fixed since it is a prospect based on the market analysis described in chapter 3. Hence the relation between the number of aircraft produced versus the unit price is plotted in figure 15.1.

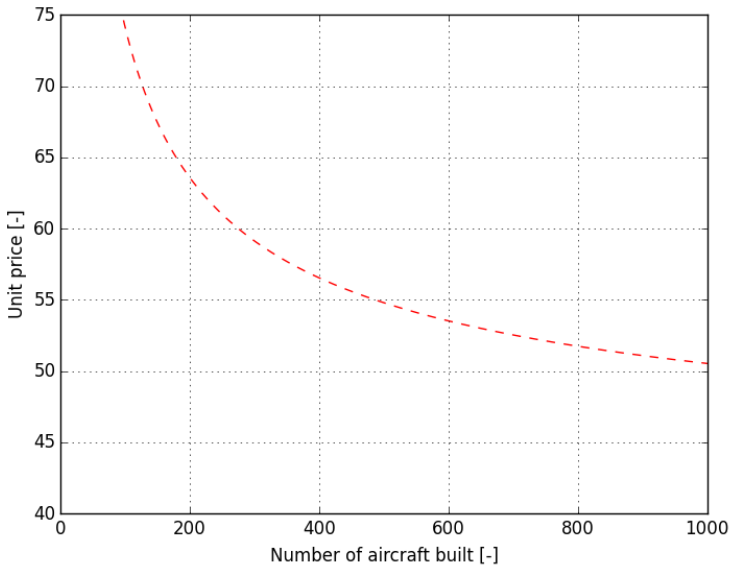

Figure 15.1: Unit cost vs. number of aircraft built.

The figure above shows that the unit price has decreased significantly after the production of 200 aircraft. The SRJ is however not competitive yet with regards to its competitors. The minimum number of produced aircraft is 500 to approach an existing competitor such as the Embraer E190-E2. On the other hand, the Bombardier CS100 is easily beaten on unit price due to its different mission profile. Eventually the unit price levels off to a value of 50.60 million USD. This is more expensive than most competitors besides the previously discussed two. The unit price could of course easily be reduced by setting a lower profit margin. However this may have a catastrophic impact on the return on investment. In other words, it would take significantly longer to earn the RDTE investment back. Additionally, it is expected that the price of composites will decrease in the upcoming years as it becomes an increasingly more common material in the field of aviation, as the Boeing 787 family already shows [72]. Both measures would reduce the unit price of the aircraft and will make it more competitive, though the latter is purely beneficial whilst the former is definitely risky to undertake.

15.2 Direct Operating Cost

The direct operating costs are specified as the costs directly related to operating an aircraft. According to *Roskam*, it consists of crew, fuel, depreciation, maintenance, fees and financing cost. On the contrary with the unit cost, the *Roskam* book is not a general guideline for the DOC estimation if more exact, accurate or up-to-date methods are applicable and available. Only when explicitly mentioned, the *Roskam* method is used. Every contributor will be discussed individually in the upcoming subsections.

15.2.1 Crew

The computation of crew cost is simply the hourly rate of a crew member; either flight deck or cabin. The determination of the hourly rates is done according to recent numbers published by *Phoenix East Aviation* [132]. Knowing that the aircraft has two pilots and four cabin attendants, earning 80 USD/h and 40 USD/h respectively, the total crew cost per hour is 320 USD/h.

15.2.2 Fuel

The fuel cost per hour is the fuel burned per hour multiplied with the cost of fuel. The fuel burn for a nominal mission has been obtained by the performance analysis previously conducted in section 10.1. With the same analysis, it is also possible to obtain the fuel burn for different missions as the SRJ will not perform a harmonic mission every single flight. By looking at live aircraft data from different airports, it is concluded that a 600 NM mission would be the most regularly performed mission for this class of airliner. Hence, the fuel consumption for a nominal mission of 600 NM is computed and multiplied with a fuel price of 170 USD cents per gallon, according to Transstat, resulting in a fuel cost of 831 USD/h [133]. The fuel cost estimate is definitely conservative with respect to the Transstat numbers. This is done purposely to account for fluctuations in future fuel prices.

15.2.3 Depreciation

Similarly to cars, aircraft "lose" value over time. This process is called depreciation. In consultation with an expert in the field of air transport and operations, a straightforward approach has been validated for this stage of the design. The residual value of an aircraft is assumed to be 20% of the unit price with a potential life time expectancy of 20 years. This lifetime estimate seems rather high but with current and future sustainable design and development technology in mind it should be achievable. To convert this number to the hourly depreciation, the total depreciation is divided over the utilisation. The overall utilisation equals the product of the total life, the numbers of days per year and the daily utilisation of the aircraft. The utilisation of an aircraft ranges from 8 to 12 hours a day, depending on the business model of the airline. For this preliminary estimate, the average is taken into account resulting in a depreciation of 601 USD/h.

15.2.4 Maintenance

The maintenance cost is determined according to the *Roskam* method and resulted in an estimated maintenance cost of 613 USD/h. The method is noticeably detailed and consists of two cost components namely tools and labour. Moreover, tools and labour costs for maintenance on both the airframe and the engines are taken into account. Since the method is designed in the late eighties, the outcome is converted as a result of inflation.

15.2.5 Fees

The fees are estimated based on data of reference aircraft as it proved to be difficult to assess this cost with an analytical model. The results found using for instance the *Roskam* approach did not result in valid results with respect to numbers found from extensive research. As a consequence, a presentation published by Sukhoi is deemed as trustworthy since it showed data of multiple aircraft [134]. Moreover, the presentation was one of the most up-to-date sources found as it published in 2013. The cost is eventually set at 450 USD/h. This number is significantly less than the reference aircraft but this assumption is valid since the SRJ has a reduced fuel consumption, noise footprint and maximum take-off weight, hence the fees will be reduced due to its outstanding performance.

15.2.6 Financing

The final cost is the financing cost. This particular cost accounts for an operator requires to pay the fleet. An example would be the fee an airline pays to lessors for utilising the aircraft, but also insurance is included. According to *Torenbeek* it is a fixed percentage of the total DOC and since limited information is available is assumed to be 7% or 212 USD/h.

The sum of the five previously mentioned costs leads to an estimated direct operating cost of 3,026 USD/h. It is very common to plot the results of a DOC analysis in a pie chart, as shown in figure 15.2.

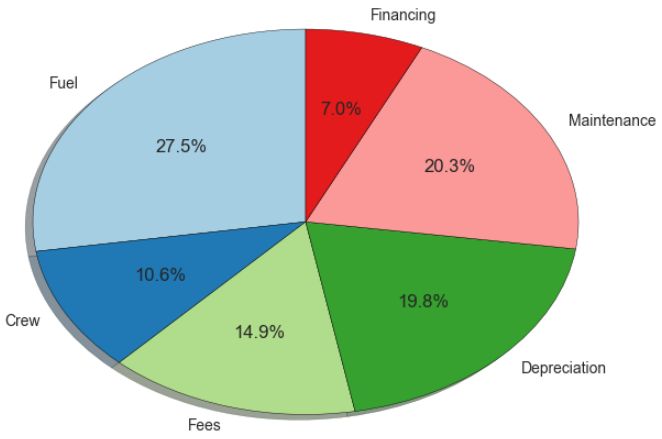

Figure 15.2: Direct operating cost breakdown.

15.3 Return on Investment

The return on investment is divided over two categories. The return of investment from manufacturer's perspective, the number of aircraft to the break-even and the operator's return of investment, which results from the higher unit cost.

15.3.1 Manufacturer's Return

With the design of a new aircraft, an enormous amount of money is spent on the initial phase of research and development. This has been quantified earlier as the RDTE cost in section 15.1. A manufacturer is primarily interested in the point when the company actually starts to earn money. This happens from the so called break-even point onwards. According to the market analysis, 500 aircraft will be produced. With a unit cost of 48.71 million USD and a profit margin of 12.5%, a profit of 6.09 million USD is earned per aircraft sold. The total research and development cost is 754.27 million USD, hence dividing this by the profit yields in the number of aircraft that should be sold to break even. In short, if 500 aircraft are ordered in total, 124 deliveries equal the total investment made by the customer. The remaining 376 aircraft result in a 2,289.84 million USD profit. As mentioned before, 500 is the minimum to be able to place the SRJ in the market at a competitive price, namely 54.80 million USD. Its slightly higher unit price is of course compensated by its considerably lower operating costs, but minimising the operators investment and thus risk is also an important consideration. Obviously the RDTE costs remain equal for every number of aircraft sold and so does the profit margin. Figure 15.3 clearly shows that producing more aircraft, resulting in a reduced listing price according to figure 15.1, requires more orders to reach the break-even point. Subsequently, the return on investment takes longer. This specific return on investment time will only increase by ordering more aircraft as an asymptote exists at roughly 140 aircraft, as can be seen in figure 15.3.

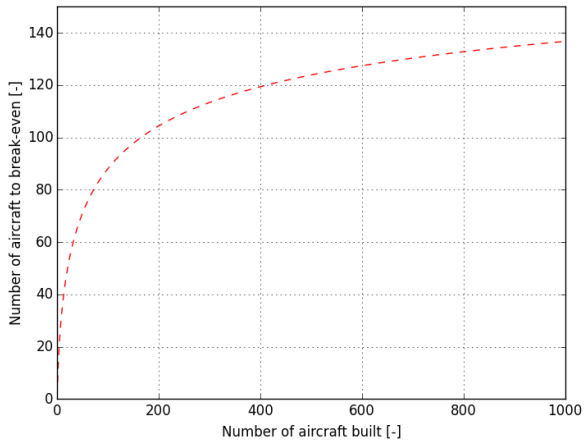

Figure 15.3: Aircraft number required to reach the return on investment versus number of aircraft produced.

In addition the plot illustrates that at least 84 aircraft should be produced to have a return on investment possibility. Below this number the manufacturer will actually lose money due to the cost of RDTE and this is underpinned by figure 15.4. It must be stressed that the unit prices at that particular number is relatively high, more than 80 million USD, and the sales potential is not taken into account when constructing these graphs. Therefore the loss up to the competitive price of 500 aircraft would be significantly higher if the aircraft were already produced by that time, a consequence of having to sell the SRJ at a market competitive price anyway. Nevertheless, figure 15.4 shows a constant increase in profit by increasing the number of aircraft built. The exponential trend has changed too a linear trend because, while the number of aircraft built increases, the unit cost and break-even number level off to a fixed number. From the targeted number of 500 on, the profit line is representative and can be regarded as the actual profit.

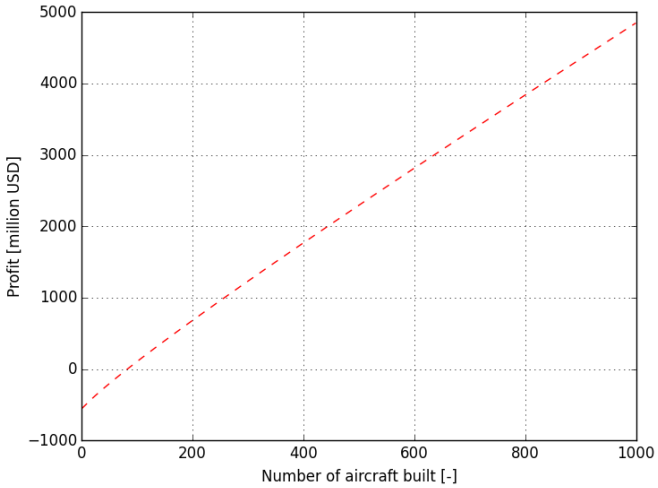

Figure 15.4: SRJ project profit vs. the number of aircraft built.

15.3.2 Operator's Return

As mentioned in the unit cost section of this chapter, the aircraft will go on sale for 54.8 million USD. This is significantly higher than the requirement which was set at a unit cost of 40.0 million USD. There are however an inherent advantage of the design which may be able to justify the increase in unit cost.

The requirement for the direct operating cost per block hour was set at 3,670.70 USD. As shown in this chapter the direct operating cost for the SRJ110 is estimated at 3,026 USD per block hour. This is quite a significant difference, equal to approximately 644 USD per block hour. This means that every hour that the aircraft is in service for the operator, the operator saves this amount compared to the initial requirement that was set. In order to make up for the higher unit cost, the aircraft has to fly 22,982 hours for a break even point to occur. At a conservative estimate of nine block hours a day for 365 days a year this would mean that after seven years the operator would have made up for the higher sale price due to the lower direct operating cost [135]. After year seven, the aircraft starts making more and more profit for the operator than was initially required. As airlines generally tend to hold on to their aircraft for more than seven years, the aircraft will still be extremely competitive on the market. To summarise, the higher unit cost is compensated by a significant reduction in direct operating cost. This ensures that the SRJ110 remains an attractive option for customers around the world for many years to come.

16 Verification & Validation

This chapter concisely describes all verification and validation procedures undertaken during the final design stage of the SRJ110. The verification and validation actions performed have been mostly executed throughout the design process instead of at the very end. Hence, some verification and validation is also explained in the respective analysis section.

16.1 Verification

Verification is a crucial step to be included in any analysis involving computational models. Verification is required in order to check the efficiency and the accuracy of the developed tools. For this project, this entails various *Python* scripts and *Excel* sheets. As a matter of fact, verification needs to be carried out on the code itself as well as on the entire simulation programme. This section is structured as follows. First, a code verification method valid for all tools is presented in subsection 16.1.1. Subsequently, a deep analysis of all the intermediate results is done. This is discussed in subsection 16.1.2. Finally, the integrity of the model is ensured by executing a system test as elaborated in subsection 16.1.3. As the following verification approach is applicable to all analysis introduced in the present report, the general method is presented without going into detail per design department.

16.1.1 Code Verification

Prior to verifying the outputs of the analyses performed in this report, particular attention is paid to the identification of all syntax and spelling mistakes in the *Python* scripts and *Excel* sheets. This is an integral part of the verification process since neglecting this step will most likely result in time consuming code examinations later on. Programming errors such as incorrect indentation, wrong index and punctuation marks, are also important to identify as early as possible in the code verification process.

Once the code scripts are clear of coding errors, the focus is on the proper use of units. Most of the time, the input parameters have their unit expressed according to the SI unit system. If this is not the case, a proper conversion factor has to be applied. To facilitate the technical analyses presented in the present report, an input data sheet accessible to all team members has been created. All *Python* and *Excel* scripts are linked to it such that updates are done automatically. This made the team work more time efficient and less tedious than working with offline data. Since this report contains the final development design of the low-noise medium-range airliner, the main focus is on technical analysis. Therefore, accuracy and reliability of the methods and inputs used have been primordial. Furthermore, the highly-iterative character of the entire design process could be more easily managed using shared data.

16.1.2 Unit Tests

Unit testing involves the breakdown of the computational tools in smaller portions. In this way, the intermediate outputs can easily be checked and verified before further use. As a matter of fact, some intermediate outputs are also inputs for subsequent calculation steps. Therefore, a deep analysis of the results is important. Each technical department is responsible for the proper follow-up of the acquired data and the update of the common input data sheet.

Moreover, the theory behind the functions implemented in the different *Python* and *Excel* scripts need to be fully understood to make sure the correct models are developed. Additionally to the proper functions interpretation, the functions have to be correctly implemented into the programme. This is checked by using simplified inputs such that the result can be easily evaluated. Calculations by hand can also be used as crosscheck. A sanity check is also more than required in order to compare the gathered inputs with reference aircraft or theoretical values found in literature.

16.1.3 System Test

Now that the individual functions of the *Python* and *Excel* scripts have been separately verified, the data consistency needs to be checked. Integration of all the functions into one single interface is challenging since the functions themselves can not be altered and two different computational tools have been used. However, by updating the input data sheet, an overview of the design can be obtained and design inconsistencies can be rapidly identified and resolved.

When discrepancies are observed between the generated and expected results, corrective actions have to be taken. However, if the above verification procedures have been carefully applied, the risk of getting inconsistencies in between the results is rather low.

16.2 Validation

Validation is proof that the developed system accomplishes the intended purposes based on the customer expectations. Several ways exist to validate the methods used to design the SRJ110. For concept configurations comparable to already proven solutions, similarity can be used to validate the concepts. Basically, this means that the generated data is compared to reference aircraft in order to perform a sanity check. This validation technique is the most referred to in this report. However, the lack of available data due to airline, manufacturer and authority policies has several time hindered proper validation actions. If the analyses themselves were based on reference data, no validation is done as it is valid by definition. This is for instance the case for the sizing of the vertical tail. In the following subsections, the validation for various analyses methods is discussed.

16.2.1 Weight Estimation

The weight estimation is carefully validated during and at the end of the process. As already described by figure 6.5, the integral role of the weight estimation required a continuous and close validation. This was done by first validating the input parameters in close discussion with all team members. Sensitive parameters were identified and therefore closely kept track off to prevent major fluctuations in the weight estimation. Moreover, *Torenbeek* provides weight breakdowns of several relevant aircraft, hence the SRJ is compared to existing designs and no significant or noticeable deviations have been found [40]. Finally, the gross weights are compared to the reference aircraft found in table 6.1. In comparison with the four most modern aircraft listed in that particular table, the Sukhoi SJ100, Mitsubishi MRJ90, Comac ARJ21-90 and Embraer E190, the SRJ is remarkably similar to what is available on the market nowadays. The operative empty weight is slightly higher than average but no detailed weight reduction measures have been undertaken or researched at this stage of the weight estimation. The weight reduction by the composite fuselage is assumed to be outweighing the "neglected" mass of the noise mitigation measures. These measures were not taken into account as no data is available. Moreover, no empirical relations exist for these innovative features. Hence the results are regarded as plausible. Moreover, the SRJ has a lighter maximum take-off weight which is the result of its outstanding performance in fuel efficiency. Conclusively, the outcome of the weight estimation is deemed valid with this substantiation.

16.2.2 Design Space

The design space was of the utmost importance as it resulted in two key parameters, the wing area and required thrust. Both parameters however were strongly dependent on the results of the weight estimation, since the weight potentially could have nullified the value of the weight and thrust loading analysis. Therefore the conclusion of the previous subsection is the first step in being able to validate the design space results. In addition, the design space itself was validated with respect to reference aircraft. A renowned source, *Janes' All The World's Aircraft*, provided the wing and thrust loading for a dozen of aircraft such that the SRJ's wing and thrust loading could be compared to existing designs [136]. With regards to the reference aircraft listed in table 6.1, no exceptional deviations have been found when data was available for comparison. In addition, the imposed constraints to determine the design point have been discussed with the other design teams constantly. This validation ensured the feasibility of the intermediate steps. An example of such a constraint is already stressed in section 6.3; the maximum lift coefficient at take-off. However, multiple constraints have been set and none was found to be unfeasible with respect to the performed analyses.

16.2.3 Stability & Control Analysis

This subsection elaborates on the validation actions undertaken to check the compliance of the outputs of the S&C analysis with the customer requirements as well as with the overall design integrity. Firstly, the method followed to generated the loading diagram, the centre of gravity range and the scissor plot is validated. Combining these graphs, the horizontal tail surface area is defined as well as the tail arms. Comparing these data with reference aircraft is additional proof of the correctness of the S&C analysis.

Loading Diagram
Construction of the loading diagram required numerous inputs. Most of them directly resulted from the weight estimation performed in chapter 6. Other parameters needed to be evaluated based on common engineering sense and reference aircraft; e.g. the location of the centre of gravity of the various aircraft components and the cargo holds properties. One validation procedure consisted of checking the location of the centre of gravity of the aircraft at operational empty weight with respect to the position of the main landing gear at 66% of MAC. Since X_{OEM} is at 24% of MAC, tip-over of the aircraft at operative empty weight is prevented. Furthermore, the most aft position of the centre of gravity during loading never goes behind 30% of MAC, which remains in front of the main landing gear. Finally, the loading diagram is slightly shifted forward which reflects the aircraft configuration with engines attached to the wing.

Centre of Gravity Diagram
The only component to be checked in this module is the moment created by all aircraft components with respect to the aircraft nose. Since the positioning of the components has been previously defined to generate the loading diagram and as the component weight directly results form the Class II weight estimation, the moment is likely to be correct. In this way, the centre of gravity of the aircraft's OEM can be found for different longitudinal wing positions as explained in chapter 7. New loading diagrams have been generated to highlight the most front and aft centre of gravity location for each wing positioning. From these results, the range of centre of gravity as a function of the wing positioning has been illustrated in a plot. Even if reference data is not available, the trend of the curve indicates the validity of the model to some extent.

Scissor Plot
Many parameters are required in the different relations that determine the stability and controllability regions of the SRJ110. A number of inputs were required to come from reference aircraft. All input values were validated and checked for validity. The outcomes of the analysis are the stability and controllability graph. These are hard to validate. By comparison to known scissor plots, they are deemed realistic. A sensitivity analysis was performed as well. The input values that either come from references or are assumed are changed within a margin to observe the effect they have on the result. The tail arm was found to have the most significant influence on the result. Nothing was found to be out of the ordinary though. As the plots following from the calculations do not exactly provide meaningful values, they are hard to validate. The validation can only be done in the end, after combining with the centre of gravity range, for the tail size, centre of gravity range and mean aerodynamic chord position.

A step further to validate the above diagrams is to combine them in a particular way such that the tail can be sized. In particular, the optimal horizontal surface area and the tail arms can be determined. A surface of 14.75 m^2 has been found which is rather low but close to 15.61 m^2, the horizontal tail surface area of the Avro RJ100 [34]. This smaller tail surface is compensated by a slightly longer horizontal tail arm of 17.918 m in order to satisfy the S&C requirements. More advanced validation procedures have been discussed in section 7.5.

16.2.4 Aerodynamic Characteristics
In this section, the validation actions taken to demonstrate the accuracy of the aerodynamic results obtained in chapter 8 are presented. Throughout the entire analysis, validation has been performed. Final, as well as intermediate outputs, have been compared to reference aircraft data. This has allowed to identify miscalculations and to justify the validity of the method used.

Airfoil Selection
A major part of the remarks and uncertainties concerning the airfoil selection have been listen in chapter 8.1. The main uncertainty is in the models and software. For the airfoil selection, $JavaFoil$ was used in order to determine characteristics of the different airfoils that were taken into consideration. Research confirmed that $JavaFoil$ is good enough for the purpose of analysing and comparing airfoil characteristics. However, it has to be noted that $JavaFoil$ does not take transsonic behaviour into consideration. For instance for the drag computation, wave drag is not taken into account. These observations were confirmed by an expert at the faculty who also noted that $JavaFoil$ consistently underestimates the (maximum) lift coefficient. This was also noticed in the verification that was performed with $Xfoil$. All other outputs of the comparative analysis - moment coefficient, slope and stall angle - were realistic with respect to both $Xfoil$ and real-life values.

Full Wing Analysis
The full wing analysis was done using $XFLR5$. As with all models, $XFLR5$ does not perform optimally in every aspect. Generally, the model is deemed accurate enough for the determination lift, moment and angle of attack values. For drag, again, high-speed drag is not taken into account. Therefore, a drag estimation was performed separately, following book methods. Another issue with $XFLR5$ is that it does not model the stall behaviour. Instead of showing a decline in slope and a top, the $C_L - \alpha$ outputs of $XFLR5$ linearly rise until they stop, where stall is supposed to be. The maximum clean lift coefficient of the wing determined using $XFLR5$ is around 1.7: a realistic value for the wing of this kind of aircraft, as confirmed by multiple professors of the faculty.

Drag Estimation
The drag estimation has been carefully carried out following the method presented in the *ADSEE* lecture slides [45]. Assumptions have been made after motivating their necessity. For instance, the total drag has been evaluated using the equation for uncambered wing. This decision primarily follows from the moderate wing camber of the selected airfoil. Values of drag components such as induced drag, zero-lift drag and wave drag are more difficult to validate. However, an intelligent and consistent way of checking the validity of the entire model is by looking at the ultimate output resulting from the drag estimation analysis, namely the lift-to-drag ratio. Typical values for subsonic jet aircraft range from 15 to 20 [46]. Values of 15.85 and 16.38 have been found for the L/D ratio without and with winglet, respectively. These values, compared to the value found in the Mid-term Report for Concept 1, are much more realistic and, to a certain extent, validate the drag estimation analysis.

Aileron Design
When designing the ailerons, particular attention has been paid on the compliance with the roll performance defined by the regulations. The roll performance criterion has not been used as input to design the ailerons, but as target value. Again, stringent guidelines have been followed. However, it was challenging to check intermediate results. These include the aircraft roll authority and the roll damping derivative. These types of data are really sensitive to the type of aircraft and therefore, are hard to define. However, proper use of units, in particular radians or degrees has been checked. *Excel* has been used to perform this analysis. Implementation of the equations has been attentively done and verified. Additionally to the roll performance requirement, integration of the ailerons on the wing planform together with the flaperons and spoilerons had to be ensured. Therefore, the goal of this analysis was to validate the ability of the ailerons to meet the roll performance requirement while having a limited length due to other systems previously implemented on the wing planform.

16.2.5 Structural Analysis
Validation procedures for the structural analysis are divided between the wing box design and fuselage design.

Wing Box
Although verification has been performed for the wing box, validation is much more difficult. No test data is available for the wing loading. Furthermore there are no reference aircraft using a full composite wing box. For a general sense of dimensions of a wing box, the aircraft hall at the Faculty of Aerospace Engineering was visited. The skin thicknesses were on the higher side compared to the VFW-613 but this can be attributed to the absence of stringers. From inspecting the only available aircraft with a fully composite wing, it was validated that the spar thickness is indeed considerably larger than the skin.

Fuselage
The *Python* code for the fuselage structural design has been carefully verified. However, in a programme of 2,000 lines of code, it cannot be ruled out that there is still a minor mistake in it. For this very reason, validation should be done. The input data of a Boeing 737 were used and the output was checked with real-life data provided by the SVV course [80]. Some discrepancies were found. For instance, the floor takes more stress in real-life, the shear stresses are not modelled entirely correct and the von Mises stress distribution is more pronounced along the whole fuselage. These differences are mainly due to the fact that the weight has been modelled as a discrete load (whereas it actually is a distributed load), and because the floor might have been modelled with too few booms. However, the order of magnitude of the stress and its maximum and

minimum location are in accordance with the real-life case, and thus the model is considered a good starting point for the preliminary fuselage design.

16.2.6 Performance Analysis

In this section, the validation procedures of the performance analysis are presented. First of all, the results found from cruise altitude, cruise speed and fuel consumption analysis are validated. Next, some important remarks are made on the climb performance characteristics of the aircraft. Lastly, the airfield performance of the SRJ110 is validated.

Cruise Altitude, Cruise Speed and Fuel Consumption

During the determination of the cruise altitude, cruise speed and fuel consumption, collaboration with other departments was of utmost importance. The earlier mentioned performance parameters were sensitive to aerodynamic changes as well as changes in weight. One of the parameters which was most influential on the fuel consumption is the specific fuel consumption (SFC). As mentioned before, engine manufacturers are reluctant to share this value because it would give competitors an advantage. Using the emissions database, however, an approximation of this value could be determined based on the rated power output of the engine and the corresponding fuel flow. This analysis has been conducted for the PW1500G engine series once again due to the fact that the PW1700G which was selected is not in the certification database.

The specific fuel consumption has been determined for all three cases listed in the emissions database; take-off, climb-out and approach [5]. This was done by first finding the maximum rated power output of the engine. The power for the corresponding take-off, climb-out and approach phases is determined from multiplying the respective thrust settings with the maximum rated power output of the engine [137]. By dividing the fuel flow by the power output the specific fuel consumption is obtained. For the PW1521G engine the SFC at take-off, climb-out and approach was found to be equal to 0.25 $lb/lbf/hr$ for all three cases. This value however does not reflect the effect of altitude on the engine performance, because the testing is conducted at sea level conditions. In order to compensate for this altitude effect, the ratio between sea level SFC and SFC at cruise altitude has been determined from a civil turbojet/turbofan database [138]. A wide variety of engines were gathered and the ratio between the cruise specific fuel consumption and sea level specific fuel consumption has been determined to be approximately 1.68. Following this ratio the PW1521G engine should have a specific fuel consumption at cruise altitude of 0.42 $lb/lbf/hr$. Putting things into perspective, for the fuel consumption model a specific fuel consumption at cruise altitude of 0.50 $lb/lbf/hr$ was used. This means that the fuel consumption model overestimates the fuel consumption during the cruise segment. As a result, the fuel consumption of the aircraft could be even better than presented.

Next to the specific fuel consumption parameter, the entire fuel consumption has been put through a validation exercises too. Two aircraft, the Sukhoi SSJ100 and the Bombardier CS100 were put through the fuel consumption model in order to determine the accuracy of the model. The results are shown in table 16.1.

Table 16.1: Comparison of the fuel efficiencies determined from the model and reference values [134, 139].

Aircraft:	**Model** [$kg/PAX/NM$]**:**	**Reference** [$kg/PAX/NM$]**:**	**Difference** [%]**:**
SRJ110	0.0376	-	-
Sukhoi SSJ100	0.0462	0.0467	-1%
Bombardier CS100	0.0352	0.0342	+3%

A small reservation has to be made with respect to the aerodynamic characteristics of the aircraft that were compared. Due to the limited detailed data available for these aircraft, the same aerodynamic drag parameters were assumed and the fuel efficiency parameters adjusted based on the ICAO engine database [5]. In addition, basic aircraft parameters such as the wing area, aspect ratio and passenger count were altered too. Even though this if not a perfect representation of reality (in fact, aerodynamic characteristics may vary quite significantly between the aircraft) the model shows a deviation which is well within the acceptable range. Even if the fuel consumption is three percent worse than calculated, the requirement is still met without any issue. For even more detailed design the recommendation is made to elaborate on the current model to account for these changes. Implementing said improvements could lead to an even more accurate representation of the actual fuel consumption of the aircraft.

Climb Performance

The most important parameter for determining the climb rate is the engine net thrust. The engine thrust decreases with increasing altitude and velocity. In order to model this, an existing model which predicts this

behaviour accurately for the engine on the Boeing 747-400 has been scaled down to fit the PW1700G. This means that the net thrust changes with airspeed and altitude in the same way as it does for the 744's engine. In reality this might not be the case since the size of the engines and the bypass ratio's are not the same. The model however is the closest approximation available. The actual climb rates might seem high when the maximum values are observed. However, many of these altitude and speed combinations will never be operated in reality, e.g. flying 150 m/s at sea level. When looking at the climb rates straight after rotation where the airspeed is constant for a short amount of time the climb rate for the Embraer E190 has been estimated at 11.6 m/s using *Flightradar24*. The SRJ110 has a maximum rate of climb of 13.6 m/s right after take-off for comparison. It has to be noted that the climb rate of the E190 probably was not on maximum thrust setting. If this is taken into account the rates of climb are very close. Additionally one of the original design goals for the SRJ110 was to have a high climb rate in order to reduce perceived noise. The SRJ110 has a service ceiling just over 35,000 ft at start of cruise weight. The E190 has a marketed service ceiling of 41,000 ft, however it is not specified at which weight and may have been selected favourably [140]. The climb gradient results from the climb rate so it does not require to be validated separately.

Airfield Performance

The take-off and landing distances depend on a number of coefficients which have a significant impact on the computed values for take-off and landing distance. The take-off distance of an actual Avro RJ100 on London City is just under 800 m determined by analysing footage of an Avro RJ100 taking off. If the specifications and weights of the Avro are used as inputs in the take-off distance model, the resulting take-off distance is 748 m. In the same way as the take-off distance, the landing length of the Avro at London City is estimated around 600 m. The landing distance from the model predicts a result of 540 m. This is only a bit lower than the real situation, but does not take into account the pilot skill or whether or not full braking force was used. For several reference aircraft the take-off and landing distances have been found [136]. These are presented in table 16.2.

Table 16.2: Take-off and landing distances for reference aircraft.

Aircraft:	**Take-off distance [m]:**	**Landing distance [m]:**	**Ratio [-]:**
B737-200	1,616	1,372	1.18
SSJ100	1,515	1,352	1.12
F100	1,720	1,350	1.27
E170	1,483	1,228	1.2
E190	1,598	1,267	1.26
CRJ700	1,779	1,596	1.11
SRJ110	1,070	925	1.15

In the table all the ratios between the landing and take-off distance are presented. In this way these can be compared to the values found for the SRJ110. With a ratio of 1.15, the SRJ110 falls right in the trend from reference aircraft.

16.2.7 Cost Analysis

A decent cost analysis is key, which is why a proper validation of the applied method has been conducted. Especially since it became clear during the process that cost, either for DOC or unit cost, was a rather difficult parameter to quantify. The unit cost, however, is easily validated because the market analysis provides the listing price of multiple reference aircraft. With a potential number of sales at 500, a listing price of 54.8 million USD was found. This number could decrease if the number of ordered aircraft, thus built, is increased resulting in a listing price of 50.6 million USD at 1,000 SRJ's. As long as the number of aircraft is beyond 500, the listing price is reasonable in comparison with some of reference aircraft, particularly the new Embraer E190-E2, seen as a close competitor. It is however hard to state a definitive conclusion since the range of listing prices is about 40 million USD, if the Sukhoi SSJ100 is compared to the Bombardier CS100. On top of that, the listing price of the SRJ is subject to change. However, it can be seen that it is at least within the outer margins of the reference aircraft, thus the results are deemed valid.

The DOC costs are even more variable than the unit cost. It is dependent on the eventual sales price and fluctuating numbers as fuel price, crew cost and interest. Consequently, validating the DOC at this point in time might yield a different conclusion with regards to the future. In addition, all aircraft are subject to these abrupt and almost unpredictable changes. Therefore comparing the DOC breakdown of the SRJ to reference aircraft would also lead to false conclusions. Hence the direct operating cost is not validated as a result of the uncertainties.

17 Operations and Logistics

This chapter focuses on determining the logistics and operational procedures. Section 17.1 first gives the functional breakdown and flow. In section 17.2 the payload-range diagrams are presented. Section 17.3 describes the operational procedures during take-off, approach and landing that contribute in the reduction of noise impact on the airport surroundings. In section 17.4, procedures and regulation at London City Airport specifically are described. The reliability, availability, maintainability and safety of the aircraft during the whole process is defined in section 17.5. Finally, section 17.6 explains the communication mechanism of an aircraft during operations.

17.1 Functional Breakdown and Flow Structure

The functional flow and breakdown diagrams represent the logical flow of operations the product shall perform during its lifetime. The breakdown diagram will be presented first in subsection 17.1.1 and shows a top-down AND-tree of the product functions. Then the flow diagram will be presented in subsection 17.1.2, which shows the logical flow of operations.

17.1.1 Functional Breakdown Diagram

In figure 17.1 the functional breakdown diagram is shown. The diagram should be read from left to right and from top to bottom. As can be seen, there is one top level function the aircraft has to fulfil: transport passengers. From this, four level-one functions originate, each marked in a different colour. Each of these four functions can then again be split up in further level-two and level-three functions.

Note that this diagram does not represent a chronological order of actions; it only shows all the functions the aircraft should be able to perform. The chronological order of these actions is shown in the functional flow diagram, figure 17.2, where the same numbering is used.

17.1.2 Functional Flow Diagram

The functional flow diagram presented in figure 17.2 shows the same grouping of operations as in the breakdown diagram. The difference between them is that the flow diagram presents the actual chronological flow of operations. It also allows for showing alternate paths in case of an operation failing to succeed. This can be seen in block four "Fly safely from A to B" where each G represents a successful conclusion and each $\overline{G}$ represents a failed operation, leading to an alternate path of operations coloured in red.

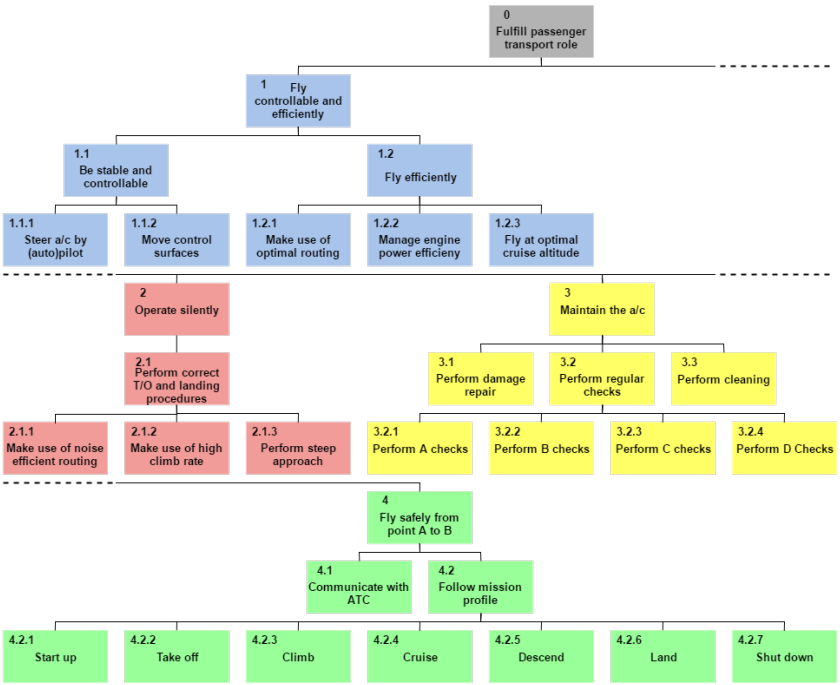

Figure 17.1: Functional breakdown diagram for a low-noise medium-range airliner. The diagram should be read from left to right and from top to bottom.

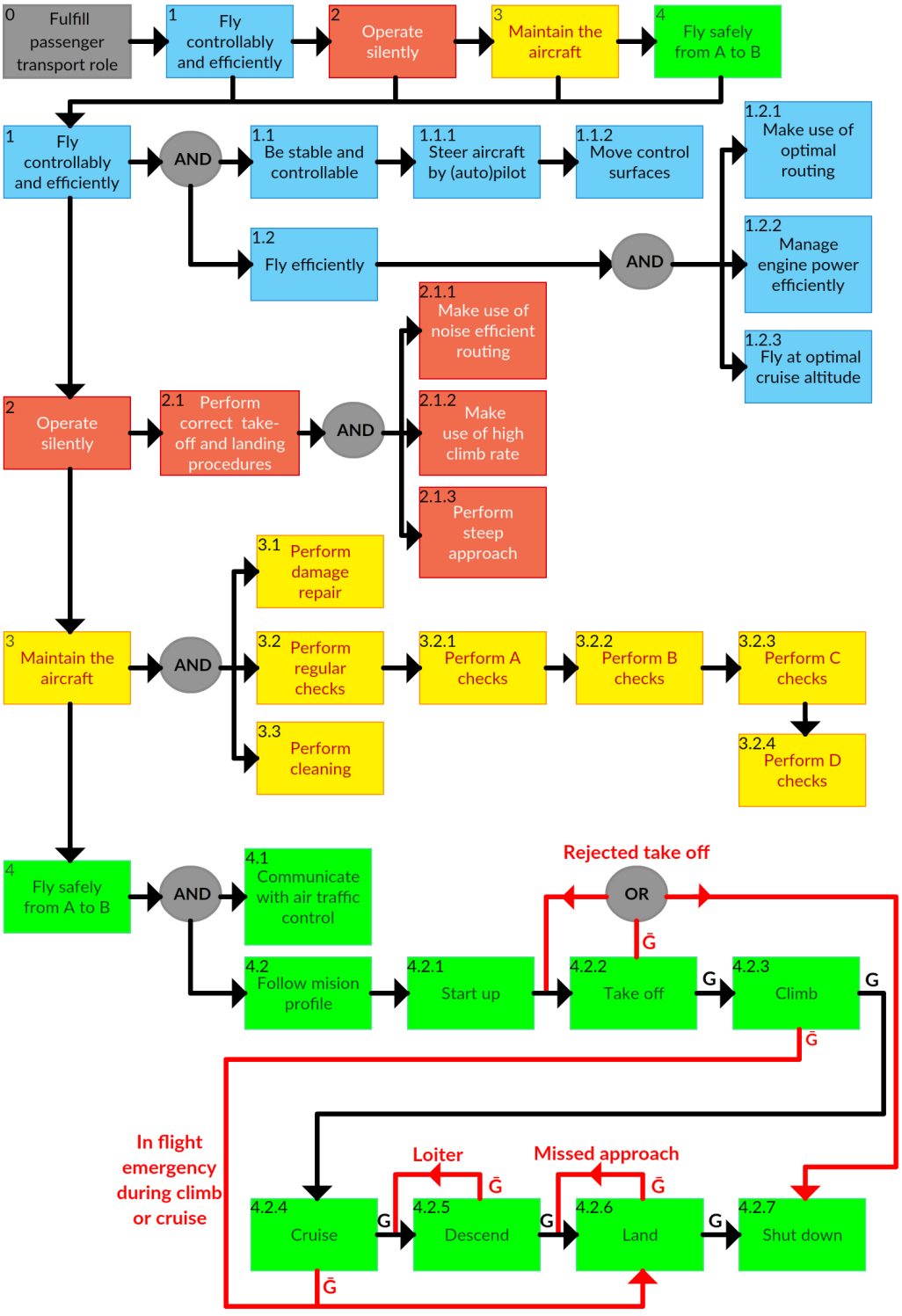

Figure 17.2: Functional flow diagram for a low-noise medium-range airliner.

17.2 Payload-Range Diagram

A payload-range diagram reflects the operational capacity of an aircraft. Even though the SRJ is designed for transporting 110 passengers, it will often perform flights with a load factor less than 100%. This is also illustrated by the requirement on LCY operations at a 80% load factor. Consequently, the range the aircraft could actually fly is different for every payload case. Furthermore, typical ranges such as harmonic and ferry range are displayed in this diagram. The harmonic range is the range an aircraft can fly at its maximum

payload. The SRJ is designed in such a way it can perform a 1,500 NM mission according to the defined requirement. The harmonic range is therefore 1,500 NM, located at the first kink in shown in figure 17.3. From that point on, fuel is added by lowering the payload until the point of maximum fuel capacity, 14,000 litres. This results in a range of approximately 3,200 NM with 5,750 kg of payload. When the maximum fuel capacity is reached, the remaining payload is unloaded up to the ferry range. The ferry range is the range the aircraft can fly without any payload on board. The SRJ is capable of flying up to 4,100 NM. This is useful for delivery and relocation flights. Moreover, it underpins the feasibility of a business jet.

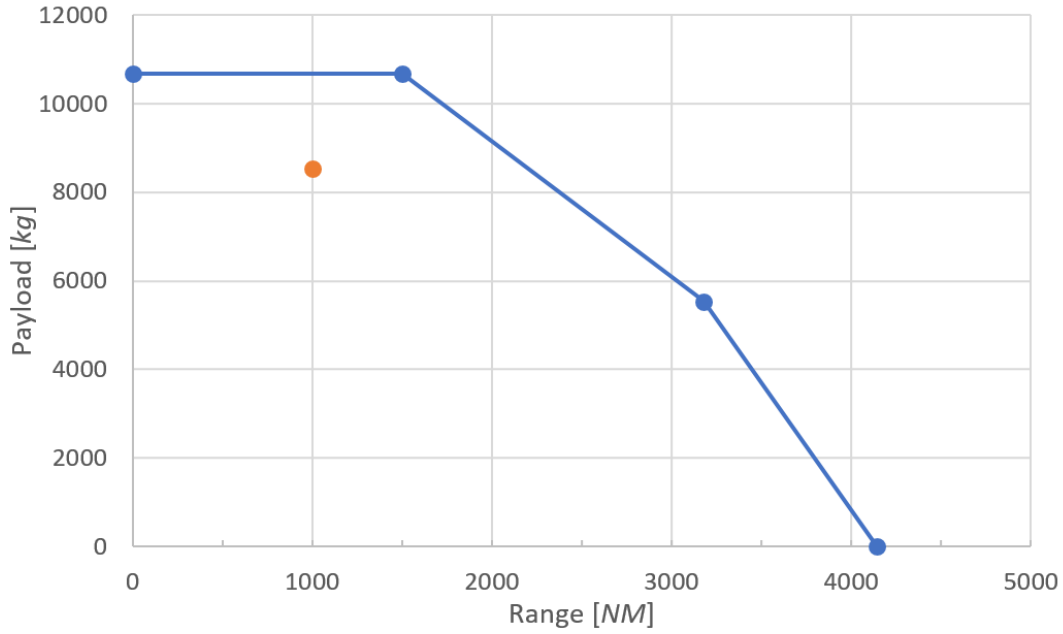

Figure 17.3: The payload-range diagram of the SRJ110. Requirement SRJ110-PERF-LCY-A1 is indicated in orange.

17.3 Operational Noise Mitigation Procedures

Besides designing an aircraft with less noise emission, certain operational procedures can also contribute to noise reduction. Various standards exist, both for take-off and approach/landing. These are presented in subsection 17.3.1 and 17.3.2, respectively.

17.3.1 Take-off Procedures

As explained in subsection 12.3.1, the measuring point for flyover noise is at 6,500 m from the start of the take-off roll. This means there is no fixed altitude above the measuring point and this depends on the climb performance of the aircraft. A higher altitude will translate in less noise, especially using the engine on top configuration. This can be achieved by a shorter take-off roll and/or higher climb rate.

Depending on airport specific noise abatement procedures, the flight management system (FMS) can compute the most optimum track for minimum noise. Boeing has developed a Quiet Climb System which takes into account obstacle clearance and noise abatement to calculate the ideal airspeed, climb angle and thrust reduction and restoration altitudes [141]. A similar system can be included in the SRJ. Automation of noise abatement in the autopilot system through the FMS also reduces crew workload and can increase compliance, leading to less fines for airlines flying to strictly noise-controlled airports. For certification purposes, thrust cutback is also allowed for the flyover measurement above a height of 300 m for two-engined aircraft [102].

17.3.2 Approach and Landing Procedures

During approach, a commonly used procedure to reduce noise is the so called continuous descent approach (CDA), visualised in figure 17.4. Using this procedure, the aircraft establishes on the glide path to the runway at distance further from the runway threshold. Consequently, the aircraft smoothly descends to the runway at a constant angle. This concept eliminates the necessity to level off at certain flight levels during a regular,

stepwise descent which would entail an increase of thrust. This results in a decrease in noise and fuel burn. Another feature is a reduced flap setting during approach. As aerodynamic noise is more profound during approach when the engines are at idle, this can have a significant influence on the noise emission. The reduced flap approach is a standard operating procedure at Amsterdam Airport Schiphol, and almost all aircraft are capable of performing this procedure [142]. A flight management system can calculate the optimum flap and glide path settings for lift, speed reduction and noise during the final flight phase.

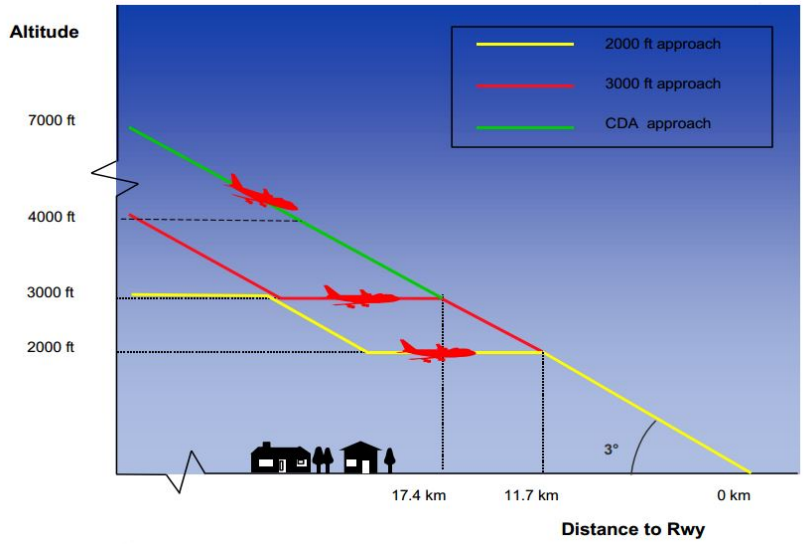

Figure 17.4: Image showing the CDA approach in green versus the stepwise approach paths [142].

It is also possible to delay the aerodynamic noise coming from the landing gear if the latter is extended at a later point during the approach. Normally, an aircraft needs to be fully configured, i.e. all flaps and gear should be in the landing position, at 1,000 ft altitude. This means the gear comes down between 1,500 and 2,000 ft altitude, or 9 to 11 km from the runway. Delaying the gear extension will reduce the noise effected area further from the airport. A new landing gear extension mechanism, able to deploy the landing gear faster and with a high reliability, will be sought. Furthermore, in order to introduce this method, airworthiness authorities and airlines need to be consulted for implementation in certification and standard operating procedures. Additional investigation needs to be performed what can be the extension moment at the latest, taking into account the change in drag and stability of the aircraft.

17.4 London City Procedures and Regulations

Besides nominal missions, requirement SRJ110-PERF-LCY-A1 states that the SRJ110 has to operate from London City Airport (LCY). This airport is known for its very short runway (1,199 m effectively) and urban location and therefore has special regulations, as stated by the London City Airport Consultative Committee (LCACC) and by EASA in Appendix Q of CS25 [11, 143].

Firstly, aircraft that fly to and from LCY have to qualify for a Steep Approach Landing (SAL), as determined by CS25 regulations and requirement SRJ110-PERF-LCY-A1-04. This requires aircraft to fly at an approach path angle greater than or equal to 4.5° (or 7.9 %) instead of the normal 3° (or 5.2%). However, the LCACC requires 5.5° (or 9.6 %). During the design of the SRJ110, it has been ensured that the aircraft satisfies the most stringent requirement. This is done by installing slats and flaps that provide a high lift coefficient to compensate the lower approach speed. Furthermore, the flare will be initiated before reaching the screen height, to make sure that the rate of descent before touchdown is smaller than 3 ft/s (SAL 25.5.b.ii) [11]. Lift dumpers, reverse thrust, a load factor of 80% and effective brakes guarantee that the aircraft comes to a stop within the runway length. This is also proven in section 10.3.

Secondly, standard instrument departures (SIDs) are steeper than normal, with a required climb gradient of 10.4% instead of the normal 5-7% [144]. This, in combination with the short runway, requires an aircraft with high lift and climb performance. A load factor of 80% and the ground effect caused by the low wing already improve the take-off performance. Additionally, the SRJ110 has a high take-off lift coefficient and excess power to be used in case of LCY departures. All these measures assure the aircraft is able to take-off safely and to follow SIDs without any problem, as was also shown in section 10.2.

Lastly, London City Airport enforces a regulation about maximum wingspan. As can be seen in figure 17.5, the taxiway is so close to the stands, that aircraft have to park with their nose facing to the taxiway. Therefore aircraft with a wingspan larger than 36 m are not allowed at LCY. The SRJ110 has a wingspan of 28 m and thus meets the requirement.

Figure 17.5: Image showing the aircraft line-up at LCY gates. All aircraft are facing the taxiway, instead of the terminal [145].

17.5 Reliability, Availability, Maintainability and Safety

RAMS (Reliability, Availability, Maintainability and Safety) is a method used to guarantee and describe the quality of a product. In subsection 17.5.1 to 17.5.4, these parts will be elaborated on. The RAMS method depends on the company and the main focus. Figure 17.6 shows the relations between the different RAMS aspects.

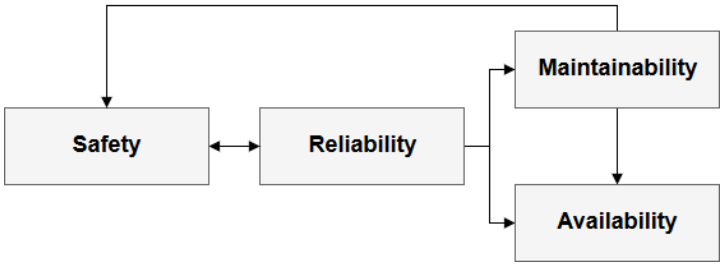

Figure 17.6: Relation between reliability, availability, maintainability and safety [146].

17.5.1 Reliability

Knowing the reliability of an aircraft is important to establish quality and safety. Reliability is subdivided in subsystem reliability and dispatch reliability.

Subsystem Reliability

Knowing the subsystem's reliability will ensure checks will be performed in time and the probability of accidents decreases by adding redundancy where necessary and possible. An approach on how this is done is described below.

First of all, the reliability shall be modelled using block diagrams of all individual subsystems. Afterwards, prediction models have to be designed or applied if already existing. These models should be able to quantify the reliability of each subsystem by calculating the probability of failure in a given period of time. In this way it is possible to identify the critical components and add redundancy if feasible. The most commonly used design reliability analysis method is FMECA (Failure Mode, Effect and Criticality Analysis), which identifies all possible failure modes. It has three main steps: determining the probability of occurrence, assessing the criticality number and constructing the criticality matrix [146]. The reliability of all systems should be checked and agreed on by all stakeholders in order to establish satisfaction. Furthermore it is important to investigate whether all systems comply with regulations and industry standards. Besides the design considerations, also

regular maintenance checks should be performed, according to CS25 regulations [11]. Afterwards, all parts should undergo integrated testing. Examples of to be tested parts are high lift devices, control services, landing gear and engines. For instance, the engines should be tested for water and bird ingestion. Furthermore the overall structural integrity should be tested as well. During operational life all failure modes should be recorded to improve future designs.

Dispatch Reliability
As stated in requirement SRJ110-S&R-REL-A1, the SRJ110 shall have a dispatch reliability of at least 98%. Dispatch reliability is determined as the percentage of flights that depart within a certain margin, which is mostly set at 15 minutes. The dispatch reliability depends on the airline, but also on maintenance issues, weather, etc. In table 17.1, the dispatch reliability of comparable aircraft is shown. As can be seen, the average dispatch reliability is 99.20%. From this it can be concluded that the SRJ110 will meet its requirement easily as it is designed for rather conventional missions.

Table 17.1: Dispatch reliability of comparable aircraft.

Aircraft:	Dispatch Reliability [%]:	Source:
B737NG	99.67	*boeingblogs.com*
A320NEO	99.70	*flightglobal.com*
SSJ100	99.70	*aviationweek.com*
ERJ170/175	98.20	*Embraer Status Report* [16]
CRJ900NG	99.67	*bombardier.com*
CS100	99.00	*flightglobal.com*
RJ100	98.00	*regional-services.com*
B717	99.65	*mediaroom.boeing.com*
Average	**99.20**	

17.5.2 Availability
Availability illustrates the probability of the readiness of a system, when required for use. Due to delays, time and money can be lost; a significant disadvantage for all stakeholders. Therefore it is crucial to have a good availability prediction and thus a clear maintenance plan. Three types of availability will be used to predict the reliability of availability, the inherent availability, the achieved availability and the operational availability. The first two are under ideal circumstances, without taking into account delays. Firstly, inherent availability is without any scheduled maintenance actions, hence this is regarded as a conceptual plan. The second one, achieved availability, includes scheduled or preventive maintenance checks. The second is obviously more advanced than the first but still preliminary. In future stages, the third one will be determined, namely the operational availability. This is the probability of availability in a real environment, taking into account delays. This approach is needed to identify the critical points in availability and prevent mistakes or delays as much as possible.

17.5.3 Maintainability
The maintenance of a design should be constructed in such a way that the least amount of time and money is spent and to still ensure safe operations.

When determining the maintainability of the aircraft, certain factors need to be taken into account. Firstly, the fine balance between elapsed time and labour-hours is the a major factor [146]. More people means having a shorter elapsed time, but it increases the labour hours and thus labour costs. This balance should be as economical and ergonomic as possible. Secondly, the human factors are regarded. This considers the ability to observe errors without using instruments. Furthermore, the maintenance tools should be designed considering the ease of use and the health impact for humans. Thirdly, the frequency factors are taken into account. These are dependent on the reliability of a single subsystems. The reliability models together with the regulations determine the frequency of maintenance checks. An additional factor considers logistic support. This represents to the availability of equipment, facilities and personnel, as well as the organisation of the maintenance. Lastly, there is cost. Most of the previous factors aim to be as economically efficient as possible. Cost directly relates to market attractiveness and satisfaction of the customer. All previous factors need to be regarded when setting up the maintainability requirements.

17.5.4 Safety

Safety engineering is designed to protect the system, the people and the environment. First of all, the system should be designed to avoid failure, or in case of failure, it should not cause any hazard. For example, when a leakage occurs in the fuel tanks, explosions could be avoided by self sealing tanks. This should ensure that not the whole system is lost in case of failure. In case of failure during operation, the aircraft occupants should be safe as well. Emergency plans should be thoroughly worked out and well explained to the passengers. Moreover, the systems should have redundancy or frequent maintenance checks in order to avoid failure during operation. Lastly, the design should also be safe for the environment, mainly taking into account pollution. The pollution mitigation for the SRJ110 considers CO, CO_2, HC and NO_x emissions. Furthermore the aircraft is designed to have a low noise pollution as well. Additionally, assuming that the aircraft might crash, the surroundings should be affected as less as possible, by for example using self sealing tanks. Besides operational safety, the design and the manufacturer should ensure production safety. Labourers should not be harmed during the manufacturing of the aircraft. All risks occurring in the design and during operations are thoroughly analysed and mitigated in the technical analysis chapter 4.

17.6 Communication Flow Diagrams

The average annual growth of air traffic in Europe is estimated to be 1.3% according to *Eurocontrol* [147]. The number of daily air operations all around the world is continuously rising, increasing the need for improved and sophisticated communication systems. In order to keep safety to an acceptable level and to ensure efficient air traffic operations, reliable communication between the different involved parties is crucial. This mainly includes pilots, air traffic operators and flight attendants.

Air traffic management is organised such that operations are in any circumstances handled in an efficient, reliable and safe way. To do so, the airspace has been divided into different regions corresponding to different flight mission phases. Figure 17.7 provides the vertical division of the airspeed in terms of altitude.

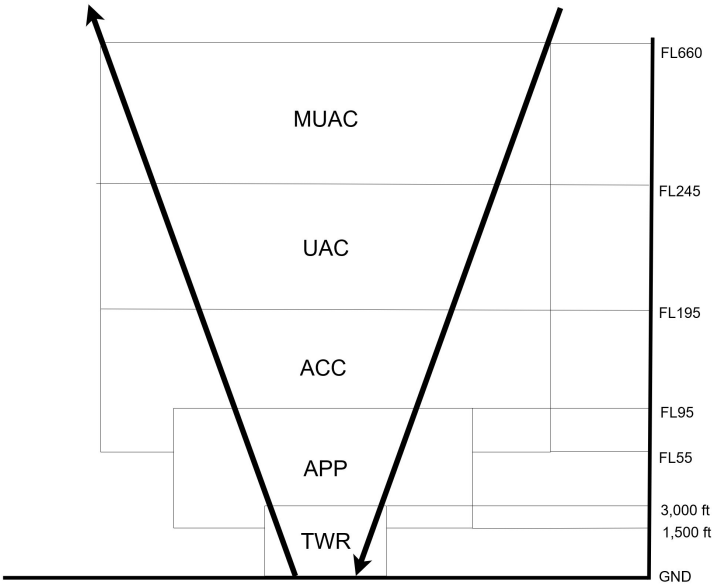

Figure 17.7: Vertical organisation of the different air traffic control centres.

Airport Traffic Control Towers (TWR) provide ground traffic control, take-off and landing control. The airport traffic area typically covers a region of 5 NM around the tower and vertically extends from ground up to 3,000 ft. Direct communication is made with the pilots and other relevant parties on the ground by means of radio systems. Visual traffic awareness is supported by Terminal Approach and Surface Movement Radars [148].

Another terminal area facility is the Approach Control Centre (APP) responsible for approaching and departing traffic. The airspace layer covered by APP ranges from 1,500 ft to $FL95$, namely 9,500 ft.

Communication at higher altitudes is ensured by the En Route control centres, also known as Air Route Traffic Control Centres (ARTCC). Between $FL55$ and $FL195$, Air Traffic Control Centres (ACC) are responsible for the air traffic. On top of the ACC, Upper Area Control Centres (UAC) extend up to $FL245$. Finally, the Maastricht Upper Area Control Centre (MUAC) is responsible for the air traffic in Europe at altitudes ranging

from $FL245$ to $FL660$. Two different services are provided by these control centres. On one hand, transition from one altitude to another - on pilot request or for safety reasons - is performed. This phase approximately lasts ten minutes. On the other hand, navigation and guidance during cruise is provided. The flight time during cruise can vary from twenty minutes to several hours.

Communication is of great importance during the entire flight mission. From engine start-up to parking at the gate of destination, clear instructions are provided to pilots to efficiently manage the operations on ground and in the air. In case of emergency, an effective communication is also required to best handle the situation. The communication system should therefore be designed in a way to ensure an undisturbed flow of information from the system to the environment, for instance by including system redundancy.

Due to the fragmentation of the airspace, the communication is highly dependent on the flight phase. Pilots have to interact with the appropriate control unit according to the flight altitude and flight phase. However, communication in between the pilots, flight attendants and passengers is possible all along the flight mission, notably for safety reasons and information. Also independent of the flight phase, communication with the airline company at any time during the flight is ensured by the Aircraft Communications Addressing and Reporting System (ACARS). Information exchanged through the ACARS is airline administrative control, engineering data and air traffic control command. Direct communication between pilots of other aircraft is possible as well.

In figures 17.8 and 17.9, communication flow diagrams are presented. Figure 17.8 displays the communication chain depending on the flight mission phase. The diagram in figure 17.9 illustrates the communication occurring independently of the flight phase. In both cases, the flow of information is represented by arrows. As expected, the pilot is the central element of these diagrams.

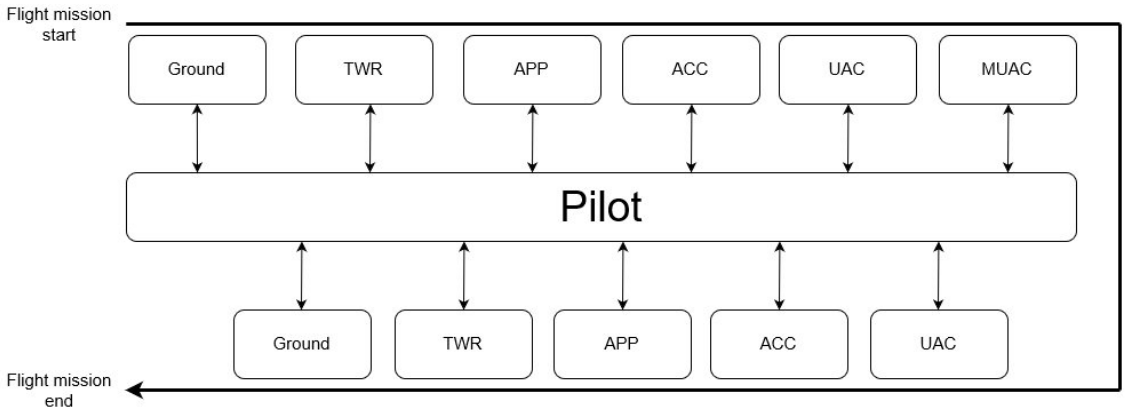

Figure 17.8: Communication flow diagram depending on the flight phase of the SRJ110.

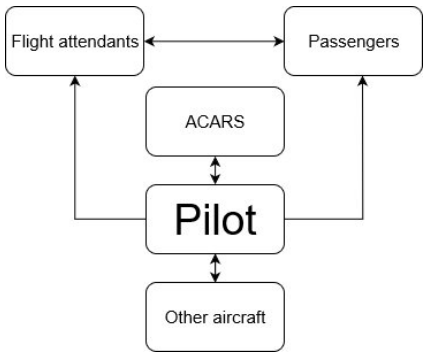

Figure 17.9: Communication flow diagram of the SRJ110 independent on the flight phase.

18 Sustainability Strategy

For companies, a proper sustainability strategy is indispensable in current times. The airline industry is no exception to this rule. As a matter of fact, airlines share a great deal of responsibility with respect to sustainability due to the significant carbon dioxide emissions and noise pollution. Sustainability has been one of the most driving criteria in the entire design process. Every group member working on a certain part of the design was aware of the responsibility aerospace engineers share with respect to sustainable design. A brief analysis of the important role sustainability played in the main design departments is presented in the following paragraphs.

The Aerodynamics Department was tasked with making the aircraft fly with the least amount of drag possible. Minimising drag is one of the key tasks of aerodynamicists and the effects related to sustainability are significant. Drag is one of the main drivers of fuel consumption which in turn determines the emission of pollutants such as carbon dioxide as well as nitrogen oxides, hydrocarbons, soot and others. In addition, drag is responsible for a large part of the noise generated by the airframe. The aerodynamics group performed a detailed design of winglets as well as an elaborate airfoil selection process in order to achieve the lowest drag configuration possible. The winglets reduced the total drag with 3.25% and the supercritical airfoil ensures low drag levels at higher cruise speeds.

The flight performance and propulsion team spent significant time and effort into engine selection, as well as determining the most optimum flight conditions for the aircraft. The PW1700G was selected as the engine for the SRJ110 due to its excellent power output, superior specific fuel consumption and low noise levels. With respect to the cruise altitude and cruise speed the optimum combination, to minimise fuel consumption, was determined. These results were of particular importance to the aerodynamics department. Last but not least, the flight performance of the aircraft proved to be a key input to the analysis of the noise contours of the aircraft. Optimising the climb gradient after take-off yields a significant reduction in noise levels on the airport surroundings.

The aerospace structures and materials department performed elaborate research on reducing the aircraft weight without making compromises to aircraft and passenger safety. The weight of the aircraft is reduced by clever design and application of novel materials, hence reducing the required aircraft lift. Less lift also implies less drag, and the results of lower drag have already been discussed earlier in this chapter. The use of carbon fibre composites has been embraced due to the superior aircraft performance, albeit at a higher unit cost and more challenging end of life solutions. The excellent aircraft performance outweighed the disadvantage of the more challenging recyclability of the composite materials. In addition, a lot of research is currently conducted in the field of recycling composite structures [149]. Research in this field is not expected to decline anytime soon due to the more and more widespread application of composites. It is likely that by the time the aircraft has to be disassembled, recycling technologies for composites have been improved significantly. This would mitigate one of the major downsides into the application of composites in current time setting. Last but not least, some important remarks about the manufacturing process were also made.

Next to environmental sustainability, economical sustainability is not to be underestimated. Making sure that the aircraft is attractive to customers at the moment it is introduced as well as during its entire life cycle contributes vastly to sustainability. An elaborate cost analysis was performed to determine the competitiveness of the aircraft on a unit cost basis as well as a direct operating cost basis. Even though the unit cost of the SRJ110 is higher than required, the lower direct operating cost still gives the aircraft a significant advantage over the competition. The lower direct operating cost also ensures that the aircraft remains an attractive option for long term use. As a result the aircraft life time should be increased significantly.

The effect of noise on sustainability is not to be underestimated. The impact of aircraft noise on the environment ranges from public complaints and possible health issues to animal migration. An elaborate research study has been performed by the noise research group into the concept of noise combined with a wide variety of possible mitigation measures. After the application of various noise mitigation measures to the SRJ110, an analysis with *INM* has been conducted to investigate the extent to which the noise levels have been reduced. The results emphasised the improved noise characteristics of the SRJ110 over the competition without making compromises to important parameters such as fuel efficiency and direct operating cost. It is safe to say that the SRJ110 sets a new industry-wide standard with respect to low noise operations.

The SRJ110 design team is satisfied sustainability has been integrated and considered throughout the design process and is confident that the aircraft will contribute towards current trends tending towards a greener society.

19 Requirements Compliance

The final task to perform is demonstrating compliance with the initial requirements defined in chapter 2. This step is crucial in the delivery of the final design as the obvious goal was to comply with all customer requirements. The compliance is illustrated by a so called compliance matrix. The matrix is shown and discussed in section 19.1. The outcome of this section is subjected to discussion and evaluation, which is carried out in section 19.2.

19.1 Compliance Matrix

The compliance matrices are divided over the topics introduced in chapter 2. Hence, a compliance matrix, or table, exists per topic. These are displayed in the following subsections. The structure of each compliance table is however constant for every set of requirements. Firstly the prefix is identified in the left cell, followed by the general parameter of interest in the cell right next to the requirement identification. The required value is then restated such that it can be compared to the achieved value, so the compliance can be ticked off in the second to last column. The final column refers to the respective (sub)section where the compliance or non-compliance is discussed and found.

19.1.1 Capacity and Operational Requirements

Below, the compliance of the capacity and operational requirements is shown. The detailed (sub)requirements and the performed requirement analysis can be found in subsections 2.2.1 and 2.3.1. In conclusion, all requirements with respect to this particular topic are met. Accordingly, the demand of the customer to develop a 110 PAX aircraft with a certain comfort standard are satisfied.

Table 19.1: Compliance matrix for capacity and operational requirements.

Requirement:	Parameter of interest:	Required value:	Achieved value:	Compliance:	(Sub)section:
SRJ110-OPS-CAP-A1	PAX [#]	110	110	✓	14.1
SRJ110-OPS-CAP-A1-01	Seat pitch [in]	30	31	✓	14.1
SRJ110-OPS-CAP-A1-02	Seat width [in]	18	18.5	✓	14.1
SRJ110-OPS-CAP-A1-03	Aisle width [in]	20	23.7	✓	14.1
SRJ110-OPS-CAP-A1-04	Lavatories [#]	2	2	✓	14.1
SRJ110-OPS-CAP-A1-05	Galleys [#]	3	3	✓	14.1

19.1.2 Performance Requirements

The goal to offer the customer an aircraft with an outstanding performance has definitely driven the design. Therefore a great amount of effort has been allocated to meeting requirements. The detailed system requirements and subsystem requirements including the requirement analysis is discussed in subsection 2.2.2 and 2.3.2 respectively. Conclusively, all performance requirements are met and thus the SRJ is able to operate from London City Airport, identified as a key requirement.

Table 19.2: Compliance matrix for the performance requirements.

Requirement:	Parameter of interest:	Required value:	Achieved value:	Compliance:	(Sub)section:
SRJ110-PERF-CRU-A1	True air speed [m/s]	216	229	✓	10.1
SRJ110-PERF-RAN-A1	Range [NM]	1,500	1,500	✓	17.2
SRJ110-PERF-LCY-A1	Range [NM]	1,000	1,000	✓	17.2
SRJ110-PERF-LCY-A1-01	Slope [°]	5.5	6.5	✓	10.3.2
SRJ110-PERF-LCY-A1-02	Descent gradient [%]	7.9	11.39	✓	10.3.2
SRJ110-PERF-LCY-A1-03	Climb out gradient [%]	3.5	19.4	✓	10.2.2
SRJ110-PERF-LCY-A1-04	Steep approach landing	-	-	✓	10
SRJ110-PERF-LCY-A1-05	Landing distance [m]	1,207/1,309	925	✓	10.3.2
SRJ110-PERF-LCY-A1-06	Take-off distance [m]	1,199	1,071	✓	10.3.1

19.1.3 Safety and Reliability Requirements

Safety and reliability are important as it reflects the operational performance of the aircraft. Even though only two requirements were set in this field, the one related to safety was rather extensive. Hence, the compliance with that requirement is shown in this stage but further discussion will be done in the next section. The requirements themselves can be found in subsection 2.2.3.

Table 19.3: Compliance matrix for the safety and reliability requirements.

Requirement:	Parameter of interest:	Required value:	Achieved value:	Compliance:	(Sub)section
SRJ110-S&R-REL-A1	Dispatch reliability [%]	98	99.2	✓	17.5.1
SRJ110-S&R-SAF-A1	CS25	-	-	X	-

19.1.4 Sustainability Requirements

Sustainability was identified as one of the most important topics for the SRJ's development, since it entails both fuel efficiency and noise. Therefore from early stages on, the progress has been carefully monitored resulting in compliance with all requirements.

Table 19.4: Compliance matrix for the sustainability requirements.

Requirement	Parameter of interest:	Required value:	Achieved value:	Compliance:	(Sub)section:
SRJ110-SUS-POL-A1	NO_x [%]	50%	52.2%	✓	10.1
SRJ110-SUS-POL-B1	CO_2 [$g/PAX/NM$]	134.3	118.4	✓	10.1
SRJ110-SUS-POL-C1	CO, HC [$g/PAX/NM$]	0.004263/0.004263	0.00376/0.00376	✓	10.1
SRJ110-SUS-POL-D1	Fuel consumption [$kg/PAX/NM$]	0.04263	0.376	✓	10.1
SRJ110-SUS-POL-E1	Noise [dBA]	256.8	247.0	✓	13.3
SRJ110-SUS-POL-F1	Noise Exposed Area [km^2]	35.2	35.6	X	13.4.2

19.1.5 Cost Requirements

The unit cost and DOC reflect the commercial viability of the aircraft. Complying with the customer's desires is of the utmost importance, so that the customer is capable of earning profit using the SRJ110. The previously defined requirements are listed in subsection 2.2.5. In conclusion, only one of the requirements is met.

Table 19.5: Compliance matrix for the cost requirements.

Requirement:	Parameter of interest:	Required value:	Achieved value:	Compliance:	(Sub)section:
SRJ110-CST-CST-A1	Unit cost [million USD]	40.0	54.8	X	15.1
SRJ110-CST-DOC-A1	DOC [USD/h]	3,671	3,026	✓	15.2

19.1.6 Miscellaneous Subsystem Requirements

The origin of the miscellaneous subsystem requirements differs per requirement. It was either the logical consequence of the design process or engineering considerations. The requirements have all been met regardless.

Table 19.6: Compliance matrix for the miscellaneous subsystem requirements.

Requirement:	Parameter of interest:	Required value:	Achieved value:	Compliance:	(Sub)section:
SRJ110-WIN-DIM-A1-01	Wingspan [m]	36.0	28.0	✓	8.2
SRJ110-INT-LUG-A1-01	Luggage compartment [L]	5,000	8,100	✓	14.1
SRJ110-INT-LUG-A1-02	Cargo volume [L]	12,000	12,000	✓	14.1
SRJ110-RES-TEAM-A1-01	Time [weeks]	10	10	✓	-
SRJ110-RES-CST-A1-01	RDTE [million USD]	1,700	754.27	✓	15.1

19.2 Discussion and Evaluation

The general conclusion of the compliance tables is straightforward. Three requirements are not met in this stage of the design. The respective requirements are once more listed below:

- SRJ110-S&R-SAF-A1 The aircraft shall be in compliance with the CS25 regulations. *Considered a driving requirement.*

- SRJ110-CST-CST-A1 The unit cost of the aircraft shall not exceed 40 million USD. *Considered a key requirement.*
- SRJ110-SUS-POL-F1 The area exposed to Sound Exposure Levels of greater than 65 dBA shall be less than 35.2 km^2.

The requirement SRJ110-S&R-SAF-A1 is not complied with, even though in a later stage it must definitely be proven as it is of the utmost importance to the SRJ110 commercial viability. If the aircraft is not proven to be airworthy, it will never be allowed to operate. The airworthiness regulations described by CS25 are very extensive, containing an enormous amount of regulations. Hence at this stage it is respected to the most elaborate extent but not completely complied with. An example of the SRJ's compliance would be steep approach landing at London City Airport or the fuselage design. However, CS25 contains regulations on topics that have not been treated yet, such as bird strikes and foreign object ingestion by engines. Consequently, it is concluded that overall the SRJ does not meet all set regulations, but the first steps are taken for doing so.

The unit cost was already identified as one of the most stringent requirements in an early stage of the report. Even the basic estimate performed in the Mid-term Report showed the requirement may not be met [31]. However, a more detailed analysis was first conducted before drawing conclusions. As expected, the more detailed analysis performed resulted in similar results. The requirement of 40 million USD can not be met. To resolve this incompliance, an open discussion was held with the customer to see what would be acceptable from his perspective. In conclusion, both parties agreed on accepting the current listing price under the condition that the direct operating cost would be less than foreseen. The cost analysis carried out in chapter 15 did show a significant reduction in DOC in comparison with the requirement. Thus, eventually the customer is satisfied with the current results.

Requirement SRJ110-SUS-POL-F1 is not met by an almost negligible margin of 0.4 km^2 or 0.8%. As previously discussed in subsection 13.4.2, one of the most promising measures is not yet taken into account: the engine shielding due to the wing. The model utilised, *INM*, was not able to model the potential noise reduction due to this noise mitigation measure. Hence, the requirement is not complied with in this stage but the design team is certain that in a later stage, with a more advanced model, the desired results will unequivocally be attained.

In conclusion, out of all requirements only three have not been met. Even though the team always strove to satisfy all top-level requirements to the best possible extent, the results are clear. Two out of three non-compliant requirements can and will be met in the future, which is why these are still considered feasible. In close consultation with the customer, the requirement on unit cost is deemed unfeasible and that is why the current result is accepted. The unfeasibility of this particular requirement is underpinned by the validation in chapter 16.

20 Post-DSE Planning

This chapter introduces the planning of the post-DSE activities. Identifying the actions to be taken once the conceptual design phase is concluded gives insight about the future functioning of the engineering company. In section 20.1 the project design & development logic will be explained. Section 20.2 presents the Gantt chart of the project. Finally in section 20.3, the production plan for manufacturing the SRJ110 is provided.

20.1 Project Design & Development Logic

In this section, all phases to be executed post-DSE are discussed and subsequently visualised by means of a project design & development logic diagram in figure 20.1. The starting point of the diagram consists of the DSE output, namely the conceptual design of a low-noise medium-range airliner. Three main phases are highlighted in the diagram: the detailed design phase, the industrial phase and the in-service phase. Hereafter, a brief explanation of each phase is provided.

20.1.1 Detailed Design Phase

In the first phase, the remaining part of the design is completed. The DSE-output is a conceptually designed aircraft, which still has to go through the preliminary design and detailed design phase. Class III and Class IV weight estimations will be performed and highly detailed structural components will be designed. Also, other systems will be designed in sufficient detail in order to go into production. Such systems are, among others, the flight computers, auto-flight and cockpit systems, electronics, high lift devices, landing gear, etc. All along the development phase, verification and validation campaigns are constantly performed to check the accuracy and reliability of the acquired outputs. Furthermore, due to the highly-iterative character of the engineering design process, procedures need to be set up for an efficient system development.

20.1.2 Industrial Phase

Once the final aircraft configuration is presented and approved by the customer, the industrial phase will be initiated by defining the assembly process. Prior to manufacturing the components, materials and tools will be collected, and facilities will be arranged. Simultaneously with the assembly of the aircraft, certification of the software (S/W) and hardware (H/W) will take place. Qualification tests will also be performed. This will be followed by the elaboration of operations manuals. After that, the flight tests will be undertaken. Shorter after the compliance of the system with the regulations and certifications, the production series will start. This is also known as the industrial ramp up production [150].

20.1.3 In-service Phase

The in-service phase will be kicked off by delivering the aircraft to the customer. However, prior to the Entry In-Service (EIS), the customer will perform a complete and detailed check of the system including, amongst others, ground check and acceptance flight [151]. Moreover, training of personnel will already be initiated. During the entire operational life of the aircraft until disposal, maintenance will be performed to make sure the quality standards defined by the manufacturer and design company are reached. Furthermore, the engineering company will remain available and provide support to the customer. However, not all material will be disposed, as sustainability is a main factor in the design of this aircraft. It will be possible to recycle used materials and potentially reuse it in the manufacturing and assembly phase.

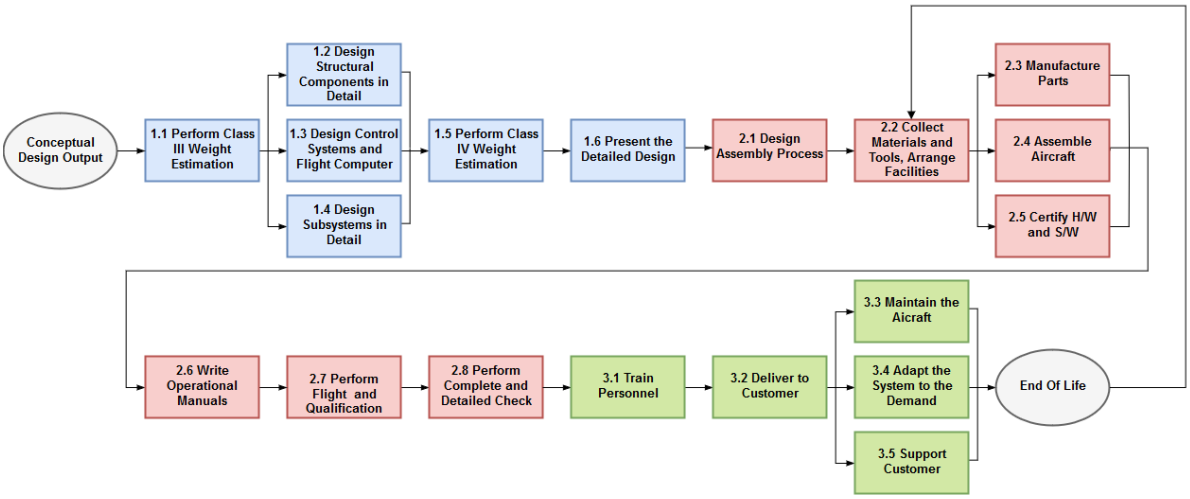

Figure 20.1: Project design and development logic with the design phase blue, the industrial phase red and the in-service phase green.

20.2 Project Gantt Chart

The Gantt chart shown in figure 20.2 shows the chronological order of tasks to be performed after the DSE. The Gantt chart directly results from the Project Design and Development Logic diagram presented in section 20.1. The Gantt chart is a living document, meaning that it requires regular update in order to keep an accurate overview of the project progress and the ongoing tasks. The gray bars represent the different phases identified in the Project Design & Development Logic diagram. The in-service phase is evaluated to last approximately 30 years. However, due to limitations of the program used to construct the Gantt chart, the final three steps, namely 3.3, 3.4, 3.5, end around 25 years after start.

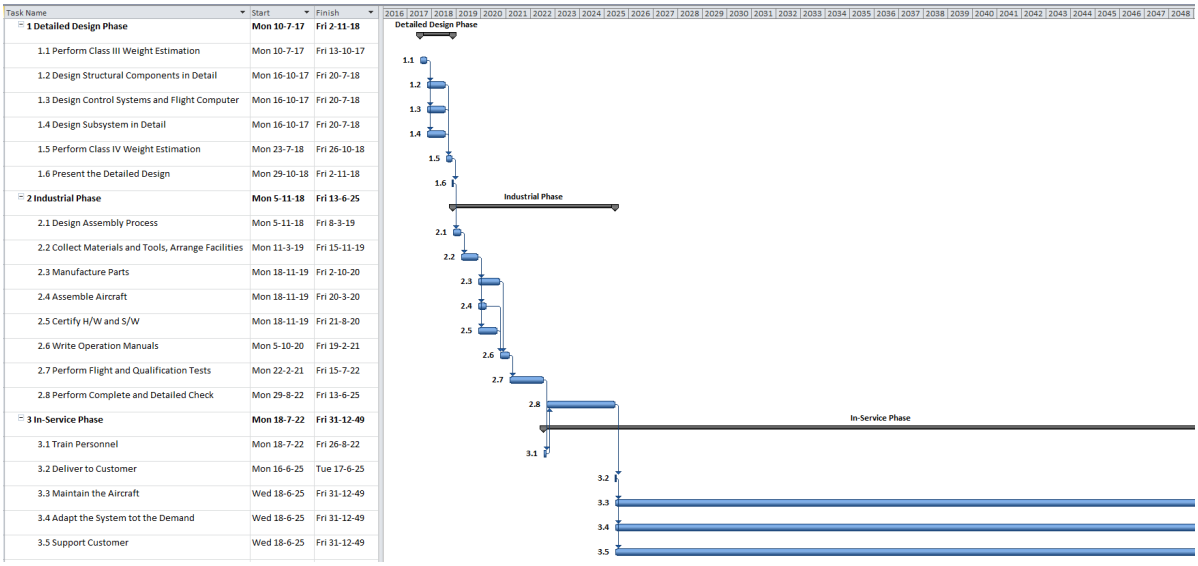

Figure 20.2: Gantt chart of post DSE tasks, including work breakdown structure.

20.3 Production Plan

This section provides the manufacturing, assembly and integration plan for the production of the SRJ110. A time ordered outline of the production activities is illustrated by means of two flow diagrams. The first diagram focuses on the manufacturing, while the second one presents the assembly activities of the SRJ110. The diagrams are presented in subsections 20.3.1 and 20.3.2 respectively, together with a brief explanation.

20.3.1 Manufacturing Plan

The first step in producing an aircraft is the manufacturing of the parts as shown in figure 20.3. This starts with determining the required resources and sourcing them. The materials and equipment collected need to be transported to the facility where the raw material will be transformed to aircraft subsystem components. Occasionally, this facility is also the place where assembly happens. In some cases, an extra step needs to be added of transporting the components to a dedicated workshop where the certain parts are made. Afterwards, these parts are stored in a warehouse. Those are components made in batches, meaning they are processed as a group. These batches are made in a dedicated workshop, not in the assembly facility. The finished batches go to a warehouse until they are retrieved for use in the assembly line. When the batch is beneath a certain critical number, a new order is submitted to the workshop. The assembling of the subsystems is presented in the next subsection.

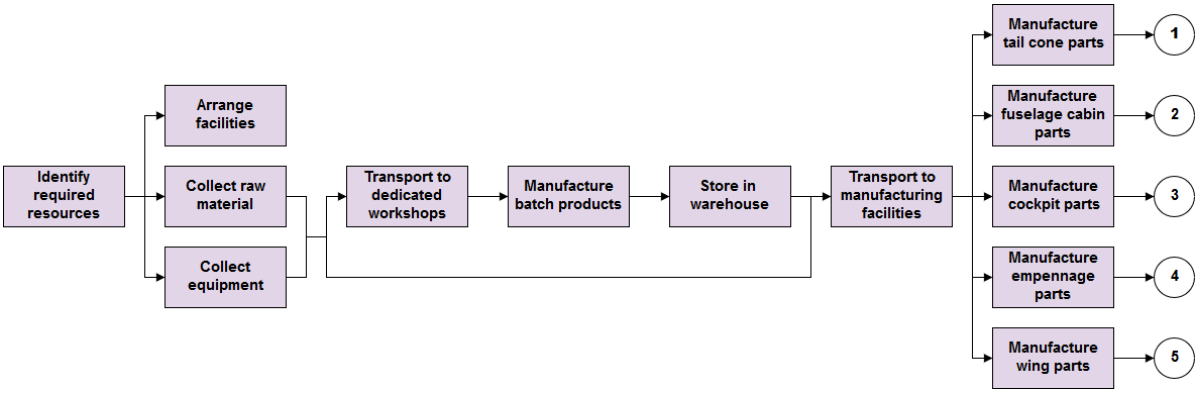

Figure 20.3: Manufacturing plan for the SRJ110.

20.3.2 Assembly and Integration Plan

Aircraft are complex systems made of numerous components that need to be assembled in a specific and ordered way. Designing an assembly and integration plan is therefore helpful to ensure an interrupted flow of actions once the assembly process is initiated. As a matter of fact, a strict assembly procedure allows an efficient and cost effective production process [152].

Nowadays, aircraft production follows a line production model. Line production is characterised by a main assembly line fed by subassembly lines as illustrated in figure 20.4. Fluidity of the assembly is one of the key points of this specific assembly method. For this particular reason, production series can easily be implemented.

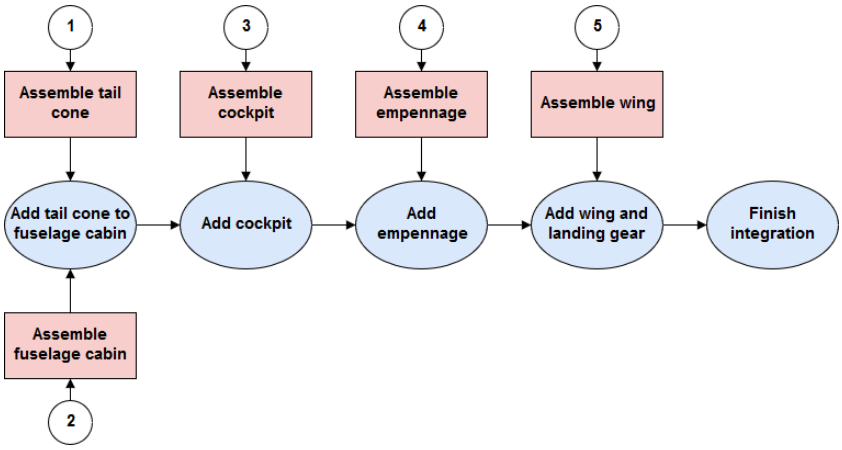

Figure 20.4: Assembly and integration plan of the SRJ110. The assembly activities are presented in the squared boxes, while the integration activities in the circular boxes.

Figure 20.4 presents the assembly sequence chart of the SRJ110 from aircraft component to the final design integration. The sub- and main assembly lines are shown as pink rectangles and blue ovals, respectively. The numbers ranging from 1 to 5 are linked to the manufactured aircraft parts as presented in figure 20.3.

Every subassembly line consists of several stations responsible for the assembly of one specific aircraft component, such as the tail cone, the cockpit section, the empennage and the wings. Specialists are assigned to each station where they perform the same tasks, in a specific amount of time, at subsequent aircraft during the production series. This allocated time is the same for each station such that parts can be moved to the next station in a fluid manner. Once the components are assembled, they are merged to the aircraft in development in the main assembly line. Before the wings are added to the final aircraft design, the landing gear and the engine are integrated to the wing structure. The integration process is finished by fixing the engines at the proper location, attaching instruments and other subsystems.

The level of detail provided in figures 20.3 and 20.4 is rather low, they only provide an overview of the production process of the SRJ110. As soon as the system enters the detailed design phase, more elaborate charts will be generated.

21 Conclusion

The objective of this report was to present the preliminary design of a revolutionary medium-range airliner, specifically aimed at operating from noise-sensitive airports, without significantly compromising efficiency, capacity, cost, environmental impact and safety. After ten weeks of dedicated work, the first prototype of the *Silent Regional Jet 110* has emerged. Through a detailed selection process performed in the Mid-term Report, the configuration of the SRJ110 has been defined based on noise and performance capabilities [31]. It unequivocally resulted in a T-tail jet aircraft with two turbofans on top of the wing.

Prior to defining the design characteristics of the SRJ110, a detailed market analysis has been performed in order to predict the market demand. The SRJ110 will undoubtedly have a place in this large and still growing market, estimating to sell about 450-500 aircraft in the first 15 years after introduction. Versatility of the design in order to create an aircraft family is projected to be lucrative, especially to lower the production and development cost. The main focus is on the European market, however the Latin American and the Asian market show favourable prospects for the future.

Several technical analyses have then been performed to verify the compliance of the design with predefined customer requirements. First, a weight prediction has been carried out. The aircraft gross weight is determined using Class I and Class II weight estimation methods. With almost 60 iterations, accuracy of the obtained results is ensured. Compared to modern reference aircraft, the SRJ110 is lighter, with a maximum take-off mass of 45,734 kg, resulting in excellent performance in fuel efficiency. The operational empty mass is slightly higher compared to reference aircraft, as no detailed weight reduction measures have been accounted yet at this stage of the development process.

Next, the stability and control of the SRJ110 has been investigated. Stability and control is ensured for an horizontal tail surface area of 14.75 m^2, an horizontal and vertical tail arm of 17.89 and 15.39 m, respectively, and a wing positioning at 13.74 m from the aircraft nose. Furthermore, in order to provide ground stability during landing, take-off and taxiing, the landing gear position needed to be examined. A conventional tricycle landing gear configuration has been selected. The main landing gear is attached on the wing but mainly stored in the fuselage, as it was to large to be entirely embedded in the fuselage.

Additionally, the aerodynamic characteristics of the SRJ110 have been investigated. A supercritical airfoil with varying thickness along the span was determined to be most suitable for the design, namely the NASA SC(2)-0610/12/14. The aspect ratio, the wingspan and the wing surface area are evaluated to be 8.925, 28 m and 87.82 m^2, respectively. Raked tips and blended winglets are added to the wing design to enhance the aerodynamic properties. Furthermore, high lift devices are designed, as well as ailerons, rudder and elevator.

The most optimal wing box material, for carrying stresses compared to weight, is a composite skin with inside a honeycomb structure. After analysing the fuselage without wing, the maximum stress is located at the main landing gear. This was used to size the fuselage. The fuselage will be made out of a carbon composite, namely CFRP T800 3900 series, for its performance in tension and compression. Even though it will increase the unit cost, due to the weight savings (20%) the operational cost will decrease significantly.

In the design of the SRJ110, some structural noise mitigation measures are included. First of all, having engines on top is beneficial for the fly-over noise. Additionally, combining it with a low wing configuration also allows for shorter landing gear, hence reducing the airframe noise. The landing gear noise is also mitigated by implementing fairings. Furthermore, to mitigate the noise of the high lift devices, trailing edge brushes are added along with wing fences at the edges of the slotted flaps. The latter is a highly innovative way to minimise flap drag, thus noise. At the leading edge a droop nose slat is used to reduce the noise, together with sealing as much slat-track-cut-out as possible. Engine noise exists out of two parts, jet noise and fan noise. To mitigate the jet noise, chevrons will be used to smooth the airflow. Whereas the mitigation for jet noise requires a large fan and bypass, reducing fan noise requires the opposite. A trade-off has been performed to have the most optimal engine diameter. Another mitigation measure for the fan noise are acoustic liners, they absorb radiated acoustic energy. A gearbox is implemented as well, allowing the fan to spin at a lower RPM, hence decreasing noise. All these mitigation measures together reduce the overall aircraft noise significantly when compared to the Avro. A predicted trajectory has been constructed for both the Avro and the SRJ110. These trajectories along with the corresponding engine net thrust have been fed into a noise prediction program. The results from this analysis have shown that the SRJ110 reaches the targeted noise reduction required at the certification measuring points. Additionally the area which experiences sound levels of over 65 dBA has reduced around 30 %, right on the requirement. The cabin noise will be mitigated by a

combination of extra shielding, isolation and active noise control.

Whereas structural noise mitigation measures have to be implemented in the design, certain operational procedures can be applied as well in order to reduce the noise at the measuring points. To decrease fly-over noise, the aircraft could climb steeper to be at a higher altitude above the measuring point. Moreover, a flight management system can be used for computing the most optimum track for minimum noise. When implemented in the autopilot system, it also decreases crew workload. Typical procedures for landing are the continuous descent approach and a deferred extension of the landing gear. The latest extension moment still needs to be investigated in a future stage. General operational characteristics of the aircraft are the cruise speed and altitude. The aircraft will be able to fly Mach 0.77, in other words 229 m/s at $FL350$. The aircraft has a fuel consumption of 0.0376 $kg/PAX/NM$, which is 12% better than required.

The total development time of the SRJ110 is currently estimated around seven years. The SRJ will have a unit cost of 54.8 million USD, which was higher than the required 40 million USD established by the customer. However, the operating cost will compensate for that, with a direct operating cost of 3,026 USD per block hour. This is approximately 644 USD per block hour less than originally planned on. In other words, the operator will make up for the higher unit costs after seven years, which is not long in aviation terms.

With respect to the requirement defined by the customer, the aircraft does not meet CS25. However, the team is confident this requirement will be meet at a later development stage. Moreover, a discrepancy is found on the noise exposed area requirement. Even though the area was reduced by 29.2%, 0.8% more is required, the equivalent to 0.4 km^2. Due to software utilised, one of the most important noise mitigation measures is not yet taken into account; wing shielding. Hence the design team is confident that the requirement will be met in a later stage.

All in all, the *Silent Regional Jet 110* is well on its way to become the most sustainable aircraft of its time in terms of noise, performance and fuel efficiency.

Bibliography

[1] Gill, E. Verification and Validation for the Attitude and Orbit Control System. University Lecture, 2017.

[2] BAe Systems. BAe146/AVRO RJ100 Versatility. https://www.regional-services.com/wp-content/uploads/2016/06/146-RJ-Versatility-8pp-brochure-Civilian-2015-FOR-WEB-2.pdf. Accessed: 26/06/2017.

[3] Pratt & Whitney. PurePower brochure. http://www.purepowerengines.com/brochures.htm. Accessed: 26/04/2017.

[4] Embraer Commercial Aviation. Embraer E-jets E2 folder. http://www.embraercommercialaviation.com/MarketInfo/Embraer_E-Jets_E2_Folder_V3_052915c.pdf. Accessed 26/04/2017.

[5] ICAO. Aircraft Engine Emissions Database. Excel file downloaded from https://www.easa.europa.eu/document-library/icao-aircraft-engine-emissions-databank. Accessed: 18/06/2017.

[6] Park, Y. and O'Kelly, M.E. Fuel burn rates of commercial passenger aircraft: variations by seat configuration and stage distance. *Journal of Transport Geography*, 41:137–147, December 2014.

[7] European Aviation Safety Agency. Noise Database, Issue 25 and 27, February 2017. https://www.easa.europa.eu/document-library/noise-type-certificates-approved-noise-levels. Accessed: 12/05/2017.

[8] Federal Aviation Administration. Details on FAA Noise Levels, Stages, and Phaseouts. https://www.faa.gov/about/office_org/headquarters_offices/apl/noise_emissions/airport_aircraft_noise_issues/levels/. Accessed: 12/05/2017.

[9] International Civil Aviation Organisation. Fourth Meeting of the ALLPIRG - Appendix WP28. http://www.icao.int/Meetings/AMC/MA/2001/Allpirg4/wp28app.pdf, 2000. Accessed: 26/04/2017.

[10] Koninklijke Luchtvaartmaatschappij. Seating plan Embraer 190. https://www.klm.com/travel/nl_nl/prepare_for_travel/on_board/seating_plans/ERJ-190.htm. Accessed: 25/04/2017.

[11] European Aviation Safety Agency. Certification Specifications and Acceptable Means of Compliance for Large Aeroplanes. https://www.easa.europa.eu/system/files/dfu/CS-25%20Amendment%2018_0.pdf. Accessed: 25/04/2017.

[12] NATS Aeronautical Information Service. Airport Charts. http://www.nats-uk.ead-it.com/public/index.php%3Foption=com_content&task=blogcategory&id=92&Itemid=141.html, http://www.bvartcc.com/charts/EGLC/AD/EG_AD_2_EGLC_en_2011-05-05.pdf. Accessed 25/04/2017.

[13] Reuters. Embraer launches next E-Jets to strong demand, SkyWest orders up to $9.4 billion. http://www.reuters.com/article/us-airshow-embraer-idUSBRE95G09W20130617. Accessed: 26/06/2017.

[14] PR Newswire. Global Market for Regional Aircrafts - 2017-2025 - Market Dynamics, Competitive Landscape, OEM Strategies & Plans, Trends & Growth Opportunities, Market Outlook through 2025. http://www.prnewswire.com/news-releases/global-market-for-regional-aircrafts---2017-2025---market-dynamics-competitive-landscape-oem-strategies--plans-trends--growth-opportunities-market-outlook-through-2025-300410256.html. Accessed 1/5/2017.

[15] SuperJet International. 2016-2035 Market Outlook. http://www.superjetinternational.com/download/SJI_Market_Outlook_2016_2035.pdf.

[16] Embraer. Dispatch Reliability Status. embraerki.republika.pl/lot.ppt. Accessed: 22/06/2017.

[17] Bombardier Aerospace. CRJ Series Status Report. http://www.bombardier.com/content/dam/Websites/bombardiercom/supporting-documents/BA/Bombardier-Aerospace-20150630-CRJ-Series-Program-Status-en.pdf. Accessed 2/5/2017.

[18] Bhaskara V. Battle Of The Regionals – ERJ vs CSeries vs MRJ vs SSJ: Introduction and Market Overview. https://airwaysmag.com/industry/battle-of-the-regional-market/. Accessed 1/5/2017.

[19] FlightGlobal. Mitsubishi delays MRJ deliveries by two years.

https://www.flightglobal.com/news/articles/mitsubishi-delays-mrj-deliveries-by-two-years-433402/. Accessed: 26/06/2017.

[20] Bombardier Aerospace. CSeries Status Report. http://www.bombardier.com/content/dam/Websites/bombardiercom/supporting-documents/BA/Bombardier-Aerospace-20161231-CSeries-Program-Status-en.pdf. Accessed 4/5/2017.

[21] Forecast International. Regional Aircraft Market Stabilizing; Long-Term Growth Projected. https://globenewswire.com/news-release/2016/09/23/874245/10165297/en/Regional-Aircraft-Market-Stabilizing-Long-Term-Growth-Projected.html. Accessed 2/5/2017.

[22] Embraer. Specifications E190. http://www.embraercommercialaviation.com/Pages/Ejets-190.aspx. Accessed 2/5/2017.

[23] Superjet International. SSJ100 Product Brochure. http://www.superjetinternational.com/download/SSJ100_product_brochure.pdf. Accessed 2/5/2017.

[24] Mitsubishi Aircraft Corporation. Fly the MRJ. http://www.flythemrj.com/. Accessed 2/5/2017.

[25] Bombardier. C Series CS100 Factsheet. http://commercialaircraft.bombardier.com/content/dam/Websites/bca/literature/cseries/C%20Series_CS100_Factsheet201607_EN.pdf. Accessed 2/5/2017.

[26] Bombardier. CRJ Series CSJ 1000 Factsheet. http://commercialaircraft.bombardier.com/content/dam/Websites/bca/literature/crj/CRJ%20Series_CRJ%201000_Factsheet_201607_EN.pdf. Accessed 2/5/2017.

[27] Swartz, K.L. Great Circle Mapper. http://www.gcmap.com/mapui?P=AGP,+TRD,+KEF,+CTA,+OTP,+SVO,+AYT,+CMN,+HEL,+TUN&R=1500nm%40ams,c:navy%0d%0a1000nm%40lcy,c:red%0d%0a&PM=b:disc7%2b%25t&RS=outline&RC=%23ff0000&RW=3&DU=mi. Accessed 25/04/2017.

[28] Jetcraft. Jetcraft 10-Year Market Outlook. http://jetcraft.com/outlook/Jetcraft-10-Year-Market-Forecast-2016.pdf. Accessed: 04/05/2017.

[29] Gaens H., Harms T., Hendrickx R., Hofman S., Pruijsers T., Van Sunten R., Van de Sype L., Verhellen S. and Wink R. Design Synthesis Exercise - Baseline Report. Technical report, Delft University of Technology, 2017.

[30] Gaens H., Harms T., Hendrickx R., Hofman S., Pruijsers T., Van Sunten R., Van de Sype L., Verhellen S. and Wink R. Design Synthesis Exercise - Project Plan. Technical report, Delft University of Technology, 2017.

[31] Gaens H., Harms T., Hendrickx R., Hofman S., Pruijsers T., Van Sunten R., Van de Sype L., Verhellen S. and Wink R. Design Synthesis Exercise - Mid-term Report. Technical report, Delft University of Technology, 2017.

[32] La Rocca, G. SEAD Lecture Slides. AE3211-I Systems engineering and Aerospace Design, TU Delft, 2017.

[33] European Union. Commission Regulation (EC) No 859/2008 of 20 August 2008. http://eur-lex.europa.eu/LexUriServ/LexUriServ.do?uri=OJ%3AL%3A2008%3A254%3A0001%3A0238%3AEN%3APDF.

[34] Butterworth-Heinemann. Civil Jet Aircraft Design. https://booksite.elsevier.com/9780340741528/appendices/data-a/default.htm. Accessed: 12/05/2017.

[35] Bombardier. The CRJ series. http://commercialaircraft.bombardier.com/content/dam/Websites/bca/literature/crj/Bombardier-Commercial-Aircraft-CRJ-Series-Brochure-en.pdf. Accessed: 12/05/2017.

[36] Civil Aviation Company of China. Advanced Regional Jet for 21th century. http://www.icas.org/media/pdf/ICAS%20Congress%20General%20Lectures/2010/ICAS-2010-0.5_ARJ21-700_en.pdf. Accessed: 12/05/2017.

[37] Airbus. A318, the World's Best 100-seat Jetliner. http://www.airbus.com/aircraftfamilies/passengeraircraft/a320family/a318/. Accessed: 12/05/2017.

[38] Fokker Technologies. Fokker 50, 70 &100 Regional Jets. http://www.flyfokker.com. Accessed:

12/05/2017.

[39] Melkert, J.A., Vos, R. and Zandbergen, B.T.C. Aerospace Design and Systems Engineering Elements I - AE1222-II. Powerpoint. Accessed: 12/05/2017.

[40] Torenbeek E. *Synthesis of Subsonic Airplane Design.* Kluwer Academic Publishers, 1982.

[41] Pratt and Whitney. PW1700G & PW1900G Engines. https://www.pw.utc.com/Content/Press_Kits/pdf/ce_pw1700g-1900g_pCard.pdf. Accessed: 25/06/2017.

[42] Ukraine International Airlines. UIA Passenger Fleet - Embraer E190. http://www.uiacargo.com/poloz/UIA%20E190.pdf. Accessed 07/06/2017.

[43] Embraer Commercial Aviation. Embraer E190 - Ground. http://www.embraercommercialaviation.com/AircraftPDF/E190_Ground.pdf. Accessed 07/06/2017.

[44] Barua, P., Sousa, T., Scholz, D. Empennage Statistics and Sizing Methods for Dorsal Fins. Technical Notes. Accessed: 12/06/2017.

[45] Elham A., Steenhuizen D. Aerospace Design and System Engineering Elements II AE2111-II - Wing Design. Powerpoint. Accessed: 26/05/2017.

[46] Sadraey, M. *Aircraft Design: A Systems Engineering Approach.* John Wiley & Sons, 2012.

[47] Roskam, J. *Airplane Design; Part IV: Layout of Landing Gear and Systems.* DARcorporation, Lawrence, Kansas, 2000.

[48] Civil Engineering Handbook. Aircraft Design - Wing Planform Geometry. https://www.civilengineeringhandbook.tk/aircraft-design/wing-planform-geometry.html. Accessed 12/06/2017.

[49] Rajendran, S. Design of Parametric Winglets and Wing tip devices - a Conceptual Design Approach. https://www.diva-portal.org/smash/get/diva2:547954/FULLTEXT01.pdf. Accessed 12/06/2017.

[50] International Nurflügelmeeting des MFC Osnabrück. Winglets - A close look. http://www.mh-aerotools.de/airfoils/winglets.htm. Accessed 14/06/2017.

[51] Enviro.Aero. Wingtip devices. https://aviationbenefits.org/case-studies/wingtip-devices/. Accessed 12/06/2017.

[52] Irvin J., Davies R. US Patent and Trademark Office - Wing Tip Device. http://appft1.uspto.gov/netacgi/nph-Parser?Sect1=PTO2&Sect2=HITOFF&p=1&u=%2Fnetahtml%2FPTO%2Fsearch-bool.html&r=1&f=G&l=50&co1=AND&d=PG01&s1=20050133672&OS=20050133672&RS=20050133672. Accessed 14/06/2017.

[53] Raymer, D.P. *Aircraft Design: A Conceptual Approach.* American Institute of Aeronautics and Astronautics, Reston, Virginia, 1999.

[54] Gleason, B. Blended Winglets - One Operator's Perspective. 2005 Performance and Flight Operations Engineering Conference - Southwest Airlines. Accessed: 14/06/2017.

[55] Elham, A. Aircraft Aerodynamic Analysis - Drag. AE2111-II Aerospace Design and Systems Engineering Elements II, TU Delft, 2016.

[56] Mason, W.H. Transonic Aerodynamics of Airfoils and Wings. AOE 4124 Configuration Aerodynamics, Virginia Tech, 2017.

[57] Gudmundsson, S. *General Aviation Aircraft Design.* Butterworth-Heinemann - Elsevier, 2014.

[58] Elham A. Aerospace Design and System Engineering Elements II AE2111-II - Aileron Design. Powerpoint. Accessed: 22/0-/2017.

[59] Warwick, G. Alcoa offers alloys to cut 787 weight. *Flight international*, 2007. https://www.flightglobal.com/news/articles/alcoa-offers-alloys-to-cut-787-weight-213707/.

[60] Hibbeler, R.C. *Mechanics of Materials in SI units.* Prentice Hall, eighth edition, 2011.

[61] ASM Aerospace Specifiaction Metals Inc. Aluminum 7075-t6. http://asm.matweb.com/search/SpecificMaterial.asp?bassnum=MA7075T6.

[62] US Department of Transportation. *Aviation Maintenance Technician Handbook: Chapter 07.* Federal Aviation Administration, 2012.

[63] Ashby, M.F. *Materials Selection in Mechanical Design.* Butterworth-Heinemann, third edition, 2005.

[64] Pichler, D. Give us affordable carbon fiber! http://www.compositesworld.com/columns/give-us-affordable-carbon-fiber, feb 2016. Accessed on: 22/06/2017.

[65] ASM Aerospace Specifiaction Metals Inc. Aluminum 7475-t7651. http://asm.matweb.com/search/SpecificMaterial.asp?bassnum=MA7475T765.

[66] Hale, J. Boeing 787 from the ground up. *Aeromagazine*, (24), 2006.

[67] Wu, G. , Yang, J. M. The mechanical behavior of GLARE laminates for aircraft structures. *Materials Science and Engineering*, 57(1):72–79, jan 2005.

[68] Smith, R.A. Composite Defects and Their Detection. *Materials Science and Engineering*, 3, 2009.

[69] Cheng, L., Tian, G.Y. Surface Crack Detection for Carbon Fiber Reinforced Plastic (CFRP) Materials Using Pulsed Eddy Current Thermography. *IEEE*, 11(12):3261–3268, may 2011.

[70] Woerden, H.J.M., Sinke, J., Hooijmeijer, P.A. Maintenance of Glare Structures and Glare as Riveted or Bonded Repair Material. *Applied Composite Materials*, 10(4):307–329, jul 2003.

[71] MIT. Material Type Cost (USD/kg) Density. http://web.mit.edu/course/3/3.11/www/modules/props.pdf. Accessed on: 22/06/2017.

[72] Shama Rao N., Simha T. G. A., Rao K. P. and Ravi Kumar G.V. Carbon Composites Are Becoming Competitive And Cost Effective. https://www.infosys.com/engineering-services/white-papers/Documents/carbon-composites-cost-effective.pdf, 2015.

[73] Constellium. Aluminium recylcling in aircraft life cycle. http://www.constellium.com/markets/aerospace/commercial-aircraft/aircraft-recycling-process, apr 2013. Accessed on: 20/06/2017.

[74] de Haan, A.R.C. *Fiber Metal Laminates*. Springer-Science, 2001. Editors: Vlot, A., Gunnink, J.W.

[75] Carberry, W. Airplane Recycling Efforts Benefit Boeing Operators. *Aeromagazine*, 2008.

[76] Boeing Fire Department. 787 Aircraft Rescue & Firefighting Composite Structure. http://www.boeing.com/assets/pdf/commercial/airports/faqs/787_composite_arff_data.pdf, apr 2013. Accessed on: 20/06/2017.

[77] Massachusetts Institute of Technology. Wing Bending Calculations; Lecture Notes. https://ocw.mit.edu/courses/aeronautics-and-astronautics/16-01-unified-engineering-i-ii-iii-iv-fall-2005-spring-2006/systems-labs-06/spl10.pdf. Accessed: 11/06/2017.

[78] Tencate. NOMEX® HONEYCOMB - AEROSPACE GRADE, product datasheet. http://www.tencate.com/emea/Images/prodcomp_28-25505_NomexAERO_V7_DS_Web_082114.pdf. Accessed: 18/06/2017.

[79] Aerospace Engineering Blog. Fancy a Sandwich? http://aerospaceengineeringblog.com/sandwich-panel/. Accessed: 18/06/2017.

[80] van der Wal, W. SVV Lecture Slides. AE3212-II Simulation, Verification and Validation, TU Delft, 2017.

[81] Bourier S., Hofman S., de Jong C., de Kok S., Nieuwerth G. and van der Pluijm A. Technical Report. Technical report, Delft University of Technology, 2017.

[82] Faber N., Gaens H., Mavrocordatos N., Stienstra A., Taams M. and Knobbout J.J. Technical Report. Technical report, Delft University of Technology, 2017.

[83] Hale, J. Boeing 787 From The Ground Up. http://www.boeing.com/commercial/aeromagazine/articles/qtr_4_06/article_04_2.html. Accessed: 10/06/2017.

[84] Hradecky, S. Hard Landing. http://avherald.com/h?search_term=hard+landing&opt=0&dosearch=1&search.x=0&search.y=0. Accessed: 10/06/2017.

[85] Hall, N. Shape Effects on Drag. https://www.grc.nasa.gov/www/k-12/airplane/shaped.html. Accessed 13/6/2017.

[86] Megson, T.H.G. *Aircraft Structures for Engineering Students*. Elsevier, 2013. Fifth Edition.

[87] Baird, F. Dreamliner Cabin Pressure Tech Reduces Altitude Sickness, Benefits PaxEx. https://apex.aero/2015/12/10/turning-down-the-cabin-pressure. Accessed 15/6/2017.

[88] Callister, W.D. and Rethwisch, D.G. *Materials Science and Engineering*. Wiley, 2011. Eighth Edition.

[89] Walraet, S. Compression-compression and tension-compression fatigue of textile woven carbon-epoxy composites. Literature Study, TU Delft, 2017.

[90] Hudson, C.M. A Study of Fatigue and Fracture in 7075-T6 Aluminium Alloy in Vacuum and Air Environments. Technical report, NASA, 1973. Accessed: 18/06/2017.

[91] Reis, P.N.B, Ferreira, J.A.M., Costa, J.D.M. and Richardson, M.O.W. Fatigue life evaluation for carbon/epoxy laminate composites under constant and variable block loading. Technical report, University of Beira Interior, University of Coimbra and University of Portsmouth, 2008. Accessed: 23/06/2017.

[92] Warwick, G. Opening Doors. *Flight International*, January 2007.

[93] FAA. El Al Flight 1862, Boeing 747-200F, 4X-AXG, Accident Overview. `http://lessonslearned.faa.gov/ll_main.cfm?TabID=1&LLID=38&LLTypeID=2`. Accessed: 19/05/2017.

[94] Grönstedt, T et al. First and Second Law Analysis of Future Aircraft Engines. *Journal of Engineering for Gas Turbines and Power*, 135, 2013.

[95] Airbus Flight Operations Support & Line Assistance. Getting to grips with fuel economy. `http://ansperformance.eu/references/library/airbus-fuel-economy.pdf`. Accessed: 18/06/2017.

[96] IATA. Carbon Offset Program - Frequently Asked Questions. `https://www.iata.org/whatwedo/environment/Documents/carbon-offset-program-faq-airline-participants.pdf`.

[97] Ruijgrok, G.J.J. *Elements of Airplane Performance*. Delft University Press, 2009.

[98] UK Met Office. Climate Extremes in the UK. `http://www.metoffice.gov.uk/public/weather/climate-extremes/#?tab=climateExtremes`. Accessed: 26/06/2017.

[99] Janszen G., Grande A.M., Bettini P., Di Landro L. INTEGRATED SOLUTIONS FOR SAFE FUEL TANKS. *Int. J. of Safety and Security Eng*, 4, 2014.

[100] Experimental Aircraft Info. Hydraulic Principles. `http://www.experimentalaircraft.info/articles/hydraulic-principles.php`. Accessed: 23/06/2017.

[101] Boeing 757-200/300 - Hydraulic System. `http://craigmiddleton.co.uk/757/Biggles/www.crjresets.ca/z-Mcon/Hard2Find/B757/757_rr/hydraulics/general.html#top`. Accessed: 23/06/2017.

[102] Ruijgrok, G.J.J. *Elements of Aviation Acoustics*. Delft University Press, 2004.

[103] van Hemelen, T. Investigation of Aircraft Noise Metrics. Master thesis, Delft University of Technology, 2017.

[104] Smith, M.J.T. *Aircraft Noise*. Cambridge University Press, 1989.

[105] Flight Operations Support & Line Assistance. Getting to grips with aircraft noise. . Technical report, Airbus Customer Services, 2003.

[106] European Aviation Safety Agency. Technology and Design; Aircraft Noise. `https://www.easa.europa.eu/eaer/topics/technology-and-design/aircraft-noise`. Accessed 12/05/2017.

[107] Dickson, N. ICAO Noise Standards. `https://www.icao.int/Meetings/Green/Documents/day%201pdf/session%202/2-Dickson.pdf`. Accessed: 22/05/2017.

[108] Herr, M. Efficient and Airworthy Passive and Active Airframe Noise Control Strategies. `http://elib.dlr.de/78650/1/herr.pdf`, mar 2012. Accessed: 26/04/2017.

[109] Finez, A., Jacob, M.C., Jondeau, E. and Roger, M. Broadband Noise reduction With Trailing Edge Brushes. Technical report, American Institute of Aeronautics and Astronautics, 2010.

[110] Slooff, J.W., de Wolf, W.B., van der Wal, H.M.M., Maseland, J.E.J. Aerodynamic and aero-acoustic effects of flap tip fences. Technical report, Nationaal Lucht- en Ruimtevaartlaboratorium, 2002.

[111] Brook, T.F., Hutcheson, F.V. and Humphreys Jr., W.M. Noise Radiation from a Continuous Mold-line Link Flap Configuration. *aeroacoustics*, 10(5&6):565–588, Apr 2011.

[112] Herr, M. , Rossignol, K.S. , J. Delfs , Mobner, M., Lippitz, N. Specification of Porous Materials for Low-Noise Trailing-Edge Applications. Technical report, DLR, Jun 2014.

[113] Autonomous Slat-Cove Filler Device. `https://technology.nasa.gov//t2media/tops/pdf/LAR-TOPS-87.pdf`. Accessed: 12/05/2017.

[114] Dejiu, Z., Xunnian, W. and Yong, L. Control Strategies For Aircraft Airframe Noise Reduction. *Chinese Journal of Aeronautics*, 26(2):249–260, 2012.

[115] Hovelmann, A. Aerodynamic Investigations of Noise-Reducing High-Lift Systems for Passenger Transport Aircraft. Technical report, DLR, Royal Instute of Technology Stockholm, Mar 2011.

[116] Pott-Pollenske, M., Wild, J., Herr, M., Delfs, J.W., Rudenko, A. and Buscher, A. Slat Noise Reduction By Means Of Adaptive Leading Edge Devices. Technical report, DLR, Airbus Operation, Sep 2014.

[117] Herr, M. , Pott-Pollenske , M. , Ewert , R. , Boenke , D. , Siebert , J. , Delfs , J. , Rudenko, A., Buscher , A., Friedel, H. , Mariotti, I. Large-Scale Studies on Slat Noise Reduction. Technical report, DLR, Jul 2015.

[118] Martens, S. Jet Noise Reduction Technology Development at GE Aircraft Engines. http://icas.org/ICAS_ARCHIVE/ICAS2002/PAPERS/842.PDF. Accessed: 24/05/2017.

[119] Leylekian, L., Lebrun, M. and Lempereur, P. An Overview of Aircraft Noise Reduction Technologies. *Aerospacelab*, 7:1–15, 2014.

[120] Dunn, D.G., Butzel, L.M., DiBlasi, A., Filler, L. and Jacobs, L.D. Aircraft configuration noise reduction vol. 1: Engineering analysis. Technical report, Boeing Commercial Airplane Company and Federal Aviation Administration, 1976.

[121] Berton, J.J. Noise Reduction Potential of Large, Over-the-Wing Mounted, Advanced Turbofan Engines. Technical report, Glenn Research Center, NASA, 2012.

[122] Joseph, P., Powell, S. and Sóbester, A. Fan Broadband Noise Shielding for Over-Wing Engines. Technical report, University of Southampton, 2012.

[123] Bombardier. Flybe Takes Delivery of Its 50th Bombardier Q400 Airliner. https://customer.aero.bombardier.com/webd/Bag/CustSite/BRAD/OpenSite.nsf/vwWebNews/19C28323AEED04E1852575BE0060369D?opendocument. Accessed: 21/06/2017.

[124] Bombardier. CRJ Fact sheet. http://news.commercialaircraft.bombardier.com/wp-content/uploads/2015/06/C-Series-Factsheet_CS100.pdf. Accessed: 12/05/2017.

[125] Boeker, E.R. et al. INM 7.0 Technical Manual. https://www.faa.gov/about/office_org/headquarters_offices/apl/research/models/inm_model/inm7_0c/media/INM_7.0_Technical_Manual.pdf. Accessed: 28/06/2017.

[126] Roskam, J. *Airplane Design; Part III: Layout Design of Cockpit, Fuselage, Wing and Empennage: Cutaways and Inboard Profiles*. DARcorporation, Lawrence, Kansas, 1989.

[127] Embraer. Embraer 190. http://www.iaso.net/downloads/docs/Embraer190.pdf.

[128] Aegean Airlines. Cabin Baggage Allowances. https://en.aegeanair.com/travel-information/baggage/cabin-baggage/.

[129] Air Moldova. Flota - E190. https://www.airmoldova.md/fleet-ro/. Accessed: 24/05/2017.

[130] Roskam, J. *Airplane Design; Part VII: Airplane Cost Estimation: Design, Development, Manufacturing and Operating*. DARcorporation, Lawrence, Kansas, 2000.

[131] Moores, V. Fourth Embraer E190-E2 test aircraft completes maiden flight. http://atwonline.com/airframes/fourth-embraer-e190-e2-test-aircraft-completes-maiden-flight. Accessed: 22/06/2017.

[132] Phoenix East Aviation. AIRLINE PILOT SALARY - What do pilots earn? https://www.pea.com/airline-pilot-salary/. Accessed: 22/06/2017.

[133] Bureau of Transportation Statistics. Airline Fuel Cost and Consumption (U.S. Carriers - Scheduled). https://www.transtats.bts.gov/fuel.asp. Accessed: 22/06/2017.

[134] Sukhoi Civil Aircraft. Operational and Economic Comparison. http://energy-leader.net/SSJ-100%E8%B6%85%E7%BA%A7100/20150708-03%20Superjet100-%20E190%20A319%20Comparison%E8%B6%85%E7%BA%A7100%20%E5%90%8C%E7%B1%BB%E9%A3%9E%E6%9C%BA%E5%AF%B9%E6%AF%94.pp. Accessed: 23/06/2017.

[135] Hartjes, S. Airline Costs, Productivity and Business Models, 2017. Airline Planning & Optimization - AE4423 lecture slides.

[136] Gunston, B., Willis, D., Munson, K., Peacock, L.T., Jackson, P., and Bushell, S. *Jane's All The World's Aircraft*. Jane's Information Group, 2015-2016.

[137] Madden, P. CAEP Combustion Technology Review Process and CAEP NOx Goals. http://www.forum-ae.eu/system/files/2-forum_caep_goals_review_process_emissions_presentation.pdf. Accessed: 26/06/2017.

[138] Meier, N. Civil Turbojet/Turbofan Specifications. http://www.jet-engine.net/civtfspec.html.

Accessed: 26/06/2017.

[139] Bombardier. C Series environmental product declaration. http://www.bombardier.com/content/dam/Websites/bombardiercom/supporting. Accessed: 27/06/2017.

[140] Embraer. E190 Specifications. https://www.embraercommercialaviation.com/commercial-jets/e190/. Accessed: 27/06/2017.

[141] Boeing Commercial Airplanes. Quiet Climb. http://www.boeing.com/commercial/aeromagazine/aero_21/quietclimb_story.html.

[142] Joustra, T. Environmental issues Amsterdam Airport Schiphol. University Lecture, 2016.

[143] LCACC. Airport Operations. http://oldsite.lcacc.org/operations/operations.html. Accessed: 12/05/2017.

[144] Jeppesen. EGLC Charts. http://www.uvairlines.com/admin/resources/charts/EGLC.pdf. Accessed: 15/05/2017.

[145] Vict20. London City Airport Morning Traffic November 2015. Tower View. https://www.youtube.com/watch?v=Veufut64nPM. YouTube screen shot. Accessed: 15/05/2017.

[146] Hamann, R.J., van Tooren, M.J.L. Systems Engineering & Technical Management Techniques Part II, jan 2006. AE3200 Design Synthesis Lecture Notes.

[147] Eurocontrol. EUROCONTROL Seven-Year Forecast. https://www.eurocontrol.int/sites/default/files/publication/files/seven-year-flights-service-units-forecast-2013-2019.pdf. Accessed 23/06/2017.

[148] Mijatovic - Jovanovic, D. Insight ATM - Introduction to Air Traffic Management. Airport of the Future - AE3501-14 Air Transportation (Q1 2016-2017).

[149] Toray. Leveraging the Power of Materials to Change the World. fhttp://www.toray.com/csr/download/pdf/dow_2016_e.pdf. Accessed: 28/06/2017.

[150] Pilarski F. Methodology for System Design. ENAC Lecture Notes. Accessed 1/6/2017.

[151] Airbus. Delivering to the Customer. http://www.airbus.com/company/aircraft-manufacture/how-is-an-aircraft-built/delivering-to-the-customer/. Accessed 02/06/2017.

[152] Sinke J. *Production of Aerospace Engineering Systems.* Delft University, 2017.

A Task Distribution

This appendix contains a detailed description of the work performed by each team member for the final design stage of the SRJ110. Technical personal contributions are covered. Clearly, the author of each section is provided as well as the team members involved in the research part. Please note that the table does not represent the amount of work each student spent on particular tasks. The frequency of a person's initials in the table is not representative of the amount of hours spent.

Table A.1: Task distribution (Part I).

Section:	Author:	Research Fellow:
Preface	RS	RS
Summary	HG	HG
1 Introduction	SV	SV
2 Requirements Analysis and Overview	TH	RS, TH
3 Market Analysis	HG	HG
4 Risk Assessment	RH	RH
5 Concept Selection	RS	ALL
6.1 Class I Weight Estimation	TH	RW, TH
6.2 Class II Weight Estimation	TH	TH
6.3.1 Thrust and Wing Loading	TH	RW, SH, TH, TP
6.3.2 Flight Envelope	SH	SH
6.4 Integrality, Iterations and Results	TH	TH
7.1 Preliminary Tail sizing	SV	RH, SV
7.2 Loading Diagram	SV	SV, TH
7.3 Centre of Gravity Range	SV	SV
7.4 Scissor Plot	HG	HG
7.5 Optimal Tail Sizing	SV	HG, SV, TH
7.6 Landing Gear Positioning	RS	RS
8.1 Airfoil Selection	HG	HG
8.2 Wing Design	SV	HG, SV, TP
8.3 Wing Tip Design	SV	SV
8.4.1 Full Wing Analysis	HG	HG
8.4.2 Drag Estimation	SV	RW, SV
8.5 High Lift Devices	RS	RS
8.6 Ailerons, Elevator and Rudder	SV	SV
9.1 Material Choice	LS	LS
9.2.1 Wing Loading Diagrams	RS	RS
9.2.2 Wing Box Design	RH	RH, RS
9.2.3 Final Wing Box Layout	RS	RH, RS
9.3 Fuselage Structure	SH	LS, SH
9.4 Engine Mount Design	SH	SH
10.1 Cruise Altitude, Cruise Speed and Fuel Consumption	RW	RW, TP, TH
10.2 Climb Performance	TP	RW, TP
10.3 Airfield Performance	TP	RW, TP
11 Subsystem Design	RH	RH

Table A.2: Task distribution (Part II).

Section:	Author:	Research Fellow:
12.1 Noise Concept	RS	RS
12.2 Noise Sources	RS	HG, LS, RS
12.3 Noise Regulations	RS	RS
12.4 Noise of Comparable Aircraft	RS	RS
12.5 Noise Contour	RS	RS
13.1 Aerodynamic Noise Mitigation	HG	HG, LS, SV
13.2 Engine Noise Mitigation	RS	HG, RS
13.3 Final Noise Reduction	RS	RS
13.4.1 Model Explanation	TP	RW, TP
13.4.2 Discussion of Results	RW	RW, TP
14.1 Final Fuselage Design	HG	HG
14.2 Final Wing Design	SV	HG, RS, SV, TP
14.3 Final Tail Design	SV	HG, SV
14.4 Final Landing Gear Design	HG	HG, RS
15 Cost Analysis	TH	RW, TH
16.1 Verification	SV	SV
16.2.1 Weight Estimation Validation	TH	TH
16.2.2 Design Space Validation	TH	TH
16.2.3a Loading Diagram Validation	SV	SV
16.2.3b Centre of Gravity Diagram Validation	SV	SV
16.2.3c Scissor Plot Validation	HG	HG
16.2.4a Full Wing Analysis	HG	HG
16.2.4b Drag Estimation Validation	SV	SV
16.2.4c Aileron Design Validation	SV	SV
16.2.5a Wing Box Validation	RH	RH, RS
16.2.5b Fuselage Validation	SH	SH
16.2.6a Cruise Altitude, Cruise Speed and Fuel Consumption Validation	RW	RW
16.2.6b Climb Performance Validation	TP	RW, TP
16.2.6c Airfield Performance Validation	TP	RW, TP
16.2.7 Cost Analysis Validation	TH	RW, TH
17.1.1 Functional Breakdown Diagram	SH	SH, TP
17.1.2 Functional Flow Diagram	TP	SH, TP
17.2 Payload-Range Diagram	TH	TH
17.3 Operational Noise Mitigation Procedures	RS	RS
17.4 London City Procedure and Regulations	SH	SH
17.5 Reliability, Availability, Maintainability and Safety	LS	LS, SH
17.6 Communication Flow Diagrams	SV	SV
18 Sustainability Strategy	RW	RW
19 Requirements Compliance	TH	TH
20.1.1 Detailed Design Phase	RH	LS, RH, SV,
20.1.2 Industrial Phase	SV	LS, RH, SV
20.1.3 In-Service Phase	SV	LS, RH, SV
20.2 Project Gantt Chart	LS	LS, SV
20.3.1 Manufacturing Plan	LS	LS, SV
20.3.2 Assembly and Integration Plan	SV	LS, SV
Conclusion	LS	LS
CATIA expert	TP	-
Report format	RS, TH	-

B Technical Drawings

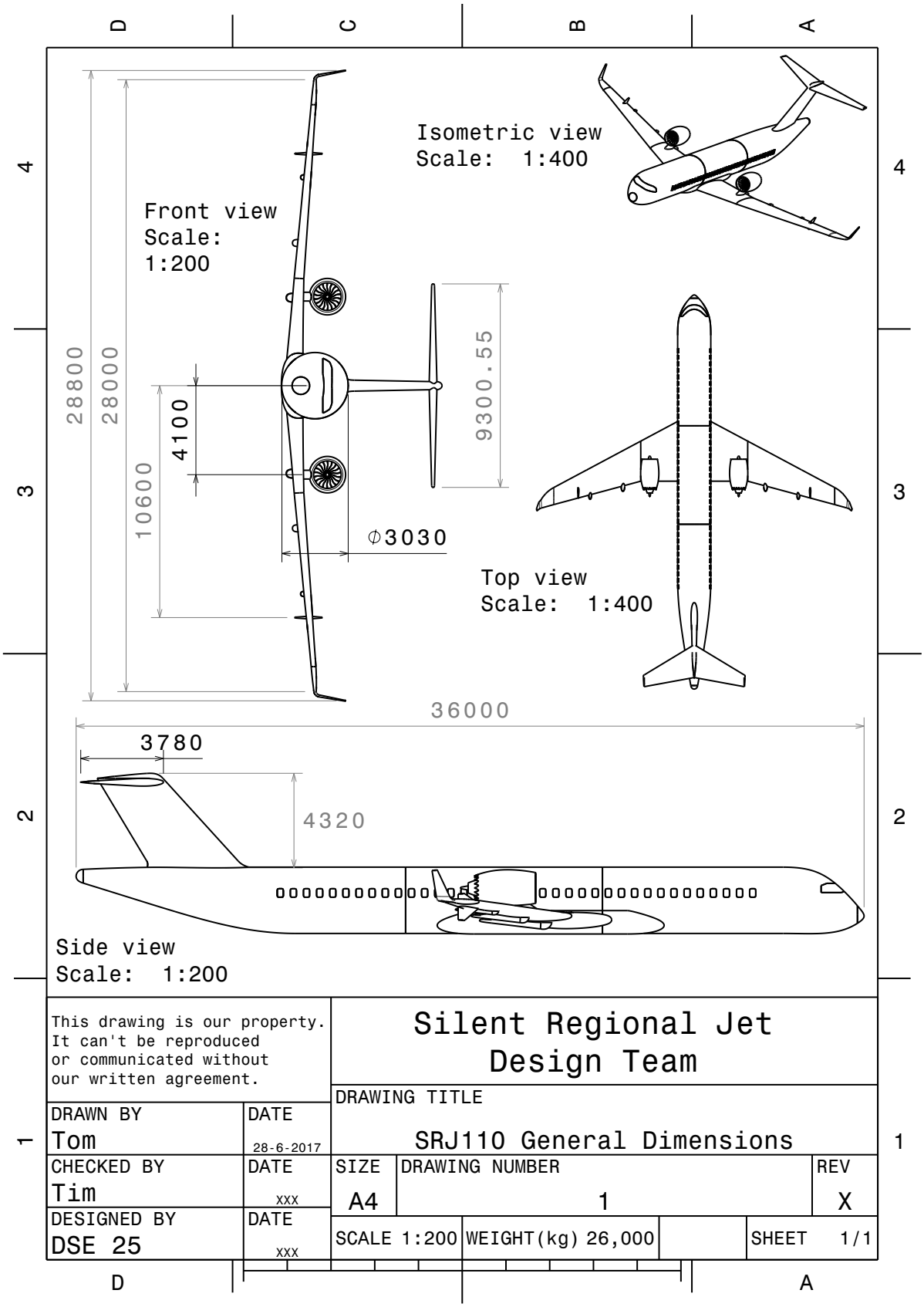

This drawing is our property. It can't be reproduced or communicated without our written agreement.		Silent Regional Jet Design Team		
DRAWN BY: Tom	DATE: 28-6-2017	DRAWING TITLE: SRJ110 General Dimensions		
CHECKED BY: Tim	DATE: XXX	SIZE: A4	DRAWING NUMBER: 1	REV: X
DESIGNED BY: DSE 25	DATE: XXX	SCALE 1:200	WEIGHT(kg) 26,000	SHEET 1/1

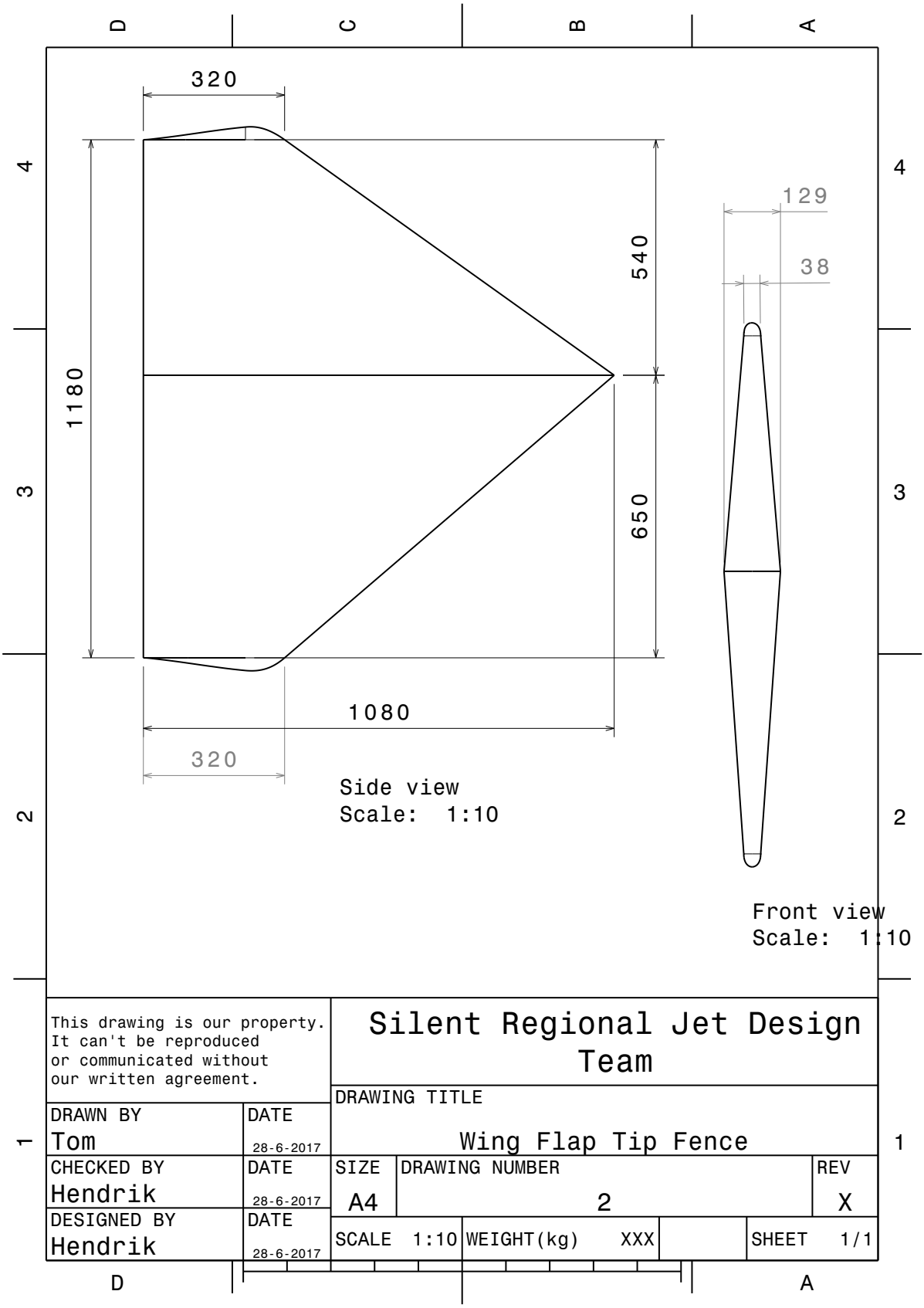
D
C
B
A
320
540
1180
650
1080
320
Side view
Scale: 1:10
129
38
Front view
Scale: 1:10
4
3
2
1
This drawing is our property.
It can't be reproduced
or communicated without
our written agreement.
Silent Regional Jet Design Team
DRAWING TITLE
Wing Flap Tip Fence
DRAWN BY
Tom
DATE
28-6-2017
CHECKED BY
Hendrik
DATE
28-6-2017
DESIGNED BY
Hendrik
DATE
28-6-2017
SIZE
A4
DRAWING NUMBER
2
REV
X
SCALE 1:10
WEIGHT(kg) XXX
SHEET 1/1

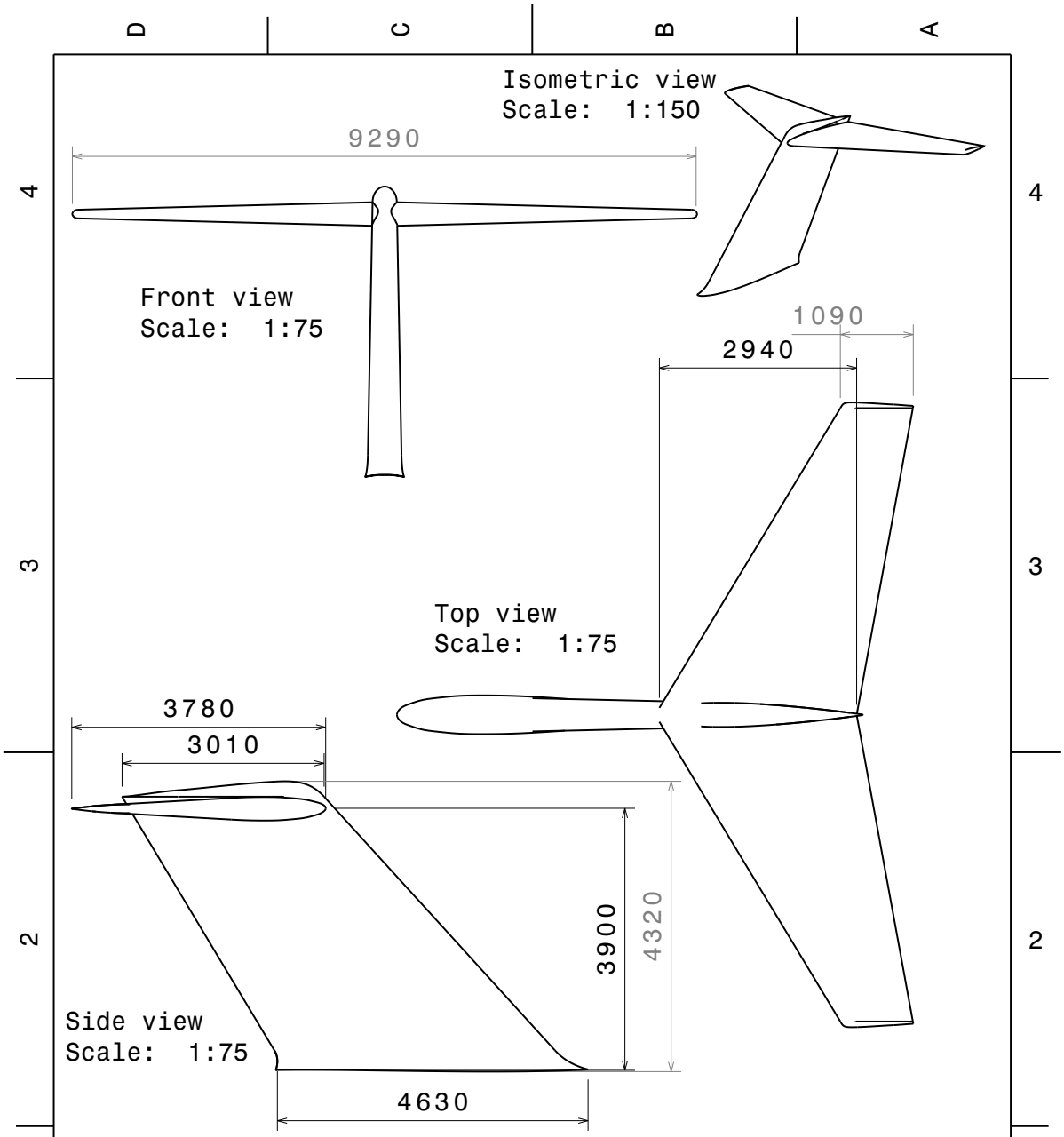

This drawing is our property. It can't be reproduced or communicated without our written agreement.		Silent Regional Jet Design Team			
DRAWN BY: Tom	DATE: 28-6-2017	DRAWING TITLE: SRJ110 Tail Section			
CHECKED BY: Tim	DATE: 28-6-2017	SIZE: A4	DRAWING NUMBER: 3		REV: X
DESIGNED BY: Saranne	DATE: 28-6-2017	SCALE: 1:75	WEIGHT(kg): XXX		SHEET: 1/1